HYDROGEOCHEMISTRY AND PHYSICAL HYDROGEOLOGY OF THE NEWFOUNDLAND ZINC MINE, DANIEL'S HARBOUR NEWFOUNDLAND

WENDY DOREEN DIAZ, B.Sc. (Honours)

HYDROGEOCHEMISTRY AND PHYSICAL HYDROGEOLOGY OF THE NEWFOUNDLAND ZINC MINE, DANIEL'S HARBOUR, NEWFOUNDLAND

BY

© Wendy Doreen Diaz, B.Sc. (Honours)

A thesis submitted to the School of Graduate Studies in partial fulfillment of the requirements for the degree of Master of Science

Department of Earth Sciences
Memorial University of Newfoundland

1990

St. John's Newfoundland

ISBN 0-315-65336-1

ABSTRACT

The Newfoundland Zinc Mine, located in a karstified carbonate platform, has large groundwater inflows along joint, fault and bedding planes. Sinkholes are prominent along the hingeline of the dominant anticlinal structure in the area. The karst nature of this aquifer is exhibited by sinkholes and other surface features, as well as by the close correlation of groundwater geochemistry and flow rates with surface recharge fluctuations. Drill logs and previous hydrogeological work suggest that aquifer permeability decreases with depth and has both diffuse and conduit elements.

Measured fracture orientations indicate t o dominant fracture plane strike and dip orientations of 039/89 and 310/88. The near horizontal bedding planes form an important third set due to their ability to conduct large volumes of water. The mine drawdown cone shape established by mine dewatering is a manifestation of underground workings and dewatering operations. Irregularities in its shape and anisotropy observed in pump tests may be caused by the orientation of these two fracture sets and faults with similar orientations. The highly variable tritium values (1-41 TU) and atypical mid-depth groundwater chemistry may be the result of localized fracture flow dominated by these sets. Local flow lines are a function of the mine drawdown and the topography.

Groundwaters are $Ca-HCO_3$ and Na-Cl type waters and most are of a meteoric origin. The $\delta^{18}O$ vs $\delta^{2}H$ data indicate an evaporated surface water contribution to some groundwater samples

and suggest a nearby lake as a source of shallow mine inflows. Apparent tritium ages indicate portions of these groundwaters have been recharged in the last 33 years. Inflows collected from different mine levels (L-Zone and T-Zone) are of two types 1) oxidized shallow inflows with low total dissolved solids and chloride (<40 ppm Cl) that may carry up to 4457 ppb zinc and 2) reducing, deeper saline groundwaters having high chloride (114-990 ppm) and sulphate (170-370 ppm) concentrations. Dissolution of gypsum or other soluble minerals locally may explain the salt content of some shallow groundwaters. The $\delta^{13}C$ vs DIC data suggest different evolutionary paths for the shallow and deep groundwaters and imply mixing of relict seawater with deep groundwater during the evolution of T-Zone groundwater.

Geochemical modelling indicates shallow groundwater evolution requires the dissolution of dolomite first under open or closed pCO_2 system conditions. This suggests recharge areas for this local flow system must be underlain by dolostone. Groundwater undersaturated with respect to carbonate minerals may reflect greater mixing with rainwater and/or saline groundwater, or slow kinetics of mineral dissolution. The decrease in $\delta^{18}O$ with increasing Cl in deeper waters suggests they are a mixture of seawater and regional groundwater recharged at higher elevations. The $\delta^{18}O$ values inferred for the meteoric component of the deep saline water implies that recharge occurred during the last post-glacial epoch.

ACKNOWLEDGEMENTS

The author wishes to thank the following mine personel: Roland Crossley, David Tiong and Gerry O'Connell for assistance during the summer and winter field work as well as supplying maps and unpublished data. The author also wishes to acknowledge the excellent assistance of Glenn Bursey, Gerry Whelan, Denny Christian and Darren Perry during the summer field program, and of Shawn Perry and Derrick Payne during the winter sampling work. Sampling of lakes was made easier by a 1986 Helicopter Scholarship from Sealand Helicopters Ltd., Nfld., to the author.

Thanks are owing to Tyson Birkett and the Geological Survey of Canada for their financial support and interest in this project under the contract #23233-6-6-0579/01 ST. Personal funding came from the Graduate Studies Bursary and Supervisors' support payments.

For providing information pertinent to this study the author is very appreciative of Mike Maher of Golder Associates Ltd., St. John's, and of Tom Lane who assisted greatly in the geology.

Although many Earth Science graduate students contributed to this thesis by many helpful discussions, two individuals stand out in their contributions. The author sincerely appreciates Bob Macleod for his help with computer programs and the author is very thankful to David Van Everdingen for his approachability and genuine helpfulness in the computer work as well as other aspects of this thesis.

I wish to thank my two supervisors; Dr. John Welhan and Dr.

John Gale collectively for their guidance during the work of this thesis. I am especially grateful to John Welhan for his continued support, enthusiasm, flexibility and suggestions during and up to the completion of this thesis. Dr. Robert Van Everdingen provided helpful criticisms on the final text.

And lastly, I truly thank Floyd Diaz for his faithful support and Amy Diaz for her unwitting inspiration.

TABLE OF CONTENTS

APPENDICES

LIST OF TABLES

LIST OF FIGURES

LIST OF PLATES

Chapter 1

INTRODUCTION

1.1 Description of Study Area and Setting

The Newfoundland Zinc Mine is located 9.5 km northeast of Daniel's Harbour, on the Great Northern Peninsula of Western Newfoundland, (Figure 1.1). The mine is situated in a sequence of predominantly dolostone beds of the St. George Group. Since the mine's discovery in 1963 by personnel of Leitch Gold Mine Ltd. and its opening in June 1975 by Teck Exploration Ltd., drilling has outlined total ore reserves of 7.1 million metric tonnes averaging 8% zinc (Crossley and Lane, 1984). As of April 1986, a total of 5,902,118 metric tonnes had been mined from 12 ore zones (R. Crossley, pers. comm., 1986) covering approximately 16 km^2 (Figure 1.2). Sphalerite ore was excavated from open pits and underground drift workings (by room and pillar method) at relatively shallow depths (L-Zone) to a maximum depth of approximately 260 m (T-Zone). Exhaustion of ore reserves forced the closure of the mine in 1990.

The mine is located near the centre of a flat-lying to undulating coastal plain with numerous small lakes. The local relief of 50 to 100 m is marked by flat-topped hills (Figure 1.3), (Proudfoot and St. Croix, 1987). This plain has many intermittent streams with scattered swamps and black spruce forest in well-drained areas. The coastal plain is underlain by an autochthonous cover sequence of Ordovician dolostone and limestone sediments. These sediments lie unconformably upon

Figure 1.1 Location map of the study area. The Newfoundland Zinc Mine is located on the Great Northern Peninsula of Newfoundland.

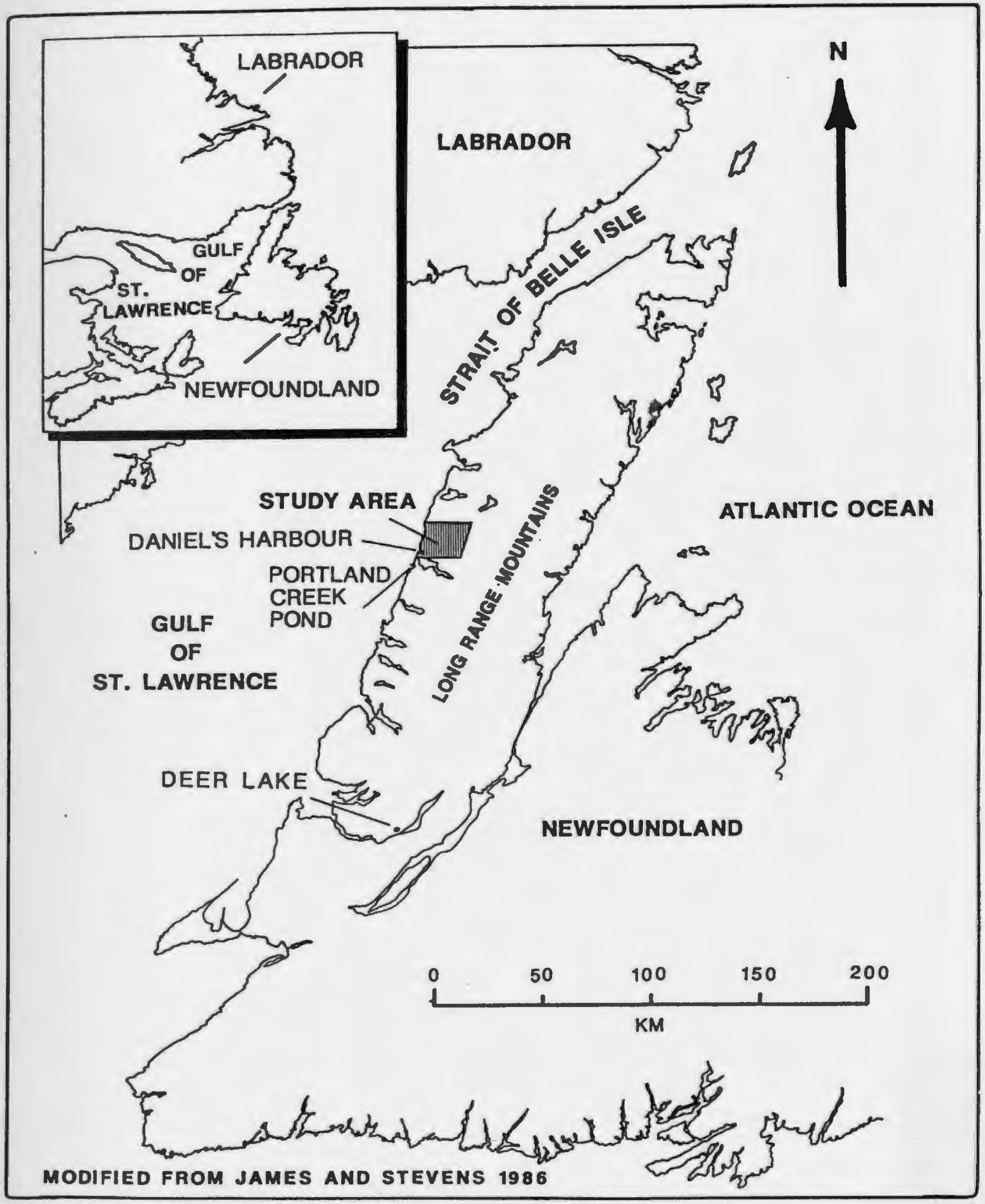

Figure 1.2 Detailed map of study area showing boundaries, lakes, major drainage routes. The mine underground workings projected to ground surface are shown in solid black. (modified from Hornbrook et al., 1975).

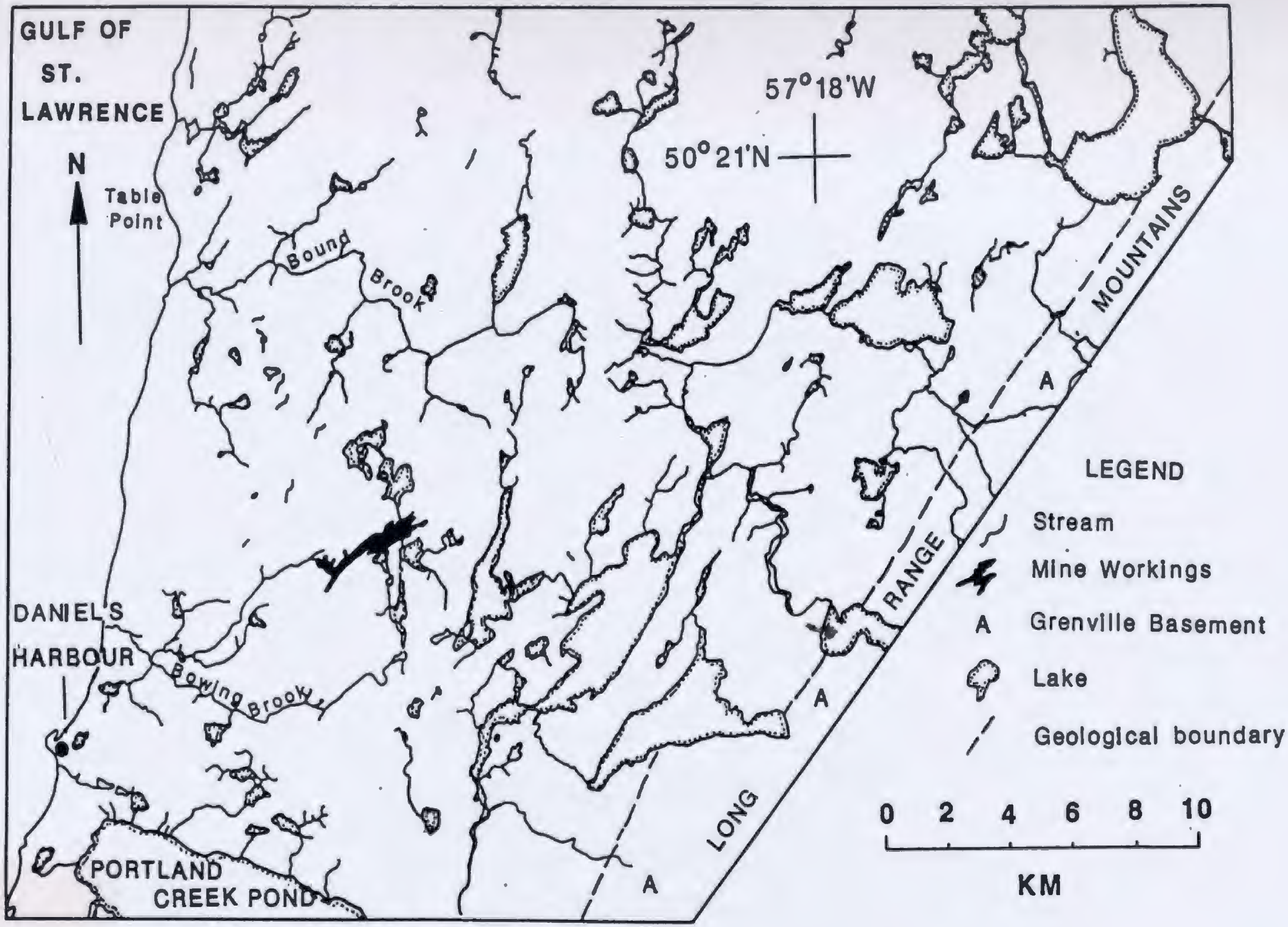
GULF OF
ST.
LAWRENCE
N
Table
Point
Bound
Brook
57°18'W
50°21'N
MOUNTAINS
RANGE
LONG
A
DANIEL'S
HARBOUR
Bowing
Brook
PORTLAND
CREEK POND
LEGEND
Stream
Mine Workings
A Grenville Basement
Lake
Geological boundary
0 2 4 6 8 10
KM

Figure 1.3 Contour elevation map of the study area. Some contour lines have been omitted in the Long Range Mountain area due to the steepness of topography.

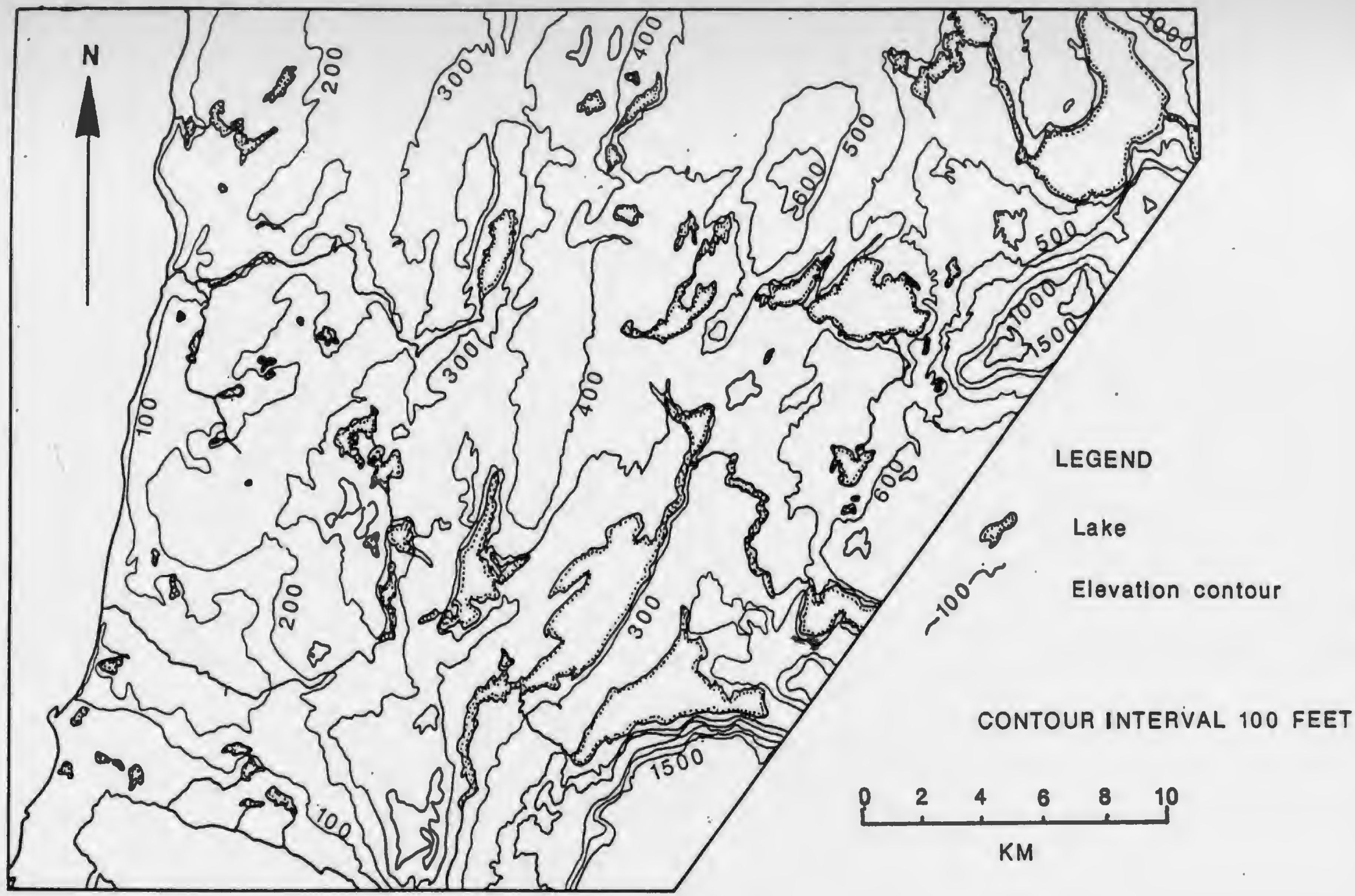
N
100
200
300
400
500
600
1000
1500
LEGEND
Lake
Elevation contour
100
CONTOUR INTERVAL 100 FEET
0 2 4 6 8 10
KM

the Grenville basement which outcrops as the Long Range Mountains.

The study area centres around the underground workings of the mine and encompasses the open pits as well as the surrounding lakes within a radius of about 10 km (Figure 1.2). The Long Range Mountains, located 17 km due east of the mine, form the eastern boundary of the study area with an elevation of 457 to 673 m. The shoreline along the Gulf of St. Lawrence forms the western boundary of the study area. The study area's southern-most extent is Portland Creek Pond and its northern limit is arbitrarily marked by the Table Point peninsula. Access to the study area is by paved road along the coastal highway.

1.2 General Mine Hydrogeology

The Newfoundland Zinc Mine is situated on a karstified carbonate platform and consequently has large groundwater inflows. These inflows caused a significant subsurface dewatering problem throughout the mine's 12 years of operation. Inflows into the mine are primarily from steeply dipping faults and joints, subhorizontal bedding planes and boreholes of various orientation. Peak underground mine inflow exceeds 56,780 l/min in the spring of the year, while in the winter months less than 22,710 l/min has been pumped.

Several hydrogeologic studies were done by Acres Consulting Ltd. (1974a&b, 1975a&b, 1976, 1977, 1978, 1979) to determine the most efficient and economical method of pumping. Mine dewatering at the Newfoundland Zinc Mine was done by underground pump stations that relayed water to storage sumps where it was eventually pumped to surface. Grouting of drill holes, major joints and faults was also recommended by Acres to control groundwater inflows. Water table drawdowns in the mining area exceeded 60 m, due to the sink created by the mine.

Karst landforms are in evidence across the plain as abundant sinkholes and springs; small sinkholes in dry lake bottoms (e.g., Lead and Spring Lakes) are seen near the mine site. Many small intermittent lakes and streams are found in the area, and these may also be indicative of early karst development. Hornbrook et al. (1975) found evidence for many streams flowing for some distance underground in the north-central part of the region.

1.3 Previous Work

Previous hydrogeological studies have been done by Acres Consulting Ltd. (1974a&b, 1975a&b, 1976, 1977, 1978, 1979) during the mining development. Acres' field investigations included pump tests, piezometer and pump discharge monitoring as well as tracer tests around the mine site. A compilation of previous hydrogeological work done on the Northern Peninsula was written by Nolan and Associates (1979); their report contained no new field work.

Detailed geological work at the mine site has been done by Lane (1984), Coron (1982), Crossley and Lane (1984), Collins and Smith (1975) and Cumming (1968). Structural geological mapping at the regional scale was done by Cawood and Williams (1986), Knight (1985), and Williams (1979). Stratigraphy and sedimentology of the region has been extensively covered by James et al. (1989); Knight and James (1987), Knight (1984), Haywick and James (1984), and Klappa, Opalinski and James (1980). Fracture analysis of rocks on the peninsula is limited to one previous study near Parson's Pond (Kunkle, 1986).

A lake sediment study and exploration geochemical survey was carried out in the Daniel's Harbour area by the Newfoundland Department of Mines (Hornbrook et al., 1975). The most recent mapping of Quaternary deposits was done by Proudfoot and St. Croix (1987).

1.4 Purpose and Scope

This thesis is a followup to preliminary work done by Welhan and Gale (1986) and is the first intensive groundwater study in the region using both hydrogeochemistry and detailed fracture analysis. Prior to 1985, there had been no detailed fracture or geochemical analyses of the mine area and groundwaters, respectively. Quantifying the fracture network, using computer techniques, aids in determining specific directions of anisotropy in the rock mass. A statistical analysis of fracture patterns in outcrop and mine drifts proved necessary for two reasons 1) studies by Acres (1974a) showed that rock mass anisotropy seemed to be caused by two major joint sets and 2) karst groundwater is known to occupy both solution-derived conduits as well as bedding planes, joints and other modes of diffuse flow (Smart & Ford, 1986).

The objectives of the thesis are:

1) to assess the physical components of the karstic groundwater flow regime in and near the mine;

2) to characterize the groundwater chemistry and stable isotope variations in order to delineate flow systems and to define the chemical evolution of groundwater and temporal/spatial effects on the hydrogeochemistry; and

3) to develop a conceptual model of the mine hydrology and related flow systems by hydrogeochemical and hydrogeological mapping.

Chapter 2

METHODOLOGY

2.1 Water Sample Collection and on Site Laboratory Work

2.1.1 Sampling locations

The field work for this study consisted of water sampling, measuring of water table depths, fracture mapping and drilling. Most of the field work was done during the unusually dry summer of 1986. Consequently, there were no inflows into the shallowest parts of the L-Zone underground workings (East drift), water levels in drill holes dropped significantly or became blocked, and bodies of surface water dried up in 1986. These conditions restricted water sampling to deeper levels of the L-Zone, and to exploration drill holes outside the perimeter of the greatest mine drawdowns, and also limited drilling of new holes to areas close to or within hauling distance of a water source. Including the preliminary work of Welhan and Gale (1986), a total of 110 water samples were taken during the 1985 and 1986 summer and 1987 winter seasons. Sample locations are shown in Figure 2.1 for the surveyed lakes, two flowing springs, and one river sample which were also sampled in 1986 and 1987. Figure 2.2 shows the locations of the remaining samples.

Four new diamond drill holes (DDH1,DDH2,DDH3 and DDH-4-86) were drilled using a J.K.S 15 Winkie Drill in 1986, see Figure 2.2. These holes were no more than 15 metres in length and their diamond drill logs are given in Appendix A. Drilling of DDH-4-86

Figure 2.1 Lake and spring water sample location map.

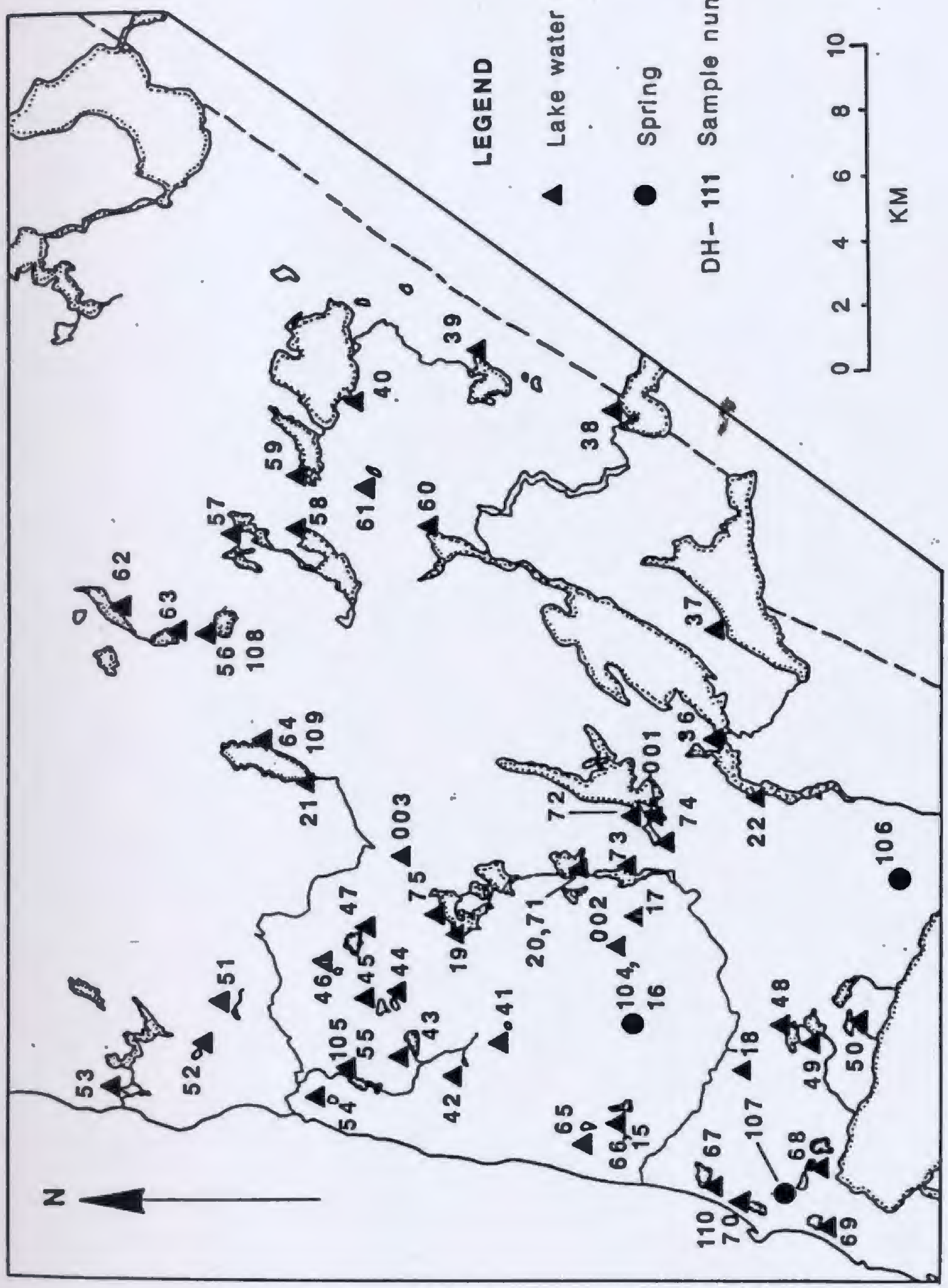

Figure 2.2 Location of mine groundwater samples. This base map is used repeatedly throughout this thesis and is a modification of the base map produced by Glenn Bursey in 1986.

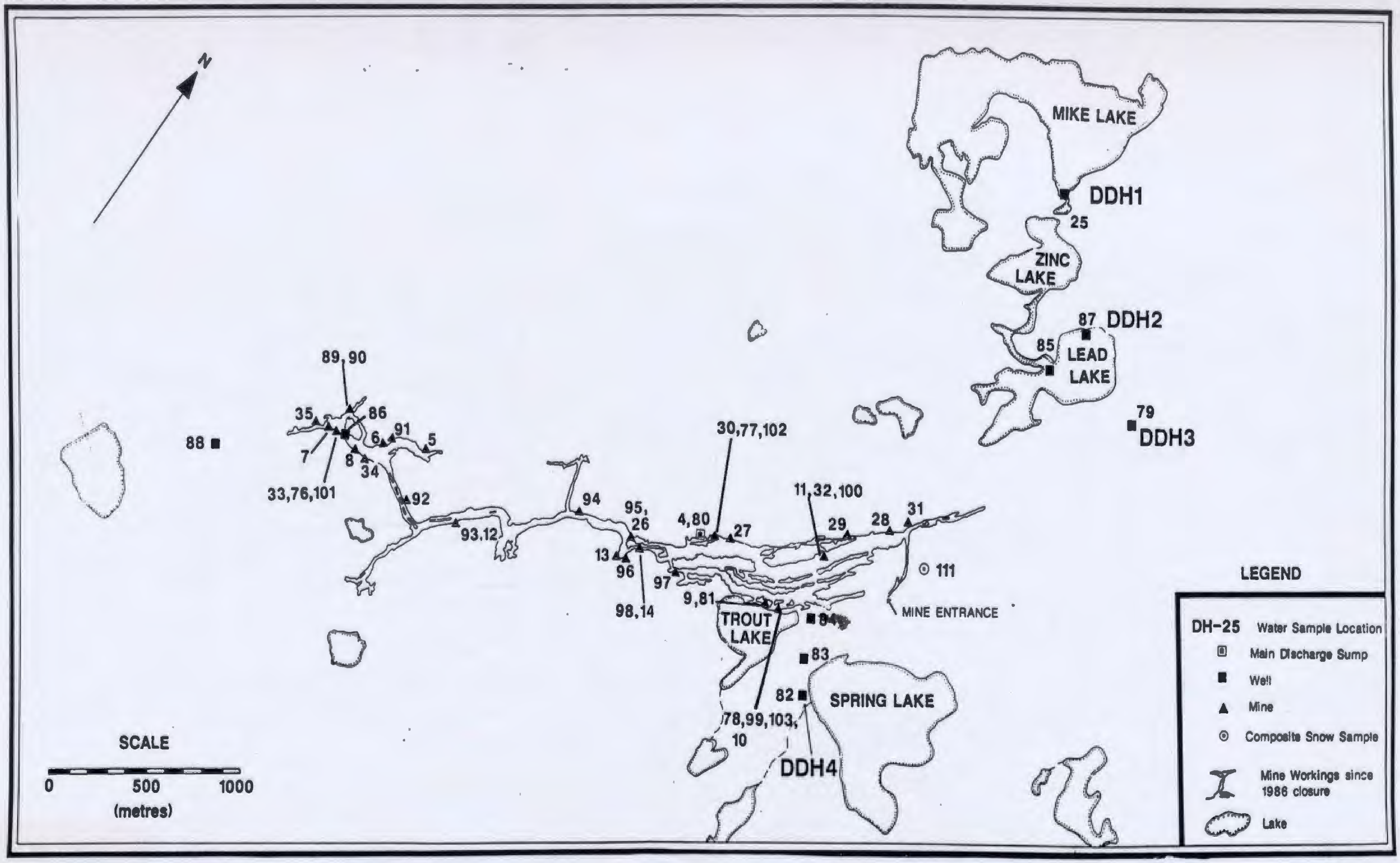
N
MIKE LAKE
DDH1
25
ZINC LAKE
87 DDH2
85
LEAD LAKE
79
DDH3
89,90
35
86
91
5
6
7
8
34
88
33,76,101
92
93,12
94
95,
26
4,80
27
30,77,102
11,32,100
29
28
31
13
96
97
98,14
9,81
© 111
MINE ENTRANCE
TROUT LAKE
84
83
82
SPRING LAKE
78,99,103,
10
DDH4
SCALE
0
500
1000
(metres)
LEGEND
DH-25 Water Sample Location
Main Discharge Sump
Well
Mine
Composite Snow Sample
Mine Workings since 1986 closure
Lake

was stopped at 34 feet, due to the inflow of tailings from Spring Lake at depths of 25 to 30 feet and the anticipated danger of sanding the drill rods.

2.1.2 Sample collection and storage procedures

Water samples obtained for major ion analyses were taken in pre-cleaned polyethylene bottles. All water samples were refrigerated during storage.

A 'Waterra' hand pump attached to polyethylene tubing was used to sample water in drill holes. An airtight flow cell was used to obtain Eh-pH measurements from surface drill holes and a bucket into which water was continuously flowing was used to obtain these measurements in the mine. Lake samples were taken by hand at the shoreline, and underground mine samples were taken from various orifices. A photo of a mine sampling site is shown in Plate 1 and a list of other site descriptions, including the type of orifice that was sampled, is given in Appendix B. Detailed descriptions were only made by the author for the 1986 sampling sites; three of these sites were repeatedly sampled at three different times during the summer field season.

Samples referred to as 'spot samples' (DH-89 to DH-100) were obtained in the mine without supporting pH, Eh, temperature and conductivity measurements and were analysed for major cations only.

Samples for total inorganic carbon analysis were taken in 250 ml glass bottles with "polyseal" phenolic caps and liners to

Plate 1. Underground sampling site of sample DH-35, T-Zone. The arrow points to the exact drill hole that was sampled.

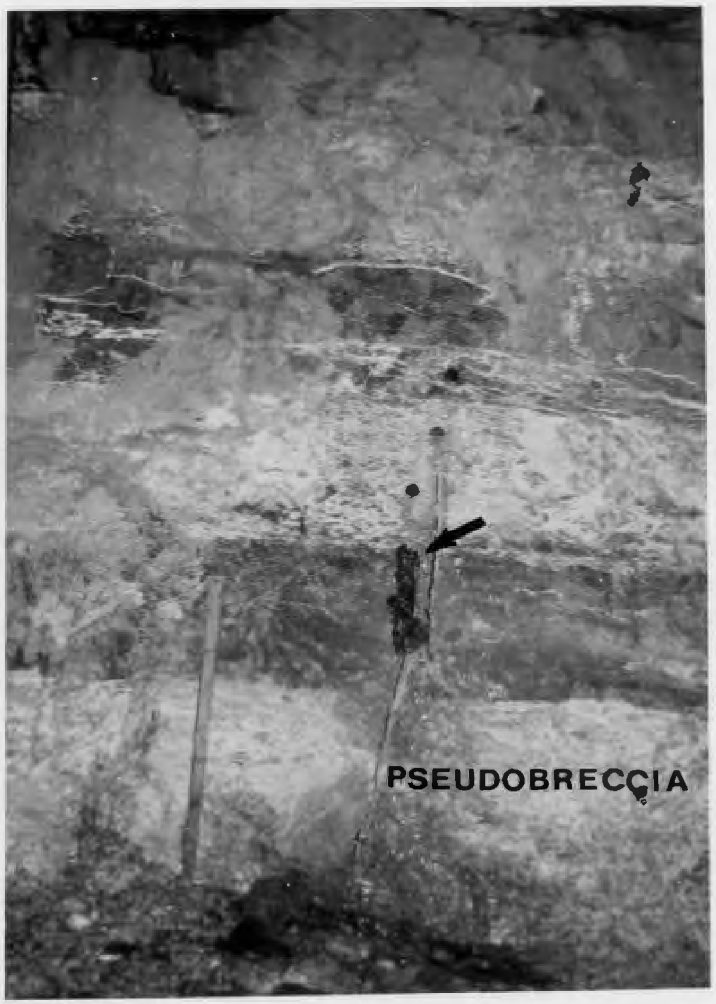

prevent CO_2 gas loss. A few grams of mercuric chloride were added to prevent microbial degradation. Samples for carbon-14 and tritium analyses were collected using methods outlined by Fritz (1983) in 20 l polypropylene carboys and 500 ml flint glass bottles, respectively. Samples for dissolved oxygen analysis were taken in 60 ml B.O.D. glass bottles for a modified Winkler titration analysis. Water samples for stable isotope analysis were taken in 20 ml scintillation vials of borosilicate glass with "polyseal" plastic lined caps.

2.1.3 Field measurements

Field measurements included temperature, pH, Eh, and conductivity. Storage-sensitive geochemical measurements (temperature, pH, Eh, dissolved oxygen) were done in the field at the sample site. Temperature, pH and Eh measurements were taken using an Accumet pH meter. A Pt-Ag/AgCl electrode was used to measure electrochemical potentials and then corrected to absolute Eh potentials. Temperatures taken with a thermocouple (precision of +/- 0.1^{o}C) were occasionally checked with a mercury thermometer (+/- 0.2 ^{o}C). The pH meter was calibrated using standarized, temperature-equilibrated buffers.

A Lakewood pH/conductivity meter was used in the 1986 field season to measure conductivity and was standardized before each measurement with a TDS/Conductivity standard solution of 2070 micromhos/cm. Two conductivity measurements were taken for each sample to check precision. Precision estimates for pH, Eh and conductivity are +/- 0.02 pH units, +/- 30 mvolts, and +/- 2 % of readings, respectively. Different conductivity meters were used in the 1985 and 1986 field seasons. A comparison test between the two conductivity meters showed that the meter used in 1985 gave higher values than the Lakewood meter (up to 500 micromhos /cm higher for samples > 2400 ppm Cl) for the same water sample.

2.1.4 Laboratory work and sample treatment

Some storage-sensitive measurements (dissolved oxygen and alkalinity titration) and other procedures for the preservation of water samples were completed at the mine laboratory on the same day the sample was taken. Both cation and anion samples were filtered with 0.45 micron cellulose acetate filters before they were stored for shipment. The alkalinity titration was done with 30 ml of water before filtering. After filtering, 2 ml of concentrated nitric acid were added to the cation sample which was also used for trace element analysis. Filtering of some water samples was delayed a day due to slow filtering caused by low water pressure at the mine site.

Carbon-14 samples (25 l) were treated with 500g of barium chloride and 30 ml of sodium hydroxide according to a procedure developed by the Department of Earth Sciences, University of Waterloo which quantitatively precipitates dissolved inorganic carbon as $BaCO_3$.

A modified Winkler Method (phenylarsine oxide standard solution as titrant) was used to measure the dissolved oxygen content with a detection limit of 0.01 mg/l (ppm). Alkalinity titration was done on all samples, except for the first 15 lake samples (DH-36 to DH-50) since the pH meter was not working on the day these samples were taken. The bicarbonate alkalinity for these samples was estimated by linear regression analysis of the other lake HCO_3/Ca data. Each titration was done immediately after the sample was exposed to air, to minimize CO_2 degassing. Precision of the alkalinity calculations is +/- 4 % .

2.2 Stable Isotope Analytical Procedures

2.2.1 Total dissolved carbon extraction and carbon-13 measurement

A high vacuum system (see Figure 2.3) was used to convert the total dissolved inorganic carbon (DIC) in the water sample to CO_2 gas and to purify it for DIC and $\delta^{13}C$ measurement.

Carbonate ions in the water sample reacted with 98 % orthophosphoric acid to form CO_2 gas. This gas was separated from water vapour and any remaining air, using liquid nitrogen baths and vacuum pumps. The CO_2 gas was then transferred by Toepler pump, to a constant volume manometer where total dissolved inorganic carbon (DIC; as CO_2) was determined by measuring the temperature (precision of +/- 0.1 ^{o}C) and CO_2 gas pressure (+/- 0.05 cm of Hg). A precision of 0.1 $^{o}/oo$ is given for the extraction procedure.

The CO_2 gas was analyzed for $\delta^{13}C$ using the V.G. Micromass

Figure 2.3. High vacuum system used to extract CO_2 gas for carbon-13 analyses.

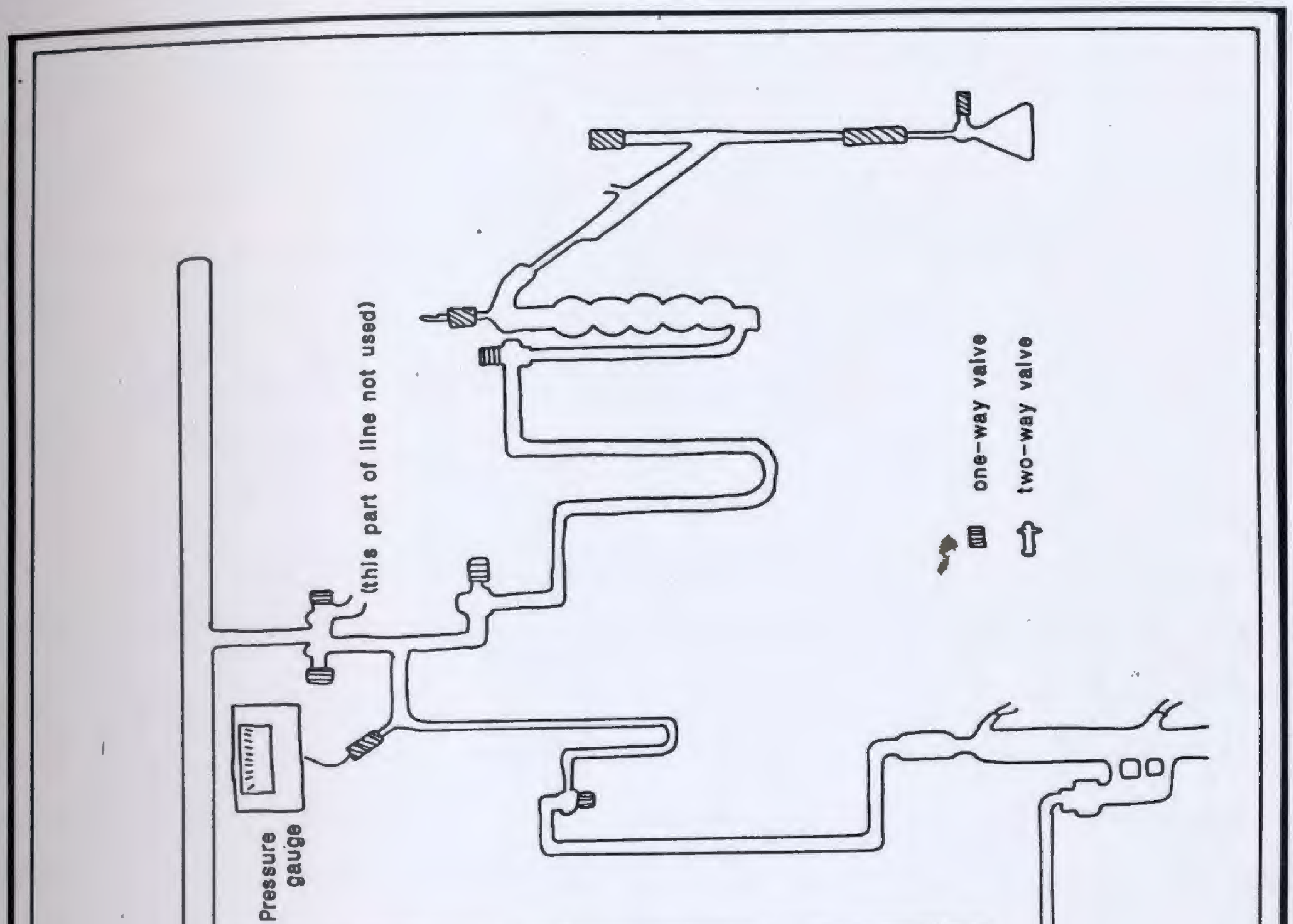

903E mass spectrometer. The "δ" is defined by the formula:

$$\delta = \frac{R_{spl} - R_{std}}{R_{std}} \times 1000, \, ^{o}/_{oo}$$

R = abundance ratio $^{13}C/^{12}C$
R_{spl} = of sample
R_{std} = of standard

Results were expressed relative to the PDB standard. Measurement precision was +/- 0.3 to 0.4 $^{o}/oo$ due to instrumental problems. An overall precision for the $\delta^{13}C$ is estimated at $^{+}/-$ 0.5 $^{o}/oo$, resulting from both the extraction and measurement errors. Reproducibility of total dissolved inorganic carbon results was determined to be approximately +/- 3 ppm.

2.2.2 Oxygen-18 and deuterium analysis

The standard method for oxygen isotope analysis is outlined by Craig (1961); deuterium was analyzed at the University of Waterloo by the standard uranium reduction method (Gonfiantini, 1981) and by the zinc method (Coleman et al., 1982) at Memorial University of Newfoundland (MUN). Similar results were obtained from both laboratories. Oxygen-18 and deuterium values are reported relative to Standard Mean Ocean Water (SMOW). Precision for mass spectrometer analyses of $^{18}O/^{16}O$ is +/- 0.2 $^{o}/oo$ and +/- 0.8 $^{o}/oo$ for deuterium.

2.3 Radioactive Isotopes

All carbon-14 and tritium analyses were done by the Isotope Laboratories at Waterloo University. Water samples were analyzed for tritium using the standard liquid scintillation beta-counter with electrolytic pre-enrichment procedure in 1985 and water samples were directly analyzed without enrichment in 1986. Tritium values are stated as Tritium Units (T.U.) which are defined as: 1 T.U. = T/H x 10^{-18} with a detection limit and precision using enrichment of approximately 1 T.U. and +/- 0.80 T.U., respectively and with a precision for direct counting of +/- 7 T.U.. Carbon-14 analyses are expressed in percent modern carbon (pmc) relative to pre-industrial/pre-nuclear wood (Fontes, 1983a) with a precision of +/- 2%.

2.4 Elemental Analysis

The 1985 cation and anion analyses were done at the Water Analysis Facility, Department of Chemistry, MUN (Welhan and Gale, 1986) by atomic absorption spectrometer and AutoAnalyzer instrumentation. All water samples collected in 1986 were analyzed in the Earth Sciences Department at MUN.

Samples taken during the 1986 field season were analyzed for anions (Cl, SO_4, NO_2, NO_3) with a Waters Associates High Performance Liquid Chromatograph (HPLC) equipped with a model 450 variable wave length UV detector and M-45 solvent delivery system. A 3390A Hewlett Packard integrator was used to convert peak heights to peak areas. Precision for Cl, SO_4, NO_2, NO_3, measurements was approximately +/- 1%, 2%, 6%, and 3%, respectively. Acidified water samples were analyzed for major cations by an atomic absorption spectrophotometer. Cation analyses are accurate to 0.2%.

Trace element analyses of acidified mine and well waters were done at Memorial University using The Inductively Coupled Plasma/Mass Spectrometer (ICP/MS). The principles of this method of analysis are outlined by Strong and Longerich (1985). Ion intensities were measured against blanks and standard solutions. Averages of repeated measurements, as well as standard deviations, were calculated for each sample. Elemental concentrations were obtained at very low detection limits of 1 ppb with an estimated precision of +/- 5% or less.

2.5 Fracture Analysis

2.5.1 Field methodology

A detailed fracture mapping survey of one surface outcrop, several open pits, and two drift walls was undertaken in the 1986 summer field season, to provide fracture data relevant to the hydrogeologic study of the mine area. A physical framework can be constructed for the development of a conceptual hydrogeochemical flow model by quantifying the fracture network. The following section describes the field methods and coding conventions used in the fracture mapping at Daniel's Harbour.

Locations of detailed fracture mapping areas are given in Figure 2.4. They include fracture mapping of vertical to near vertical surfaces in the H-Zone, F-Zone, A-Zone and two mine drifts in the entrance decline and lower L-Zone. Over half of the 923 fractures mapped were located on the near horizontal surface of a large outcrop in dry Lead Lake. Outcrop exposures are very limited and restricted to areas near some lake shores.

Figure 2.4 Locations of fracture mapping areas at the Newfoundland Zinc Mine.

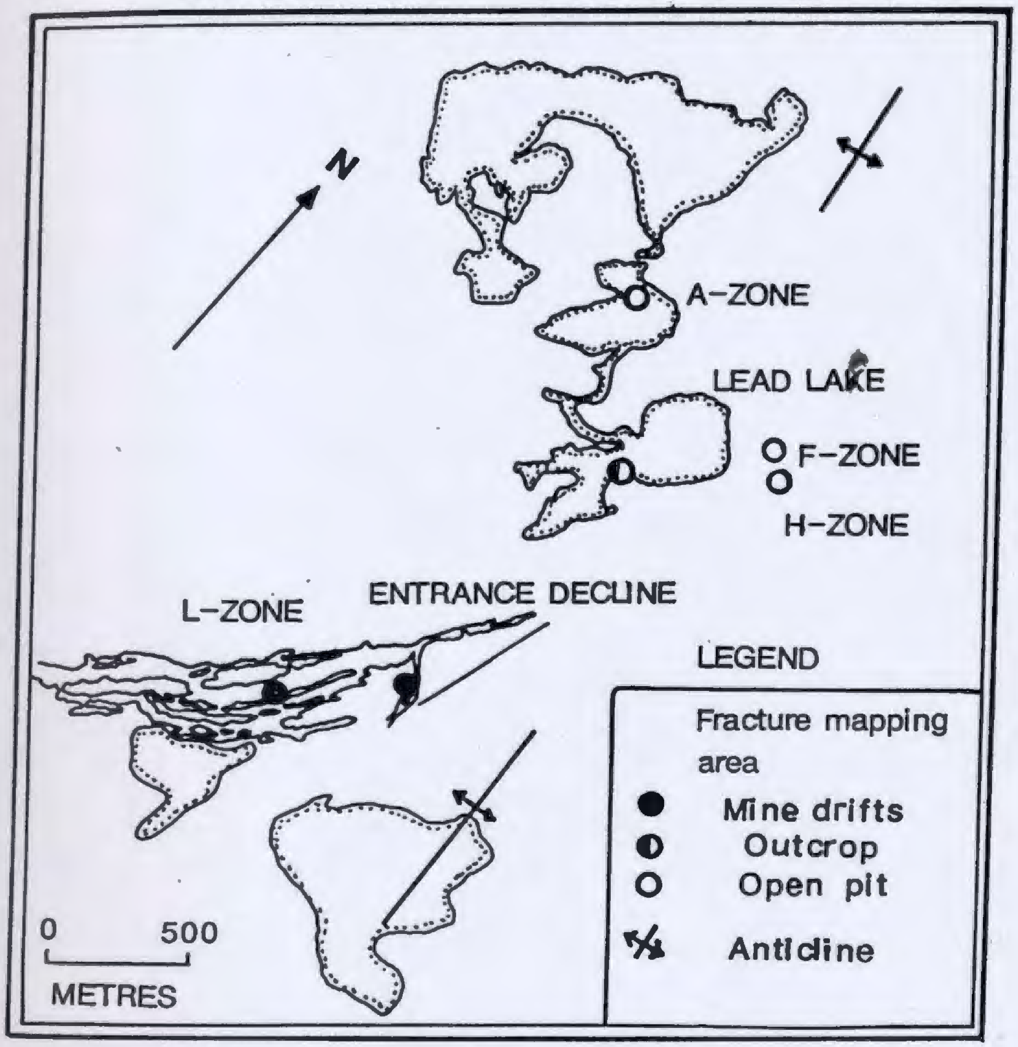

Fractures were mapped using photographs taken from a helicopter and on the ground. Overlays were drawn for each photograph of the open pits (see Appendix C), and for the photo composite of the Lead Lake outcrop (see Appendix D). An example of this line survey/photograph technique introduced by J.E. Gale is illustrated in Figure 2.5. The sampling line (henceforth referred to as the scanline) was defined by a measuring tape placed along the outcrop surface. Scanlines varied in length from 1.2 to 32 m and averaged 15.6 m. Some of the vertical mine drift walls were uneven and the accuracy of recorded scanline lengths was +/- 10 cm. All fractures, greater than 50 cm in length, intersecting the scanline were mapped by drawing the fracture trace with its number on the overlay (see Appendix C and D). Scanline orientations and basic fracture information were recorded on formatted field data sheets by using codes. Coding conventions were similar to those used by Gale and Witherspoon (1979) and their explanations are given in Appendix E.

Fracture type can be joints, veins, or bedding planes. Joints are fractures that contain no infilling minerals and have not experienced any movement along their surfaces (Rouleau and Gale, 1985a). However, joints are sometimes lined with a black, possibly dolomitic, coating. Veins are generally thin joints that contain infilling material. For simplicity, all fractures will be henceforth referred to as 'joints' since most of the fractures in this study occur as joints; and bedding planes will be referred to as such. All joints that were mapped are

Figure 2.5. Fracture mapping technique used for this study. Fractures are recorded on aerial photograph overlays of the same scale. A mapped portion of the Lead Lake outcrop is shown in this figure.

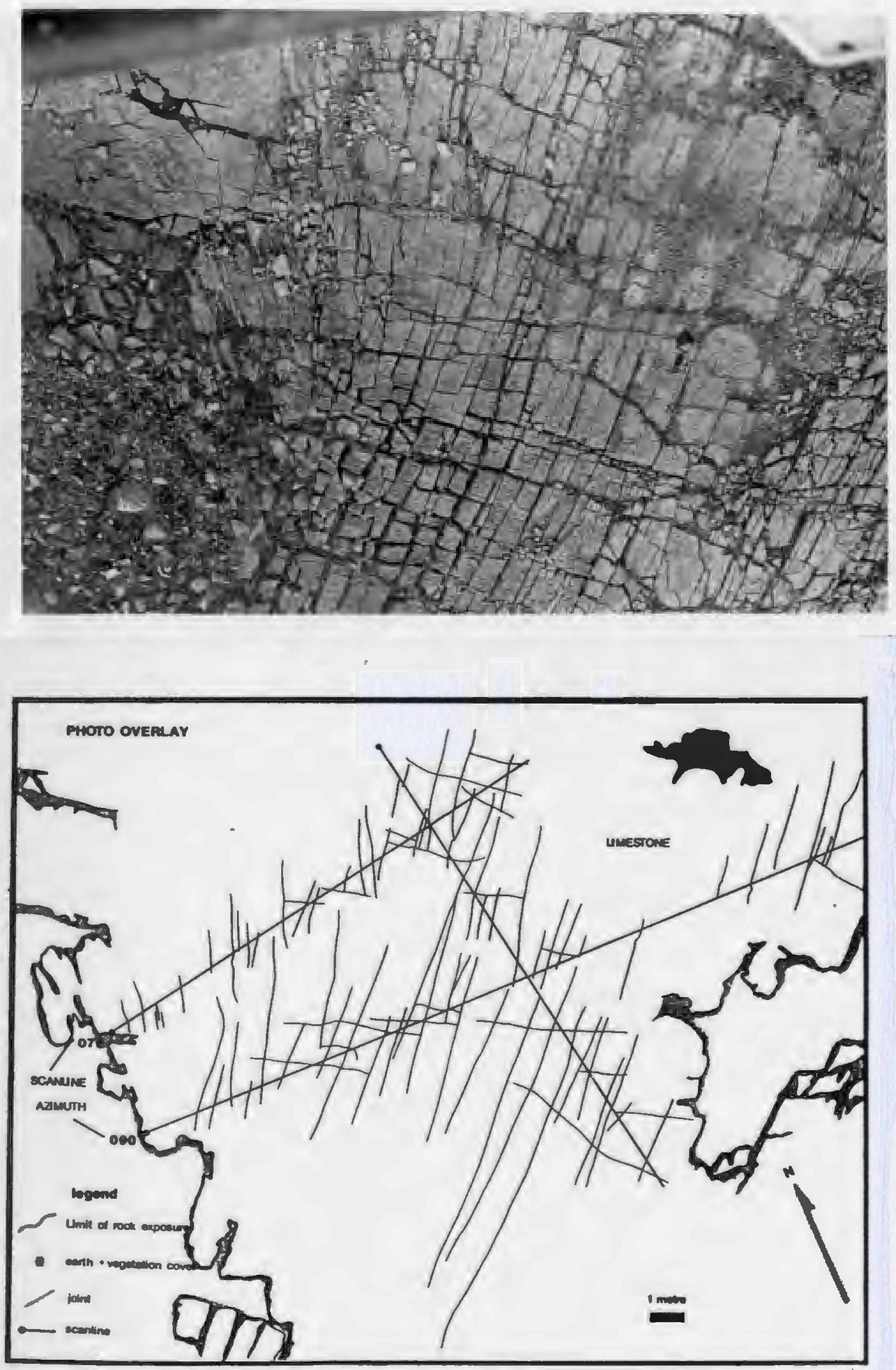

natural and were not induced by blasting. Joints induced by blasting are discontinuous, curved or botryoidal in nature.

This fracture mapping technique is affected by the following limitations. In the underground workings it was difficult to measure the entire joint length of long vertical joints, and only the portion exposed on the drift face (3 to 4 m high) was mapped. However, only a small number of the less abundant long joints were affected by this limitation. The Lead Lake outcrop is very extensive, and censoring of fractures due to outcrop limits only affected a small number of the peripheral joints and a few very long joints. The preferential sampling of joint sets perpendicular to certain rock face orientations is inherent in this procedure although an effort was made to minimize its effect by trying to map rock faces of different orientations.

2.5.2 Processing and manipulation of fracture data

Fracture data were entered into three separate files [Lead Lake (DNSHAR.DAT), Mine drifts (DNSHAR2.DAT), Open pits (DNSHAR3.DAT)] from field data sheets. Joints were segregated in this manner to facilitate comparison between areas and comparison of joints mapped with different censoring limitations. These files were combined to make a total data file of 923 joints. The complete "original" data files are given in Appendix F.

2.5.2.1 Fracture orientations

Initially, the poles to joint planes were plotted on lower hemisphere equal-area projections and contoured using the Schmidt

Method; a procedure used by Rouleau and Gale (1985a). The fracture data was processed and plotted using the STRDAT.FOR and STRPLO.FOR programs (Memorial University, 1987). Orientation plots (see Appendix G) using this method were made for comparison with similar plots produced using the SPHERE program (Diggle and Fisher, 1985). The complete fracture analysis is based on joint set orientations that were found using SPHERE, a contouring plotting program for data projected to a sphere.

The sequence of programs used in this next stage of fracture analysis is illustrated in Figure 2.6. Three programming environments were used: FORTRAN, SPSSX and the SAS system. A program DHLOOK.FOR (see Appendix H) was written by the author in order to extract orientation information from the original data files to be used by the SPHERE program. The final contoured orientation plot is accompanied by a screen output of relevant data, such as the mean or principal vector of each plot in the form of eigenvectors and direction cosines (see Appendix I).

The visual technique of delineating joint sets is similar to the method used by Rouleau and Gale (1985a). For each file the sets were defined and numbered sequentially, in order of their importance within each file. Sets that are from different files (areas) but have the same number are not interchangeable. For example, set 3 from the open pits does not have the same orientation as set 3 from the mine workings but both are the third dominant joint set in their respective files. When the sets were determined, their orientation limits (defined by drawing borders around contoured areas) were used to separate the original data file into smaller files using the modified program SETSLOOKWEND.FOR. This program assigns each fracture to a designated set if its orientation falls within the specified set range. The program outputs two files for the SPHERE program and for other trace length, spacing and orientation analysis programs. These programs are listed in Figure 2.6 as ORIENT.HIS, TRACE.HIS, SPACE.FOR, TRACE.SAS and CENSTERM.SAS.

2.5.2.2 Trace length and spacing analysis

The output file produced from SETSLOOKWEND.FOR was used to produce suitable input files for the trace length analysis programs. Frequency histograms for joint lengths were produced for each joint set by using the program TRACE.HIS. The TRACE.SAS program produced histograms segregated on the basis of censoring and termination mode. The program CENSTERM.SAS outputs univariant statistics for each level of censoring (0,1,2) only.

The SPACE.FOR program (Memorial University, unpubl.) calculated spacing between joints of the same set by processing the output files from the SETSLOOKWEND.FOR program. The SPACE.SAS program produced histograms and statistics for spacings in sets.

Spacing between joints was calculated using the distance approach method (Rouleau and Gale, 1985a) and formulae by Koch and Link (1971). This method defines spacing as the perpendicular distance between adjacent joints of similar strike. The main assumption of these calculations is that the joints of the

Figure 2.6 Sequence of programs used in the analysis of joint data from the Newfoundland Zinc Mine.

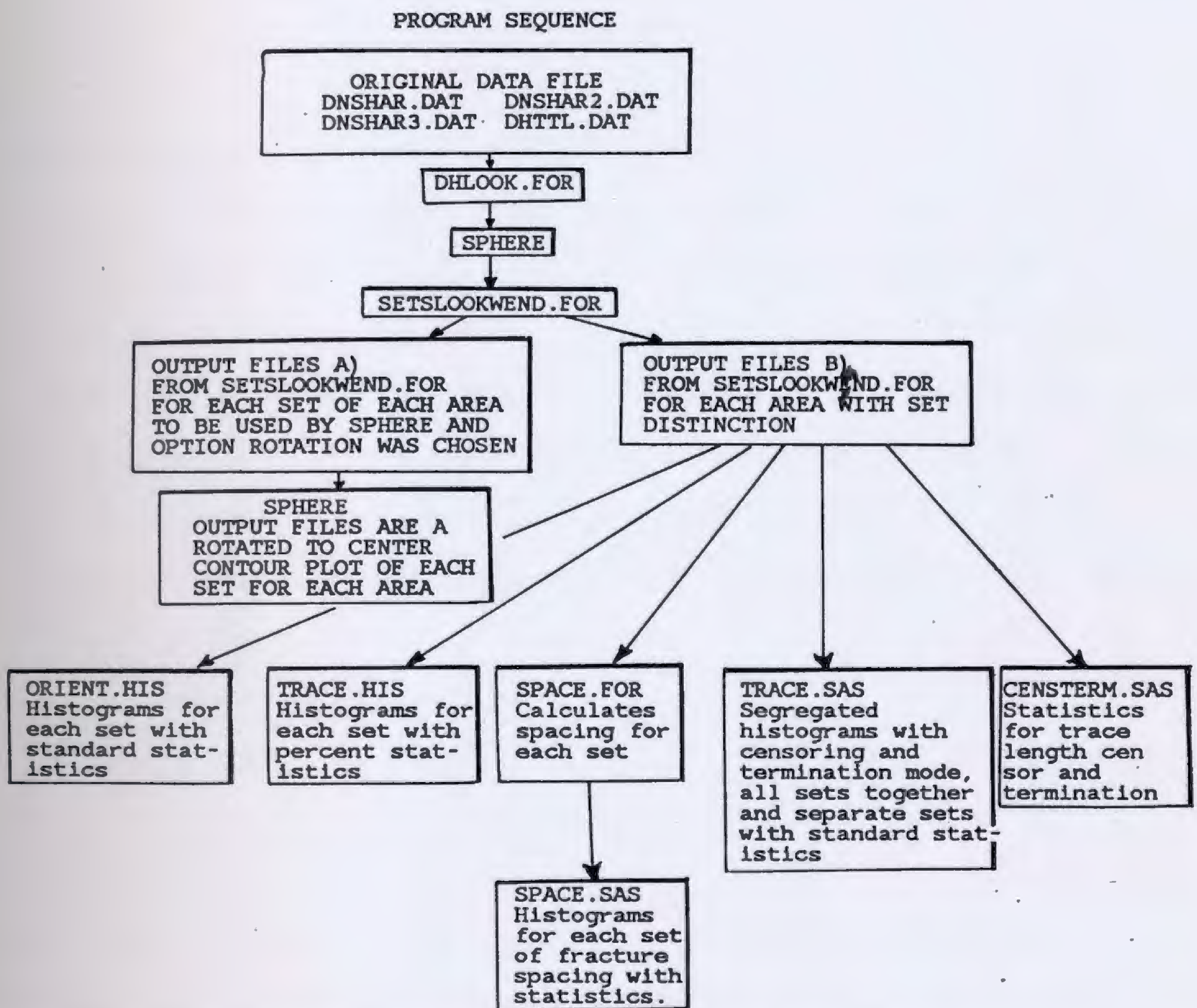

All SAS programs output two files: one that lists the desired data output with extension '.lis' and the other lists the sequence of commands that the program executed-errors can be checked in this file- with the extension '.log'.

same set are parallel to each other and equal to the orientation of the mean pole for the set. Thus, sets that are very well defined and have the least range of orientations have the best representative values for spacing. Further explanation of fracture analysis and manipulation is given in Appendix J.

2.6 Hydrogeological Measurements

Physical measurements outlined below were done in the 1986 summer field season. The study area has numerous exploration drill holes for water table measurements but problems arose during this field season due to unusually low water table conditions. Two of the shallow (10 to 15m) holes drilled in July became dry after 1/2 hour of pumping at a rate of 1 l/min. In late July, water levels in these holes fluctuated by over 50 cm.

2.6.1 Hydraulic head measurements

Water level measurements were done with a conventional 60 m water tape. A total of 83 water table levels were measured over a period of 11 days from July 26 to August 5. The "blocky" nature of the dolostone caused some older holes surveyed in 1985 to cave in and repeating measurements in these holes was impossible. In a few cases, a one metre steel rod was used to clear holes before the water tape was lowered into the hole.

Exploration drill holes that did not intersect ore zones were not cased or surveyed for elevations by mine staff. All unknown drill collar elevations and the Spring Lake level were surveyed relative to the common Teck Exploration Datum using a standard surveyors' level transit supplied by mine personnel. All relative elevations are +/- 5 cm. This arbitrary datum of 1000 ft has an absolute elevation of 343 ft (105 m) above mean sea level, as determined by altimeter. In 1987, this datum was checked by a transit survey carried out from the coast to the mine site and it was found that the datum is approximately 20 ft (6 m) below its true elevation (Bursey pers. comm., 1987).

Hydraulic head data were calculated by subtracting the casing (stick-up) from surveyed elevations and then subtracting the depth to water level from this measurement (ground surface), followed by correcting to mean sea level from the arbitrary datum. Components of the hydraulic gradients were calculated from pairs of adjacent hydraulic head measurements by dividing the difference in head by the distance between the open holes.

2.6.2 Pressure measurements

Pressure measurements were made on 19 drill holes, equipped with valves, using a 500 psi pressure gauge in the underground drifts (see Figure 2.7). All data was collected on July 31, 1986. Measurement error was estimated to be 5 to 10 psi.

Figure 2.7 Location map of pressure measurement sites in the mine underground workings.

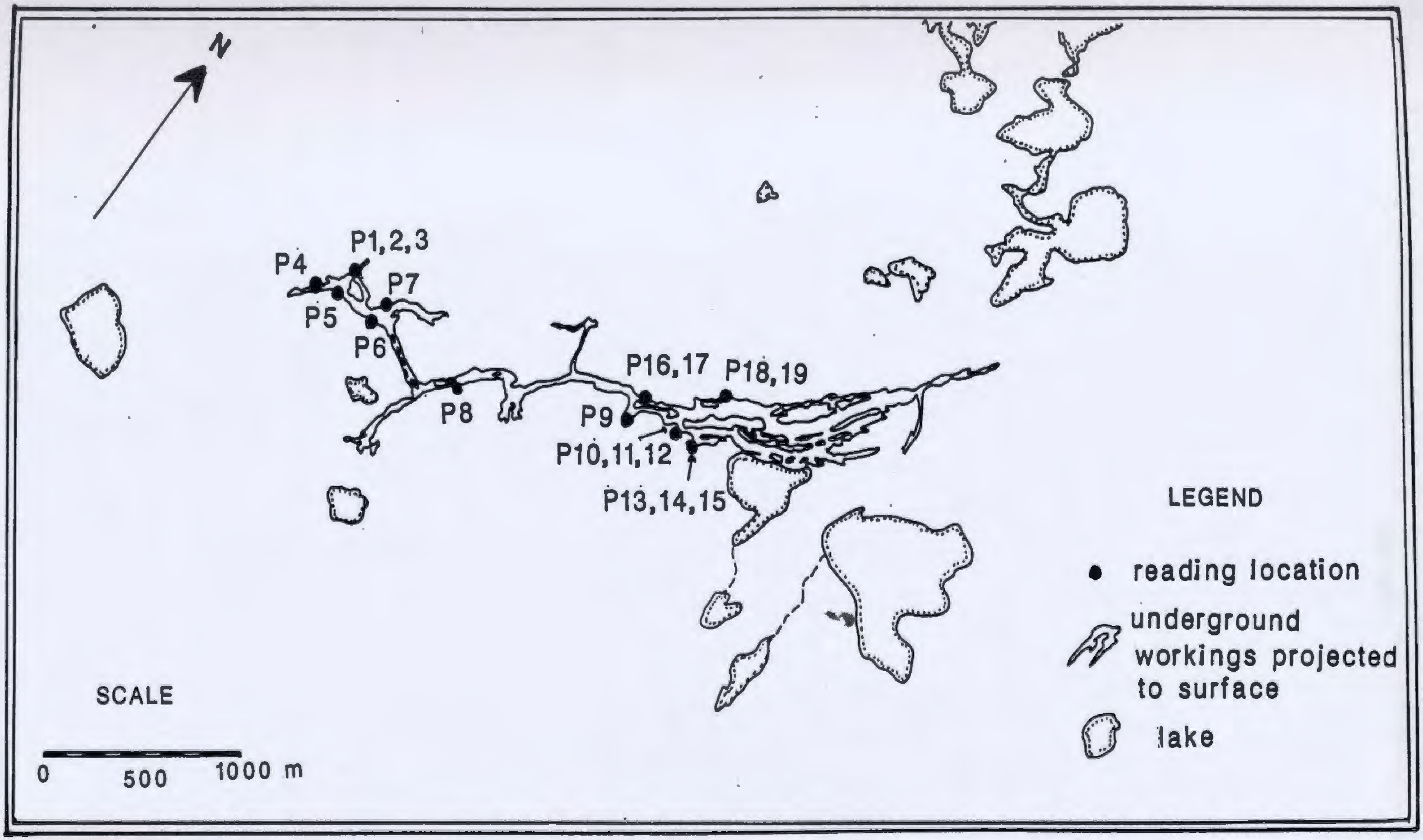
N
P1,2,3
P4
P5
P6
P7
P8
P9
P10,11,12
P13,14,15
P16,17
P18,19
LEGEND
reading location
underground workings projected to surface
lake
SCALE
0 500 1000 m

Chapter 3

GEOLOGY

3.1 General Geology

The rocks underlying the coastal plain in the study area are an autochthonous sequence of Cambro-Ordovician carbonate and clastic sediments of the Humber Zone (see Figure 3.1). These rocks lie unconformably upon the Precambrian basement which outcrops at the eastern boundary of the area as the Long Range Mountains. The basement is of Grenvillian age and largely consists of massive, slightly foliated, pink, fine- to coarse-grained granite and granite gneisses (Cawood & Williams, 1986; Knight, 1985).

The Cambro-Ordovician strata and Grenville basement are autochthonous rocks and are structurally overlain by the Humber Arm Allochthon via thrust faults (Knight, 1984) to the south of the study area. Block faulting of the Grenvillian basement marked the beginning of Humber Zone's geological evolution (Williams, 1979). From Early Cambrian to Early Ordovician times, carbonate deposition occurred over a stable marine platform with an east-dipping continental slope (Klappa et al., 1980).

The Cambro-Ordovician rocks consist of 4 groups (Figure 3.2). The Labrador Group (directly above basement rocks) is overlain in turn by the Port au Port Group, the St. George and the Table Head Group. The mine occurs in rocks of the St. George Group. The St. George group is divided into four formations: Watts Bight Formation, Boat Harbour Formation, Catoche Formation and Aguathuna Formation, see Figure 3.2 (Knight, 1984).

Figure 3.1. Regional geological map of the Daniel's Harbour study area compiled by T. Lane (in prep.). Only carbonate sediments are subdivided into major rock groups. The cross-section through the mine area assumes the carbonate sequence as well as basement rocks are transected by steeply dipping faults.

(Adapted from Lane, in prep.; Knight, 1985; Stenzel et al.[1], 1990)

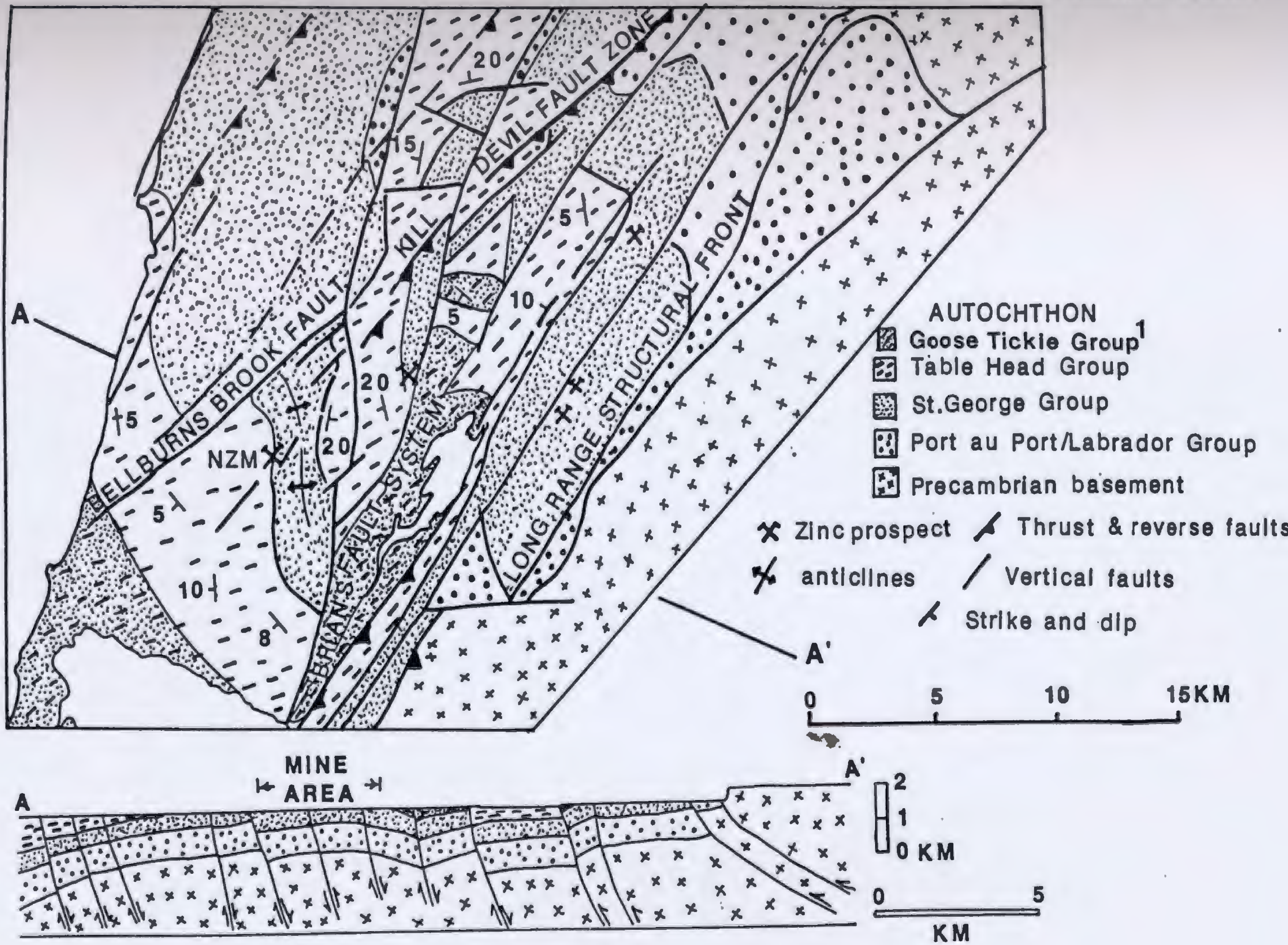

Figure 3.2. Autochthon and St. George Group stratigraphy. The Newfoundland Zinc Mine is situated in coarse dolostones of the Catoche Formation. These coarse dolostones are overlain by fine dolostones of the Aguathuna formation and underlain by limestones of the remainder of the Catoche Formation.

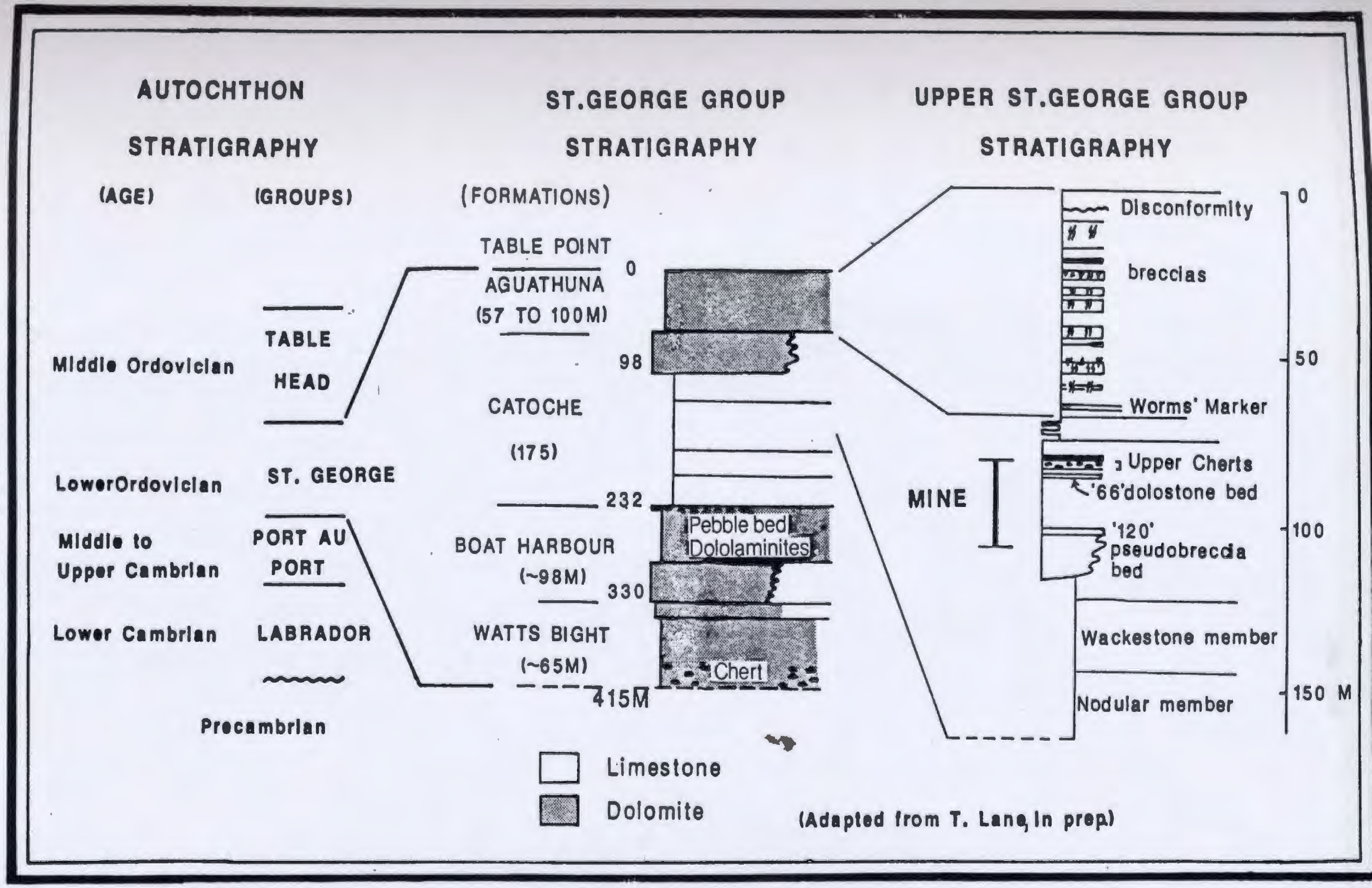

AUTOCHTHON STRATIGRAPHY
ST.GEORGE GROUP STRATIGRAPHY
UPPER ST.GEORGE GROUP STRATIGRAPHY
(AGE)
(GROUPS)
(FORMATIONS)
TABLE POINT
AGUATHUNA (57 TO 100M)
0
98
Middle Ordovician
TABLE HEAD
CATOCHE (175)
LowerOrdovician
ST. GEORGE
232
Middle to Upper Cambrian
PORT AU PORT
BOAT HARBOUR (~98M)
Pebble bed
Dololaminites
330
Lower Cambrian
LABRADOR
WATTS BIGHT (~65M)
Chert
415M
Precambrian
Disconformity
breccias
Worms' Marker
Upper Cherts
'66'dolostone bed
MINE
'120' pseudobrecdia bed
Wackestone member
Nodular member
0
50
100
150 M
Limestone
Dolomite
(Adapted from T. Lane, in prep.)

3.2 Regional Stratigraphy and Description of Rock Units

Of the autochthonous sequence, the Cambrian rocks are generally less fossiliferous and more silici-clastic than the overlying carbonate-rich St. George and Table Head Group rocks (Knight and James, 1987). The following description is restricted to formations of the St. George and Table Head groups pertinent to the study area.

The St. George Group consists of well-bedded cream to grey dolostones and grey limestones with widespread bio-turbation (Cawood and Williams, 1986). Porosity varies most in the dolomites; lower parts of the section may be silicified (Cawood and Williams, 1986) whereas higher up in the section they are vuggy (Upper Catoche Formation; Lane, in prep.). Dolomit-ization occurred in several stages and the last stage was marked by the occurrence of saddle dolomite which is found in the ore host rocks at the mine (Haywick and James, 1984). Periods of subaerial exposure are represented by sedimentary breccias, pebble and sand lags and irregular solution surfaces (Knight and James, 1987). The Table Head Group consists of fossiliferous limestones with local dolomitization and shale interbeds (Klappa et al., 1980). The contact between the St. George and Table Head Groups is at present cited as a regionally conformable contact but this contact is locally disconformable (Knight and James, 1987) at the Newfoundland Zinc Mine.

The thicknesses of the St. George Group formations at the mine site are given in Figure 3.2. Of greatest significance to this study are the Catoche and Aguathuna formations since they comprise most of the mine section.

The Catoche formation contains bedded, muddy, bioturbated, fossiliferous grey lime mudstones with algal-metazoan buildups (Ross and James, 1987; Knight, 1985). There are some diagenetic dolostones near the top of the formation (Knight and James, 1987). The dolostones of the Aguathuna contain minor limestone and shale (Knight and James, 1987). These dolostones vary in thickness laterally (Lane, in prep.). Bioturbation is extensive in the Aguathuna Formation at the mine site (Figure 3.2) and appears as mottling of the dolostones. A possible arid depositional environment and the formation of evaporites are suggested by the presence of chert with relict anhydrite (Ross and James, 1987).

The Table Point formation is the lower-most unit of the Table Head Group and is the only formation of this group that outcrops in the mine study area (Figure 3.3). It is a massive grey limestone with minor dolostone (Klappa et al., 1980). The Lead Lake outcrop (location of fracture mapping) is massive limestone with early selective dolomitization of abundant burrows and fossils (Haywick and James, 1984).

3.3 Local mine stratigraphy and rock units

The entire mine section comprises only the basal part of the Table Head Group and approximately the upper half of the St. George Group. The actual mining operations occur in the upper third of the Catoche formation (see Figure 3.2).

There is a further subdivision of the St. George and Table Head Groups' formations based on mine drill logs but it is not practical to map these sub-units at the scale of Figure 3.3 due to the abundant lateral facies changes within these units (Lane, pers. comm., 1987).

The Catoche formation can be subdivided into two units: the pseudobreccia unit and the lower limestone unit (see Figure 3.3). The Siliceous Dolomite and Dark Grey Dolomite units referred to in pump test data (Chapter 4) are subunits of the Aguathuna and Catoche formations, respectively (Knight and James, 1987).

The presence of gypsiferous pseudobreccia, gypsum in matrix breccias and in a large L-Zone vug (DDH 746; Coron, 1982), as well as the occurrence of chert with relict anhydrite in the Aguathuna formation, suggests the presence of evaporites in other parts of the carbonate sequence. Chert nodules found in various parts of the section (Figure 3.2) may have been pods of gypsum or anhydrite that have since been replaced by silica (Coron, 1982).

Matrix or collapse breccias (Figure 3.3) are referred to as pre-Middle Ordovician karst features (Crossley and Lane, 1984). The fine crystalline matrix of these bodies is relatively impermeable. Stylolites are pervasive in the mine section and are almost always lined with dolomite. They are probably contemporaneous with or earlier than the first stages of dolomitization in the limestone (Collins and Smith, 1975). Laboratory testing showed that stylolites reduce rock strength

Figure 3.3. Geological map of the Newfoundland Zinc Mine and immediate area. Underground workings have been projected to surface and open pit workings are also shown. (compiled by G. Bursey)

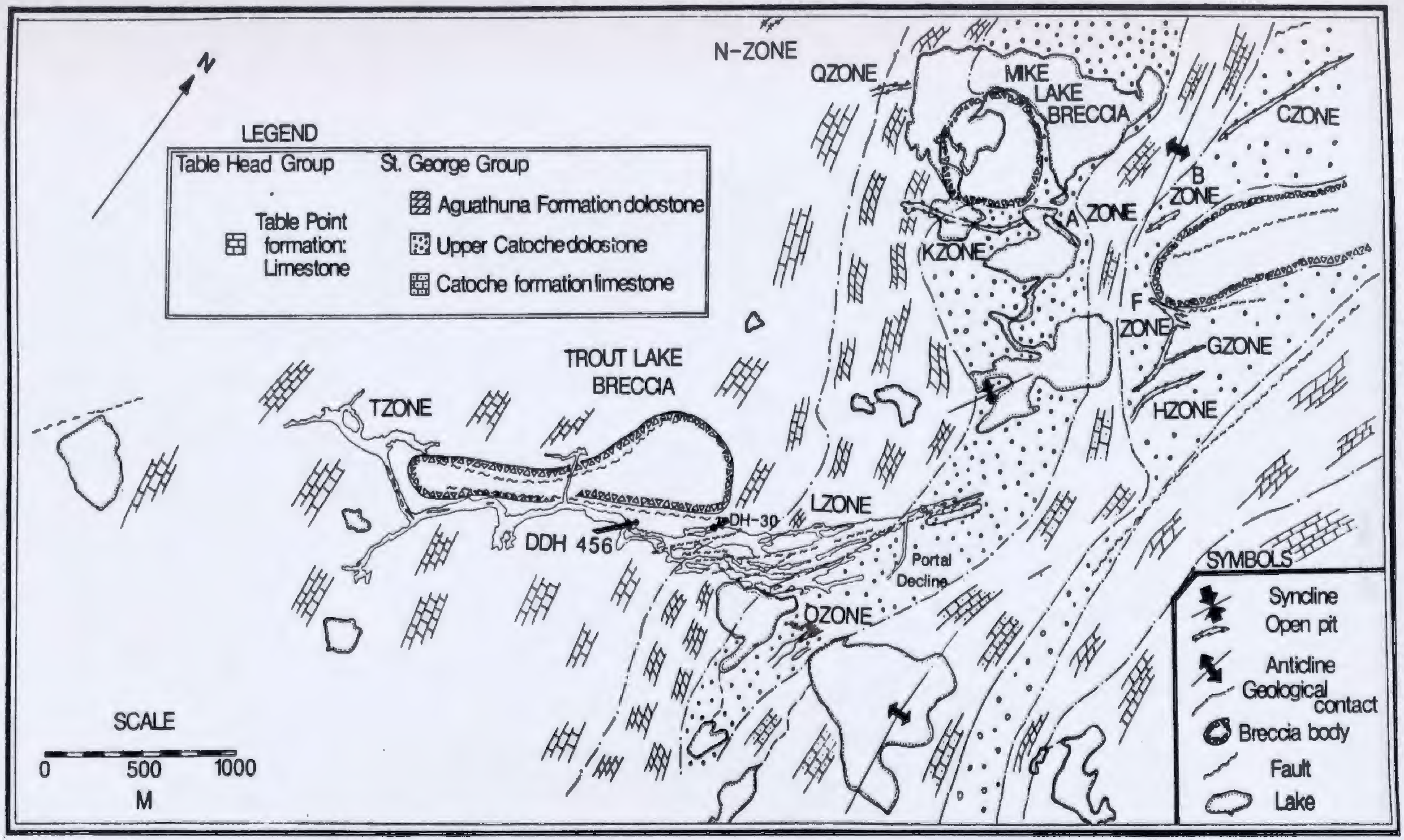
N
LEGEND
Table Head Group
Table Point formation: Limestone
St. George Group
Aguathuna Formation dolostone
Upper Catoche dolostone
Catoche formation limestone
N-ZONE
QZONE
MIKE LAKE BRECCIA
CZONE
B ZONE
A ZONE
KZONE
F ZONE
GZONE
HZONE
TROUT LAKE BRECCIA
TZONE
LZONE
DH-30
DDH 456
Portal Decline
OZONE
SCALE
0 500 1000
M
SYMBOLS
Syncline
Open pit
Anticline
Geological contact
Breccia body
Fault
Lake

and core logging showed that they decrease core recovery (Appendix M).

3.4 Description of ore and host rocks

The Newfoundland Zinc Mine is a Mississippi-Valley type deposit of the Tennessee variety (Dearin, 1976). Sphalerite was mined for its zinc in this essentially monomineralic orebody (James and Stevens, 1982). The mineralization is associated with paleokarst-derived collapse breccias and fracturing, (Lane, 1984; Collins & Smith, 1975), epigenetic veining and crystalline white saddle dolomite (Crossley & Lane, 1984; Haywick & James, 1984). The mineralization is confined to the pseudobreccia unit (Lane, 1984). Sphalerite is concentrated in long (500-4000 m), sinuous en échelon ore lenses or narrow (7-70 m) stratiform bodies bordered by faults and subparallel fracture zones (Coron, 1982). Zinc, lead and copper values decrease sharply with distance from ore (Sangster, 1968).

Sphalerite contains very few impurities of which iron (1.3%) and cadmium (0.18%) are the primary ones. Accessory minerals listed in order of abundance are galena, pyrite/marcasite, chalcopyrite-bornite, and native sulfur. Barite, gypsum and celestite crystals, considered to be late-stage mineralization (Crossley and Lane, 1984), have been found in vugs from the mine workings near DDH 456 (see Figure 3.3), and in vugs of the L-Zone near the Trout Lake Breccia associated with pyrite and chalcopyrite, respectively (Coron, 1982). Secondary hematite, limonite and smithsonite occur as supergene alteration products of the upper 6 m of mineralized bedrock (Coron,1982).

Bulk analysis of zinc ore and ore host rocks reveal the following trends: Co (7 ppm), Mo (7 ppm) and Ag (1 ppm) have minor ore association; Cd (675 ppm) is associated with Zn (>10,000 ppm); Pb and Cu are elevated in ore (70, 185 ppm) and in pyrite (44, 7 ppm) that is associated with ore (Lane, pers. comm., unpublished mine analyses).

Most of the ore zones in the mine area are aligned more or less parallel to the regional structural trend of 040 (K, Q and C-Zones; see Figure 3.3). The A-Zone is aligned to the second major trend found also in the Grenvillian basement which runs perpendicular to the 040 trend (Coron, 1982).

3.5 Surficial Geology

Quaternary deposits overlie the carbonate platform and were last deposited and reworked by glaciers probably during the late Wisconsinan Age. These glaciers originated at the dome of the Long Range Mountains and advanced westward 12,800 +/- 150 years B.P. (Proudfoot and St. Croix, 1987). The glaciers coalesced as they spread out on the carbonate platform and terminated at sea. The general direction of ice movement is indicated by striations of 270 ^{o} +/- 40 (Hornbrook et al., 1975). The marine limit at this time was about 145 metres above present sea level (Proudfoot and St. Croix, 1987). Regional thicknesses of overburden range from thin and patchy over the Long Range foothills to approximately 30 m along the coastal areas (Hornbrook et al., 1975). Some lakes underlain by St. George Group rocks have fine, white marl lake bottom sediment (Hornbrook et al., 1975). Field work in 1986 established that lakes 36, 53, 57 ,58, 64, 65, 71 (see Figure 2.1) have fine grey bottom sediment. Most of these lakes are found near the coast and they are all underlain by the St. George Group (Figure 3.1).

The mine area is covered by unconsolidated sediment forming a high-relief (75 m) dissected plain that is classified as an eroded moraine complex consisting of raised beaches, wave-modified hummocks and cobbly beach terraces (Proudfoot and St. Croix, 1987). This unit has been extensively reworked by wave action with the admixture of finer marine sediment. The surficial material is composed of carbonate detritus and granitic erratics, and thicknesses are highly variable. Depressions contain sand- and gravel-sized carbonate detritus of marine origin e.g., shell fragments (Hornbrook et al., 1975). Clay was only deposited near the coastline of the study area. Local thicknesses measured from drill logs vary between 0 and 8.5 m (Crossley, pers. comm.) and average 1.8 to 2.7 m of calcareous till (Hornbrook et al., 1975).

If the rock exposed in the open pits is neglected, outcrop is very poor due to the extensive glacial cover in the area. Suboutcroppings of sphalerite in the vicinity of the portal decline entrance and at the north shore of Zinc Lake (see Figure 3.3) weathered and produced elevated zinc levels in the soil

(Hornbrook, et al., 1975). These zinc anomalies led to the discovery of the mine.

3.6 Structural Geology

3.6.1 Regional structural geology

Mild deformation of the Humber Arm Autochthon over most of the study area resulted in the platform being transected by numerous north-northeast trending faults (both vertical and thrust) and minor folds. Cawood and Williams (1986) found that fold axes and late thrusts on the carbonate platform are subparallel. They inferred that the folding took place during the regional compression of the Allochthon and Autochthon, just before brittle fracturing and fault overthrusting of the Precambrian basement. The carbonate strata are gently dipping to the southwest. Near the contact with the Precambrian basement, strata can be more deformed and exhibit recumbent folds and recrystallization/silicification of dolomite and calcite (Knight, 1985). Based on a compilation of all previous work (see Figure 3.1), the fault contact forming the eastern border of the study area is a vertical fault (Lane, in prep.). Structural deformation of this part of the Northern Peninsula probably was manifested as numerous near-vertical faults rather than one dominant thrust which is common to the south and north of the study region (Grenier R., pers. comm., 1988).

As can be seen from the regional geological map (Figure 3.1) long, curvilinear, steep reverse faults dominate the structure in the area (Knight, 1985). They form a series of subparallel faults, trending 20 to 60 ^{o} east (Lane, 1984). The cross-section in Figure 3.1 shows these faults have a general dip-slip component displacing units upwards to a maximum of 1500 m (Lane, 1984).

It has been suggested that the shape (parallel to the Grenvillian basement) and structures of the carbonate platform reflect older structures in the Grenvillian Structural Province (Williams, 1979; Coron, 1982). The most prominent set of joints in both the Long Range gneisses and the carbonate strata trends 040 degrees. The northeast trend of the Long Range inlier itself is coincident with the general northeast trend of the faults and joints of the area. Minor east-west trending faults are found in the Grenvillian basement and in the carbonate platform.

3.6.2 Local structural geology

The local structure of the mine area (see Figure 3.3) is dominated by the gentle folding of the shallow dipping (5^{o} SW) northeasterly striking carbonate strata (Coron, 1982). The anticlinal fold axis trends in the north-northeasterly direction (from Spring to Mike Lake, Figure 3.3). Its west limb dips approximately 7 degrees to the west and the other limb gently dips approximately 10 degrees eastward. The east-west trending fault in the L-Zone area is interpreted as a second generation of faulting related to the major north-east trending faults (east of map area, Figure 3.3), (Coron, 1982). The northeast-southwest trending faults in the area have associated fracture zones that are mineralized with sphalerite and these fractures have a 040 o trend. Most authors (Knight, 1977; Cumming, 1968; Coron, 1982; Lane, 1984; Crossley & Lane, 1984) agree that structural influences controlling ore deposition were limited to fracturing and faulting of the carbonate strata. All folding is post-ore and there are post-ore faults that displace ore lenses in some areas (Coron, 1982).

3.6.3 Fracture analysis

The fracture survey was designed to investigate the suggestion (Acres, 1974a) that drawdown anisotropy in the fractured rock mass was caused by two major joint sets that are nearly vertical. Details on fracture mapping techniques and data manipulation are summarized in Section 2.5.

3.6.3.1 Fracture orientation

Figure 3.4A is a plot of all poles to fracture planes mapped at the mine area using the SPHERE program. Poles were contoured according to estimated density function values introduced by Fisher et al. (pg. 41, 1987). High density of poles have high function values and low density areas have lower function values. Pole diagrams of fractures from vertical mine drift faces and open pit walls show a significant concentration of near horizontal bedding planes and joints (see Figures 3.4C, D).

Four fracture sets for the total survey (combining all fracture sites) are defined based on a visual inspection of

Figure 3.4A) Pole diagram for the entire fracture survey measured in underground drifts, open pits and Lead Lake outcrop. Four sets can be defined by the pole clustering. Seven equally spaced contours based on miniumum and maximum function values 0 and 2.572 respectively. Contour heights are as follows: 0.184, 0.551, 0.918, 1.286, 1.853, 2.021, 2.388.

B) Pole diagram for fractures mapped from the Lead Lake outcrop only. Six contours are equally spaced by function value: Min. function value of 0 and Max. of 2.798. Contour heights are as follows: 0.233, 0.700, 1.166, 1.632, 2.099, 2.565. The black dots represent scanline orientations. Fracture sets are numbered according to their importance within each site and are not interchangeable between sites.

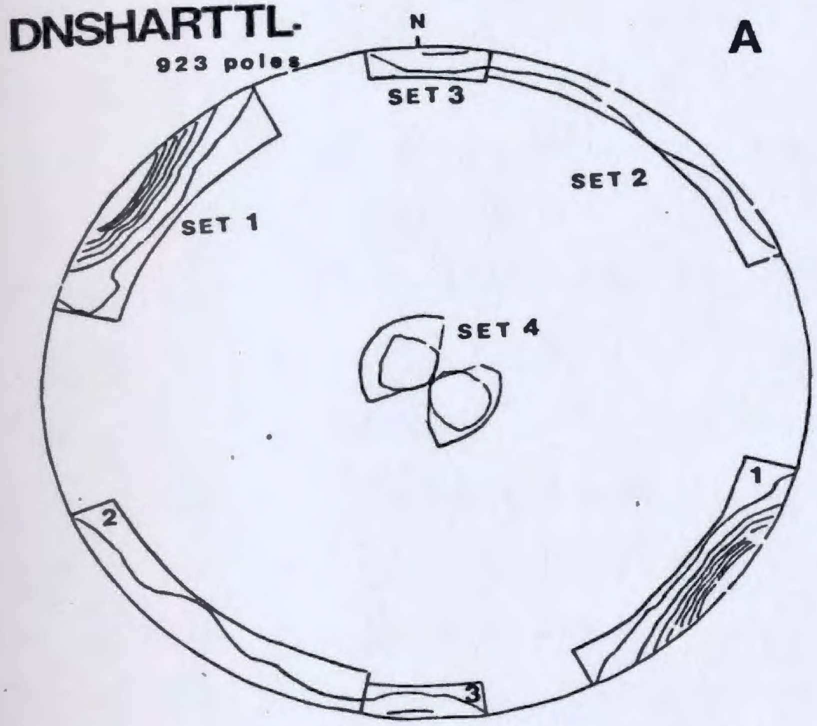
DNSHARTTL.
923 poles
N
A
SET 3
SET 2
SET 1
SET 4
1
2
3

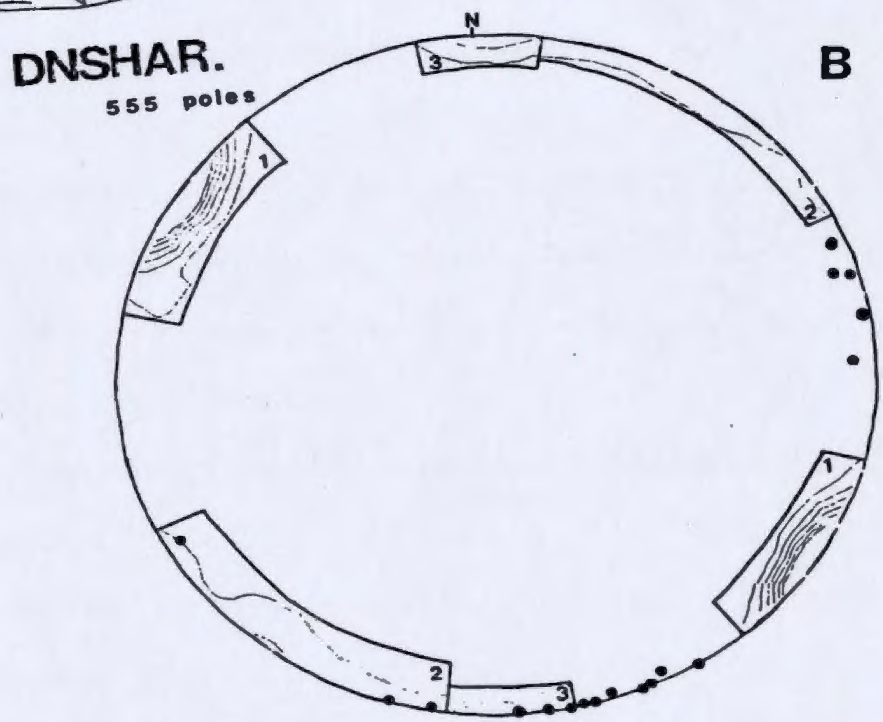
N
DNSHAR.
555 poles
B
3
1
2
1
2
3

contour line density (Figure 3.4A). Eighty-eight % of all fractures fall within the boundaries of the specified 4 sets. Seventy-seven % of the total fractures (joints) mapped are included in the two well defined major Sets #1 and #2, and 11 % of the fractures make up the somewhat weaker Sets #3 and #4. Set #1 is a steeply dipping set of joints with a north-east trend. Set #2 has a wider range of dip direction orientations and is also a steeply dipping joint set but with a north-westerly trend. A smaller third joint set is found only at Lead Lake and is steeply dipping with an east-west strike. Set #3 is separated from Set #2 on the basis of a second contour line that is only developed within the boundaries drawn for Set #3 (Figures 3.4A). A lower hemisphere equal-area projection of the same data using the STRPLO program (contouring according to density per unit area of projection) shows similar pole clusters (see Appendix G) which confirm the existing set boundaries. The shallow dipping bedding planes of Set #4 are not large in number but significant in their water conducting potential. Since they are sub-horizontal there is a very large range in strike direction.

In addition, fracture sets have been determined for each individual mapping site indicated on Figure 2.4. Fracture set orientations are given in Table 3.1. Fracture sets are numbered sequentially, according to the procedure outlined in Section 2.5.2.1, in descending order of their importance at each individual mapping site, not according to their significance within the entire fracture survey. For example, the third most

Figure 3.4C) Pole diagram of fractures measured in the underground drift workings. Five equally spaced contours based on minimum and maximumum function values of 0 and 1.463 respectively. Contour heights are as follows: 0.147, 0.439, 0.732, 1.024, 1.317. Black dots represent scanline orientations.

D) Pole diagram of fractures measured in the open pits. Five equally spaced contours based on minimum and maximum function values of 0 and 1.856 respectively. Contour heights are as follows: 0.186, 0.557, 0.927, 1.299, 1.670. Black dots represent scanline orietations.

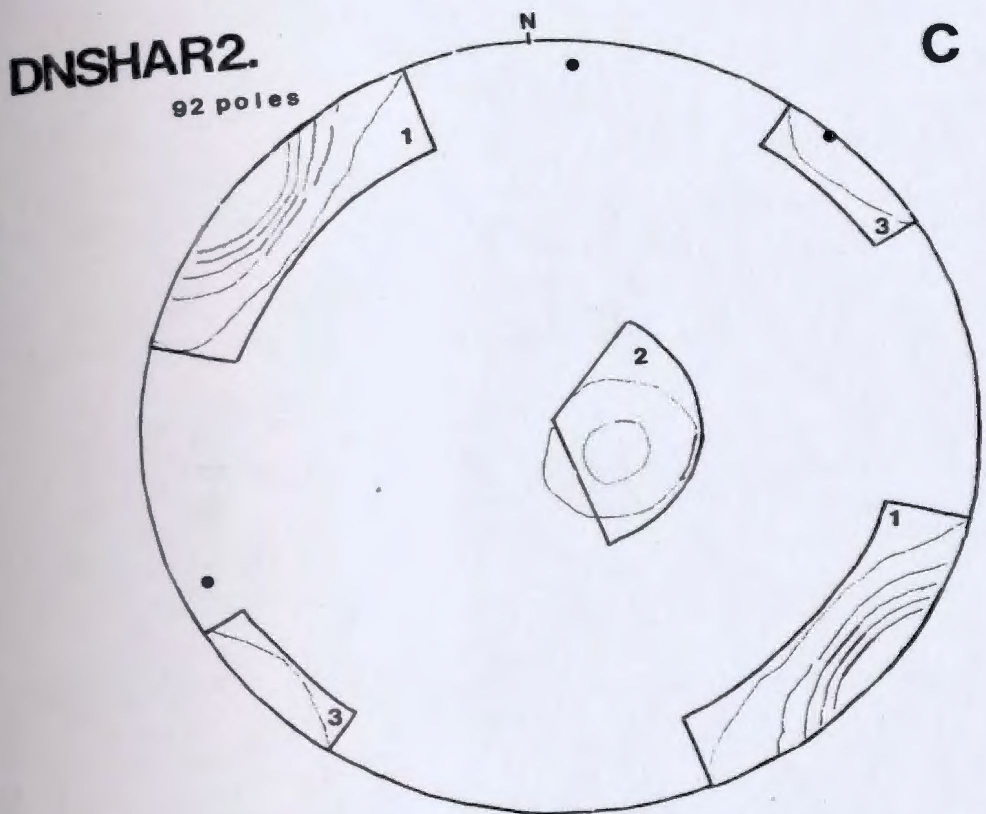
DNSHAR2.
92 poles
N
C
1
2
3
1
3

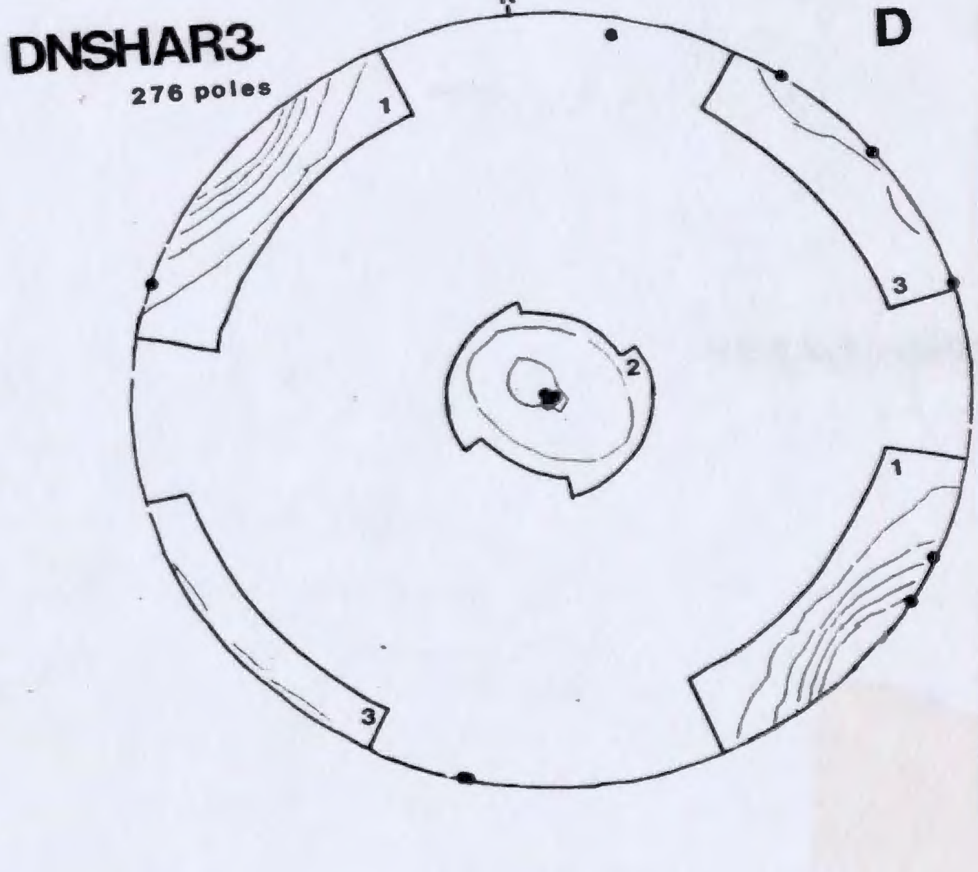
N
DNSHAR3
276 poles
D
1
3
2
1
3

Table 3.1 Orientation (dip direction and dip) limits of fracture sets defined by contoured fracture data for entire mapping survey and for individual mapping areas.

original data file

DNSHARTTL.DAT — 923 Poles to Planes (Total Fracture Set)

	#	DIP	DIP DIRECTION
SET 1		75-90	286-336
	581	72-90	107-146
SET 2		81-90	191-249
	132	75-90	011-069
SET 3		80-90	173-192
		79-90	353-359
	54		0-012
SET 4		0 -15	258-351
	44	0 -15	082-176

DNSHAR.DAT — 555 Poles to Planes (Lead Lake Outcrop)

	#	DIP	DIP DIRECTION
SET 1		75-90	285-322
	355	72-90	108-143
SET 2		81-90	191-247
	100	73-90	011-065
SET 3		80-90	352-359
			000-011
	52	80-90	172-192

DNSHAR2.DAT — 92 Poles to Planes (Mine Drift Workings)

	#	DIP	DIP DIRECTION
SET 1		79-90	289-342
	58	77-90	108-163
SET 2	12	0-25	233-343
SET 3		77-90	207-242
	7	78-90	037-062

DNSHAR3.DAT — 276 Poles to Planes (Open Pits)

	#	DIP	DIP DIRECTION
SET 1		68-90	285-341
	176	70-90	105-161
SET 2		0-20	242-353
	37	0-21	062-173
SET 3		71-90	212-260
	32	78-90	031-080

dominant set mapped in the underground drift workings (Set #3 in Figure 3.4C) does not correspond to the third most dominant set for the total fracture survey (Set #3 Figure 3.4A).

The stereograms/pole diagrams for each individual mapping area (Figures 3.4 C, D) indicate that there is areal variability in the dips of the bedding planes which can be related to the anticlinal structure in the area (see Figure 3.3). An orientation plot for the drift workings (Figure 3.4 C) shows a set of bedding planes dipping generally to the west. This is logical since the drifts are on the western limb of the anticline (Figure 2.4). Figure 3.4D represents fractures mapped on vertical surfaces in the open pits and shows east and west dip directions for the shallowly dipping bedding planes. This is because the open pits are located on both limbs of the anticline.

Well defined Joint Sets #1 and #2 of the whole fracture survey (Figure 3.4A) can be related to this anticline and the major northeasterly faults in the mining area (see Figure 3.3). Stresses that would produce an anticline with a north trending axis and faults of approximately 240 ° strike (NE-SW trend) would have a maximum principal stress in the east-west direction (Price, 1966). This is confirmed by the trend of regional compression causing the westward thrusting of the basement rocks onto the platform (see Section 3.1.1). Some bedding planes may have been important planes of slippage (Spencer, 1977) at the time of folding and thrusting of these layered rocks, which caused enlargement along the bedding plane.

Minor joint Set #3 of the total fracture survey (Figure 3.4A), is perpendicular to the fold axis and may have formed under tensional stress, although there is no direct field evidence for this, because fracture surfaces were very weathered. Set #3 is found only at the mapping site nearest the anticlinal crest, which may suggest more intense weathering of the greater joint density found near the crest of an anticline. Joint Set #3 may also be a secondary set related to the small synclinal structure (with north-east trending axis) located at the south end of Lead Lake (Figure 3.3). Joint Sets #1 and #2 of the total fracture survey may be shear joints developed in response to the east-west maximum principal stress (Price, 1966).

Frequency histograms of orientation data (see Figure 3.5), with statistics assuming a normal distribution (see Table 3.2), were produced for each set of the total fracture survey by using the dip direction limits listed in Table 3.1. For each mapping site an additional set of statistics for their respective sets is given in Appendix K. By plotting the fracture orientations in this manner, previous set divisions are reinforced by the peaked distributions found for each set, substantiating these fracture sets that were defined solely on the basis of orientation.

The majority of dip angles between 75 and 90 $^{\circ}$ for Sets #1, #2, and #3 indicate most fractures measured in the mine area are steeply dipping. Low dip angles of 0 to 20 $^{\circ}$ in Set #4 are expected for near horizontal bedding planes. A wide distribution of dip directions in Set #4 is typical when measuring dip directions of shallowly dipping planes and may not be representative of the true dip direction distribution.

The mean vector for each set of the total fracture survey (see Section 2.5.2.1) was determined by the set rotation option in the SPHERE program. Analysis of the set rotation results is given in Appendix I. The mean vectors or average pole orientations are listed in Table 3.3. The average pole orientations for Sets #1 and #2 are the same as mean poles

Figure 3.5 Frequency histograms of orientation data for each of the fracture sets determined from the total fracture survey. For the purpose of displaying orientations on an histogram with a scale from 0 to 180°, data was manipulated as follows: 180° was subtracted from dip direction greater than 180° and their dip was subtacted from 180 also. Dips > 90° were calculated for fractures with dip directions > 180°. This was done for all sets except Set 3, for which dip directions are north-south.

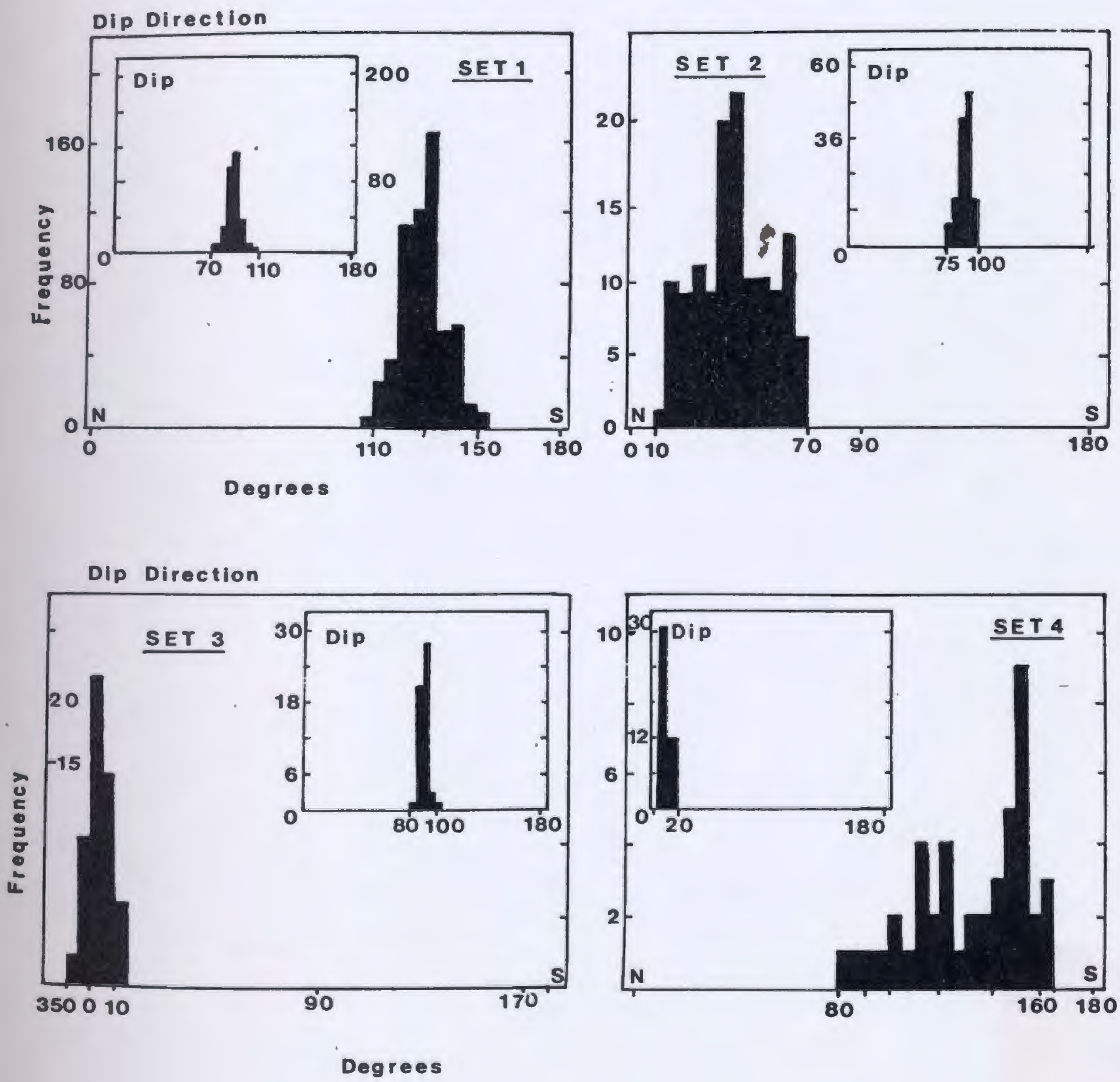

Table 3.2 Orientation data basic statistics for the four fracture sets defined for the entire fracture survey. Negative minimum for Set #3 refers to dip directions to the west of north or 360.

DNSHARTTL.DAT

Dip Direction	Set #1	Set #2	Set #3	Set #4
Mean (°)	129	41	3	132
S.D.	8	14	5	22
Min.	108	13	-6	84
Max.	156	68	12	163
No. of fractures	581	132	56	44

Dip	Set #1	Set #2	Set #3	Set #4
Mean (°)	89	88	90	9
S.D.	5	5	3	3
Min.	73	75	80	5
Max.	105	99	100	15
No. of fractures	581	132	54	44

Table 3.3 Average pole orientation for each set as determined from the SPHERE program.

	Plunge Azimuth	Plunge	Strike (of plane)	Dip	Dip Direction
Set #1	308.9	0.6	039	89	129
Set #2	220.6	1.7	310	88	041
Set #3	3.2	0.1	093	90	183
Set #4	108.3	89.2	198	01	288

determined by histogram statistics listed in Table 3.2. The discrepancies between Table 3.2 and Table 3.3 for Sets #3 and #4 can be explained by the specifics of the histogram program (subtract 180° from dip direction; see explanation in caption of Figure 3.5) and the poorly defined distribution for dip directions, respectively.

3.6.3.2 Fracture trace length

Trace length histograms for each fracture set are shown in Figure 3.6 (sorted in terms of censoring) and 3.7 (sorted in terms of termination mode). Basic statistics for the trace length analysis of the entire fracture survey are given for its 4 sets in Table 3.4. Trace length statistics for individual areas are given in Appendix K.

The distributions illustrated in the trace length histograms are skewed to the right. This positive skewness may be partially due to the 0.50 m cut-off for the trace length survey. Without a more detailed statistical analysis (ie. corrections for censoring and termination mode) of the trace length data it is difficult to compare mean lengths and determine an exact mean trace length for each set. Set #1 has some of the longest fractures, but Set #4 has consistently the longest fracture lengths of any set. Most of the fractures measured have some degree of censoring (cens = 1 or 2). Trace length histograms sorted on the basis of termination mode (see Figure 3.7) show that most of the fractures have both ends free (term. mode = 0). The two major sets may be from the same period of deformation since they very seldom terminate with each other (censoring 1 and 2).

Some fractures of Sets #2 and #3 have a splayed termination style. Although the average fracture length has not been corrected for censoring and termination mode, there does appear to be a significant difference in length between sets.

The fracture data give very little information on the

Figure 3.6 Trace length histograms for each major fracture set sorted in terms of censoring style. See appendix E for censoring code explanation.

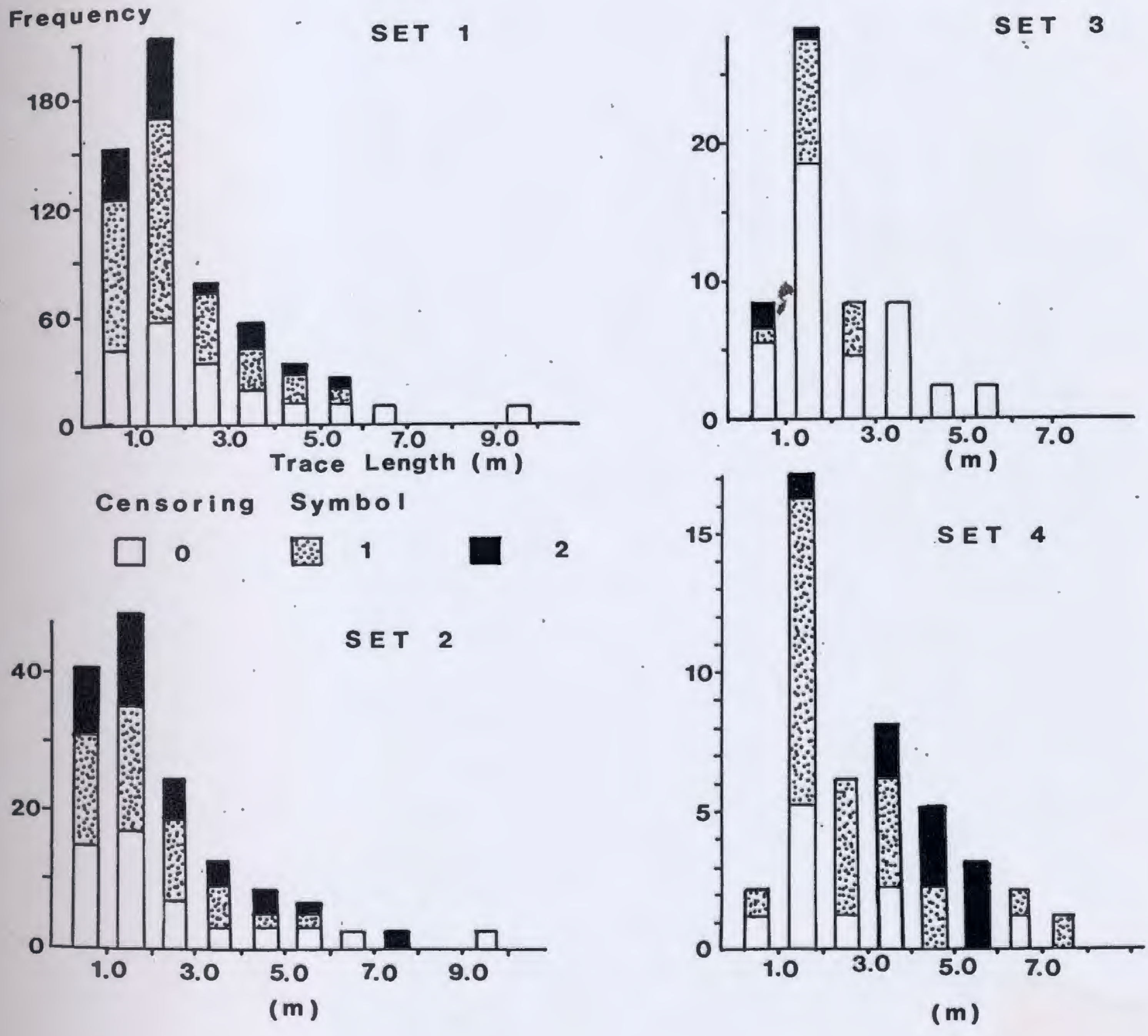

Figure 3.7 Trace length histograms for each major fracture set sorted according to termination mode. See Appendix E for coding explanation.

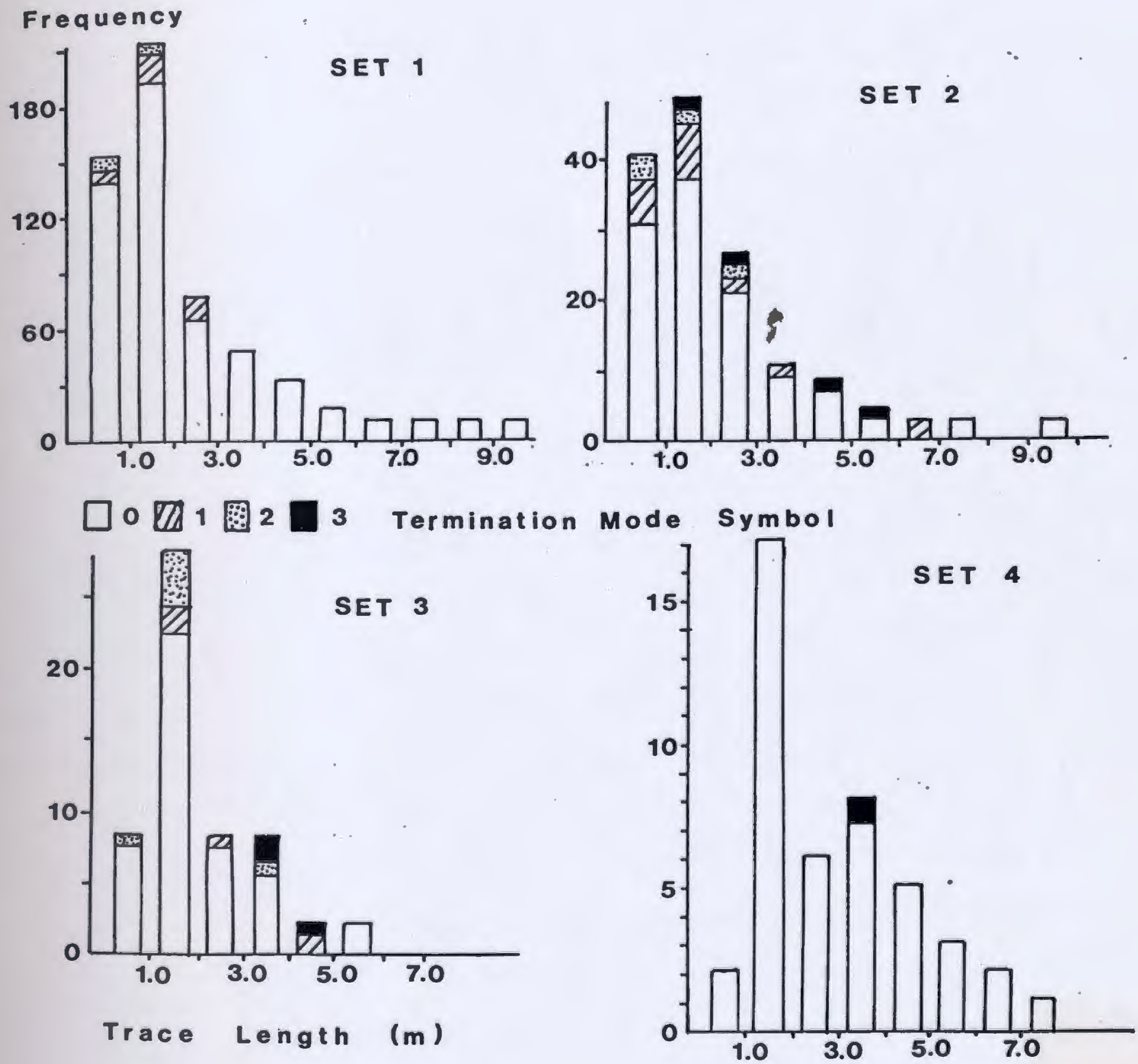

Table 3.4 Basic statistics for trace length histograms shown in Figure 3.6.

DNSHARTTL.DAT

	Set #1			Set #2		
Censoring	0	1	2	0	1	2
Mean (m)	2.93	2.20	2.30	1.58	1.97	2.11
S. D. (m)	3.04	2.28	2.09	1.36	1.56	1.73
Min. (m)	0.50	0.50	0.50	0.50	0.50	0.50
Max. (m)	16.30	15.30	10.00	6.70	9.80	7.40
No.	166	294	121	38	54	40

	Set #3			Set #4		
Censoring	0	1	2	0	1	2
Mean (m)	2.14	1.64	1.07	2.27	2.61	3.99
S. D. (m)	1.39	0.64	0.74	1.85	1.67	1.25
Min. (m)	0.60	0.60	0.50	0.70	0.90	1.40
Max. (m)	5.70	2.90	1.90	6.80	7.40	5.20
No.	39	14	3	10	25	9

relative ages of the major and minor fracture sets, because only one fracture was observed to offset another (no. 32 Appendix F). This northeasterly trending joint offsets an older northwesterly trending joint. In the underground drifts joints 478, 479 and 480 were observed to terminate at bedding planes indicating the obvious younger relationship of joints to bedding planes. A number of northeasterly trending joints belonging to Set #1, with an average pole orientation of 306/89 (NE trending), are very thin (<2mm) and are partially or completely filled with weathered, black dolomite. This type of infilling in the Lead Lake outcrop, where most joints dominantly open, may suggest that Set #1 includes joints from more than one generation. Small fracture zones of similar pole orientation (310/87) or NE-trending joint planes were also observed in the Lead Lake outcrop.

Other observations from the original data sheets (see Appendix F) show that small pits on the surface of the Lead Lake outcrop are aligned along the regional northeast (Set #1) and northwest (Set #2) trends. This indicates structural control of limestone dissolution typical in other karst regions such as the Ocala limestone of Georgia (Brook and Allison, 1983).

3.6.3.3 Fracture spacing

Spacing histograms for each set of the total fracture survey are shown in Figure 3.8 and statistics are given in Table 3.5. Spacing statistics for individual areas are given in Appendix K. Analyzing fracture maps for the calculation of fracture spacing is affected by many sources of error (Rouleau & Gale, 1985a), as indicated by the large standard deviations for the mean spacing (see Table 3.5). These data are only apparent spacings and not true spacing values because of the truncation error in this survey. An analysis was undertaken anyway, so an estimate of spacing between major sets could be determined, since there were no data available from orientated boreholes to provide better spacing values (Rouleau & Gale, 1985b).

The histograms for the 4 sets do not have the shape of a theoretical normal distribution but they are positively skewed (to the right), similar to spacing histograms at Stripa, Sweden (Rouleau and Gale, 1985b). These empirical distributions

Figure 3.8 Fracture spacing histograms for each set of the total fractures mapped. Basic statistics to accompany histograms are listed in Table 3.5.

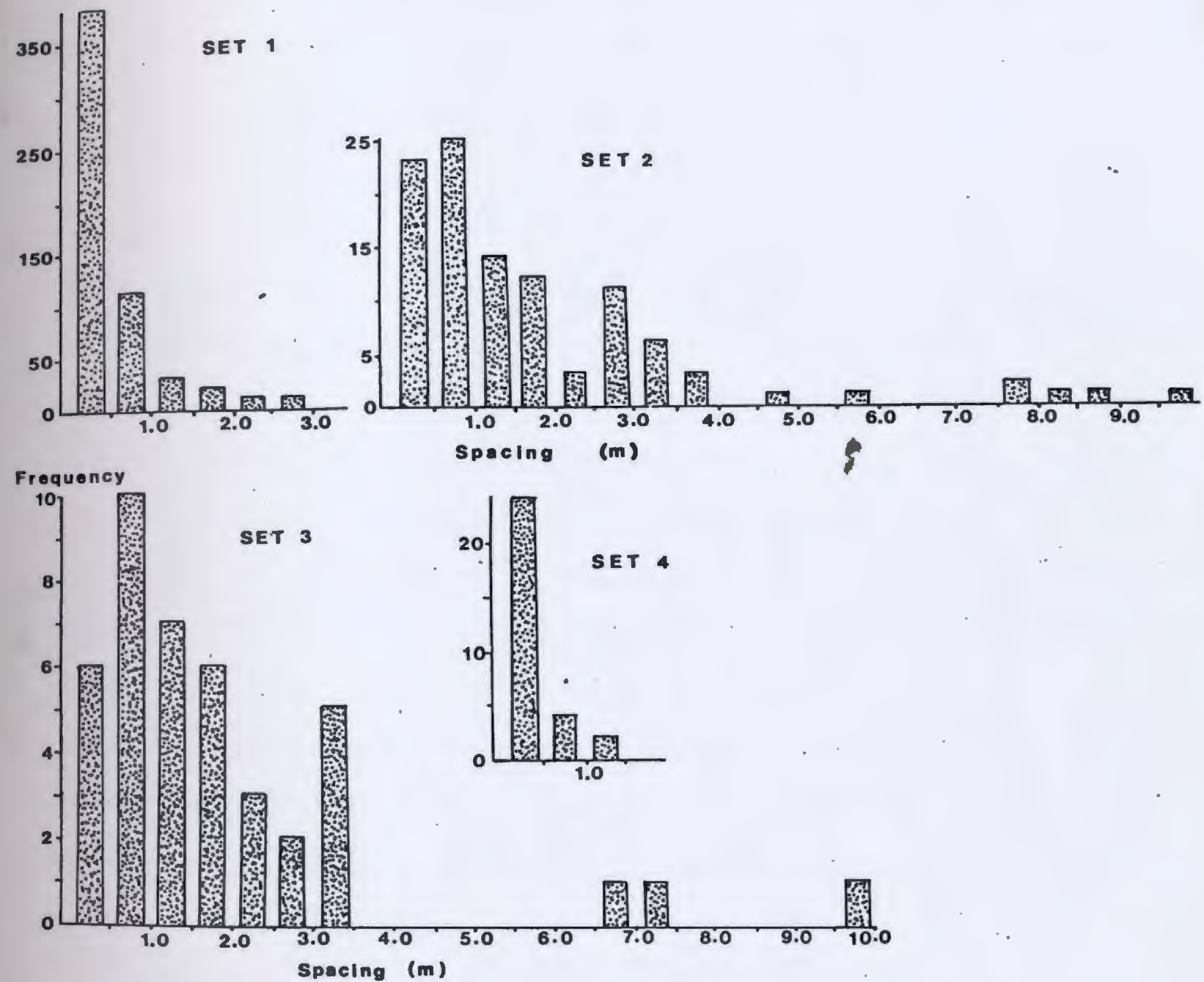

Table 3.5 Basic statistics for the calculated spacing between fractures of the same set for the entire fracture survey (DNSHARTTL.DAT).

	Set 1	Set 2	Set 3	Set 4
Mean (m)	0.55	1.75	2.01	0.32
S. D. (m)	0.90	1.88	2.31	0.30
Min. (m)	0.01	0.00	0.15	0.03
Max. (m)	11.86	9.56	13.02	1.27
No.	551	105	42	30

approximate the exponential model.

Generally, joints belonging to Set #1 are closely spaced (0.55 m), those in Set #2 are more widely spaced (average 1.75 m), and those in Set #3 are even more widely spaced. Bedding planes (Set #4) are an average 32 cm apart.

3.7 Summary

Geological components covered in this chapter will be used to construct the conceptual flow model of the mine and region. Significant geological information for the mine area and region can be summarized by Figures 3.3 and 3.1, respectively.

The layered carbonate terrain, consisting of a succession of limestone and dolostone beds that dip south-westerly, is underlain by a Precambrian basement of lower permeability. This relatively low relief platform is bordered to the east by the Long Range Mountains. In the past, subaerial exposure and ancient karstification may have caused selective dissolution of carbonates and the precipitation of gypsum, barite and anhydrite, as well as the formation of collapse breccias. These ancient geological formations suggest karstification was very important in localizing ore and is important in the development of secondary porosity of these carbonate rocks.

Quaternary deposits cover most of the area but vary greatly in thickness, both locally and regionally. Reworked by wave action during the marine inundation over 12,000 years ago, they contain abundant carbonate detritus and lack clay-sized material, except in coastal areas. Recharge through these deposits is considered to be extensive due to predominance of sorted till and coarse-grained sediment. Less infiltration is anticipated in the small areas covered by fine, lake bottom marl sediment and clay.

The northeast regional structural trend caused by regional compression and thrusting of the layered carbonate rocks is predominantly manifested by faults regionally and joints locally. Present-day dissolution may have originated along stylolites and bedding planes that have undergone slippage during regional deformation, as well as along joints in the local anticlinal axis.

The rocks of the Newfoundland Zinc Mine are transected by two major steeply dipping joint sets and shallowly dipping bedding planes. Joint Set #1 is presumed to be the most important water-conducting feature, next to the more horizontally extensive bedding planes, due to their frequency, close spacing and relatively long length. The mean fracture plane orientation for important fracture sets are:

Joint Set #1	039/89	
Joint Set #2	310/88	
Bedding plane Set #4	198/01	(sub-horizontal)

Joint Set #1, determined by local fracture mapping, is also coincident with the most prominent regional joint set of 040 degrees. The bedding planes are visibly influenced by the anticline in the area, and the joint sets may have been produced by the same stress field that caused the formation of this anticline.

Chapter 4

PHYSICAL HYDROGEOLOGY

4.1 General Hydrogeology

A physical hydrogeological framework for the mine and the regional groundwater flow regime is constructed by using air photographs, mine pumping and precipitation records, water table elevations and previous hydrogeological studies.

4.1.1 Karst landforms and surface hydrology

Lineaments visible on aerial photographs (Lattman, 1958) represent zones of high fracture concentration and may correspond to subterranean water passages or surface drainage routes in karst regions (Lattman & Parizek, 1964; Kastning & Kastning, 1981). Few lineaments can be discerned from 1:50,000/1:12,000-scale aerial photographs due to low relief, swamps and poor outcrop. A repetitive northeasterly trend, highly modified by swamps, can be distinguished in areas northeast of Mike Lake and south of Table Point (see Figure 1.2). Part of one lineament trending N028E is shown in Plate 2. In the Portland Creek watershed area (Figure 1.3), lakes like Brian's Pond exhibit some modification due to the bedrock NE-SW trending structural lineaments. Other surface drainage follows the same regional trend with the exception of Bowing and Bound Brooks (Figure 1.2) which follow the regional topography gradient towards the west.

Sinkholes are predominant in the region (Hornbrook et al., 1975) and are most visible on dry lake bottoms. Areas underlain

Plate 2. Circa 1965 aerial photograph (1:50,000) of the mine area before mining operations. The northeast structural trend of surface drainage and lakes that are presently dry due to mine pumping are indicated. Photograph courtesy of Newfoundland and Labrador Department of Energy Mines and Resources photo library.

↙ - wide strandline surrounding Lead Lake
- - - - lineament of regional NE structural trend
x - lakes dry in 1986 field season
\+ - lake/swamp with sinkholes dry prior to mining

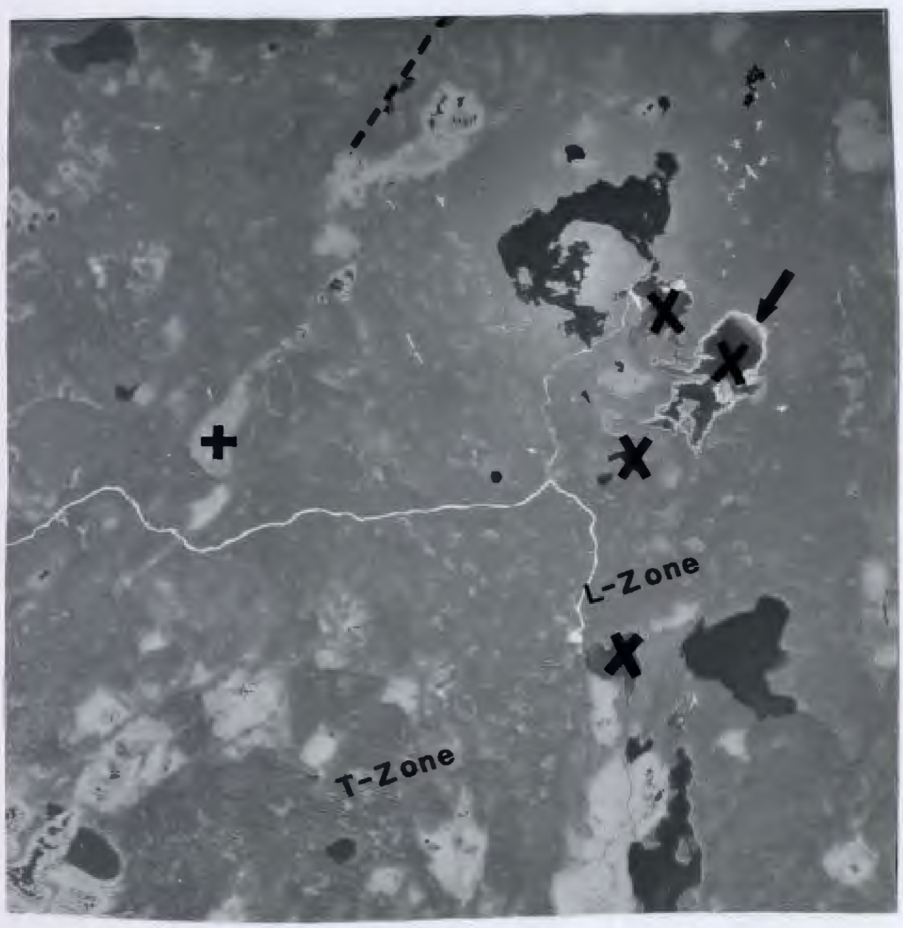

by the St. George Group (Figure 3.1) are characterized by solution-collapse terrain, disappearing streams and intermittent lakes and springs (Hornbrook et al., 1975).

Surface hydrology and sinkholes of the mine study area inferred from topographic maps, past hydrologic reports (Acres, 1974a) and 1986 field work are shown in Figure 4.1. Plate 2 shows the mine area before mining operations commenced. All lakes which are now permanently dry (shown as "x") as a result of mine dewatering are restricted to areas north and south of the L-Zone. An old dry lake bottom (marked with an "+"), with numerous small sinkholes aligned in a N026E direction, was dry before the commencement of mine dewatering. Small sinkholes (less than 5m diameter) are found in the centre of Zinc and Lead Lakes and the northwest shore of Spring Lake (see Figure 4.1). During July 1986 the Spring Lake sinkhole drained the lake at an estimated rate of 200 l/min (as much as 500 l/min in other years; Welhan and Gale, 1986). Dye tracer tests performed by mine staff did not establish a connection between the Spring Lake sinkhole and mine inflows (R. Crossley, pers. comm., 1986). Lead and Zinc Lakes are now permanently dry, but Spring Lake also became dry in August 1986, except for a small pond near its outflow.

Sinkholes indicate cavernous zones at depth in maturely karstified regions (Legrand and Stringfield, 1971). At the mine though, sinks appear to be related to an anticlinal axis (Figure 3.3) and not to large solution channels below ground surface. Rauch and White (1970) found that most caves and solution

Figure 4.1. General hydrology map of the mine area. Surface drainage divides/flow directions, sinkholes and bedding plane seeps found underground are indicated.

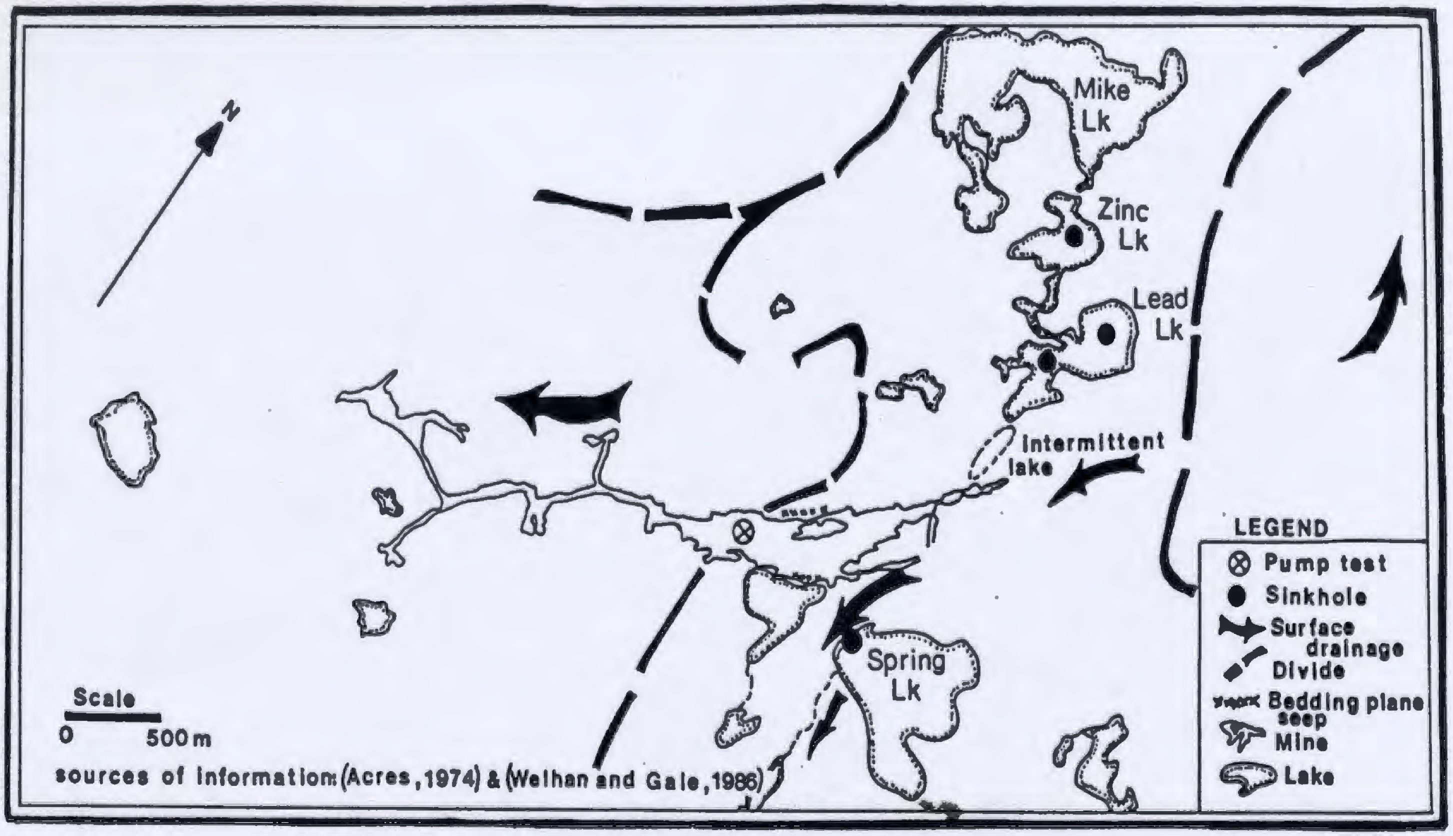
N
Mike Lk
Zinc Lk
Lead Lk
Intermittent lake
Spring Lk
Scale
0 500m
sources of information:(Acres,1974) & (Welhan and Gale,1986)
LEGEND
Pump test
Sinkhole
Surface drainage
Divide
Bedding plane seep
Mine
Lake

channels are restricted to micritic, pure limestones and not dolomites. The pervasiveness of dolomite, sparite and other impurites (eg. quartz) in the mine rocks (see Section 3.3) would tend to inhibit cave development (Rauch and White, 1970).

The broad strandline around Lead Lake shown on Plate 2 indicates fluctuating water levels in the past. An intermittent stream joining Lead Lake and Spring Lake, first reported by Acres (1974a), may have followed a zone of increased permeability between the two lakes. The intermittent nature of the stream may also have been the result of lake level fluctuations caused by sinkhole development. This stream now appears to have been destroyed by mining operations (Figure 4.1). The area north of the L-Zone provided much of the underground inflows into the mine before Lead Lake became dry (Acres, 1974a) and may still contribute to inflows during peak rainfall periods.

4.1.2 Precipitation and pumping rates

The region receives an average of 900 mm precipitation annually (Environment Canada records quoted in Nolan et al., 1979) with approximately 45 % falling as snow over 5 months of the year. Peak surface runoff occurs during late spring and early summer. The summer of 1986 with 205 mm of rainfall was significantly drier than the previous summer, when more than 300 mm fell during the same months (see Figure 4.2).

A comparison of the mine pumping data with the monthly precipitation data is shown on Figure 4.2A and B from 1984 to

Figure 4.2A Dewatering (pumpage rates) and climatological data compiled by D. Tiong of the Newfoundland Zinc Mine for the years A)1984-1985. Peak pumping rates coincide with peak rainfall periods.

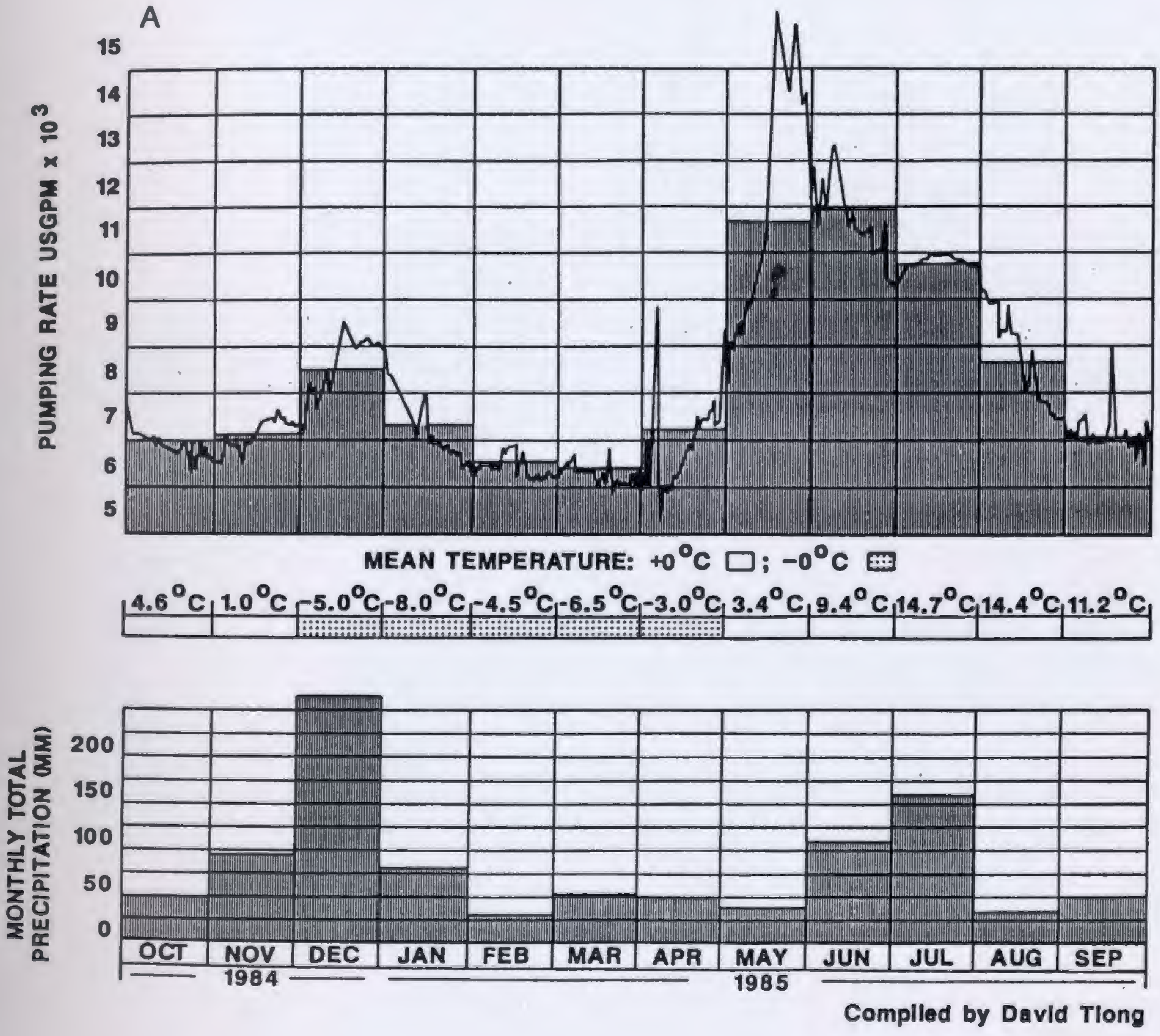

Figure 4.2 B Dewatering and climatological data for the years 1985-1986.

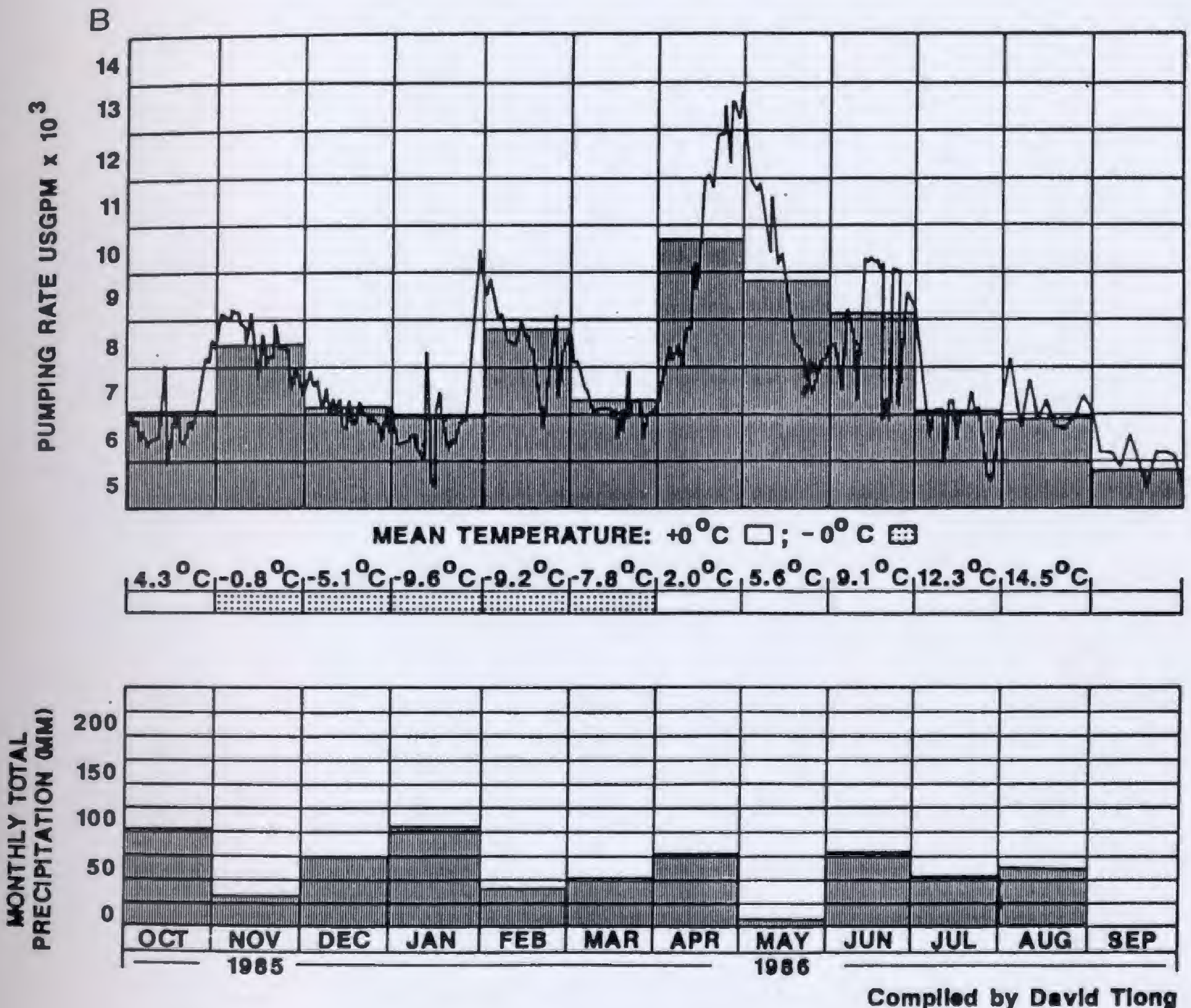

1986. These records show that variations in mine pumping rates are directly related to seasonal variations in precipitation, typical of karst groundwater regimes (Legrand and Stringfield, 1971). Large spring inflows result from high winter snow storage, whereas periods of low precipitation show a reduction in mine inflows (Acres, 1978). Peak snowfalls from November to January do not contribute immediately but in addition to the high spring rainfall they increase mine inflows substantially during the May melt. A more direct correlation between peaks in precipitation and pumping rate can be made in the summer months.

In 1985 low groundwater storage in the aquifer after minimal precipitation in August and September produced a one-month lag between heavy October rainfall and high pumping rates in November. Rapid response to changing recharge necessitates many conduits of flow from surface to underground and implies highly permeable rocks.

Other factors affecting the pumping rate are the extent and depth of underground workings. The increase in average monthly pumping rate was approximately 1890 l/min in 1976 and in 1979 rose to 3785 l/min (Figure 4A & 5B in Welhan and Gale, 1986). During this period the most extensive and shallowest (0-40 m depth) mining operations (L-Zone) took place. After 1979, the mine was extended to deeper levels (T-Zone; 40-260m). The T-Zone is less extensive and did not contribute significantly to the overall pumping rate. Pumping rates dropped after peaking at the end of 1979 (63,000 l/min) and then maintained an average

37,855 l/min. The higher pumping rates from the L-Zone may indicate that rock permeability is greater in the upper parts of the mine.

4.1.3 Mine groundwater regime

Hydraulic heads have been plotted and contoured on Figure 4.3A for 1985 and Figure 4.3B for 1986. The extent of the mine drawdown cone increased in 1986 as a result of that year's summer drought. In 1986, water table drawdowns (with respect to ground surface) ranged from 0 to >60 m in the artesian wells above the T-Zone and in wells near the L-Zone, respectively. These drawdowns were significantly larger than 1985 measurements (Welhan and Gale, 1986). Water table elevations near the hill north of the L-Zone (see Figure 4.3B) were as much as 15 m lower in 1986 than in 1985 (see Appendix L).

Drawdowns were large north of the L-Zone and substantially lower south of the L-Zone (Figure 4.3B). This drawdown cone asymmetry in the north-south direction is illustrated by the cross section through the mine workings shown in Figure 4.4. The drawdown cone's oblong shape in the east-west direction may be due to increased permeability associated with the major faults (Figure 3.3) that are sub-parallel to the axis of the mine (Acres, 1975a). However, the fact that the drawdown cone extends and deepens in the direction of the mine workings (Acres, 1978) implies that the cone's shape is likely a manifestation of the dewatering operations centered around the L-Zone.

Figure 4.3 Hydraulic head (or water table elevation) maps for the mine area in A 1985 and B 1986. Oblong drawdown cone mimics shape of underground workings. Drawdown of water table increased in extent in 1986 due to low precipitation.

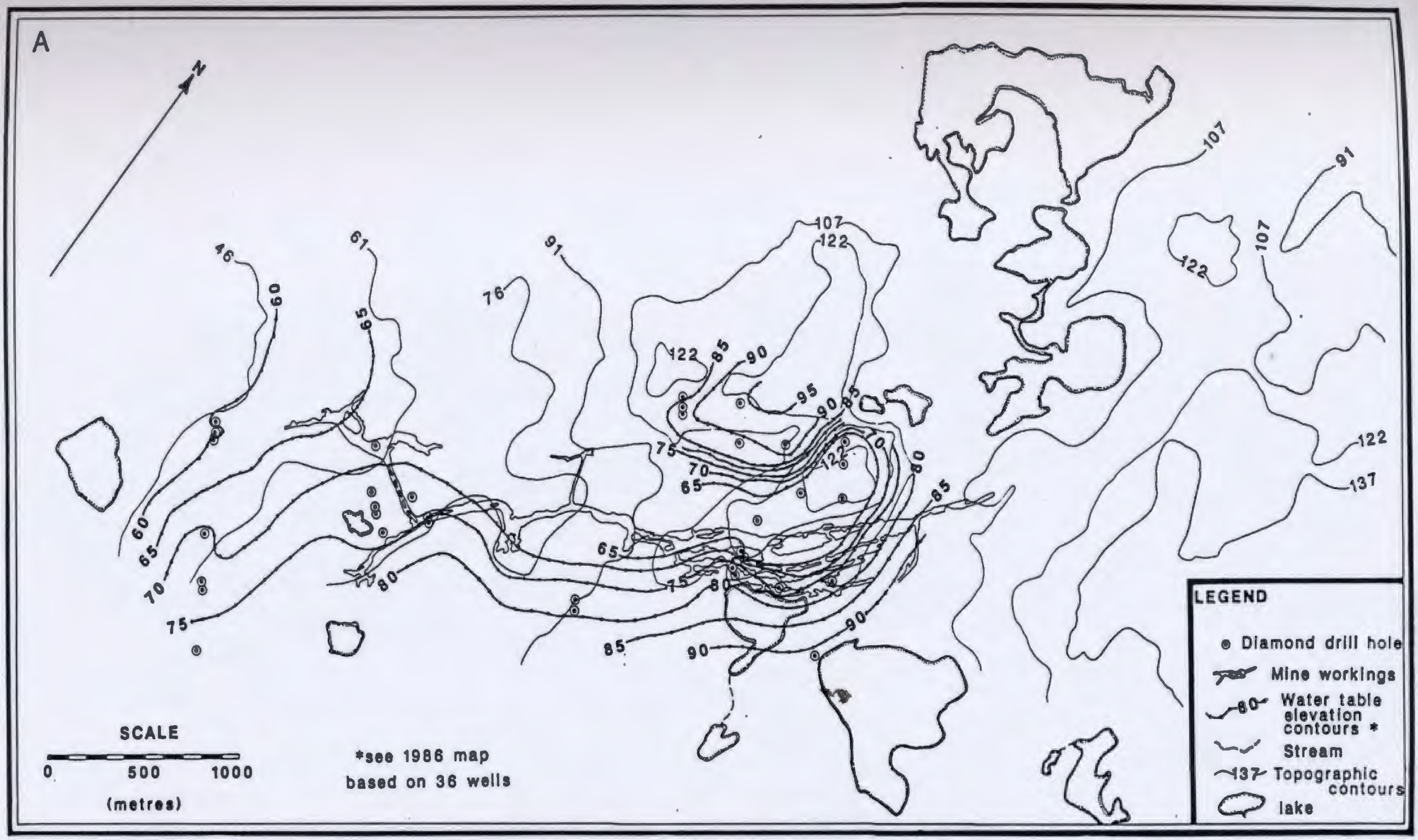
A
N
LEGEND
Diamond drill hole
Mine workings
80 Water table elevation contours *
Stream
137 Topographic contours
lake
SCALE
0
500
1000
(metres)
*see 1986 map
based on 36 wells
46
60
61
65
76
91
107
122
85
90
95
75
70
80
137

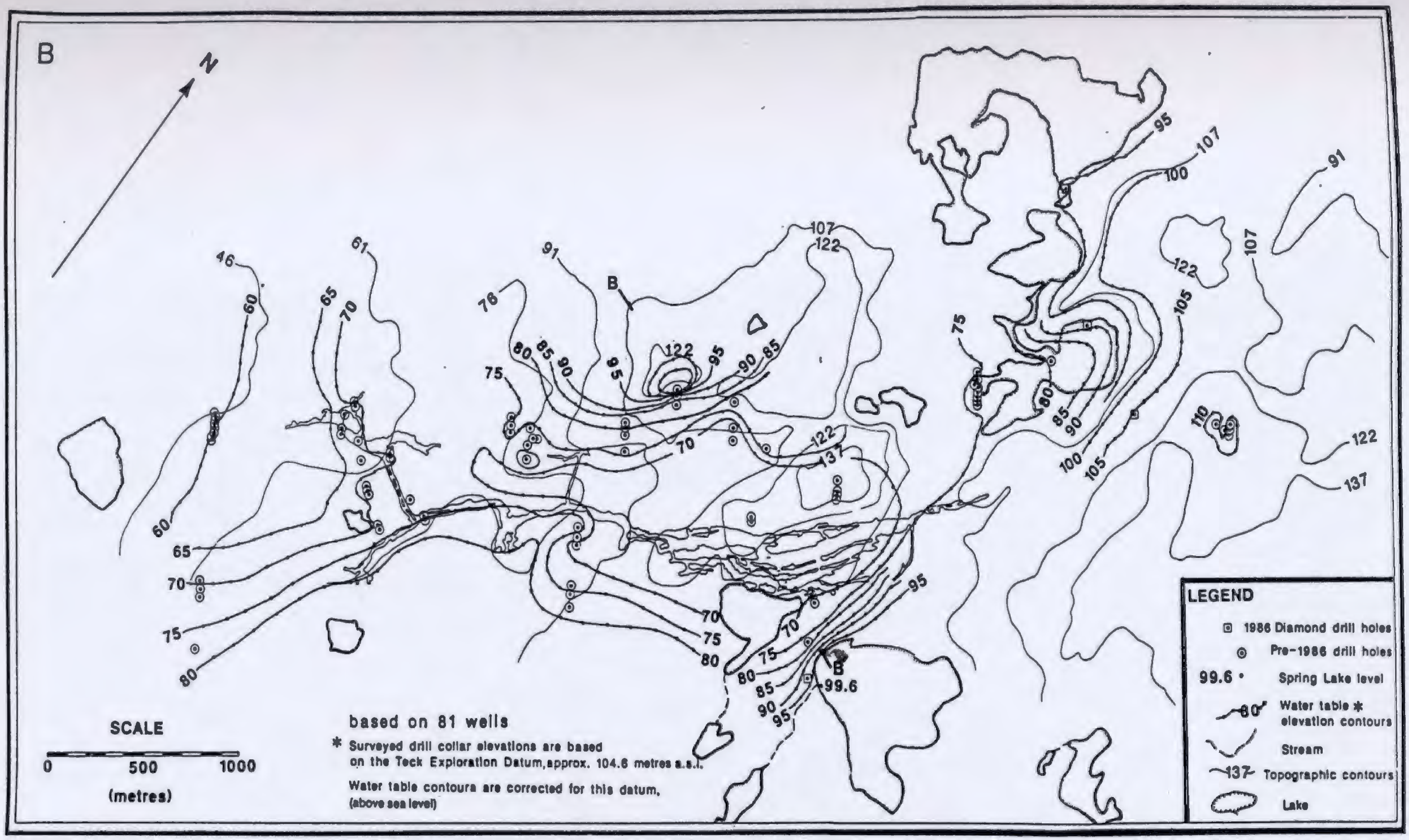
B
N
SCALE
0 500 1000
(metres)
based on 81 wells
* Surveyed drill collar elevations are based on the Teck Exploration Datum, approx. 104.6 metres a.s.l.
Water table contours are corrected for this datum, (above sea level)
LEGEND
1986 Diamond drill holes
Pre-1986 drill holes
99.6 • Spring Lake level
80 Water table * elevation contours
Stream
137 Topographic contours
Lake

Figure 4.4. Cross section B-B' through the 1986 water table map (see Figure 4.3B). The drawdown cone is asymmetrical in a NW-SE direction arould the L-Zone workings. Evidently, pumping affected the north side (B) of the mine workings more than the south side.

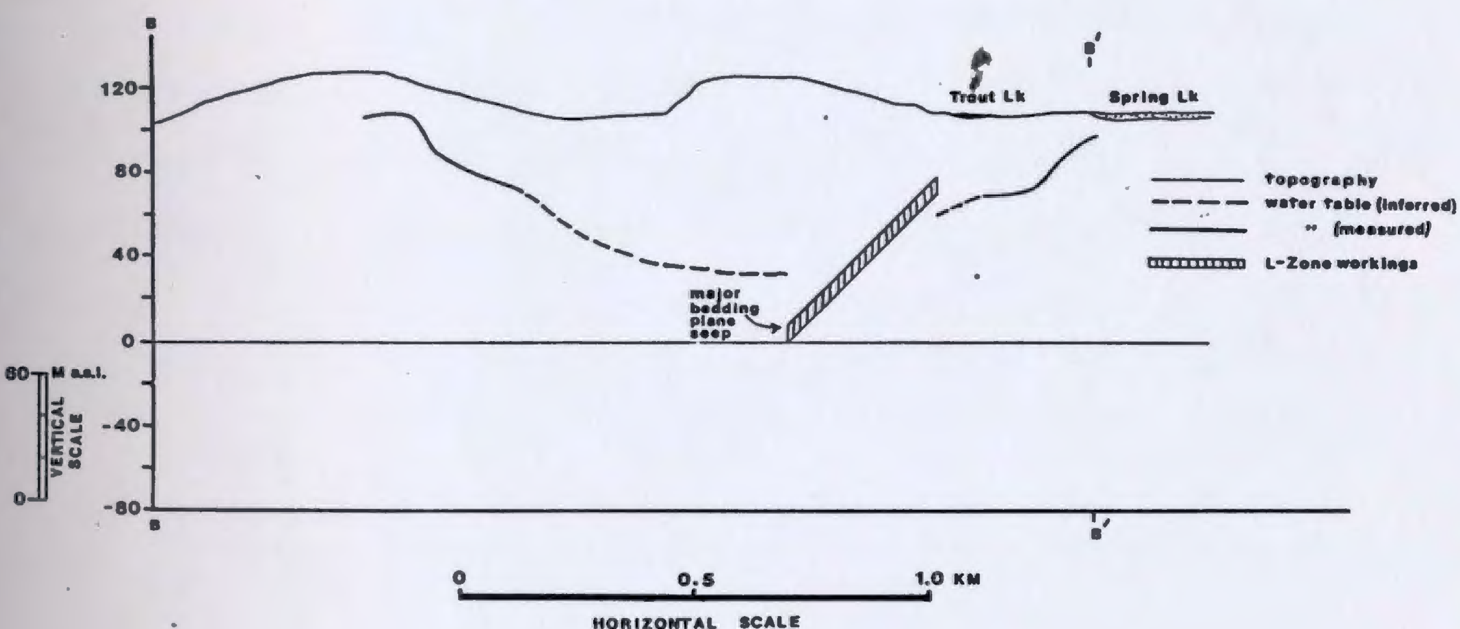

Horizontal components of hydraulic gradients calculated from 1985/1986 data are listed in Table 4.1 and are shown on Figures 4.5A and 4.5B, respectively. The well groupings for these water table surveys establish only single components of the gradient, in the directions indicated on Figures 4.5A and B. The fact that most of the gradients are small may mean that they are very large in another direction. These gradients are within the range (0.004-2.95) found at other mines in karstified fractured rock (Motyka and Wilk, 1986). About half of the gradients, calculated from water levels in wells that were measured both in 1985 and in 1986, were greater in 1986. The largest gradient increase occurred to the west in the vicinity of gradients # 17, 18, 21 and near the hill where gradient # 9 was measured (Figure 4.5B). Comparison of individual gradients between 1985 and 1986 is difficult since the well survey for each year did not consist of

Table 4.1 Components of hydraulic gradients for 1985 and 1986 surveys. Reference numbers refer to gradient labels shown on Figure 4.5A and B. Reference labels with the same number for both years do not represent the same set of well pairs for 1985 and 1986.

Ref. #	1985	1986	Ref. #	1985	1986
1	0.0286	0.0087	13	0.0054	0.0214
2	0.0165	0.0420	14	0.1029	0.0161
3	0.0098	0.0510	15	0.0476	0.0068
4	0.0120	0.00	16		0.0139
5	0.0139	0.0047	17		0.0333
6	0.1220	0.0479	18		0.1135
7	0.0240	0.0319	19		0.0084
8	0.0434	0.0802	20		0.0239
9	0.0408	0.3668	21		0.0460
10	0.0980	0.0301	22		0.0076
11	0.0609	0.6603	23		0.0089
12	0.0214	0.0197			

Figure 4.5. Component hydraulic gradient maps for a) 1985 and b) 1986. Gradients (listed in Table 4.1) are largest around the L-Zone workings and directions are in response to underground pumping.

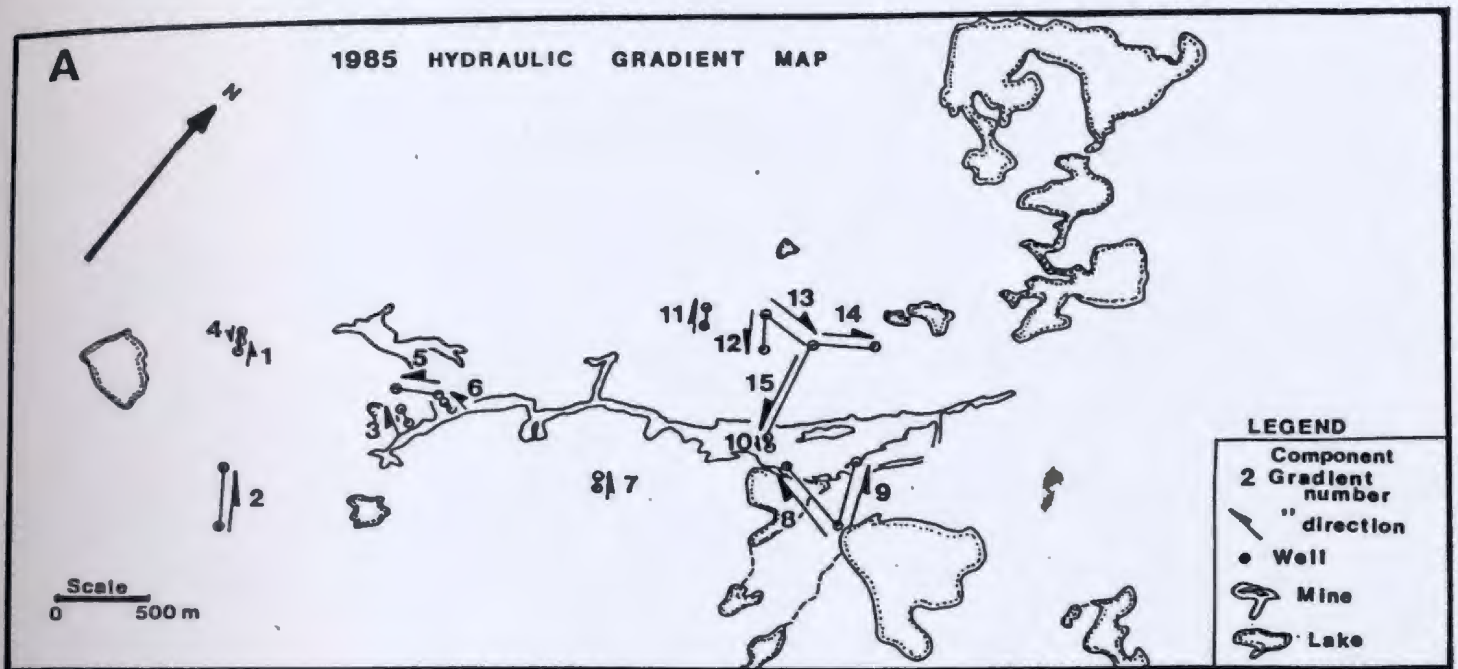
A
1985 HYDRAULIC GRADIENT MAP
N
LEGEND
Component
2 Gradient number
" direction
Well
Mine
Lake
Scale
0 500 m

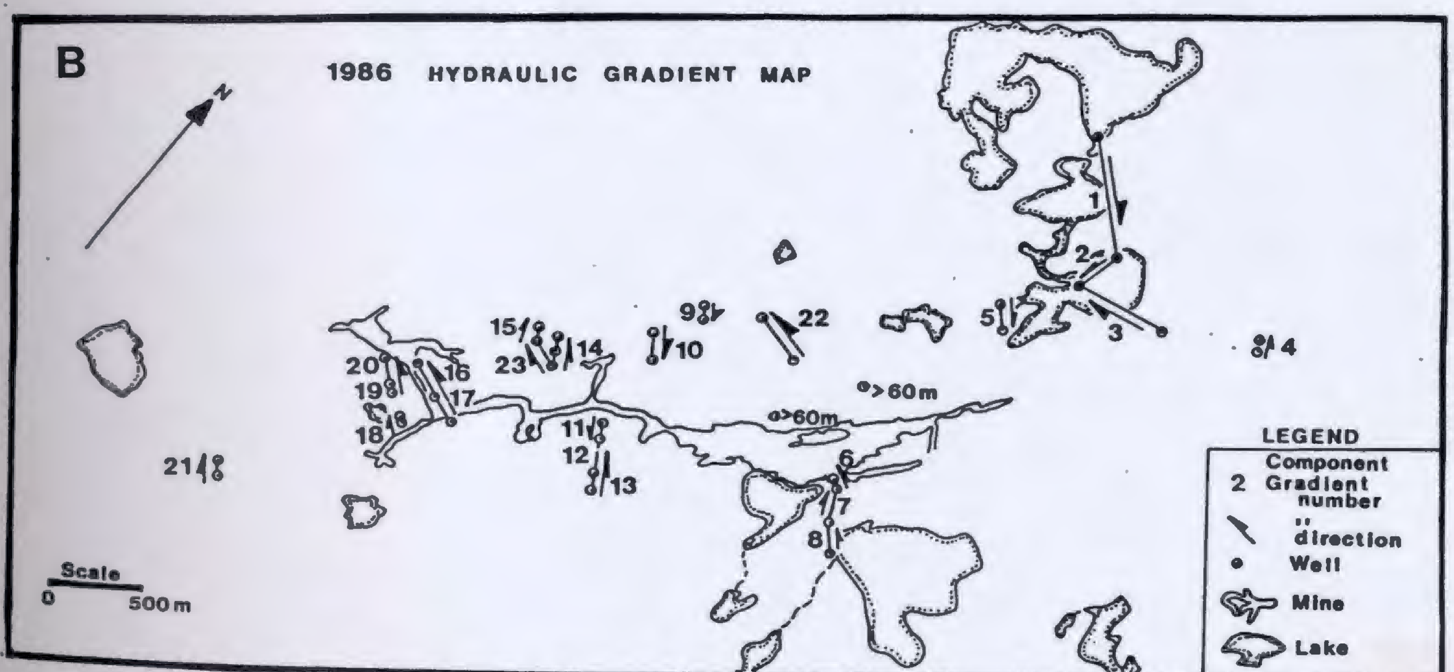
B
1986 HYDRAULIC GRADIENT MAP
N
>60m
>60m
LEGEND
Component
2 Gradient number
" direction
Well
Mine
Lake
Scale
0 500 m

the same wells and this method (see Section 2.6.1) of calculating hydraulic gradients is prone to error in anisotropic terrain (Stojic et al., 1976). Acres (1974a) concluded from piezometer monitoring that there were no significant vertical gradients. They rejected the possiblility that artesian pressures exist in the L-Zone and indicated there was no aquifer confinement by impermeable strata. This implies excellent vertical hydraulic connection.

Water (gauge) pressures measured underground, and their hydraulic head conversions, are listed in Table 4.2. The low pressure measured for P-5 (*) may be due to pressure loss when the valve was opened (see Section 2.6.2). Despite the uncertainties in these data, a general decrease in hydraulic head with depth is suggested, possibly in response to the regional topographical slope towards the west.

4.2 Permeability

Assessment of the permeability for the region and mine host rocks is based entirely on previous work because it was not possible to do pump or pressure/packer tests at the mine site during the summer of 1986 for logistical reasons. The packer equipment of the necessary diameter was not available for the newly drilled holes. A summary of the work done by others is given in Appendix N.

Major groundwater-bearing conduits in the mine workings are bedding planes, faults, and fractures. Other major sources of

Table 4.2 Pressure measurements taken underground at Daniel's Harbour Mine. See Figure 2.7 for their locations. Gauge pressures were converted to hydraulic head by the formula h = P/pg - z where p=density, g=acceleration due to gravity, and z=elevation with respect to datum. Combined error of pressure-gauge measurement and estimation of site elevation for head values is 3.5-5m. * - this pressure is anomalously low (see text).

P #	SITE	Gauge (PSI)	Pressures (kPa)	Hydraulic Head (m)	Elevation (masl)
P-1	T-Zone	265	1.827×10^3	0.7	-186
P-2	T-Zone	285	1.965 x "	15.0	-186
P-3	T-Zone	290	2.000 x "	18.0	-186
P-4	T-Zone	320	2.210 x "	36.0	-190
P-5	T-Zone	15	0.103 x "	-182.0*	-193
P-6	T-Zone	220	1.517 x "	-29.0	-184
P-7	T-Zone	150	1.034 x "	-79.0	-184
P-8	Mid-Zone	160	1.103 x "	25.0	- 87
P-9	L-Zone	105	0.619 x "	32.0	- 31
P-10	L-Zone	25	0.172 x "	18.0	1
P-11	L-Zone	60	0.414 x "	43.0	1
P-12	L-Zone	55	0.379 x "	39.0	1
P-13	L-Zone	75	0.517 x "	55.0	2
P-14	L-Zone	70	0.483 x "	51.0	2
P-15	L-Zone	70	0.483 x "	51.0	2
P-16	L-Zone	65	0.448 x "	17.0	-29
P-17	L-Zone	65	0.448 x "	17.0	-29
P-18	L-Zone	60	0.414 x "	15.0	-28
P-19	L-Zone	40	0.275 x "	0.4	-28

seepage include backs (ceilings of drifts), joint-bedding plane intersections and drill holes (Acres, 1975b).

In the mine many bedding planes are intersected but only some conduct significant inflows. These surfaces may have been planes of slippage during regional compression (see Section 3.6.3.1). Bedding planes (Set #4) are consistently longer than any other fracture type (see Section 3.6.3.2), emphasizing the role of bedding planes in conducting groundwater to the mine despite their relatively low numbers. Wet lines appear on the backs where joints intersect the bedding planes and conduct water into the open drifts. Faults with major inflows have an average orientation of 225/80 (Acres, 1975b). Flow velocities of 2.3×10^{-2} m/s to 3.1×10^{-2} m/s were calculated during dye tracer tests (Acres, 1975a) and were only an order of magnitude lower than maximum mean tracer velocities of 1.7×10^{-1} m/s for open-channel flow measured at Castleguard Meadows, Alberta (Smart & Ford, 1986).

In 1986, inflows from bedding planes were measured by timing the filling of a 500-ml container at various locations along 3 major bedding plane seeps (main decline near DH-27, see Figure 2.2). Seepage varied along the bedding planes and ranged from nil to 0.02 l/s every 3 m. A total inflow of 1.25 l/s over a length of 81 m was estimated. In the L-Zone, where a major grouted fault (216/72) intersects bedding planes (vicinity of DH-32, see Figure 2.2), inflow of 9.8 l/s over a length of 14 m was measured in 1986. The number of water-conducting features decreases with depth in the L-Zone decline, which implies rock permeability decreases as well.

RQD plots (see Appendix A) for the 1986 drill holes show that areas of dense fracturing do not appear to be related to specific (sparite) porous layers in the pseudobreccia unit. The lowest RQD values (dense fracture, low mean core length) consistently occur in the first 2-3 m of core and they are not restricted to the more vuggy sparite sublayers. The total hole RQD range was 43.9 to 79 % with a low average of 62 %; indicating poor to fair rock mass conditions. Stylolites (perpendicular to core axis) were very common in the core, and some core sections could be broken by hand along these irregular suture-like subhorizontal discontinuities (see Appendix A). Stylolites decrease rock strength, as evidenced by rock strength tests (see Appendix M), and may localize dissolution by groundwater. Diamond drill core analyses by Acres (1974a) showed that the upper 15 m of core exhibited the highest permeability due to solution-enlarged jointing and sinkholes. Thus, permeability decreases with depth as frequency and weathering of flow conduits decreases with depth.

The pressure-test data done by Acres (1974a) indicated that the upper and lower contacts of the pseudobreccia commonly had high hydraulic conductivities of 1×10^{-3} m/s. Permeability, found by pressure testing (Acres, 1974a), was greatest in the uppermost weathered zone of 1 to 10 m (most often in the upper 3 m in both the Table Head limestone and siliceous dolomite) and in zones of open conduits such as faults and bedding planes. The permeability variation can be larger within the same lithological unit than between different lithological units. These fluctuations may be caused by well bore intersections with major bedding planes or fracture seeps within each rock type. In individual units there is a minor trend to higher permeabilities laterally towards the east. This could be caused by an increase in the fracture size/or extent of dissolution as one gets closer to the crest of the anticline (see Figure 3.3). Acres' concluded that individual flow conduits such as bedding planes and fractures are very significant to the permeability distribution in the carbonate rock mass at the mine. The analysis of Acres data and the 1986 drill logs shows that permeability is not necessarily a function of lithology in this aquifer; at least not in the upper few hundred metres of the carbonate platform.

Two pump tests were undertaken in the same pumping well at different depths by Acres (1974a). Final drawdown cones and specifics for each pump test are given in Figure 4.6. The Acres pump test results were reanalyzed using the Jacob distance-drawdown method (Heath, 1983). There is a large scatter in the plotted points on distance-drawdown plots, suggesting that this aquifer is anisotropic. Newly calculated transmissivity and storativity values are given in Appendix N.

The axis of maximum transmissivity for the aquifer tested by pump test #1 (Acres, 1974a) was determined by the method of Papadopolous (1967). The N63E oriented axis (see Figure 4.6) corresponds to an average orientation between the two documented major joint sets in the mine area and the dominant regional NE trend (see Section 3.6.1). The previously mentioned major fault conduits have similar orientations as Joint set #1 and obviously contribute to the aquifer's anisotropy as well.

4.3 Conclusions

Figure 4.7 summarizes the essential physical information discussed thus far for the mine area. The regional NE stuctural

Figure 4.6 Acres (1974a) pump test data from a well located just north of Trout Lake in the vicinity of the L-Zone workings. Geology transected by wells is shown on the left of the diagram with maximum axis of transimissivity.

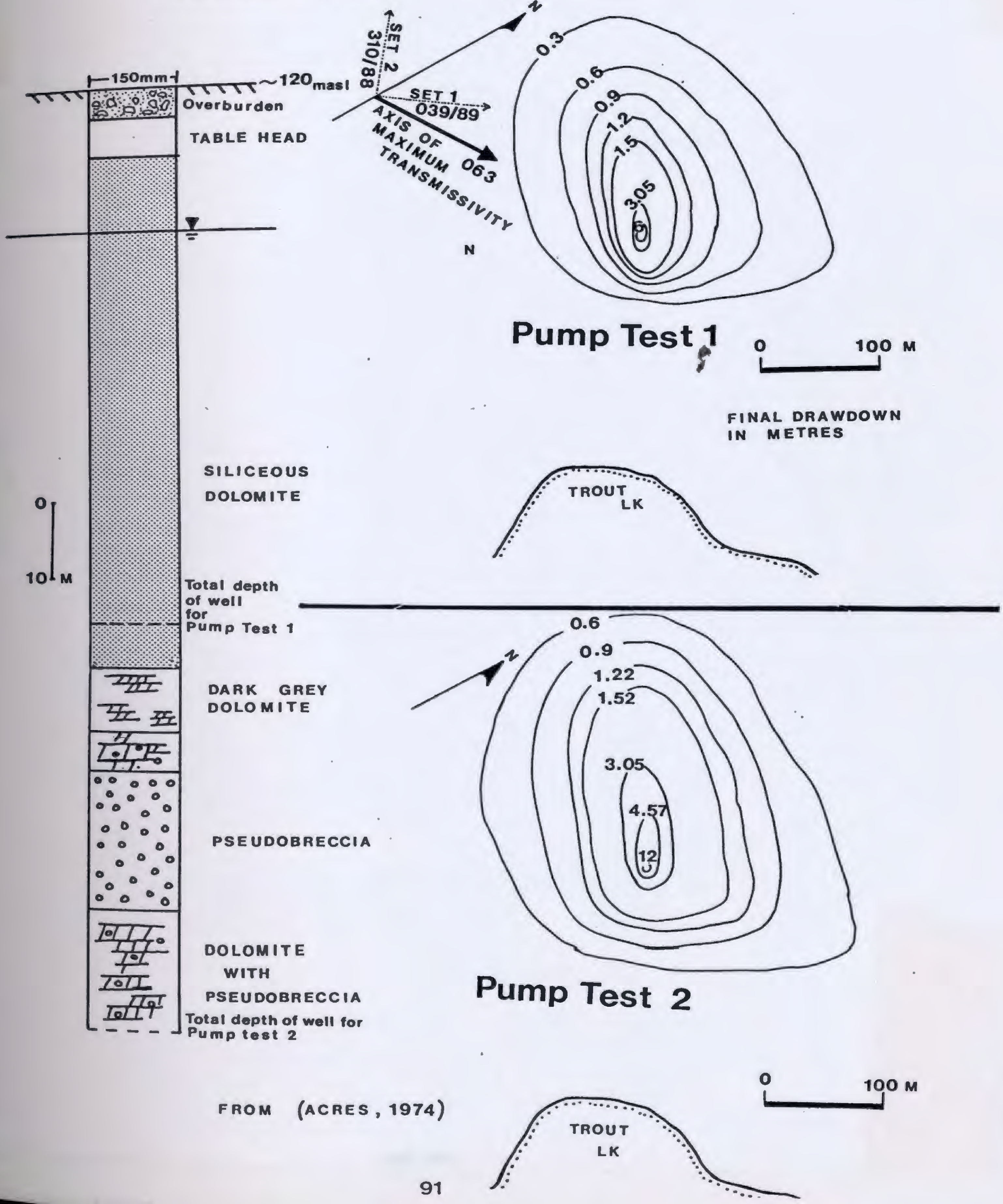

Figure 4.7 Composite map of essential hydrogeological features for the local mine area.

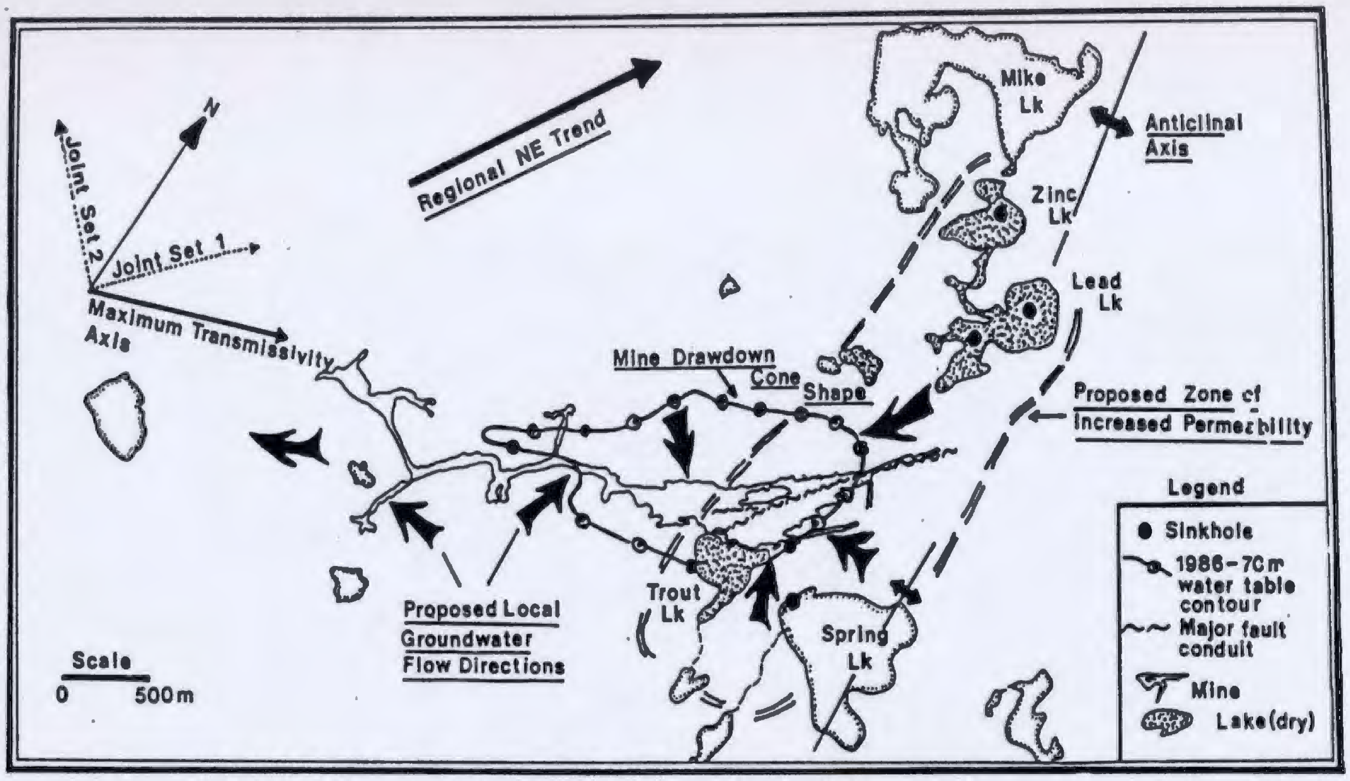
N
Joint Set 2
Joint Set 1
Maximum Transmissivity Axis
Regional NE Trend
Mike Lk
Anticlinal Axis
Zinc Lk
Lead Lk
Mine Drawdown Cone Shape
Proposed Zone of Increased Permeability
Legend
Sinkhole
1986-70m water table contour
Major fault conduit
Mine
Lake(dry)
Trout Lk
Spring Lk
Proposed Local Groundwater Flow Directions
Scale
0 500m

trend controls surface drainage, intensifies dissolution along NE lineaments (thereby controlling sinkhole development) and influences groundwater flow directions. Karst development related to structure was observed in areal photographs of this study area. The Newfoundland Zinc Mine rocks are only moderately karstified and dissolution is limited to sinkholes. Lakes with widely fluctuating water levels are also characteristic of karst regions.

Mine dewatering mainly affects areas within 2 km north and south of the eastern part of the L-Zone underground workings. Mine inflows are intimately associated with precipitation and are greatest in the shallow L-Zone workings. The Spring Lake sinkhole is an important source of recharge to the subsurface but a direct link to the L-Zone is not yet established. The shape of the drawdown cone mimics the outline of the underground workings, both being aligned parallel to the NE trending faults that crosscut the area. Hydraulic gradients are within documented ranges for karst areas (Motyka and Wilk, 1986), despite the influence of mine dewatering, but they varied between surveyed years in both magnitude and direction. Gradient and water table maps were used to infer groundwater flow directions.

The carbonate rocks in the area make up a highly anisotropic aquifer whose permeability is a function of the degree of weathering of the major conduits of flow rather than of the position of major lithological units within the carbonate sequence. The presence of local highly conductive structural features (eg. faults, bedding planes and joints) causes increased permeability in certain directions or anisotropy, and varied permeability on the local scale. Major dissolution of these conduits along the local anticlinal axis would cause a zone of increased permeability in the eastern part of the study area (see Figure 4.7). Major faults and lakes with wide strandlines (Lead Lake) may also indicate areas of greater permeabililty. The axis of maximum transmissivity is oriented N63E, again coinciding with the regional trend. Permeability generally decreases with depth but complications arise due to the above mentioned structural and lithological features (weathered lithological contacts rather than separately assigned permeabilities to the total lithologic units). Permeability profiles, results of 1986 field work, and drill core analyses show that there is no clear correlation between permeability and lithology, and indicate greatest permeability variance with depth. Good vertical hydraulic connection is probably due to the intense weathering of the predominantly vertical joints in the upper 50 m of section.

Bedding planes increase permeabililty on a small scale and the unit would be considered homogeneous with respect to its many bedding planes on the regional scale. Regionally, the Precambrian basement underlying the carbonate sequence is assumed impermeable as in other regional flow system studies (Toth, 1978).

Chapter 5

HYDROGEOCHEMISTRY

5.1 Introduction

The objective of this chapter is to describe the hydrogeochemistry of groundwaters at the mine and its environs in order to determine different groundwater types. Geochemical trends exhibited by major- and trace-ion plots help to determine the mechanisms that control elemental concentrations, thereby indicating possible evolutionary paths and mixing relationships of groundwaters. Stable isotopes are used to differentiate waters with similar major-ion compositions, and to determine origins of mine inflows and possible history of the different groundwater types. Hypotheses deduced from elemental trends are tested with geochemical modelling.

5.2 Results

Chemical analyses for waters sampled in 1985, 1986 and 1987 are given in Tables 5.1 to 5.3. Table 5.1 includes major-ion chemistry, and other chemical parameters, as well as charge balance error for the major ion analyses. Some analyses in Table 5.1 are not reliable because they have charge balance errors greater than 40 %.

Trace element analyses for all mine and well waters sampled in 1986 are shown in Table 5.2. Environmental isotope analyses for deuterium, oxygen-18, carbon-13 (of total DIC), tritium, and radiocarbon are listed in Table 5.3.

Table 5.1 Major-ion and water chemistry of the groundwater, lake and spring water sampled in and around the Newfoundland Zinc Mine. Major-ion concentrations are in ppm. Charge balance has been included as a measure of analysis reliability. The charge balance error was calculated as follows:

$$E(\%) = \frac{SUMm_c z_c - SUMm_a z_a}{SUMm_c z_c + SUMm_a z_a} \times 100$$

where m and z is the molality and ionic charge of each cation(c) and anion (a), respectively. For a complete sample site description see Appendix B. Alkalinities and charge balances for lake samples denoted with a * were estimated by linear regression.

Samples DH-001 -- DH-023 taken in July 1985
Samples DH-025 -- DH-103 taken in July-August 1986
Samples DH-104 -- DH-111 taken in March 1987

Alk. = alkalinity Diss. O_2 = dissolved oxygen
Cond.= conductivity T = temperature

Sample ID: well- sample taken from surface drill hole
sump- sample from the mine sump discharge
mine- groundwater from underground drifts
Sample AREA: location of sample site with respect to underground workings

DH-#	ID	AREA	T, °C	pH	Eh mV	Cond. µmho/cm	Diss. O_2 ppm	Ca	Mg
1985:									
1	lake	SOUTH	15	7.25	448	480		18	6.4
2	well	SOUTH	5	7.56	-32	1320		20	17
3	well	NORTH	5	6.96	365	1500		55	19
4	sump	NORTH	6.9	8.26	218	1450		54	28
5	mine	T-ZONE	5.6	7.41	-33	2750		38	32
6	mine	T-ZONE	5.8	7.42	78	4000		52	36
7	mine	T-ZONE	5.8	7.52	-59	10100		83	54
8	mine	T-ZONE	5.6	7.51	-59	5900		55	37
9	mine	L-ZONE	5.8	7.29	238	1315		51	30
10	mine	L-ZONE	6.7	7.55	310	1260		50	26
11	mine	L-ZONE	5.9	7.30	314	1570		62	33
12	mine	MID-DEPTH	5.3	7.48	-47	9400		98	84
13	mine	MID-DEPTH	4.7	7.20	52	1240		48	22
14	mine	MID-DEPTH	5.1	7.25	13	2800		56	31
15	lake	SOUTH	15	8.21	348	860		35	9.1
16	lake	SOUTH	15	7.89	392	850		29	8.4
17	lake	SOUTH	15	6.76	454	250		9.8	1.7
18	lake	SOUTH	15	7.93	404	325		11	3.4
19	lake	NORTH	15	8.37	372	760		29	11
20	lake	SOUTH	16.9	8.45	405	1225		52	28
21	lake	NORTH	15	8.22	403	650		32	7.7
22	lake	SOUTH	15	7.35	436	152		5.6	1.9
23	rain		15	5.71	218	218		1.5	0.9
1986:									
25	well	NORTH	8.5	7.13	538	930	1.3	139.20	62.20
26	mine	MID-DEPTH	5.2	7.88	410	880	2.2	60.30	34.30
27	mine	L-ZONE	6.2	7.61		530	3.1	63.50	29.80
28	mine	L-ZONE	4.1	7.57	496	430	0.9	51.60	27.10
29	mine	L-ZONE	4.6	7.60	516	640		92.30	32.60
30	mine	MID-DEPTH	5.0	7.71	15	1500	0	80.00	48.00
31	mine	L-ZONE	4.4	7.60	416	480	5.2	59.30	30.60
32	mine	L-ZONE	6.4	7.38	339	655	3.1	73.30	40.70
33	mine	T-ZONE	6.1	7.79	-18	3000	0	71.50	58.50
34	mine	T-ZONE	5.6	7.82	42	1250	0.9	54.50	32.00
35	mine	T-ZONE	5.8	7.87	32	800	0.4	38.40	27.50
36	lake*	EAST	15.5	7.50		45		3.93	1.86
37	lake*	EAST	15.6	7.80		39		2.79	1.45
38	lake*	EAST	17.8	7.70		29		0.71	0.36
39	lake*	EAST	22.2	7.90		100		14.10	2.77
40	lake*	NORTHEAST	20.0	7.75		56		5.72	2.23
41	lake*	WEST	25.0	7.50		200		28.00	7.42
42	lake*	WEST	26.7	8.40		140		16.60	5.61
43	lake*	WEST	25.0	8.20		310		38.50	19.50
44	lake*	NORTHWES	28.8	8.25		320		33.60	20.80
45	lake*	NORTHWES	25.6	8.10		130		12.40	8.32
46	lake*	NORTHWES	26.7	8.20		300		35.90	12.80
47	lake*	NORTHWES	24.4	8.40		290		38.50	16.20
48	lake*	SOUTHWES	24.4	7.50		72		5.50	2.58
49	lake*	SOUTHWES	25.6	8.10		130		19.40	3.14
50	lake*	SOUTHWES	24.4	7.80		64		2.14	1.45
51	lake	NORTHWES	16.7	8.09		300		36.40	6.82
52	lake	NORTHWES	18.3	7.67		120		9.79	4.28
53	lake	NORTHWES	18.8	8.94		260		42.70	14.40
54	lake	NORTHWES	20.0	8.52		230		26.30	9.35

DH-#	ID	AREA	Na	K	Alk.	Cl	SO_4	NO_3	NO_2	Charge Balance
1985:										
1	lake	SOUTH	4.85	0.54	70	8.4	3.4			0.06
2	well	SOUTH	62	14	298	17	8.5			-0.01
3	well	NORTH	6.5	0.59	287	12	8.2			-0.06
4	sump	NORTH	3.2	3.8	222	48	85			-0.13
5	mine	T-ZONE	190	16	284	180	90			0.06
6	mine	T-ZONE	290	19	279	329	170			0.04
7	mine	T-ZONE	500	23	209	717	310			0.01
8	mine	T-ZONE	280	15	230	354	92			0.08
9	mine	L-ZONE	12	2.4	225	25	83			-0.04
10	mine	L-ZONE	12	2.2	212	23	81			-0.05
11	mine	L-ZONE	16	2.4	292	35	83			-0.07
12	mine	MID-DEPTH	710	31	189	988	370			0.06
13	mine	MID-DEPTH	30	6.5	248	41	79			-0.09
14	mine	MID-DEPTH	150	11	230	210	80			0.03
15	lake	SOUTH	11	0.82	201	19	6.2			-0.14
16	lake	SOUTH	23	3	148	20	8			0.01
17	lake	SOUTH	6	0.61	31	11	3.1			0.01
18	lake	SOUTH	8.1	0.68	43	11	2.2			0.06
19	lake	NORTH	4.86	0.51	109	9.6	8.3			0.07
20	lake	SOUTH	12	2.4	212	25	59			0.01
21	lake	NORTH	4.92	0.58	137	9.2	3.3			-0.02
22	lake	SOUTH	3.23	0.31	17	5.1	1.9			0.11
23	rain		0.55	0.21	9	0.5	0.7			0.00
1986:										
25	well	NORTH	7.12	1.05	207	10.4	311.6	2.4	0.0	0.10
26	mine	MID-DEPTH	76.40	7.59	231	125.2	87.9	0.0	0.0	0.01
27	mine	L-ZONE	15.16	4.05	251	20.8	47.7	0.0	0.0	0.06
28	mine	L-ZONE	12.24	1.50	231	18.2	24.1	0.0	0.7	0.06
29	mine	L-ZONE	8.15	1.37	251	10.2	128.0	0.0	0.0	0.04
30	mine	MID-DEPTH	201.80	17.30	231	320.4	132.0	0.0	0.0	0.05
31	mine	L-ZONE	13.15	1.31	246	18.7	41.9	24.2	0.0	0.06
32	mine	L-ZONE	16.89	3.01	276	39.1	52.2	3.9	0.0	0.08
33	mine	T-ZONE	485.90	27.00	212	790.8	190.8	0.0	0.0	0.01
34	mine	T-ZONE	169.90	13.00	226	258.9	77.0	0.0	0.0	0.02
35	mine	T-ZONE	106.80	13.60	261	114.6	58.0	35.0	0.0	0.03
36	lake*	EAST	4.70	0.28	16					
37	lake*	EAST	5.10	0.33	11	5.1	1.4	0.0	0.0	0.15
38	lake*	EAST	3.76	0.19	3					
39	lake*	EAST	6.22	0.40	58					
40	lake*	NORTHEAST	5.27	0.28	23	5.3	0.5	0.0	0.0	0.13
41	lake*	WEST	10.17	0.76	114	14.1	4.1	0.0	0.0	0.02
42	lake*	WEST	8.70	0.09	68	10.9	7.9	0.0	0.0	0.47
43	lake*	WEST	9.93	0.65	157	15.1	7.5	0.0	0.0	0.11
44	lake*	NORTHWEST	10.10	0.75	137	17.1	4.6	0.0	0.0	0.15
45	lake*	NORTHWEST	8.97	0.38	51	11.6	2.3	0.0	0.0	0.17
46	lake*	NORTHWEST	9.93	0.63	146	18.4	5.8	0.0	0.0	0.04
47	lake*	NORTHWEST	9.03	0.56	157	13.2	6.9	0.0	0.0	0.08
48	lake*	SOUTHWEST	8.10	0.49	22					
49	lake*	SOUTHWEST	9.10	0.69	79					
50	lake*	SOUTHWEST	7.26	0.41	9					
51	lake	NORTHWEST	8.41	0.42	197	19.8	3.2	0.0	0.0	-0.17
52	lake	NORTHWEST	7.74	0.31	59	11.8	2.0	0.0	0.0	-0.06
53	lake	NORTHWEST	9.41	0.61	182	12.4	6.5	0.0	0.0	0.04
54	lake	NORTHWEST	14.75	0.51	103	24.5	6.5	0.0	0.0	0.04

DH-#	ID	AREA	T, °C	pH	Eh mV	Cond. µmho/cm	Diss.O_2 ppm	Ca	Mg
55	lake	NORTHWEST	18.9	8.61		290		41.00	15.30
56	lake	NORTHEAST	17.2	7.73		150		19.20	6.02
57	lake	NORTHEAST	17.7	8.60		220		27.90	7.30
58	lake	NORTHEAST	15.5	8.11		270		46.80	10.00
59	lake	NORTHEAST	22.2	7.83		74		8.50	3.08
60	lake	NORTHEAST	21.0	8.15		110		14.50	4.46
61	lake	NORTHEAST	21.0	8.59		120		13.20	7.12
62	lake	NORTHEAST	20.0	8.58		220		29.70	9.53
63	lake	NORTHEAST	21.7	8.39		160		27.00	7.78
64	lake	NORTHEAST	18.8	8.52		240		36.40	9.53
65	lake	WEST	17.7	8.10		290		42.00	9.53
66	lake	SOUTHWEST	18.3	8.47		390		53.40	16.70
67	lake	SOUTHWEST	16.6	7.31		100		6.36	3.26
68	lake	SOUTHWEST	18.9	7.27		88		5.72	3.20
69	lake	SOUTHWEST	17.8	7.41		120		5.00	4.04
70	lake	SOUTHWEST	17.8	7.16		110		5.50	3.68
71	lake	SOUTH	16.1	8.37		500		66.40	33.70
72	lake	SOUTHEAST	16.6	7.95		160		20.70	7.00
73	lake	SOUTH	16.6	7.68		210		34.70	14.90
74	lake	SOUTH	16.6	7.73		170		24.40	10.40
75	lake	NORTH	16.6	8.04		330		44.50	16.80
76	mine	T-ZONE	6.1	7.45	-177	3000	0	71.80	60.10
77	mine	MID-DEPTH	4.9	7.27	-175	1500	1.3	82.80	49.30
78	mine	L-ZONE	7.9	7.34	184	500	4.4	63.50	31.90
79	well	NORTH	9.5	7.62	246	485	11.8	61.10	31.60
80	sump	NORTH	5.6	7.66	175	620	10	62.70	31.60
81	mine	L-ZONE	5.9	7.13	230	500	2.2	61.00	34.50
82	well	SOUTH	10.4	7.29	236	580	10.5	70.80	38.70
83	well	SOUTH	10.5	7.11	321	540	8.3	65.10	33.00
84	well	SOUTH	10.8	7.53	224	565	7.4	82.60	34.40
85	well	NORTH	13.7	6.92	245	543	5.2	109.30	57.20
86	well	WEST	11.6	7.57	20	455	0.9	44.00	25.70
87	well	NORTH				535	10.5	64.50	38.20
88	well	NORTH	12.8	7.76	-85	448	0.9	35.10	16.70
89	mine	T-ZONE				2590		66.80	55.60
90	mine	T-ZONE				775		43.90	29.10
91	mine	T-ZONE				1600		48.60	37.80
92	mine	T-ZONE				895		45.20	28.90
93	mine	T-ZONE				3100		79.80	69.40
94	mine	MID-DEPTH				655		67.80	31.20
95	mine	MID-DEPTH				745		66.20	31.50
96	mine	MID-DEPTH				500		52.50	23.20
97	mine	L-ZONE				445		51.90	20.70
98	mine	L-ZONE				945		57.50	29.90
99	mine	L-ZONE				530		62.50	30.80
100	mine	L-ZONE				675		74.50	41.40
101	mine	T-ZONE	6.7	7.81	-106	3100	0.9	73.80	60.20
102	mine	MID-DEPTH	4.6	7.31	-97	630	1.7	39.90	30.30
103	mine	L-ZONE	6.7	7.28	148	530	7.9	63.80	32.70
1987:									
104	river	SOUTH				775		8.00	4.02
105	lake	SOUTH						7.10	2.63
106	spring	SOUTH				380		5.30	3.48
107	spring	SOUTH				380		5.60	2.63
108	lake	NORTHEAST				255		4.60	1.25
109	lake	NORTHEAST				330		6.60	1.55
110	lake	SOUTHWEST				280		1.90	1.04
111	snow	EAST				25		0.20	0.06

DH-#	ID	AREA	Na	K	Alk.	Cl	SO4	NO3	NO2	Charge Balance
55	lake	NORTHWEST	10.24	0.67	187	17.3	10.9	0.0	0.0	0.00
56	lake	NORTHEAST	6.83	0.41	79					
57	lake	NORTHEAST	5.77	0.49	128					
58	lake	NORTHEAST	6.53	0.54	177					
59	lake	NORTHEAST	5.49	0.34	34					
60	lake	NORTHEAST	5.48	0.35	69	5.2	1.0	0.0	0.0	0.01
61	lake	NORTHEAST	6.26	0.22	64					
62	lake	NORTHEAST	6.31	0.38	133					
63	lake	NORTHEAST	5.70	0.40	113					
64	lake	NORTHEAST	7.17	0.59	143					
65	lake	WEST	15.14	1.15	148					
66	lake	SOUTHWEST	15.70	1.23	217					
67	lake	SOUTHWEST	12.46	0.52	25					
68	lake	SOUTHWEST	10.13	0.56	25					
69	lake	SOUTHWEST	15.76	0.76	20					
70	lake	SOUTHWEST	15.34	0.81	20					
71	lake	SOUTH	13.63	2.06	236	22.8	48.2	0.0	0.0	0.10
72	lake	SOUTHEAST	7.20	0.53	94	9.0	2.7	0.0	0.0	0.02
73	lake	SOUTH	10.01	1.05	133					
74	lake	SOUTH	6.26	0.50	108					
75	lake	NORTH	7.77	0.52	148	10.4	39.0	0.0	0.0	0.06
76	mine	T-ZONE	470.30	26.80	207	756.0	173.4	0.0	0.0	0.02
77	mine	MID-DEPTH	206.90	17.00	226	348.0	140.0	0.0	0.0	0.03
78	mine	L-ZONE	14.43	2.32	231	21.1	13.3	0.0	0.0	0.44
79	well	NORTH	9.33	1.15	222	12.9	64.9	7.5	0.0	0.06
80	sump	NORTH	37.83	4.81	236	50.0	59.3	0.0	0.0	0.07
81	mine	L-ZONE	14.35	3.03	236	19.7	46.4	0.0	0.0	0.10
82	well	SOUTH	13.52	2.65	276	21.5	41.3	0.0	0.0	0.10
83	well	SOUTH	12.61	2.16	217	17.3	58.1	0.0	0.0	0.11
84	well	SOUTH	12.74	2.16	271	18.8	62.3	0.0	0.0	0.09
85	well	NORTH	9.38	1.10	202	12.5	73.8	29.8	0.0	0.34
86	well	WEST	23.08	9.45	261	18.6	14.5	0.0	0.0	0.04
87	well	NORTH	10.76	1.25	276	16.0	36.6	0.0	0.0	
88	well	NORTH	48.22	8.80	256	19.6	14.5	0.0	0.0	0.04
89	mine	T-ZONE	379.30	25.60						
90	mine	T-ZONE	79.40	12.40						
91	mine	T-ZONE	227.00	19.80						
92	mine	T-ZONE	103.10	12.40						
93	mine	T-ZONE	445.90	29.10						
94	mine	MID-DEPTH	33.38	4.66						
95	mine	MID-DEPTH	46.74	5.73						
96	mine	MID-DEPTH	23.00	5.98						
97	mine	L-ZONE	16.05	2.32						
98	mine	L-ZONE	91.25	9.35						
99	mine	L-ZONE	12.46	2.14						
100	mine	L-ZONE	16.81	2.99						
101	mine	T-ZONE	465.10	27.30	212	798.6	189.6	0.0	0.0	0.00
102	mine	MID-DEPTH	59.35	11.50	261	45.5	42.4	0.0	0.0	0.12
103	mine	L-ZONE	13.99	2.47	231	21.8	55.8	0.0	0.0	0.14
1987:										
104	river	SOUTH	77.10	9.42						
105	lake	SOUTH	13.00	1.35						
106	spring	SOUTH	8.70	1.36						
107	spring	SOUTH	17.40	1.74						
108	lake	NORTHEAST	7.90	0.66						
109	lake	NORTHEAST	8.00	1.10						
110	lake	SOUTHWEST	36.40	2.28						
111	snow	EAST	3.60	0.51						

Table 5.2 Trace-element analysis of groundwater samples from mine and environs done by ICP/MS in ppb. The minesump and tailings pond water samples were also analyzed. Trace elements are grouped according to their relationship with chloride (analyzed with HPLC in ppm). Group 1 elements show a positive correlation with Cl and group 2 have an inverse relation with Cl. Chloride concentrations are listed for comparison. Iron and strontium do not conform to these two groups. Refer to Table 5.1 for sample identification and location.

Terms are defined as follows: ND - not detectable
NA - not analyzed

		Group 1			Group 2			
DH-# ID	Cl	V	Rb	I	Zn	Mn	Co	Ni
1985:								
DH-001	8.4			2.5	9.4			
DH-002	17.0			3.0	12.5			
DH-003	12.0			3.0	20.8			
DH-004	48.0			2.7	18.2			
DH-005	180.0			3.6	11.7			
DH-006	329.0			4.8	12.0			
DH-007	717.0			4.9	12.7			
DH-008	354.0			5.0	11.4			
DH-009	25.0			3.1	16.9			
DH-010	23.0			2.3	20.1			
DH-011	35.0			4.1	16.9			
DH-012	988.0			4.9	17.2			
DH-013	41.0			2.1	15.5			
DH-014	210.0			3.7	13.0			
DH-015	19.0			1.9	8.7			
DH-016	20.0			2.8	11.8			
DH-017	11.0			1.7	11.3			
DH-018	11.0			1.9	ND			
DH-019	9.6			1.2	10.4			
DH-020	25.0			3.4	18.2			
DH-021	9.2			1.2	9.3			
DH-022	5.1			0.2	10.4			
DH-023	0.5			ND	ND			
1986:								
DH-025	10.4	0.3	0.8	0.8	1986.0	28.5	2.3	43.9
DH-026	125.2	1.3	3.4	2.4	51.3	0.4	1.1	13.5
DH-027	20.8	0.2	1.9	1.4	239.1	7.6	1.5	14.8
DH-028	18.2	0.2	0.9	1.4	144.8	0.3	0.7	10.3
DH-029	10.2	0.1	1.0	0.8	3428.1	7.2	2.3	40.4
DH-030	320.4	2.9	6.4	6.5	8.1	1.2	0.6	10.8
DH-031	18.7	0.3	0.9	1.6	618.3	0.6	0.5	10.8
DH-032	39.1	0.4	2.1	10.9	168.2	59.8	1.7	15.5
DH-033	790.8	6.7	11.1	15.8	8.7	0.6	0.5	8.6
DH-034	258.9	2.3	6.3	4.4	5.3	4.8	0.4	7.1
DH-035	114.6	1.1	6.5	3.2	2.9	0.6	0.3	6.5
DH-071	22.8	0.5	1.3	2.9	433.1	8.1	1.0	14.7
DH-076	756.0	6.3	11.0	14.0	58.4	1.9	0.6	12.0
DH-077	348.0	3.5	7.1	8.5	25.1	1.2	0.7	12.6
DH-078	21.1	0.3	1.4	2.5	381.3	0.3	0.7	15.6
DH-079	12.9	0.4	1.0	3.5	248.6	48.0	2.4	13.8
DH-080	50.0	0.6	2.4	2.4	478.2	9.1	1.1	14.9
DH-081	19.7	0.3	2.6	4.7	142.3	43.2	3.2	15.2
DH-082	21.5	0.6	1.6	4.2	1199.3	34.6	1.4	61.3
DH-083	17.3	0.4	1.4	2.0	1471.0	33.4	4.2	52.5
DH-084	18.8	0.5	1.4	2.0	841.6	34.1	2.3	28.1
DH-085	12.5	0.9	1.1	2.3	3756.8	36.6	1.8	80.7
DH-086	18.6	0.2	3.3	3.2	11.3	8.6	0.4	5.8
DH-087	16.0	0.8	1.1	1.4	4457.3	37.0	6.5	286.5
DH-088	19.6	0.2	3.8	1.5	11.1	12.4	0.3	5.7
DH-101	798.6	7.3	11.6	20.6	406.0	2.3	0.8	30.0
DH-102	45.5	0.6	5.2	2.0	430.4	1.0	0.6	27.7
DH-103	21.8	0.3	1.5	2.6	864.2	0.8	0.9	39.2

		Group 2						
DH-# ID	Cl	Mo	Cd	Ba	Pb	U	Fe	Sr
1985:								
DH-001	8.4	ND		18.7		ND		17.2
DH-002	17.0	ND		21.9		ND		32.7
DH-003	12.0	ND		22.6		ND		25.1
DH-004	48.0	21.8		24.2		10.3		29.8
DH-005	180.0	ND		20.3		ND		34.5
DH-006	329.0	ND		19.7		ND		36.6
DH-007	717.0	ND		18.8		ND		37.0
DH-008	354.0	ND		21.3		ND		35.9
DH-009	25.0	22.8		21.6		10.7		31.6
DH-010	23.0	23.3		24.3		10.7		31.6
DH-011	35.0	20.7		25.8		10.1		29.4
DH-012	988.0	ND		19.1		ND		36.3
DH-013	41.0	20.2		22.3		10.2		29.6
DH-014	210.0	18.2		21.9		9.3		32.0
DH-015	19.0	ND		20.2		ND		18.3
DH-016	20.0	ND		21.6		ND		26.2
DH-017	11.0	ND		15.1		ND		16.4
DH-018	11.0	ND		16.0		ND		16.3
DH-019	9.6	ND		19.9		ND		16.7
DH-020	25.0	23.1		24.5		10.4		31.2
DH-021	9.2	ND		19.9		ND		18.0
DH-022	5.1	ND		13.6		ND		15.2
DH-023	0.5	ND		ND		ND		ND
1986:								
DH-025	10.4	2.0	0.3	48.1	4.9	13.7	4329	71.5
DH-026	125.2	5.1	0.3	54.0	0.6	3.4	2194	435.1
DH-027	20.8	8.4	0.1	149.3	1.5	5.6	NA	136.8
DH-028	18.2	2.1	0.2	74.1	0.3	2.2	1618	51.5
DH-029	10.2	10.3	1.7	108.3	0.3	16.1	2763	72.9
DH-030	320.4	0.9	0.0	33.4	0.4	0.4	2287	1039.7
DH-031	18.7	2.8	0.8	76.6	0.5	4.0	1706	54.6
DH-032	39.1	4.3	0.2	160.5	1.3	4.7	2339	250.8
DH-033	790.8	0.1	0.1	11.6	0.4	0.4	1916	NA
DH-034	258.9	0.4	0.0	199.9	0.5	1.2	1610	988.7
DH-035	114.6	0.8	0.0	32.6	0.5	0.5	1137	NA
DH-071	22.8	5.3	0.5	117.9	2.2	5.5	2072	128.8
DH-076	756.0	0.1	0.3	12.0	2.9	0.4	1864	NA
DH-077	348.0	0.9	0.3	36.6	4.5	0.5	2472	1145.6
DH-078	21.1	6.8	1.4	95.8	11.4	7.0	2081	201.9
DH-079	12.9	28.5	0.9	68.6	15.7	5.8	2600	57.5
DH-080	50.0	5.7	0.4	108.2	0.5	4.5	1963	326.3
DH-081	19.7	6.0	0.3	107.4	1.1	5.5	1916	290.1
DH-082	21.5	4.1	2.1	133.2	29.1	3.9	2573	235.9
DH-083	17.3	20.1	2.3	105.8	26.2	47.7	2336	189.3
DH-084	18.8	7.0	2.1	195.2	30.6	11.2	3055	243.3
DH-085	12.5	4.1	3.1	514.0	158.0	6.7	3959	47.3
DH-086	18.6	0.6	0.0	261.5	0.3	0.3	1320	247.3
DH-087	16.0	7.7	2.6	297.2	142.0	14.1	3014	39.9
DH-088	19.6	0.6	0.0	204.1	0.3	0.2	1212	282.4
DH-101	798.6	NA	0.5	15.0	4.0	0.4	2121	NA
DH-102	45.5	NA	0.5	29.2	3.6	0.2	1309	1046.0
DH-103	21.8	7.0	1.5	107.3	5.2	7.7	2093	222.1

Table 5.3 Available environmental isotope data for selected samples. Also listed is the chloride concentration for comparison. Precision for 1986 tritium and carbon-14 measurements is +/- 7 T.U. and +/- 2% modern carbon, respectively. Detection limit and precision for 1985 analyses are 1 T.U., +/-0.8 T.U., respectively. Additional deuterium analyses for samples: DH-18,29, 30, 84, 35, 76 were done at Memorial University in 1988.
Symbols and short form explanations:

* = contamination suspected,
** = C-13 analysis for DH-25 = -7, DH-27 =-11.4 and DH-85 = -9.8 $^{o}/oo$
DIC = dissolved inorganic carbon as ppm HCO_3.

Refer to Table 5.1 for sample identification and sample location.

DH-#	Cl ppm	2H o/oo	18O o/oo	13C o/oo	DIC ppm	Tritium T.U.	C-14 %modern carbon
1985:							
DH-01	8.4		-9.0				
DH-02	17.0		-10.0				
DH-03	12.0		-10.3				
DH-05	180.0		-10.0			7	
DH-06	329.0		-10.2			1	
DH-07	717.0		-10.4			1	
DH-08	354.0		-10.1				
DH-09	25.0		-9.7			7	
DH-10	23.0		-9.5				
DH-11	35.0		-9.9			25	
DH-12	988.0		-10.5			38 *	
DH-13	41.0		-9.6				
DH-14	210.0		-10.1				
DH-15	19.0		-8.7				
DH-16	20.0		-9.2				
DH-17	11.0		-5.4				
DH-18	11.0	-74.1	-7.8				
DH-19	9.6		-7.3				
DH-20	25.0		-9.2				
DH-21	9.2		-9.7				
DH-22	5.1		-11.1				
DH-23	0.5		-12.3				
1986:							
DH-25	10.4	-75.1	-9.7			29	29 **
DH-26	125.2	-76.9	-10.1	-10.2	235	36	
DH-27	20.8	-75.1	-9.4	-7.2	195	20	58 **
DH-28	18.2		-9.9	-9.1	188		
DH-29	10.2	-75.8	-8.8				
DH-30	320.4	-79.0	-10.1	-5.7	179		
DH-31	18.7		-11.3	-12.5	246		
DH-32	39.1		-9.7	-10.6	295		
DH-33	790.8	-75.9	-9.7	-7.4	211	22	
DH-35	114.6	-77.1	-10.2	-5.8	192		
DH-76	756.0	-72.5	-9.0	-5.7	211		
DH-77	348.0	-76.4	-9.8	-11.7	180	14	
DH-78	21.1	-75.0	-8.5	-8.0	194	32	
DH-79	12.9		-10.0				
DH-80	50.0		-10.2				
DH-81	19.7		-9.8				
DH-82	21.5		-9.6				
DH-83	17.3	-74.3	-9.9			33	
DH-84	18.8	-80.0	-9.9				
DH-85	12.5	-80.8	-11.1			41	60 **
DH-87	16.0		-10.4				
DH-88	19.6		-10.2				
DH-101	798.6		-10.5	-7.6	214		
DH-102	45.5		-10.6				
DH-103	21.8		-9.4	-7.2	231		
1987:							
DH-104			-10.1				
DH-106			-10.0				
DH-107			-10.1				
DH-111			-14.0				

The range of observed calcite-saturation indices in lakes and groundwaters is shown in Figure 5.1. These indices are defined as: $SI = IAP/K_{sp}$, where IAP is the ion activity product and K_{sp} is the solubility product for calcite at the measured temperature. $SI < 1$, $= 1$ and >1 indicate the groundwater is undersaturated, in equilibrium with, and supersaturated with calcite, respectively. The saturation indices for groundwaters and lake waters were estimated from carbonate chemistry and assumed activity coefficients of unity. Major assumptions in the indices' estimation will be discussed in Section 5.5.1.2 and refined values based on chemical speciation modelling for groundwater samples only will be presented in Section 5.5.1.1.

5.3 Chemical Characterization of Waters

5.3.1 Major ion and carbonate chemistry

The percentage of each major constituent was calculated (equivalents per million) and plotted on a standard trilinear diagram (Piper, 1944), (see Figure 5.2). In all three areas of the diagram seawater composition is given as a reference. Most lake waters and groundwaters from wells are of the calcium-magnesium bicarbonate type whereas the mine groundwaters range from a calcium-magnesium-bicarbonate type to a sodium-chloride +/- sulphate type. This diagram shows chemical trends in mine groundwaters which reflect the dissolution of limestone and dolostone and the mixing of this water with a more saline endmember. Some samples lie outside the fields defined by the

Figure 5.1 Estimated calcite-saturation indices (S.I.) are shown as frequency histograms for A) lake water and B) groundwater samples. S.I.(calcite) = mCa x mCO_3/ K_{sp} $CaCO_3$, assuming activity coefficient = 1. Groundwater in equilibrium with calcite has S.I.=1.

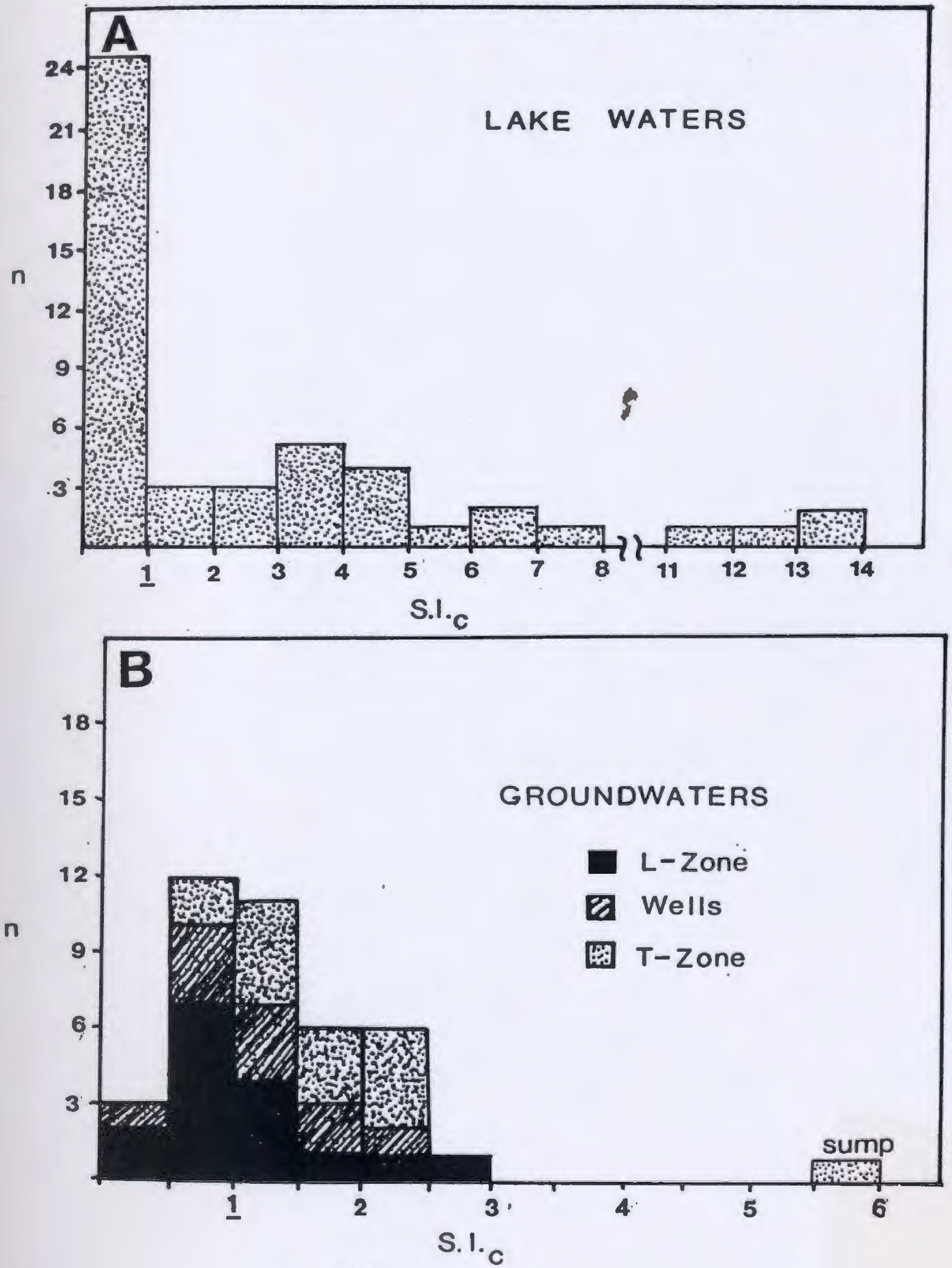

Figure 5.2 Major ion analyses are represented as percentages of total equivalents per million (epm) on this standard trilinear diagram (Piper, 1944). EPM is defined as ppm/gew, and gew is the gram equivalent weight (gram formula weight/valence). Seawater composition is indicated on each plot. Note that mine waters are scattered between well and seawater compositions. Some of the lake waters lie in two distinct fields outlined in the anion plot as having high Cl and SO_4 concentrations (see discussion for Figure 5.12).

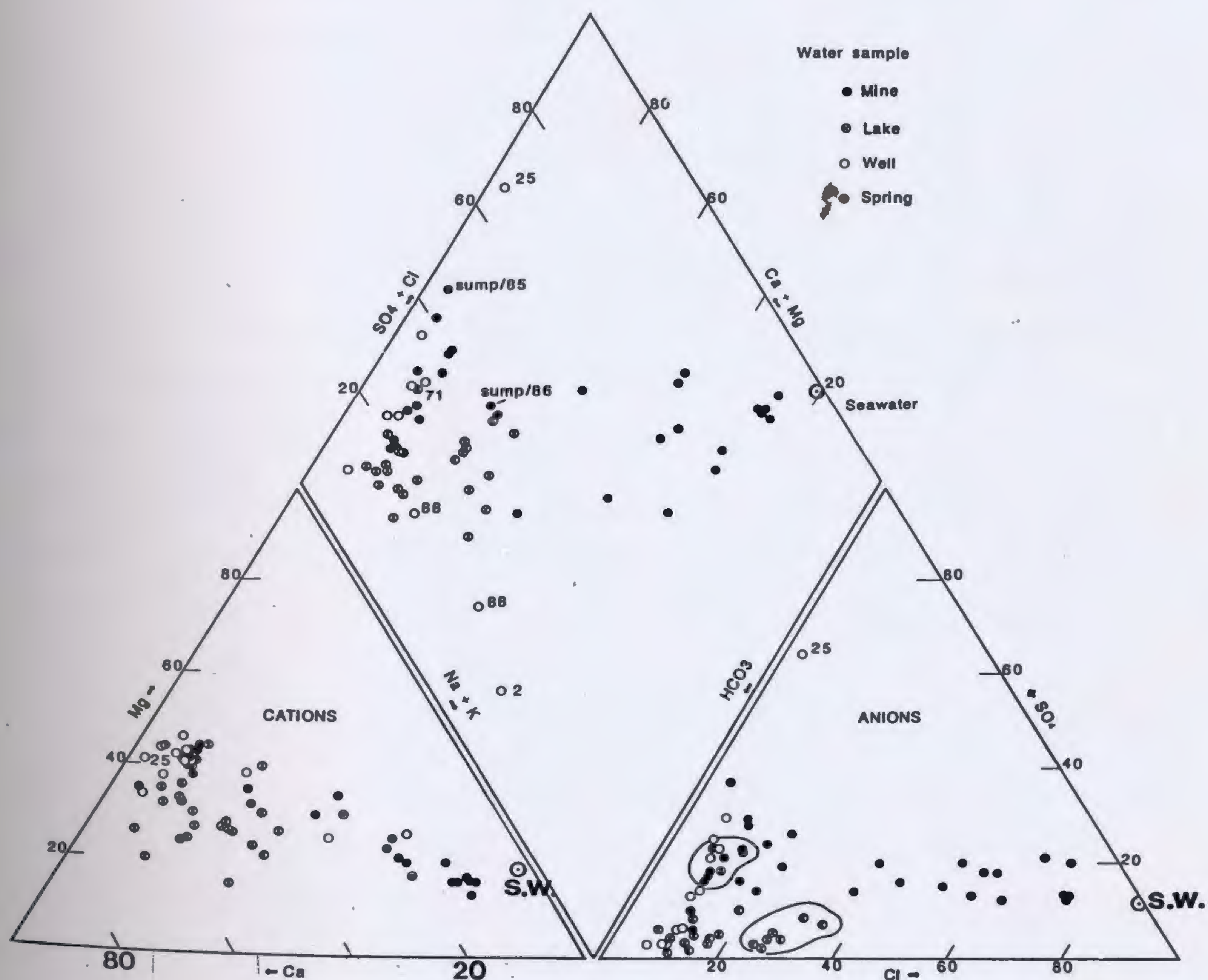

majority of samples. Saline groundwaters are typically enriched in both sulphate and chloride but the high percentage of sulphate in DH-25 is not associated with a chloride increase. DH-88, DH-86 and DH-02 are high in sodium without a corresponding high chloride concentration.

Mine samples show the greatest range in chloride content (10-988 ppm) and generally the deepest mine samples have the highest concentrations of Cl^-, Na^+, and K^+ (Table 5.1), indicating an increase in dissolved salt load with depth (see Figure 5.3). High chloride levels at mid-depths (-40 m a.s.l., see Figure 5.3) in samples DH-26,14 and DH-30,77 (deep drill hole, see Appendix B) may indicate a zone of increased permeability connecting this mid-zone depth to deeper mine waters, resulting in more mixing between shallow and deep groundwaters. DH-12 has the highest salt load and thus the greatest contribution of deep saline groundwater. Local dissolution of known occurrences of gypsum and celestite in vugs (Coron, 1982; see Figure 3.2) may be a source of high salinities in DH-26,77 and is supported by high Sr in these samples (see Table 5.2). These soluble minerals will be henceforth referred to as sulphates for convenience. Road salt may be responsible for high Na and Cl in DH-14 but does not explain the low salt content in groundwaters from the L-Zone decline where the road salt was applied. High sulphate in deep groundwaters rules out road salt as a source of T-Zone salinity.

The fact that saline waters are found at a certain depth in

Figure 5.3 The depth of mine groundwater sampling sites has been plotted against chloride concentration. Samples 30 and 77 were collected from a deep drill hole that extends several hundred feet below the indicated collar elevation. The uncertainity in depth of groundwater source is shown by arrows under these samples. Generally, chloride concentration increases with depth.

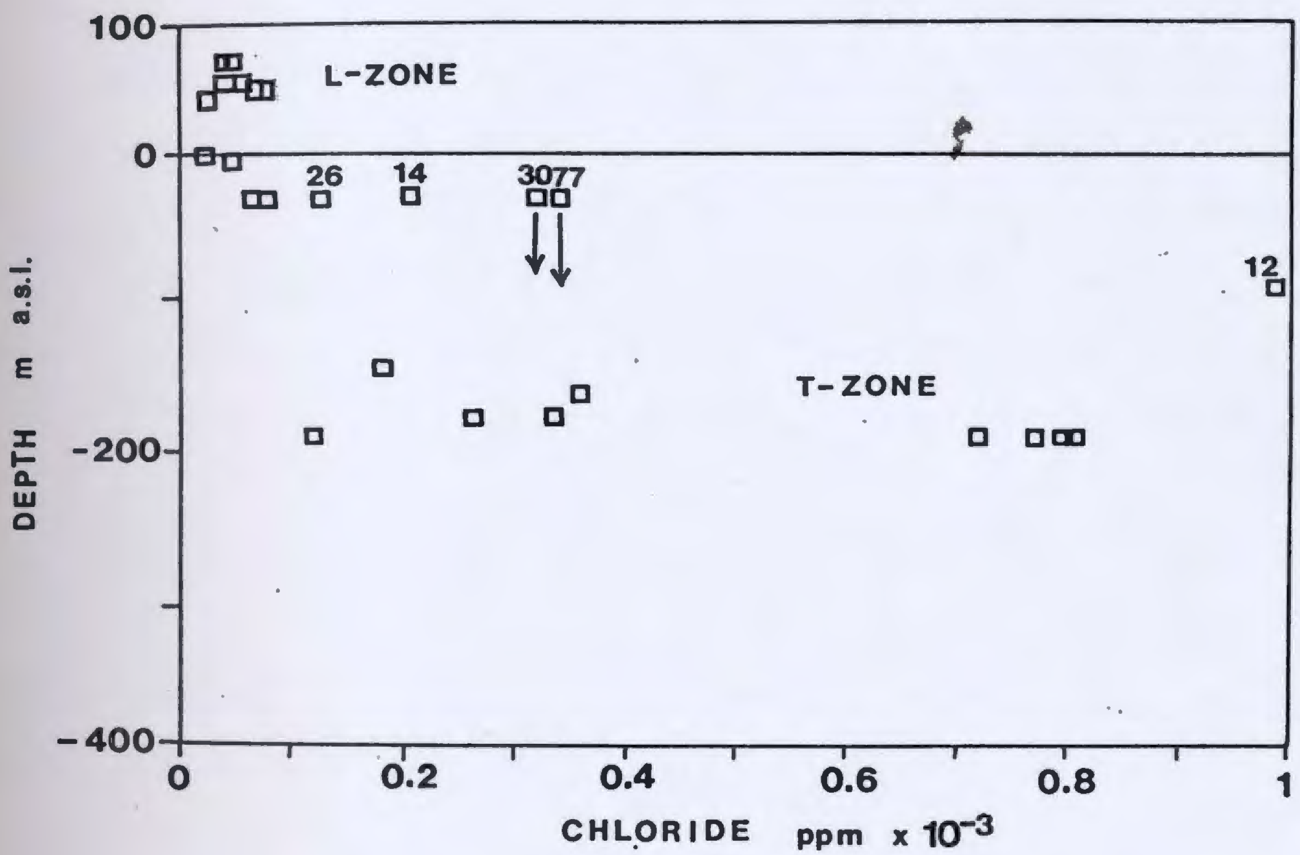

the mine implies that there is a saline water zone in this aquifer. Depth to the saline water zone is probably highly variable between localities due to the anisotropy of the aquifer, mixing of waters, and depression of the water table due to mine dewatering. However, chloride and dissolved oxygen concentrations found in the mine show that saline, near to and reducing groundwaters (>100ppm chloride and no detectable dissolved oxygen) were first intersected beneath the L-Zone workings, at about 100 m below sea level or about 175m below ground surface (see Figure 5.3 and 5.4). This depth is further substantiated by geophysical work done on N-Zone drill holes (see Figure 3.2). Saline waters were suspected to have caused a large offset in the spontaneous potential logs at 116m below ground surface or 25 m below sea level (J. Mwenifumbo, pers. comm.; 1986). Very saline water (up to 3600 ppm Cl) has been recently found in deep artesian exploration boreholes 3 km west of the mine, indicating that saline waters occur at depth, over a wide area beneath the study region. The saline interface may represent a boundary between a local (dilute) and regional (saline) groundwater flow system which may extend over a wide area.

Mine and well waters tend to have higher levels of calcium than lake waters. Calcium content gradually increases with chloride content (see Figure 5.5). This trend may be due to the ionic-strength effect whereby deeper salt-rich groundwater of higher ionic strength causes a decrease in the activity of each

Figure 5.4 The depth of sampling site vs dissolved oxygen graph shows a decrease in D.O. content with deeper sampling location.

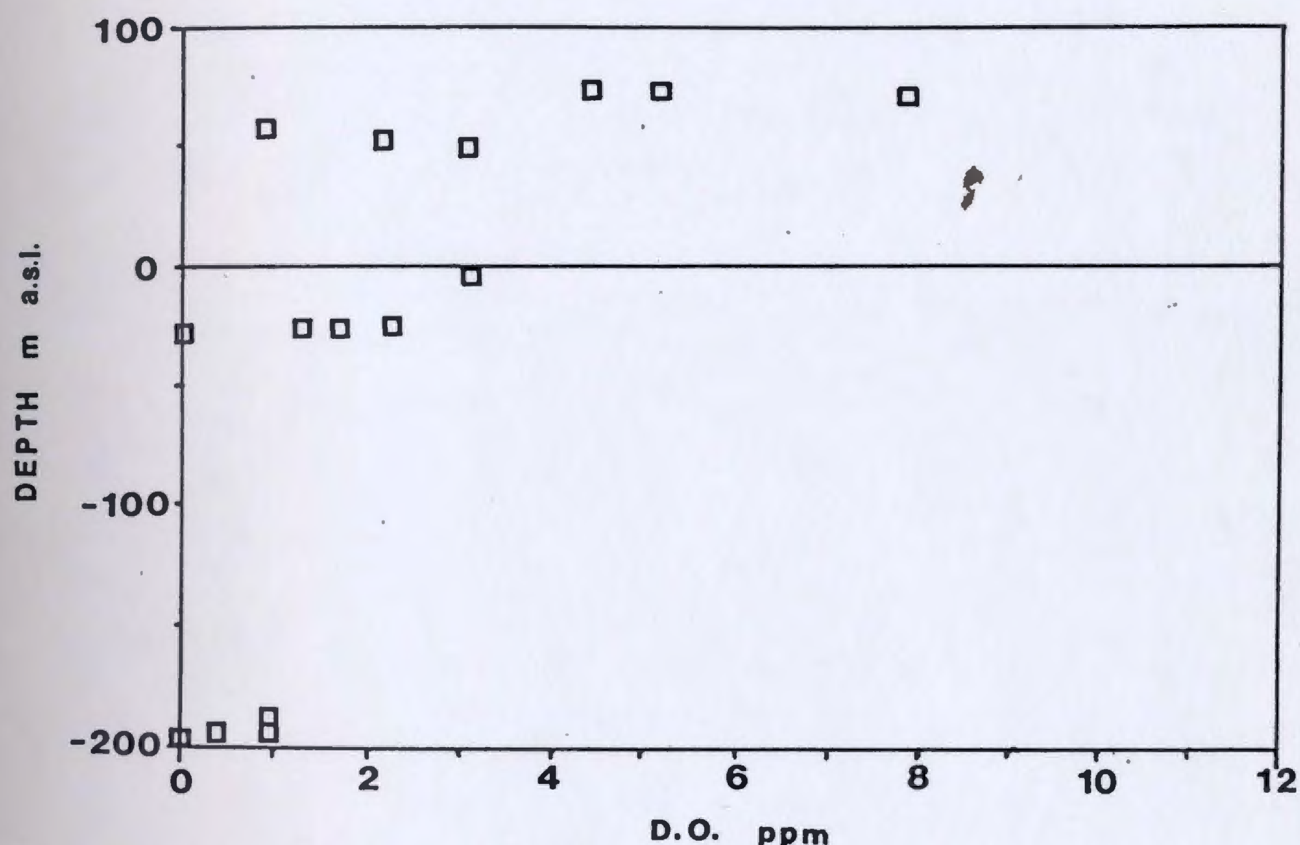

Figure 5.5 This plot shows a general increase of calcium with chloride concentration for the mine-water samples. Lake waters appear to be a mixture of rainwater (little Ca) and shallow groundwater. Some well samples have very high concentrations of Ca. Spring Lake and the mine sump are also indicated.

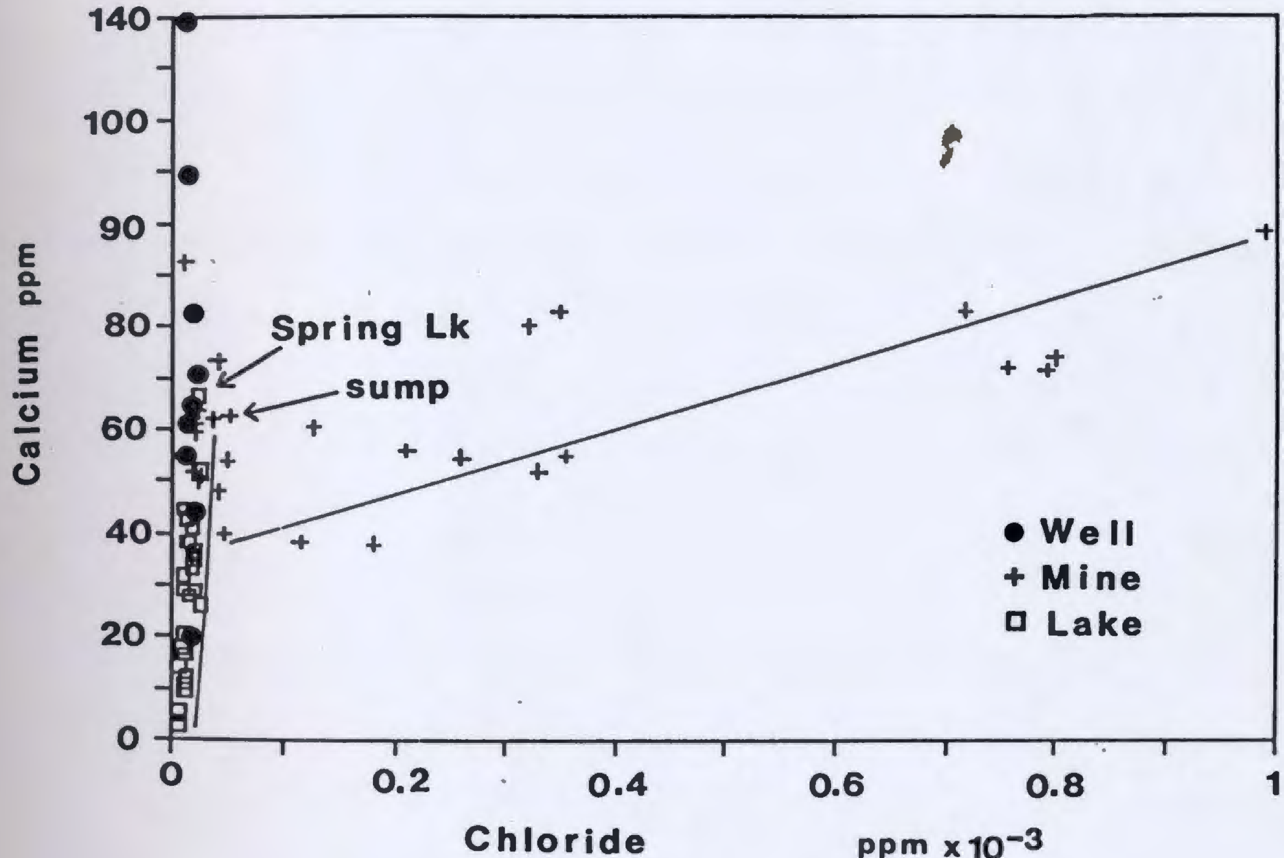

ion in the solution and thus more carbonate minerals can be dissolved until equilibrium with calcite is attained (Back and Hanshaw, 1970). Calcium may also be increased in deeper waters even after equilibrium with calcite is reached by the dissolution of Ca-bearing silicate minerals such as anorthite.

A typical shallow groundwater composition is displayed in Figure 5.6, based on the average of all shallow groundwater samples except the anomalous groundwaters (DH-25, 29, 85) and the flowing artesian wells (DH-86, 88). DH-25 is unique in that it has low sodium/chloride and high sulphate contents (Figure 5.6). Samples DH-85 & DH-29 also have higher calcium and sulphate concentrations than the average shallow groundwater. These wells may have acquired sulphate by extensive bacterial oxidation of sulphides (Hoag and Webber, 1976a), which is supported by their very high Zn concentrations (>2000 ppb), or by dissolution of minerals such as gypsum.

Flowing artesian wells DH-86 (plotted on Figure 5.6) and DH-88 differ slightly from other shallow groundwaters in that they have elevated Na and K concentrations that are possibly related to ion exchange effects. The area is located in a poorly drained mud plain with sand and compact subsurface till (Proudfoot and St. Croix, 1987), and ion exchange may occur between clay in the till and carbonate groundwater. The similarity in chemistry between DH-86, 88 and DH-02 (1985 flowing artesian well) illustrates the homogeneity of this discharge zone (about 700 m between wells).

Figure 5.6 Relative concentrations of major ions have been plotted on this percent of maximum concentration vs ion plot for shallow groundwater samples that deviate from the average shallow groundwater composition (shown on graph by patterned double line). DH-25 (dashed line) has higher than average Ca^{2+} & SO_4^{2-} concentrations whereas DH-86 (dotted line) has a high K^+ concentration.

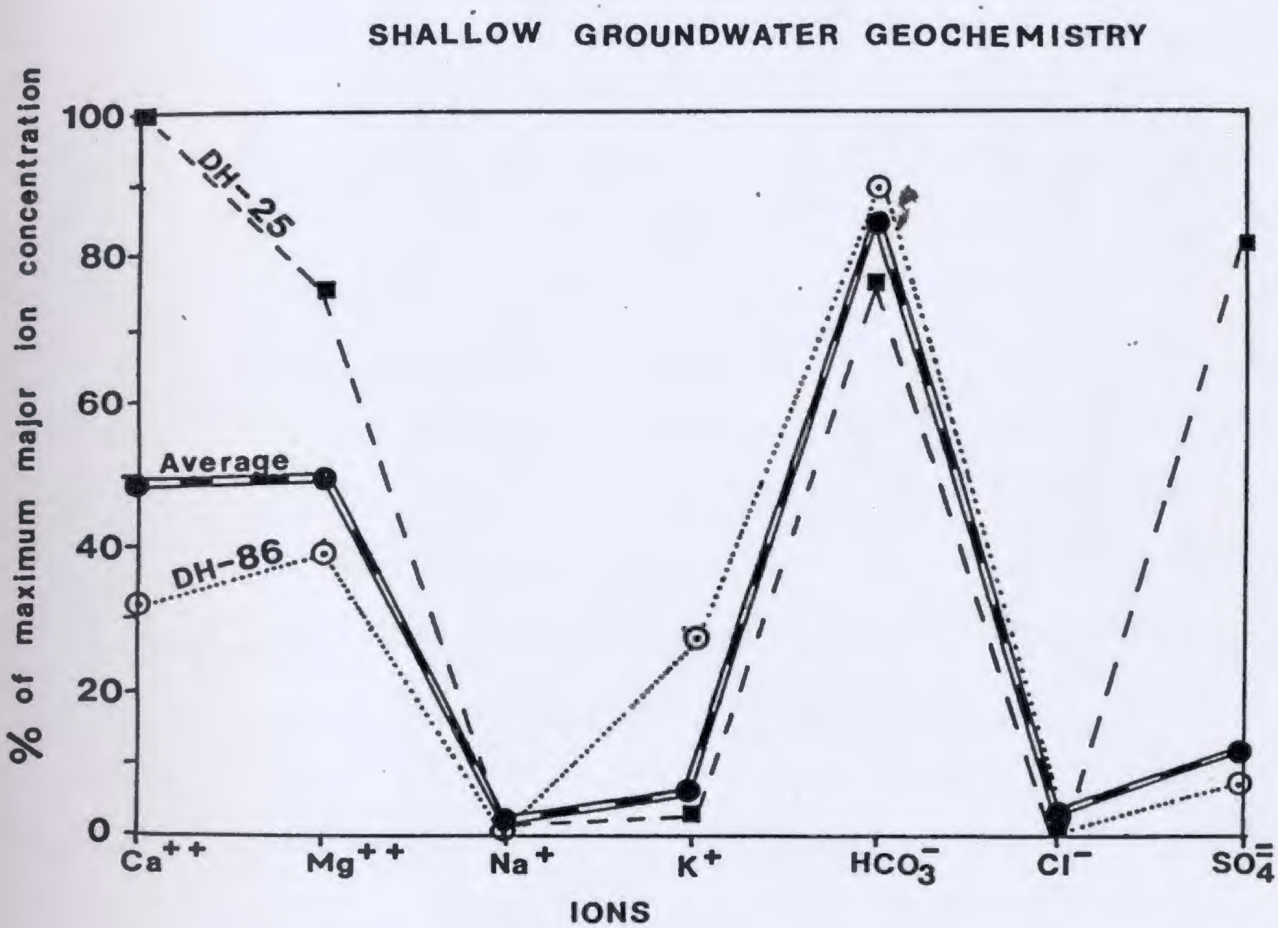

Figures 5.7 and 5.8 exhibit the mixing relations between water types shown in Figure 5.2. Surface water samples (lakes) result from a two component mixture of rainwater (DH-23 at essentially the origin in Figures 5.7 and 5.8) and dilute shallow groundwaters. Mine waters result from a mixture of these shallow groundwaters and a presumed deeper water with high salt content. These mixing trends are manifested in all major ions (eg: see Figure 5.8).

A distinct separation between 1985 and 1986 mine conductivity data is shown in Figure 5.7. Cross-checks between instruments showed measurements were consistently 400-500 umhos/cm higher for the 1985 meter than for the 1986 meter (See Section 2.1.3). The sulphate vs chloride plot (Figure 5.8) shows a similar separation of data and indicates that mine groundwaters sampled in 1985 were indeed more concentrated than groundwaters sampled in 1986, but measurement error can only account partially for the differences illustrated in Figures 5.7 and 5.8. The spread of data in Figure 5.8 suggests the additional possibility that the distinction between 1985 and 1986 water chemistry represents a sampling bias to high sulphate waters that were sampled more often in 1985. This is possible since deep groundwaters sampled in 1985 and 1986 were collected from different sites.

The low sulphate content of DH-08 measured in 1985 (see Figure 5.8) may indicate that multiple sulphate-producing mechanisms are operating in the shallow groundwaters. Much of

Figure 5.7 Conductivity (umhos/cm) vs chloride plot for 1985 and 1986 water samples. Symbols apply to both Figures 5.7 and 5.8. Two types of mixing trends are shown: one for Cl contents <25 ppm, represented by lake waters which are a mixture of rainwater and shallow groundwater and the second for Cl contents >25 ppm whereby mine groundwaters represent a mixture of dilute shallow groundwater and more saline groundwater. There are higher conductivities reported for 1985 samples than for 1986 samples.

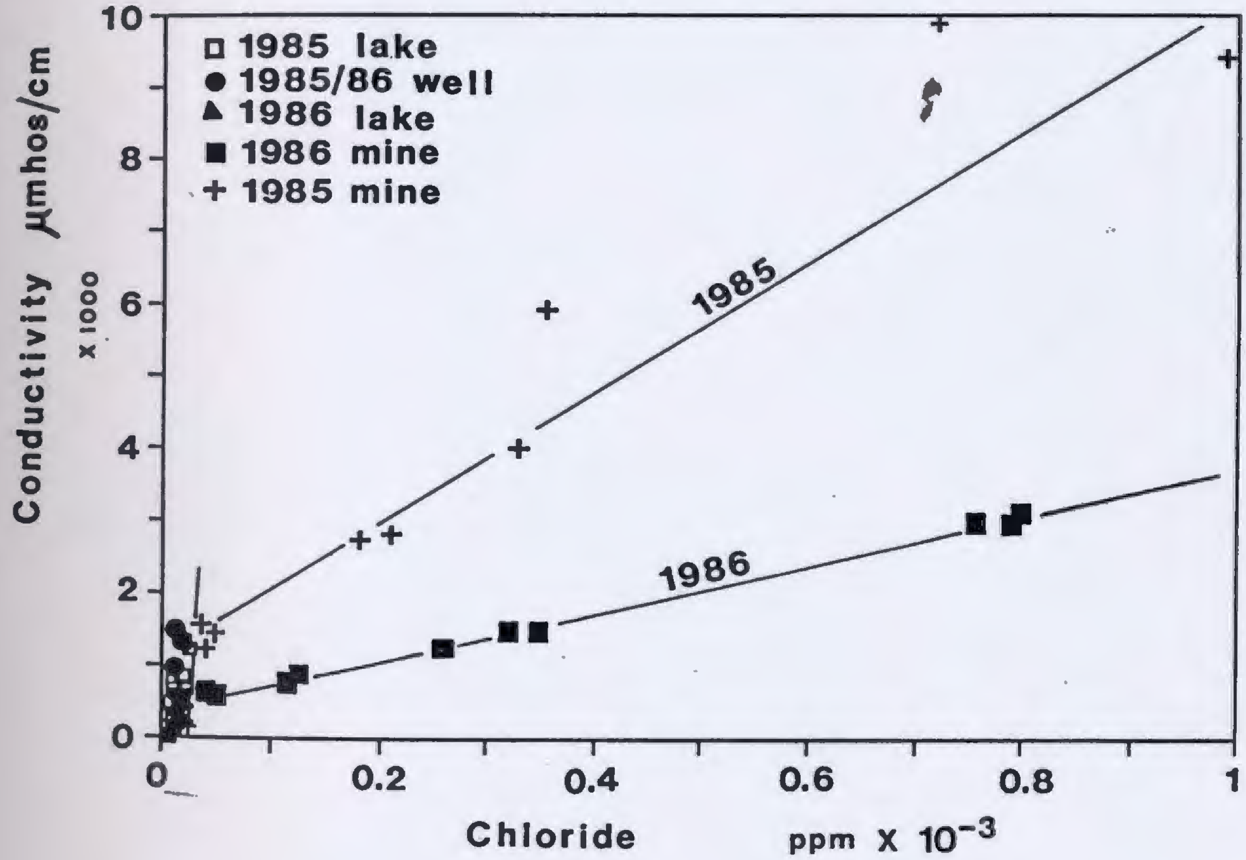

Figure 5.8 Sulphate vs chloride plot for 1985 and 1986 water samples. The same mixing trends as in Figure 5.7 are exhibited in this figure. Differences between 1985 and 1986 shown in Figure 5.7 are illustrated in this figure with some scatter (eg. DH-08).

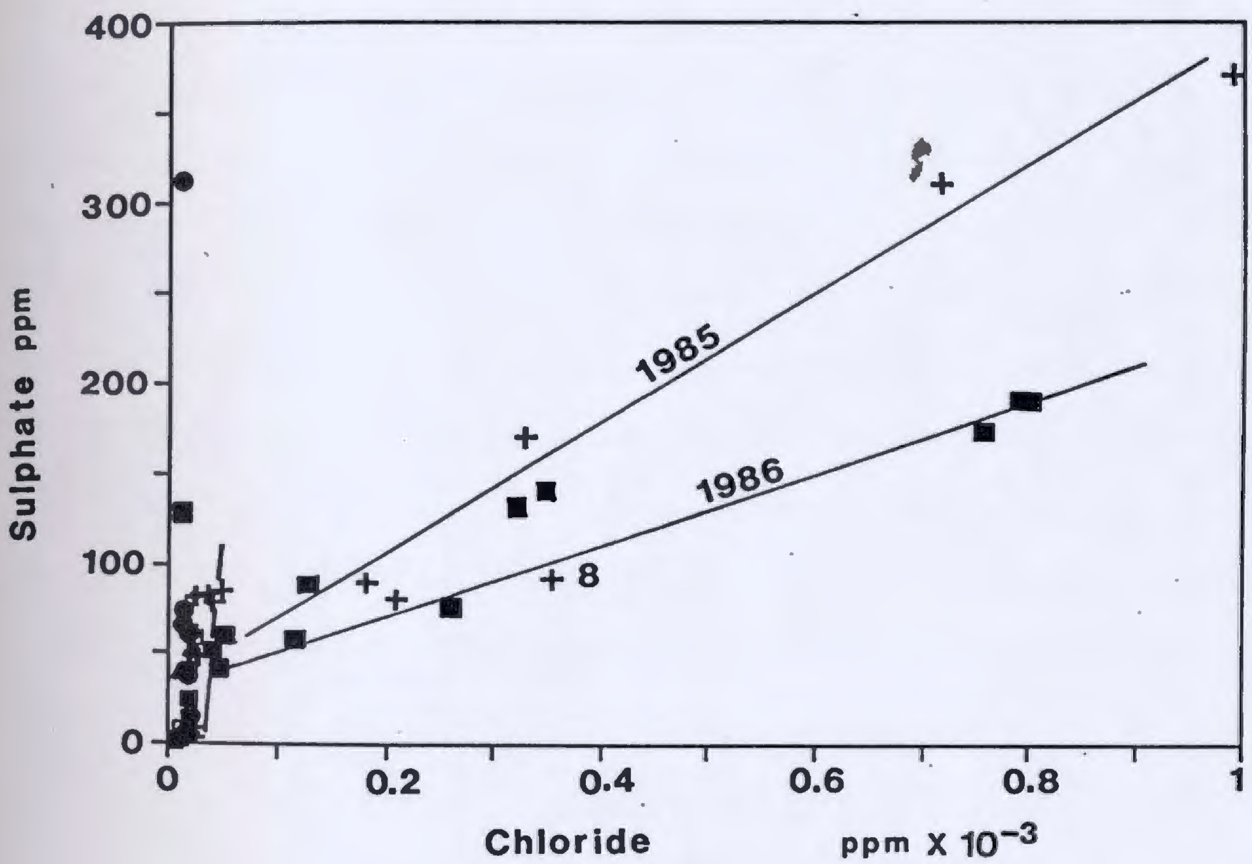

the sulphate in deeper groundwaters is not derived from sphalerite oxidation since high sulphate concentrations are found only in deep reducing mine waters and not in the shallow parts of the mine where known sphalerite orebodies and oxidizing conditions exist.

All waters range in pH from 6.76 to 8.94 for 1985/1986. The widest range is found in the surface water samples (Figure 5.9). Mine samples range in pH from 7.13 to 7.88 with a range of 7.4 to 7.8 in the deep mine waters (Figure 5.9). The high buffering capacity of the carbonate rocks prevents the development of acid-mine drainage because H^+ ions produced in sphalerite oxidation are consumed by dissolution of carbonate rocks.

The bicarbonate content is represented by the alkalinity at these pH's. Figure 5.10 shows the mixing trend of 1985/1986 lake waters between rain water and groundwater compositions. The data show good reproducibility of lake water analyses from year to year, particularly for the alkalinity measurements. The widening of the lake chemistry field (see Figure 5.10) as it approaches the groundwater composition may reflect groundwater contribution from different flow systems with characteristically different calcium and bicarbonate concentrations.

Figure 5.11 demonstrates the combined effect of rainwater-groundwater mixing (varied Ca concentration) and the loss of CO_2 (causing supersaturation). Discharging groundwaters (with high pCO_2) equilibrate with the atmosphere at lower pCO_2, causing the pH to rise. The discharged water thus becomes supersaturated

Figure 5.9 Water samples from 1985 and 1986 show buffering of deeper groundwaters by the carbonate rocks at pH 7.4 -7.8. Surface water samples (<50 ppm Cl) show the widest pH range.

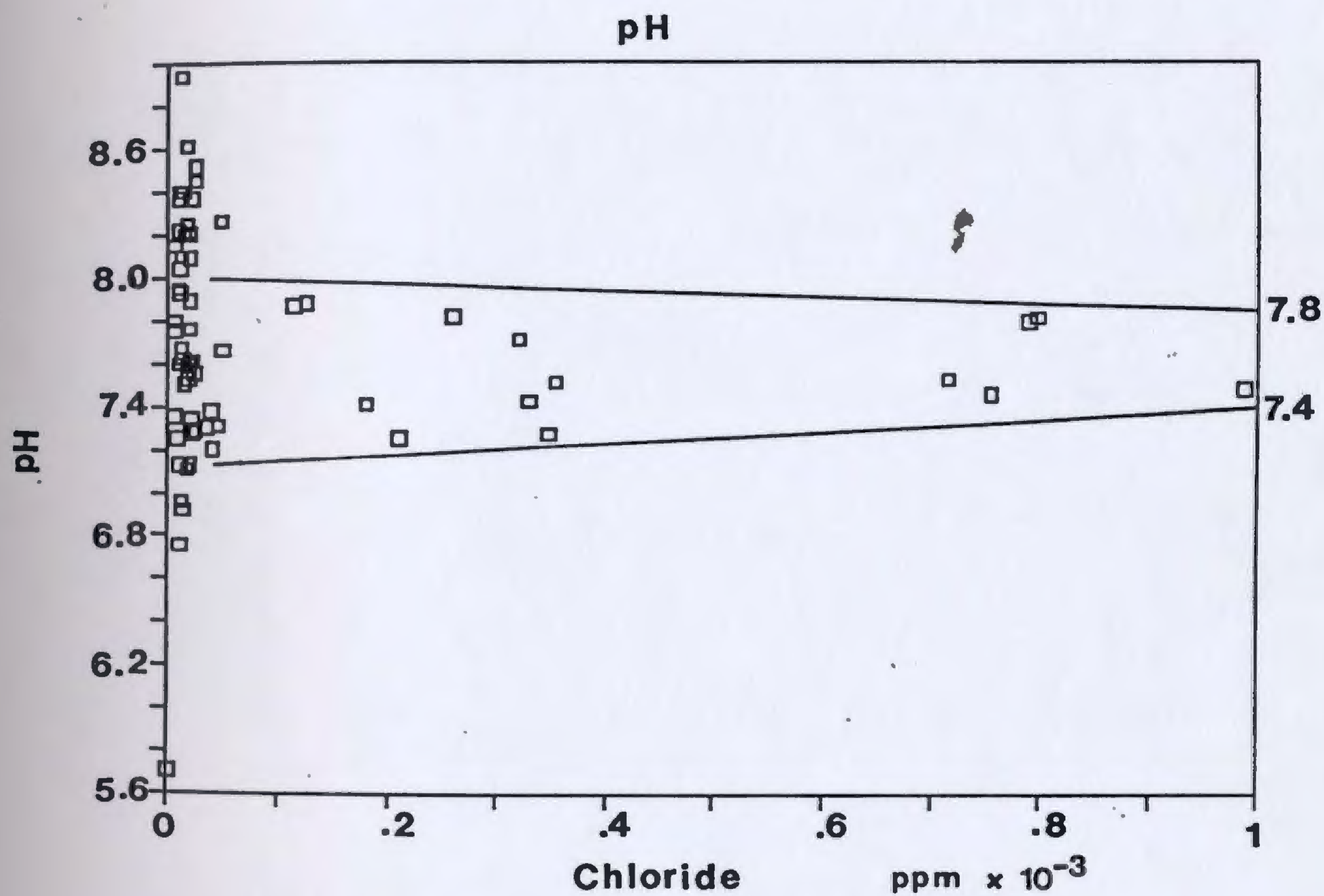

Figure 5.10 Alkalinity vs calcium plot for 1985 and 1986 data. Groundwaters fall into a distinct field and the arrow indicates increasing groundwater contribution to the lakes. Lake chemistry is the result of mixing of rainwater with groundwater. Sump discharge is a mixture of all mine groundwaters.

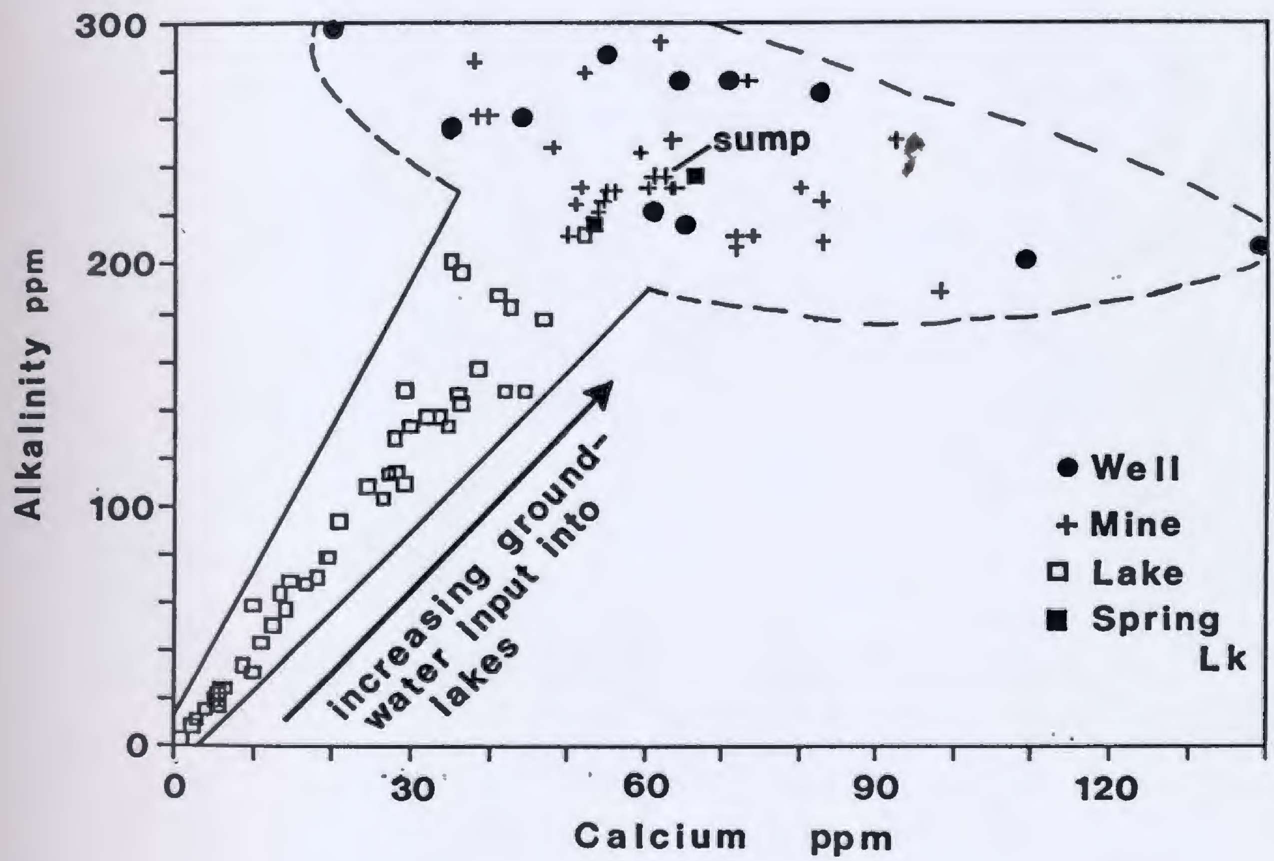

Figure 5.11 The trend seen in this plot (S.I.calcite vs Ca) is a result of the combined effects of groundwater input and CO_2 loss on lake-water chemistry. Lakes with greater groundwater input have high saturation indices. The solid line indicates calcite saturation.

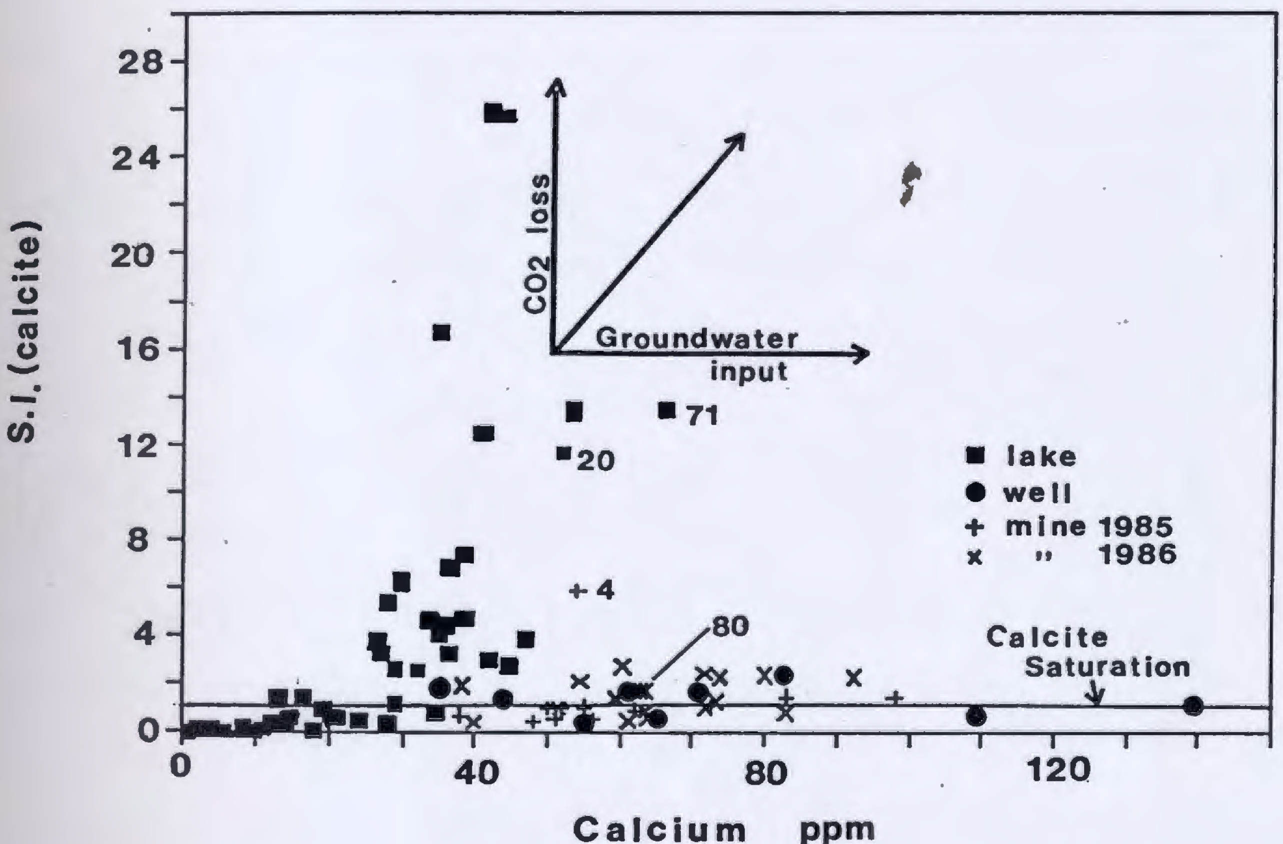

with respect to calcite and dolomite. Therefore, lakes with high saturation indices have large groundwater inputs. The sump discharge for both years (DH-04, DH-80) is supersaturated with respect to calcite and dolomite because of CO_2 loss during pumping and outflow.

Spring lake (20,71) and the mine sump (4,80) have very similar major-ion chemistry and plot near each other on major-ion graphs (see Figure 5.5, 5.10 and 5.11). Minesump water has only slightly elevated values of Na, K, Cl, and SO_4 indicating a major contribution from the shallow L-Zone and a minimal contribution from the T-Zone. The sump and Spring lake are both supersaturated with respect to calcite (Figure 5.11). This is because much of the mine outflow is discharged into Spring lake.

Lake calcite saturation indices used to construct the histogram in Figure 5.1A are displayed on a regional map of the study area in Figure 5.12. For the most part lakes supersaturated with respect to calcite occur near the coast as well as down-gradient from the mine and are classified as discharge lakes, whereas near the Long Range Mountains (regional recharge areas) only low saturation indices are observed. Lakes with marl bottom sediment are all calcite supersaturated except DH-36 (see Section 3.5). On the basis of their chemical compositions, lakes near the coast contain water derived mainly from local flow systems and not from deeper saline waters of a presumed regional flow system. However, all lakes with relatively high concentrations of SO_4 and Cl (circled in Figure

Figure 5.12 Regional map of the study area showing calcite saturation indices of lakes sampled in 1986. Most supersaturated lakes are concentrated in an area within 8-10 km from the coastline indicating this is a groundwater discharge area, possibly for regional flow.

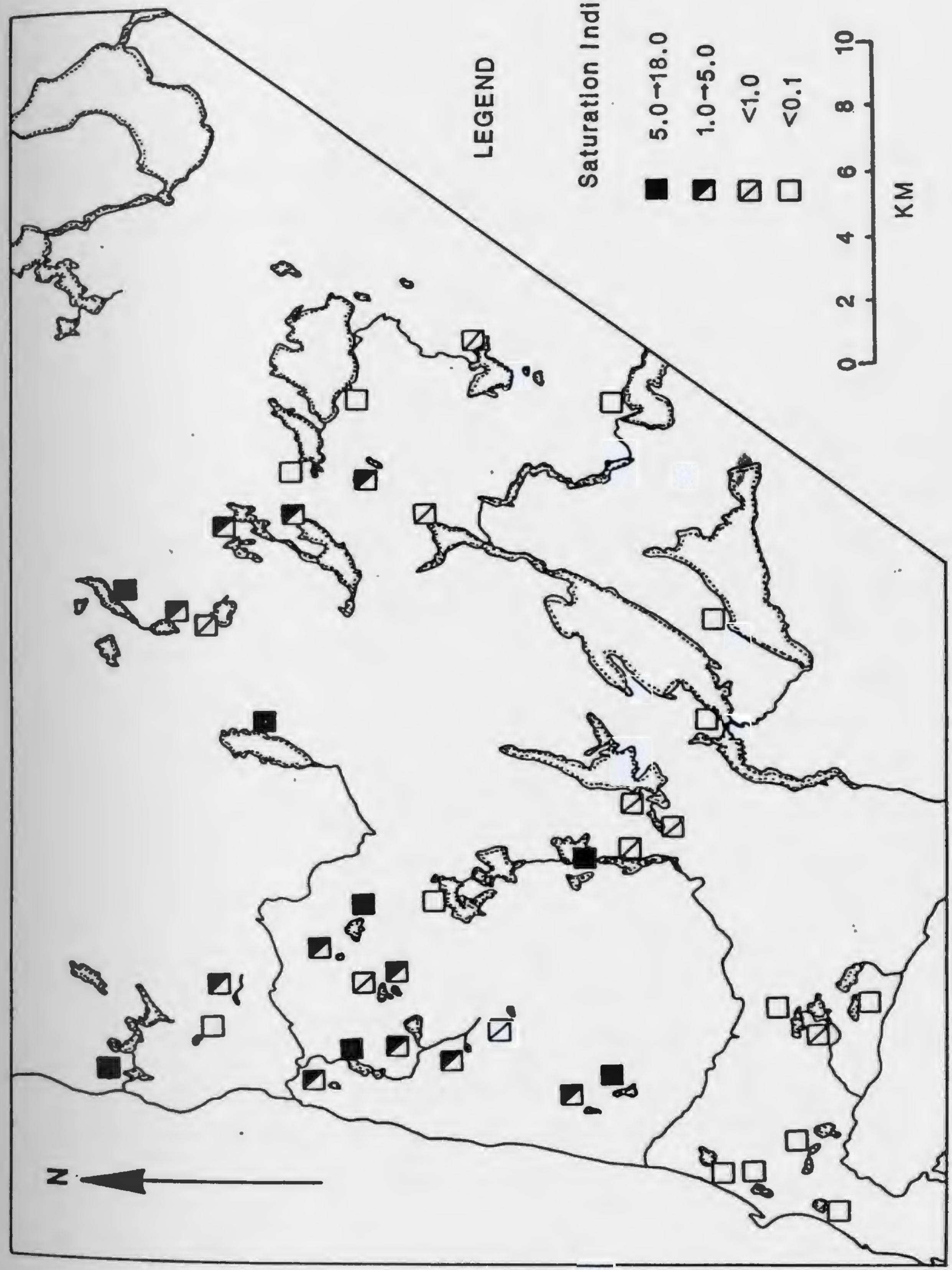
LEGEND
Saturation Indices
5.0→18.0
1.0→5.0
<1.0
<0.1
0 2 4 6 8 10
KM
N

5.2) are located in a presumed discharge area within 8-10 km of the coast and may represent a component of regional discharge.

Figure 5.4 shows dissolved oxygen content decreasing with increasing depth. Figures 5.13 and 5.14 show that reducing groundwaters (negative Eh) are low in D.O. and high in sulphate. Oxidizing groundwaters (high D.O., positive Eh) generally have low sulphate concentrations.

5.3.2 Trace-element chemistry

5.3.2.1 Trace-element abundances

With a few exceptions, trace-element abundances in groundwater are well below the recommended maximum levels for drinking water by American (Matthess, 1974) and Canadian standards (Health & Welfare Canada, 1987). Iron for all samples is consistently above the 'aesthetic objective' of <0.3 mg/l (300 ppb) listed in the Canadian Drinking Water Guidelines, (Health & Welfare Canada, 1987). The concentration of Pb in DH-85 & 87 exceed the 'maximum allowable concentration' of 0.05 mg/l (50 ppb) (Health & Welfare Canada, 1987).

The mine sump discharge and Spring Lake have very similar trace-element chemistry (see Table 5.2). Cobalt, Mo, Cd, and Pb are all elevated in groundwaters that also have zinc anomalies (> 1000 ppb Zn). Since these elements are also associated with sphalerite ore (see Section 3.4), dissolved Zn is probably derived from local ore bodies near or upgradient from the groundwater sampling points.

Figure 5.13 Lake and well waters are oxidizing whereas mine groundwaters range from oxidizing to reducing conditions. Deeper mine waters (high SO_4) are reducing. DH-25 & DH-29 (high SO_4) are highly oxidizing and may indicate sphalerite oxidation as a SO_4-producing mechanism.

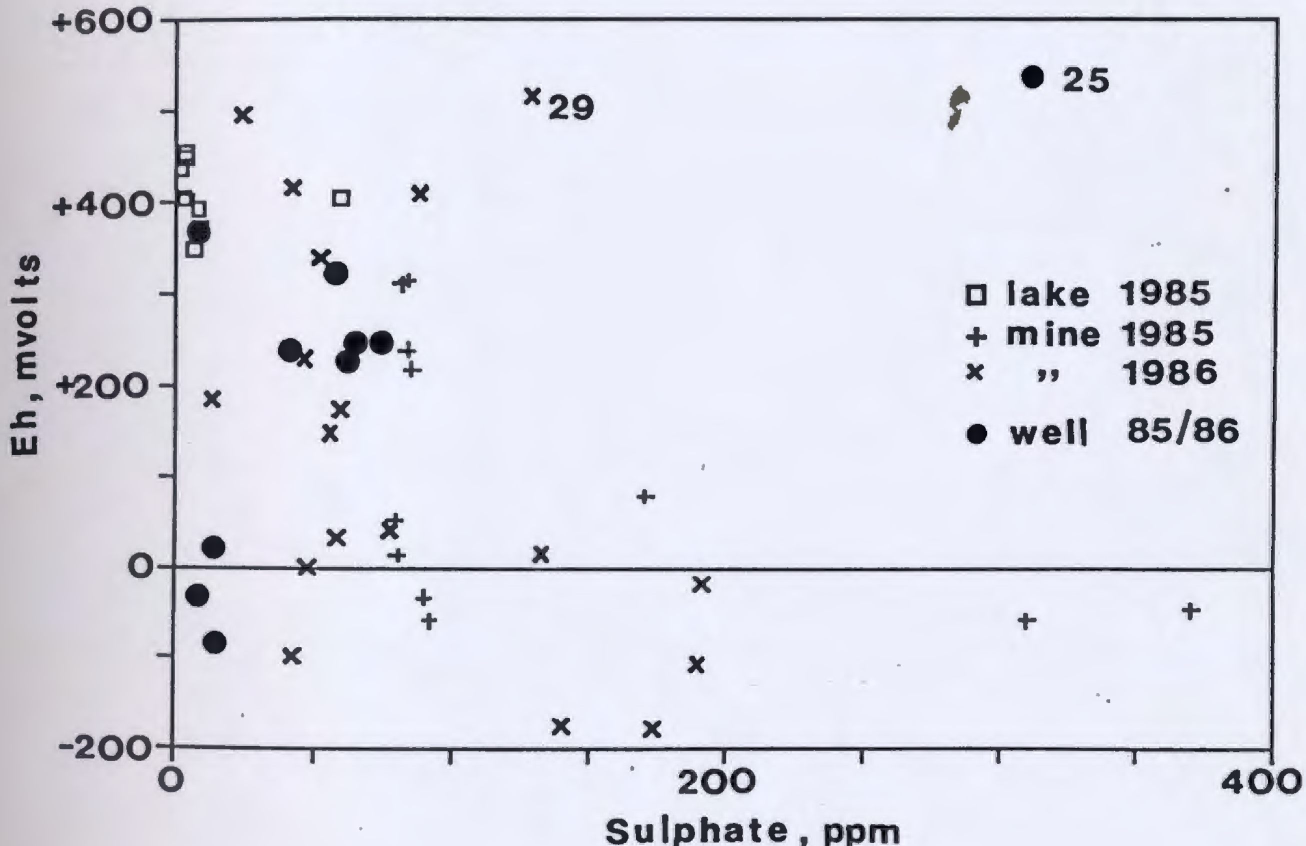

Figure 5.14 Eh vs D.O. plot for the 1986 groundwater samples. Generally higher D.O. contents (> 2 ppm) indicate oxidizing conditions; reducing waters have less than 2 ppm D.O. Well samples DH-86 and 88 may be the result of a shallow/and deep water (oxygen-depleted) mixture (see discussion of Figure 5.6). DH-80 indicates oxygenated water from mine sump discharge.

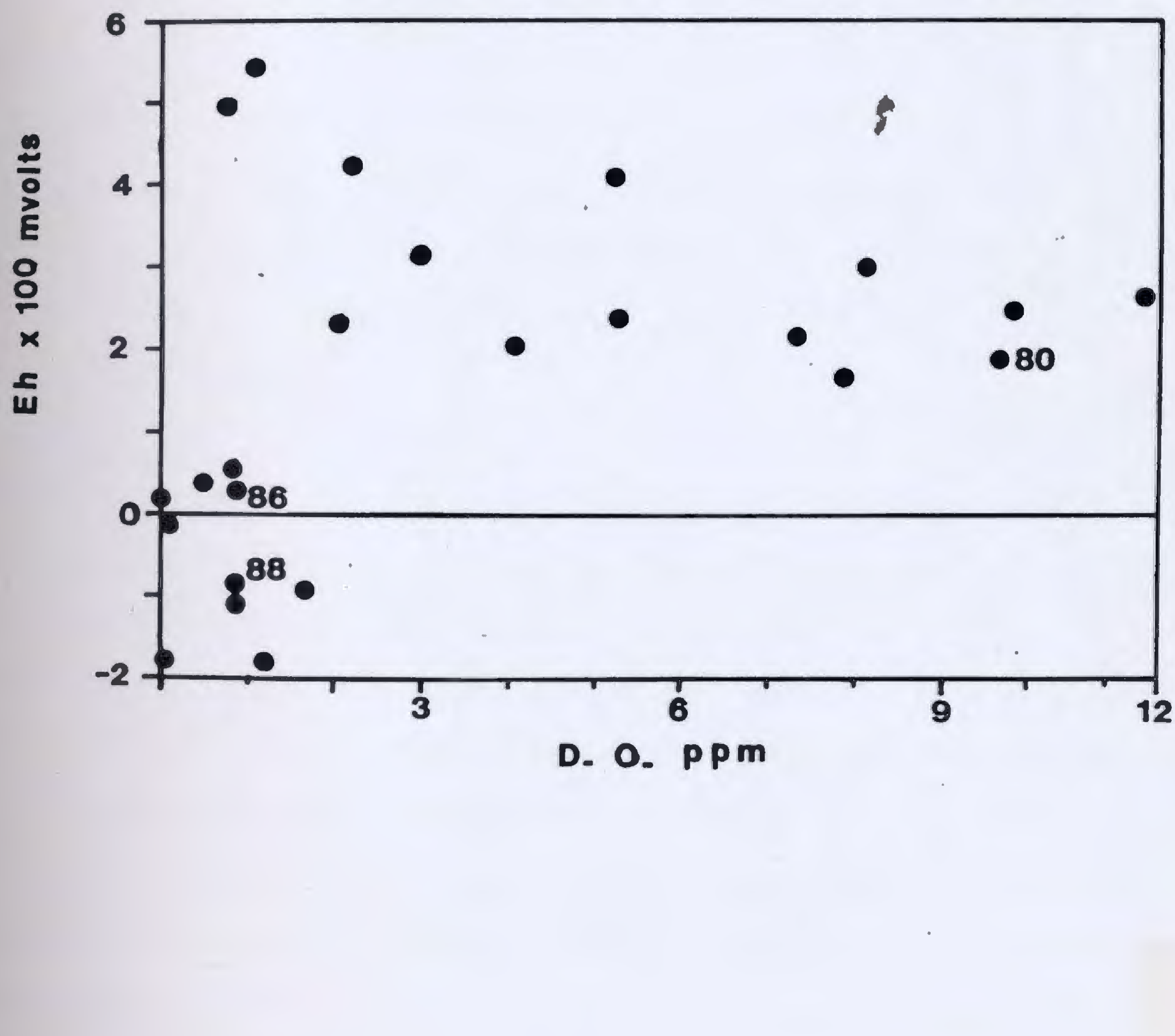

5.3.2.2 Trace-element groupings

Two different groupings of groundwaters are distinguished using the trace-element data. Group 1 elements (V, Rb, and I) show a direct correlation with Cl as illustrated in Figure 5.15. Zinc concentrations noticeably decrease in deep mine waters as salinity (Cl) increases (see Figure 5.16) and the same relationship applies to the majority of the trace elements analyzed: Mn, Co, Ni, Mo, Cd, Ba, Pb and U (Group 2 in Table 5.2). Zinc values greater than 1000 ppb are found only in the shallow mine waters (<100 ppm Cl), with the exception of sample DH-101. Iron and Sr show no or weak correlations with Cl. On a Sr vs Cl plot some samples have a direct and others an inverse relationship with Cl. The scatter of points on the Fe vs Cl plot shows no pattern although Fe and Ca are directly correlated as shown in Figure 5.17.

5.3.2.3 Groundwater residence-time control on trace elements

High iodide concentrations are found in 1986 T-Zone samples (DH-101,33,76), and high levels of Br and Li were found in 1985 T-Zone samples (Welhan & Gale, 1986). Iodide, Br, and Li are associated with easily dissolvable salt-type minerals as well as deep chemically evolved saline water, so their occurrence depends on mineral availability which would increase with groundwater residence time in the aquifer. Thus I, Br, and Li are indicators of a residence-time control on trace-element abundances in groundwater. High levels of these elements in T-Zone

Figure 5.15 The direct relationship between V and Cl is illustrative of trace element Group 1 (Rb,I) in Table 5.2.

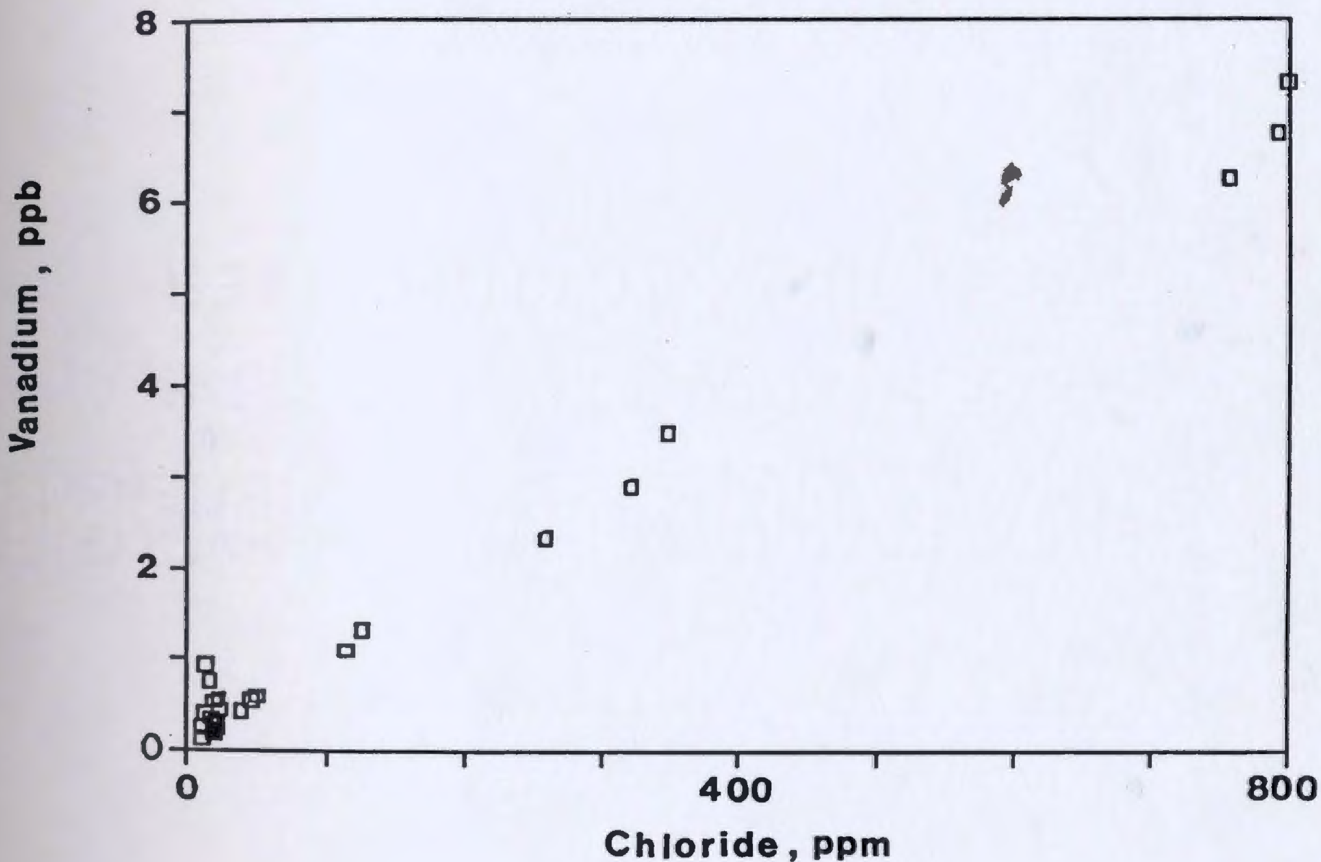

Figure 5.16 The inverse relationship between Zn and Cl in this plot is common to other Group 2 trace elements (see Table 5.2).

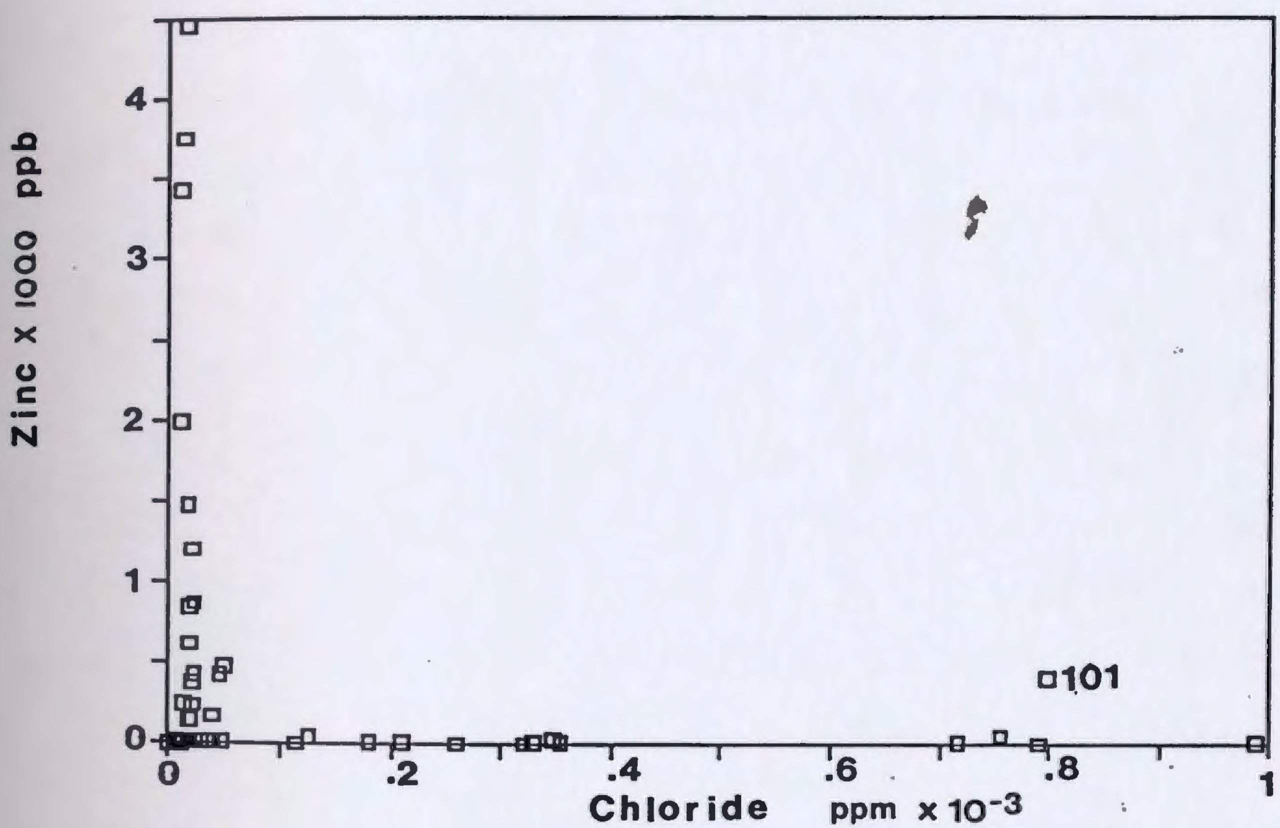

Figure 5.17 Fe vs Ca plot for 1986 groundwater data. The direct relationship between these two elements suggests Fe in groundwater is derived from the dissolution of impure carbonate rocks. Numbered data points have high Zn concentrations. Ca from ICP/MS analysis (see Appendix O).

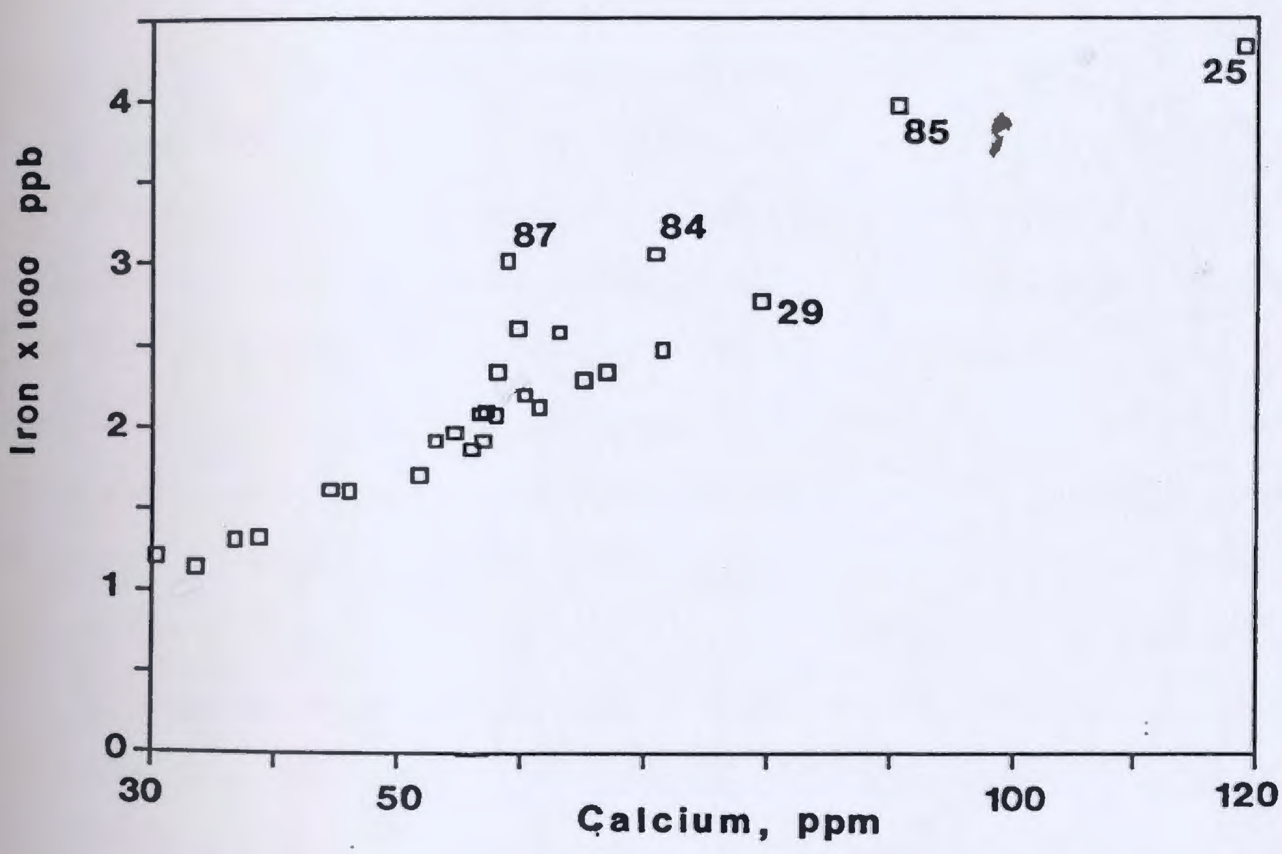

groundwaters may indicate that salt minerals along the groundwater flow path are a source for the high salinities, and suggest that these groundwaters are more chemically evolved than L-Zone waters.

Rb concentration increases in the deep saline waters. The common substitution of Rb for K in minerals such as sylvite (Faure, 1977) supports this mechanism as a source for the salinity in these deep waters which would increase with time as more salt-type minerals are dissolved.

Although vanadium and uranium are often associated (Brookins, 1988; Garrels & Christ, 1965; and Langmuir, 1978) they do not show the same relationship with chloride in these groundwaters. Vanadium is concentrated (> 2 ppb) in deep T-Zone waters whereas uranium is concentrated (> 2 ppb) in the shallow groundwaters of L-Zone. The elevated vanadium levels in the T-Zone are below concentrations necessary for equilibrium with the relatively insoluble vanadium oxides V_2O_4 and V_2O_3 which are the most stable compounds in these reducing waters of intermediate pH levels (Garrels & Christ, 1965; Langmuir, 1978). Thus, vanadium levels are not controlled by mineral precipitation. Vanadium may be segregated from uranium by its preferential incorporation into the lattice structure of clays (Brookins, 1988) which may be present in the surficial materials of this area. In this environment vanadium solubility could be enhanced by SO_4 complexing (Garrel & Christ, 1965). Positive correlation of V with Cl, like Rb and I, suggests that it has accumulated with time during groundwater chemical evolution.

5.3.2.4 Local solubility control on trace elements

Strontium is common in carbonate (Back & Hanshaw, 1970) and silicate rocks and one would expect an increasing Sr content with water residence time as the groundwater dissolves more and more rock. As groundwater dissolves carbonate rock it will quickly become saturated with respect to calcite. Both calcium and strontium concentrations may still increase if silicate minerals such as anorthite are dissolved during groundwater evolution. This is indeed the case in 1985 samples where Sr levels generally increase in the deeper mine waters. However in 1986 samples, T-Zone groundwaters contain both high (DH-34 at 989 ppb) and low Sr levels (no detectable Sr in DH-33, 35, 76, 101).

Deering et al. (1983) reported up to 32 ppm Sr in groundwaters from areas in northwestern Ohio with known celestite deposits. They explained low Sr concentrations (<16 ppm) in the same area by high sulphate values that caused $SrSO_4$ precipitation. This conclusion is irrelevant to the Sr data for 1986 T-Zone groundwaters, since samples that contain relatively high SO_4 (DH-30) also contain relatively high Sr (> 1 ppm), SO_4 and Sr concentrations found in the mine are much lower than those of the Ohio study, and equilibrium calculations indicate that T-Zone groundwaters are undersaturated with respect to celestite.

The Sr/Ca ratio for Daniel's Harbour dolomites is 0.00006 (T. Lane, pers. comm.) and for some Ordovician limestones is

0.00047 (Helz and Sinex, 1974). The same ratio for T-Zone groundwaters is much larger (0.0012), possibly due to the dissolution of local occurrences of celestite and/or strontianite. Isolated celestite occurrences apparently cause locally high Sr levels in sample DH-26 with 435 ppb Sr, and in the samples with the highest Sr concentrations (DH-30,77,102). These samples correlate with known celestite and gypsum occurrences in vugs near drill hole 456 and DH-30 (see Figure 3.3 & Section 3.3). Strontium levels are well below those needed for saturation with respect to both celestite and strontianite and thus if these minerals are indeed a source, Sr content could be controlled locally by mineral availability.

The 1985 and 1986 data indicate that Sr concentrations in groundwater may be controlled by: 1) uniform Sr distribution in rocks of the flow system as trace impurities in carbonates or possibly dispersed in primary salt and sulphate-type minerals; 2) mixing of Sr-depleted shallow groundwater and Sr-enriched deep groundwater in varying proportions; and 3) high Sr content near vug-filling celestite and strontianite.

In general, the dissolved concentrations of trace metals depend on the geochemical mobility, as well as on the presence of the metals in the bedrock. The mobility of heavy metals is dependent on the solubility of their stable solid phases (minerals), the availability of complexing anions, Eh/pH conditions, and the presence of removal mechanisms in the environment.

Iron forms soluble Fe^{2+} in the pH-Eh environment found at the mine (Hem, 1985) and it would be expected in groundwaters of this type if a source was available. The direct correlation between Fe and Ca (Figure 5.17) can be explained in part by the dissolution of Fe which commonly substitutes in impure calcite and dolomite (Faust & Hunter, 1967; Hurlbut & Klein, 1977).

Samples (DH-25, 29, 84, 85, 87) with high Ca also have high Fe and Zn (see Figure 5.17 and 5.18). There is also a direct correlation of Fe with Zn, especially in T-Zone samples, suggesting that Fe is derived from impure sphalerite as well. This is supported by chemical analysis of the zinc ore which indicates only two impurities: iron and cadmium (see Section 3.4). Thus, Fe may be linked genetically with both calcite and sphalerite. Sphalerite oxidation produces H^+ (acid production) and Fe^{2+} ions, promotes calcite and dolomite dissolution, and thereby raises the Ca and Fe as well as the Zn concentrations in groundwater. Iron may also be linked with Ca and Zn by the oxidation of sphalerite and its accessory mineral pyrite (see Section 3.4).

Molybdenum and U are enhanced in some shallow groundwaters of the L-Zone and in wells within 1.5 km north and east of the mine workings. The locations of these wells are near known ore zones and open pits (Figure 2.2 and 3.2). There is a minor association of Mo with sphalerite (see Section 3.4), suggesting an ore source for the Mo. It was demonstrated by Welhan et al. (1988) that zinc concentrations found in the mine-water samples

Figure 5.18 Zinc vs SO_4 plot for 1986 groundwater data. Numbered data points refer to groundwater from wells and mine that exceed 1000 ppb Zn. Generally, high-sulphate groundwaters have low Zn concentrations. DH-25 has a higher than average SO4 concentration and does not fit this trend.

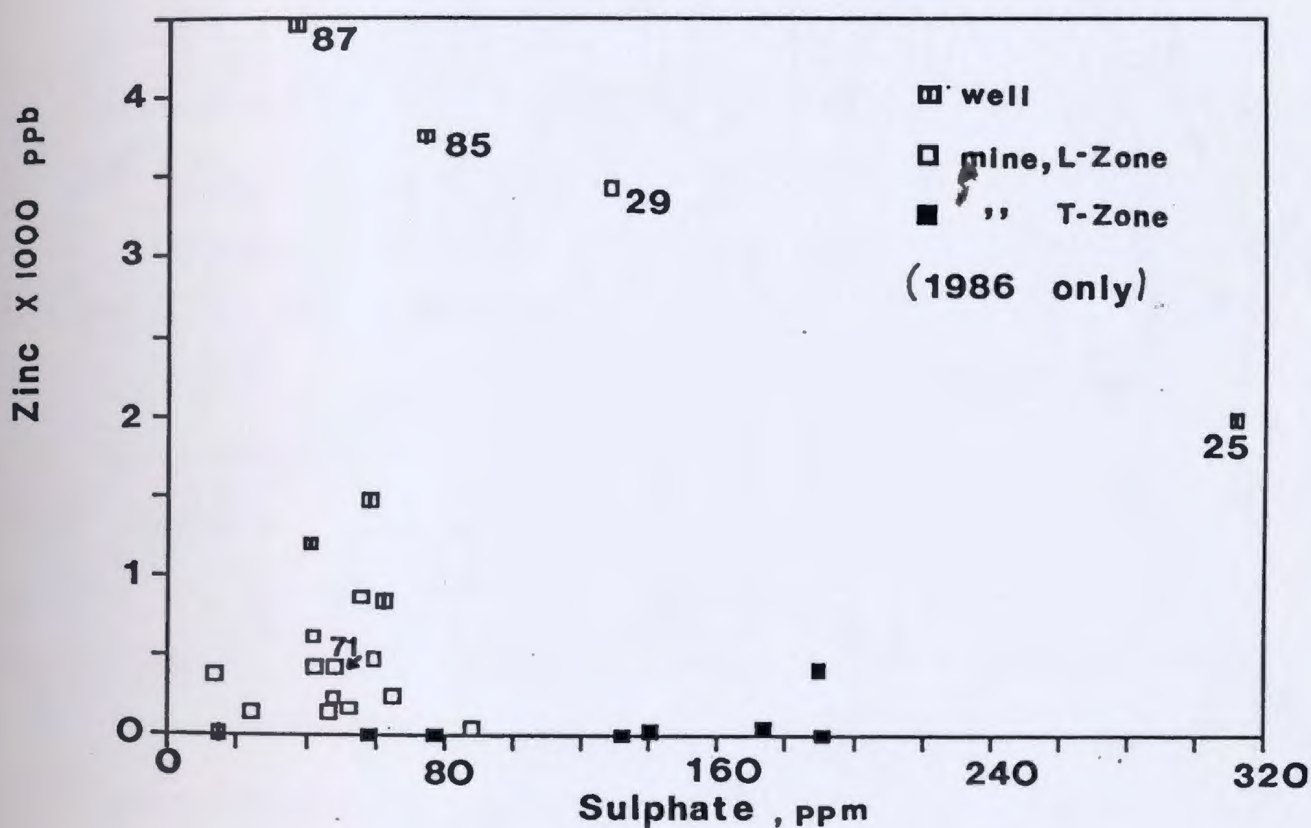

can be explained by the combined processes of sphalerite oxidation and $ZnCO_3$ precipitation. Molybdenum versus Zn data (for 1986 only) have a correlation coefficient of 0.49. Hence, the poor to fair correlation between Mo and Zn may be explained by sphalerite oxidation (producing Zn & Mo ions) and $ZnCO_3$ precipitation (decreasing Zn levels), thereby masking the genetic link between Zn and Mo in groundwater.

The low Mo values for deep waters may be due to molybdenum's lower solubility under reducing conditions (Hansuld, 1966). In alkaline-oxidizing water, molybdenum occurs as mobile anions MoO_4^{2-} and $HMoO_4^-$, and it would be expected in groundwater under L-Zone conditions near a Mo source. Barakso & Bradshaw (1971) also found high Mo contents in alkaline waters near sources of ore. Thus, the major control on Mo is the presence of local ore zones along groundwater paths.

The plot of molybdenum vs uranium (see Figure 5.19) illustrates a direct correlation for the 1986 mine and well samples. Unlike Mo, uranium is not associated with this type of sulphide deposit. However, there is a direct relationship between uranium and zinc in the shallow groundwater that is statistically significant with a good correlation coefficient of 0.77. Deeper groundwaters, if belonging to a regional flow system, may have acquired U from the granitic rocks of the Long Range Mountains during recharge; but this source does not explain the observed U levels in the some of the shallow groundwaters. Uranium and Mo may have a separate source than the zinc by

Figure 5.19 Molybdenum vs U plot for groundwater samples. There is a direct relationship between these two elements that may be related to sphalerite oxidation (source of Mo) and carbonate dissolution (source of U). Exceptions to this relationship are DH-79 & DH-25.

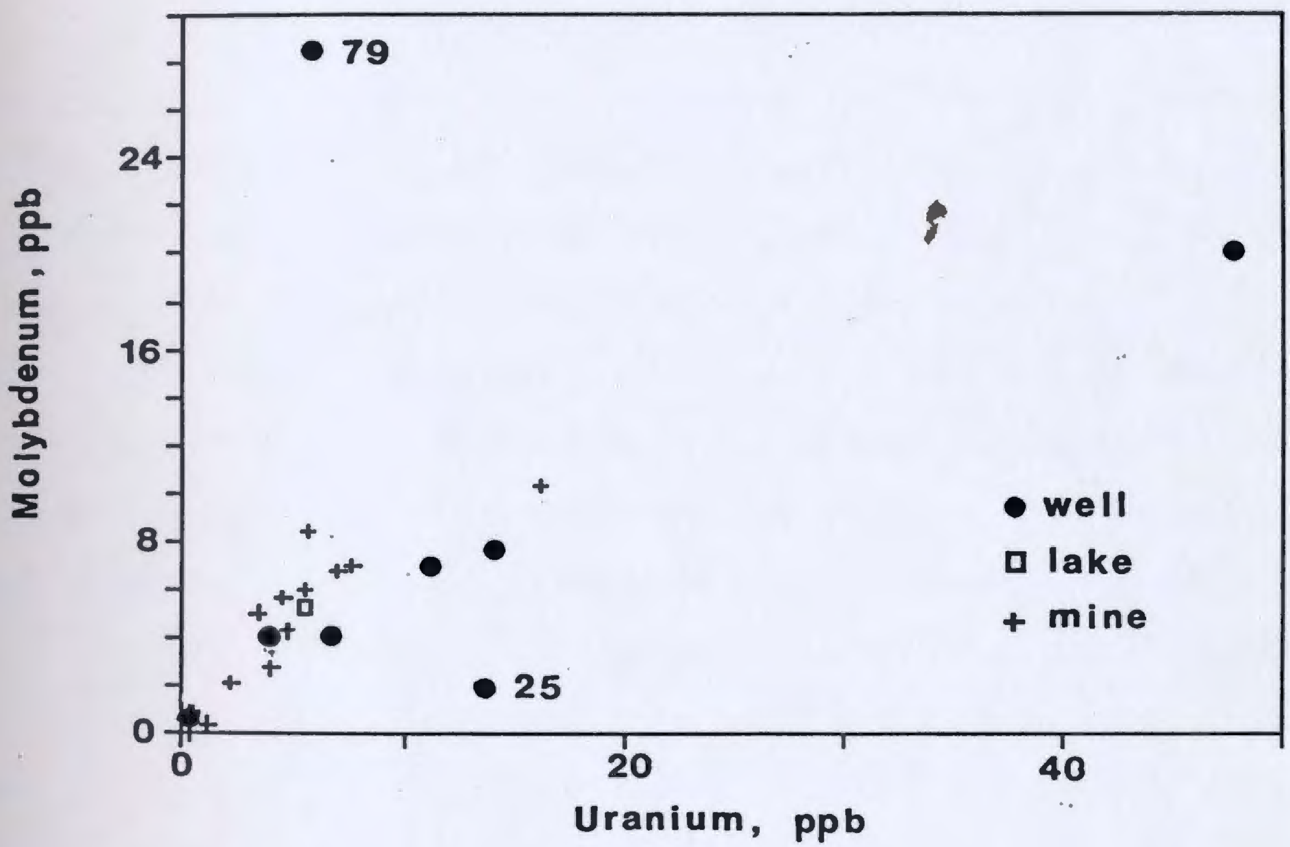

possibly being derived from the granitic erratics found in the calcareous drift which covers the mine site (see Section 3.5). There is a strong Mo-U association in the late Precambrian granites of the Long Range Mountains (P.H. Davenport, pers. comm.). However, this soil source for U and Mo does not explain the sporadic or localized occurrences of high U and Mo levels in shallow groundwaters or the good correlation between Zn and U. One would expect evenly distributed high U and Mo levels in the shallow groundwaters (eg. low values in DH-28, 31) since the entire mine area is covered with glacial drift. A possible source of U could be impurities in carbonate rocks. By analogy with the Fe-Ca-Zn relationship, a dual mechanism such as sphalerite oxidation (producing acidic waters and Mo) followed by carbonate dissolution (U liberation) could explain the U-Mo correlation despite their different sources. Uranium forms soluble mineral phases at T-Zone Eh-pH conditions since redox levels are still too high to render the uranium ion immobile. The low U concentrations in the T-Zone groundwaters may be the result of less oxidizing conditions in the T-Zone inhibiting sphalerite oxidation and thus the mechanism by which U is liberated from the carbonate rocks.

It would appear then that there are two main controls on trace elements in the groundwaters at Daniel's Harbour. These controls are the availability/local occurrence of associated minerals, and the residence-time of the groundwater. Rubidium, iodide and vanadium (Group 1) are controlled by the latter and are concentrated in deeper groundwaters; zinc, manganese, cobalt, nickel, molybdenum, cadmium, barium, lead, and uranium (Group 2) are controlled by the former mechanism and are concentrated in the shallow groundwaters. Strontium is controlled by both mechanisms and iron is likely controlled by impurities in sphalerite and/or carbonate rocks.

5.3.2.5 Controls on zinc solubility

Zinc has the highest concentrations of all trace elements analyzed; as much as 4457 ppb Zn is dissolved in shallow groundwaters (DH-87). Other studies (Hoag & Webber, 1976b) have found anomalous Zn values (up to 2920 ppb) in groundwater with pH 6.4 to 7.8 (similar to Daniel's Harbour). Van Everdingen (1970) explained high Zn contents (177 ppm) in acidic groundwater by sulphide oxidation and dissolution of zinc sulphide minerals.

Sphalerite oxidation is also a likely mechanism by which Zn is released into Daniel's Harbour shallow groundwaters. Under pH conditions and sulfur concentrations similar to the L-Zone environment, Zn will form the soluble Zn^{2+} ion in oxidizing waters (Salomons, 1984). From Figure 5.16 it appears that significant aqueous Zn concentrations are supported in the shallow, oxidizing groundwaters of the mine. Maximum Zn levels may be controlled by zinc-carbonate precipitation at high pH's and Zn^{2+} concentrations greater than several ppm (Salomons, 1984; Welhan et al., 1988). The occurrence of smithsonite in the upper, weathered portion of mineralized bedrock at the mine (see

Section 3.4) is direct evidence for sphalerite oxidation and $ZnCO_3$ precipitation.

Anomalously high Zn and traces of Fe and Mn (associated with the mineralization itself) found in the groundwaters probably indicate point sources of sphalerite since metal values in the carbonate host rock fall away rapidly to background with distance from ore (Sangster, 1968). Groundwater Zn concentrations change a great deal in the same area (ie. >1000 ppb northeast of Spring Lake to <100 ppb 500 m north; see Figure 5.20) and provide a further indication of localized sources of zinc, precipitation of $ZnCO_3$ and/or dilution soon after dissolution of sphalerite. In general, any element observed at concentrations below 0.1 ppm or 100 ppb is considered a trace constituent of groundwater (Freeze and Cherry, 1979) and thus concentrations below this value were not considered anomalous in this area.

The limited areal extent of Zn concentration anomalies in groundwater around the mine is similar to that for U-Mo anomalies. These anomalies can be correlated with open-pit ore zone locations and trends seem to be spatially related to different mine areas and depths. This is shown in the contoured Zn anomaly map (Figure 5.20). Wells with high Zn as well as Mo and U concentrations (DH-25, DH-87 and DH-85; see Table 5.2) are in the Lead Lake area, near open pit operations that at one time contained major ore zones. Other anomalous well waters (DH-82, 83, 84) are found east of the Spring Lake tailings pond and the unmined O-Zone (Figure 2.2). Further evidence for the close

Figure 5.20 Groundwater zinc analyses have been plotted and contoured to produce this groundwater zinc anomaly map. Sites with >1000 ppb Zn are considered anomalous and Zn concentrations fall rapidly away from these sites. When compared with the geology map of the same area (see Figure 3.3) the high Zn areas correspond to areas of ZnS mineralization.

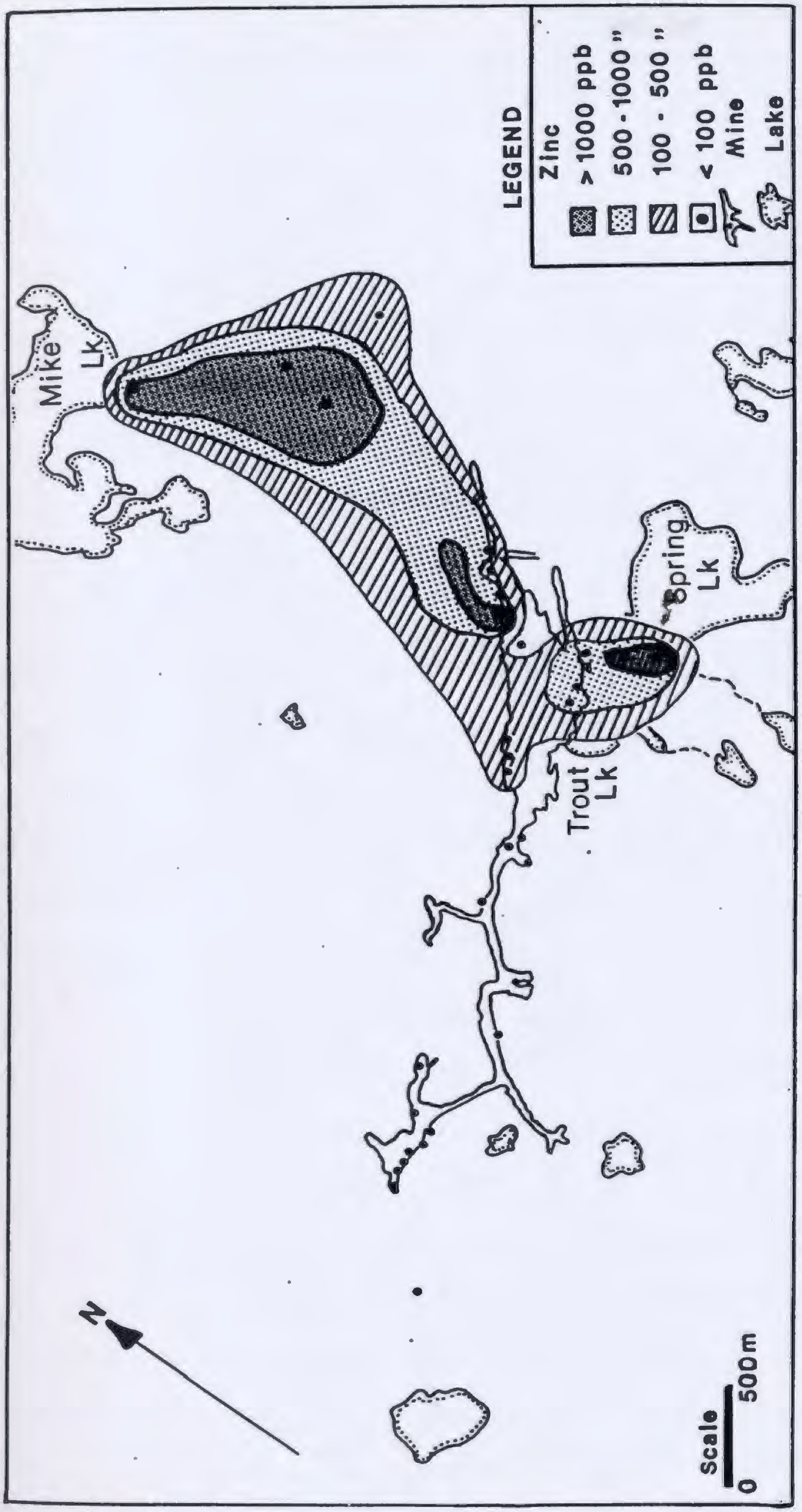
LEGEND
Zinc
> 1000 ppb
500 - 1000 "
100 - 500 "
< 100 ppb
Mine
Lake
Mike Lk
Spring Lk
Trout Lk
N
Scale
0 500m

proximity of an ore source to such Zn-rich groundwaters is that these waters have an enrichment of the less mobile Pb ion. These observations are important because trace-element anomalies in groundwater may indicate paths of groundwater flow over short distances and thus locate ore zones elsewhere.

The Zn distribution shown in Figure 5.20 is significant hydrogeologically. Patterns developed in the shaded areas may be the result of Zn-bearing shallow groundwater flowing southwest from Mike Lake and north from Spring Lake and is consistent with hydraulic gradients discussed in Section 4.1.3.

5.3.3 Sequential sampling

Three underground mine sites were sampled more than once during the summer of 1986 in order to determine temporal variations in water chemistry at different levels in the mine. Sample site descriptions are given in Appendix B and relevant data for the samples is listed in Table 5.4. Major and trace ions have been plotted for each sample site on Figure 5.21.

The last round of sampling (August) indicated a significant change in chemistry at Site 2 from the previous two rounds of sampling. There was a large decrease in major and trace constituents: Cl^-, SO_4^{2-}, Mg^{2+}, Ca^{2+}, Fe^{2+}, I^-. Ions characteristic of the deep saline waters (Cl^-, SO_4^{2-}, I^-) show the greatest dilution (see Figure 5.21). The conductivity change from 1500 to 630 μmhos/cm (Table 5.4) indicates that the groundwaters at this site were diluted with rainwater by approximately 50%.

Table 5.4 Pertinent data on sampling sites used in the sequential sampling site analysis. Each site was sampled at 3 different times during the summer of 1986 with the exception of site 3; it was sampled only twice. Accumulated rainfall between each sampling date is shown in Figure 5.21.

	July 18	July 29	Aug. 12-14
SITE # 1			
Sample#	DH-33	DH-76	DH-101
Conduct.	3000	3000	3100
$\delta^{18}O$	-9.7	- 9.97	-10.46
SITE # 2			
Sample#	DH-30	DH-77	DH-102
Conduct.	1500	1500	630
$\delta^{18}O$	-10.09	n.a.	-10.59
SITE # 3			
Sample #		DH-78	DH-103
Conduct.		500	530
$\delta^{18}O$		-8.52	-9.4

Figure 5.21 Results of the 1986 sequential sampling survey. Concentrations (log scale) of selected major, minor and trace groundwater constituents have been plotted against time. Sampling dates are underlined. Numbers 1, 2 and 3 refer to sample site locations listed in Table 5.4. Rainfall prior to the sampling date is shown at the bottom of the graph. Most ions (except Zn) show a dilution at sample site 2 during mid-August. If there was no change in water chemistry with time, each ion would plot as a horizontal line.

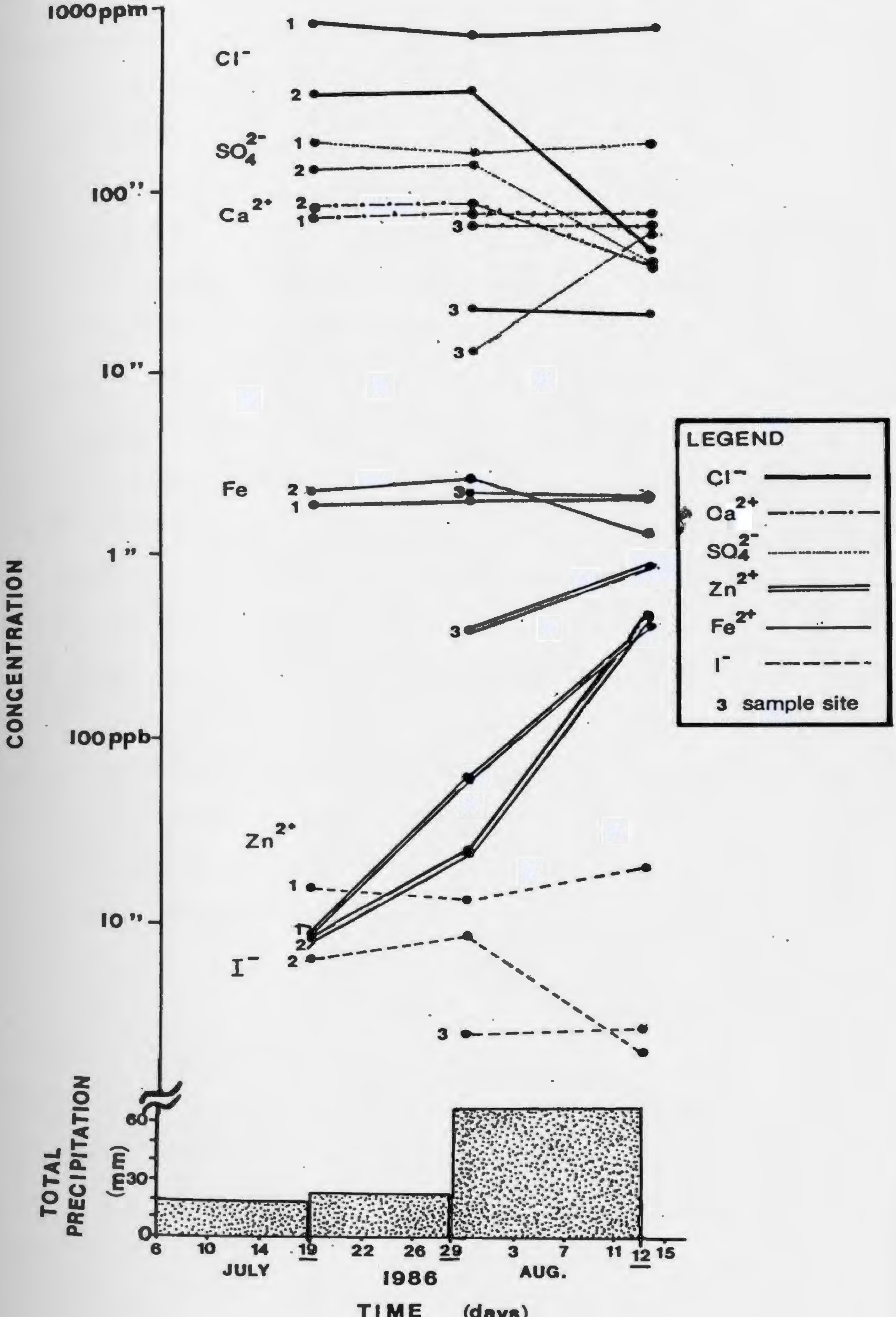

1000ppm
100"
10"
1"
100ppb
10"
CONCENTRATION
Cl⁻
SO_4^{2-}
Ca^{2+}
Fe
Zn^{2+}
I^-
LEGEND
Cl^-
Ca^{2+}
SO_4^{2-}
Zn^{2+}
Fe^{2+}
I^-
3 sample site
TOTAL PRECIPITATION (mm)
60
30
0
6 10 14 19 22 26 29 3 7 11 12 15
JULY
1986
AUG.
TIME (days)

The decrease in ion concentrations may have been caused by dilution brought about by the increase in rainfall after the second and before the third round of sampling (see Figure 5.21). The apparent association of dilute water with a high rainfall event suggests a major connection or increased permeability between ground surface, mine levels and the L-Zone, allowing more infiltration at Site 2 than at the other sites. Fontes (1983b) pointed out that a specific problem in karstic systems is the possible occurrence of inactive or 'by-passed' reservoirs which are discharged and recharged during high rain periods. If there is a physical connection (eg. fault, see Figure 3.2) between the drill hole and the surface then dilution of saline water may occur during times of increased recharge.

Fluctuations in groundwater chemistry that occur only at Site 2, and only after increased rainfall, are further evidence for aquifer anisotropy, indicating a specific zone of increased permeability due to the dissolution of carbonate rocks along faults. Major-ion chemistry and oxygen isotopes show temporal variations in groundwater that reflect changes in aquifer recharge.

5.3.4 Isotope geochemistry

Environmental isotopes were used to study the mine flow regime and to further differentiate waters of similar major-ion chemistry. These isotopes helped in flow-system delineation, determination of mixing between different waters and sources of mine inflows, and provided age estimates for the groundwaters.

5.3.4.1 Stable oxygen and hydrogen isotopes

Oxygen-18 and deuterium signatures of precipitation vary locally depending on the climate of the geographical region. As a result, $\delta^{18}O$ and $\delta^{2}H$ values will plot on a regional meteoric water line (see Figure 5.22) with the same slope as the global meteoric water line but with a different 'y'-intercept (Gat, 1981).

Figure 5.22 shows that Newfoundland Zinc Mine groundwaters are of a normal meteoric origin. Sample DH-18 is an example of surface evaporated water (lake) which plots off the meteoric water line on an evaporation slope. DH-78 is a shallow mine groundwater in close proximity to Spring Lake and its position in Figure 5.22 implies that shallow inflows may be derived from Spring Lake. This hypothesis is supported by deuterium analyses of shallow groundwater near L-Zone workings (DH-29 in Figure 5.22) which also indicate an evaporated surface water contribution.

Figure 5.23 summarizes oxygen isotope data for mine, borehole and surface waters. The T-Zone groundwaters show more scatter in $\delta^{18}O$ in 1986 [average= -10.09 o/oo, standard deviation= 0.33] than in 1985 [average= -10.25 o/oo, standard deviation= 0.19], suggesting more mixing between $\delta^{18}O$--variable L-Zone groundwater [average= -9.65 $^{o}/oo$, standard deviation= 0.80] and T-Zone groundwaters in 1986, and/or a changing

Figure 5.22 Most groundwater samples from the Newfoundland Zinc Mine have a meteoric origin. Samples 78, 76 29, have been modified by evaporation. A lake sample (DH-18) is used to illustrate the evaporated surface water contribution to mine groundwater inflows. "M.W.L." indicates meteoric water line.

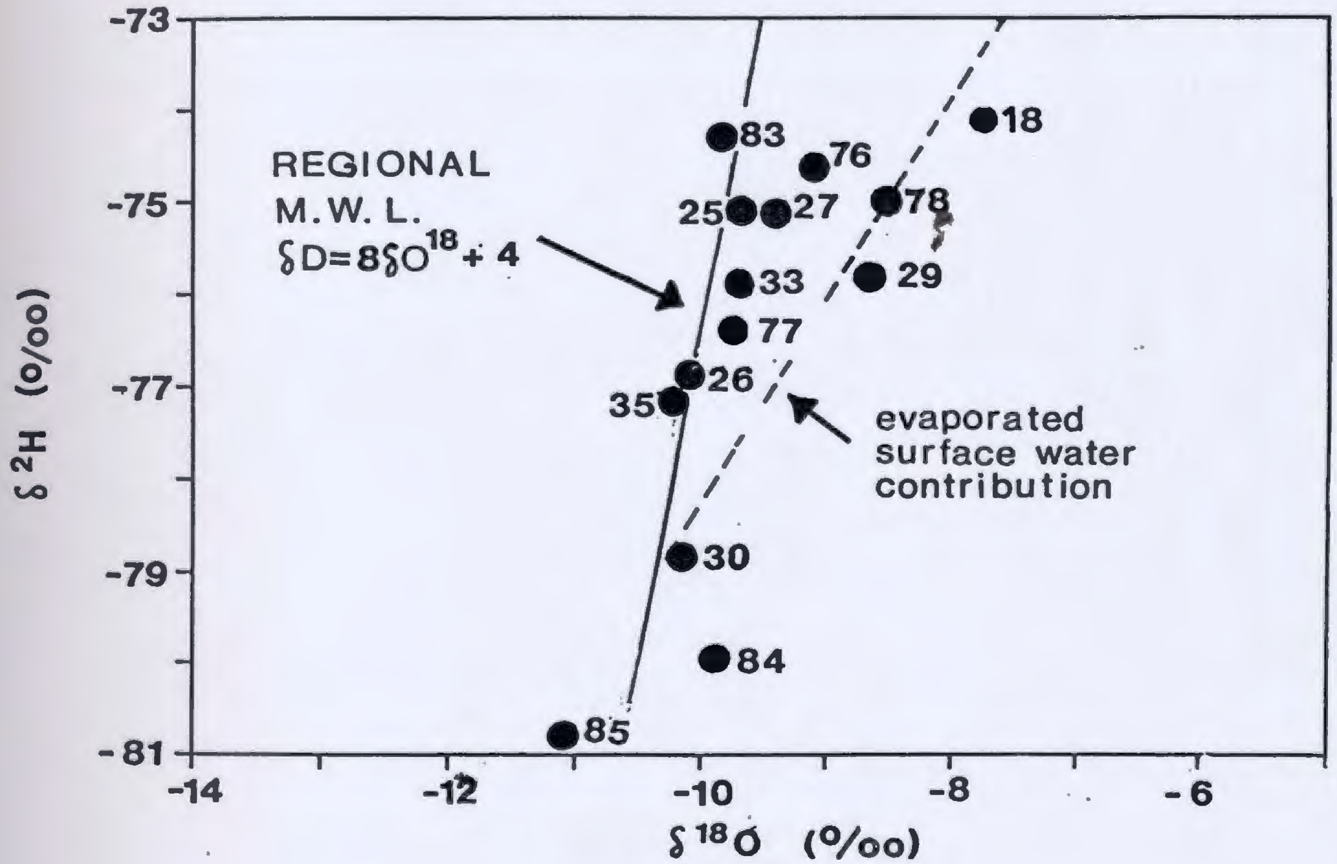

Figure 5.23 A decrease in oxygen-18 with increasing chloride content (solid line) for deep mine groundwater samples suggests a higher elevation of recharge for the deeper saline groundwaters. Saline groundwater samples above this line (circled) may indicate mixing with surface water enriched in $\delta^{18}O$.

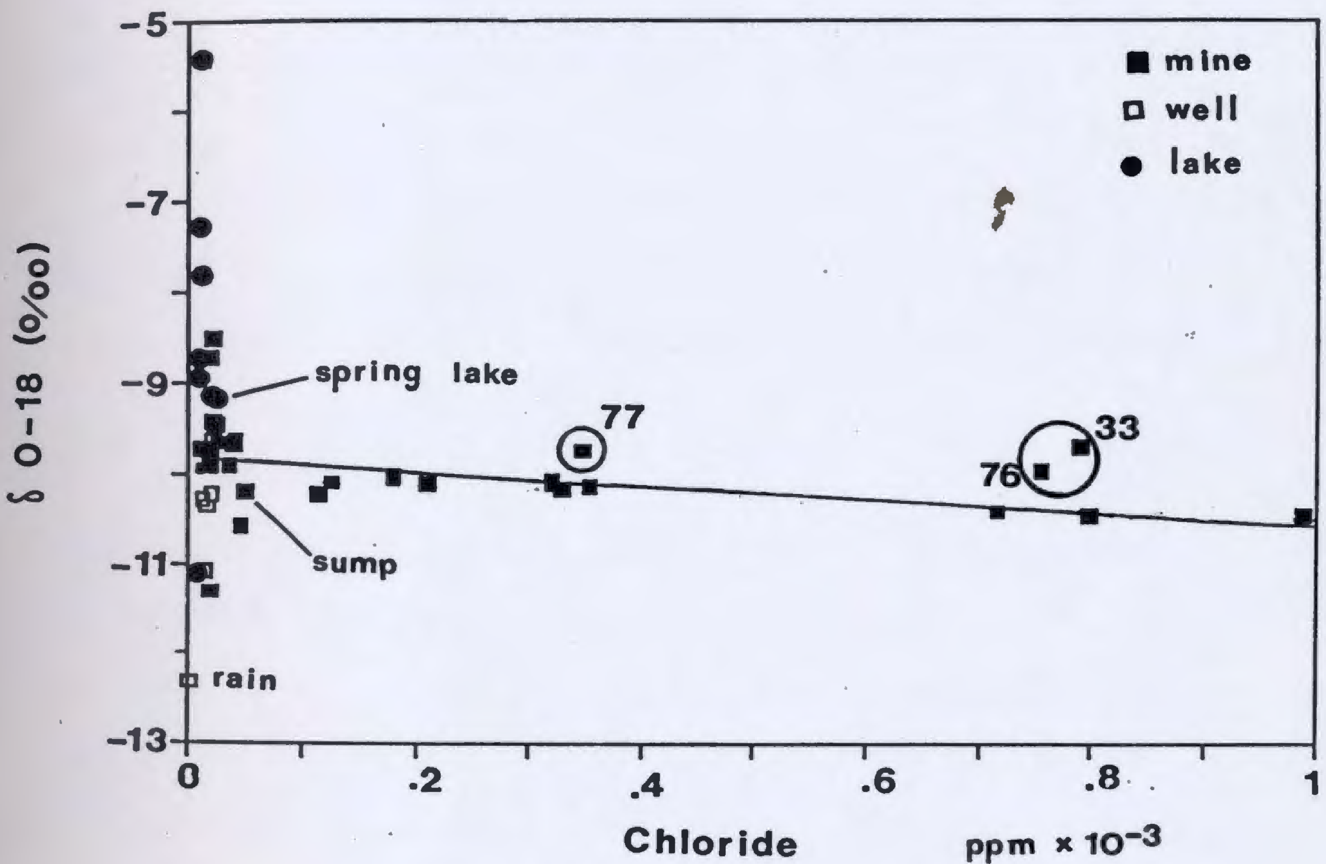

hydrogeologic flow regime during this year. Surface samples show the greatest range in oxygen isotope ratios from -5.43 $^{o}/oo$ (lake) to -13.97 $^{o}/oo$ (snow) reflecting evaporation of lake waters and the seasonal variation in precipitation (Gat, 1971).

Perennial springs (DH-106 and 107) and the flowing artesian well (DH-88) are isotopically very similar (see Table 5.3), illustrating the homogenizing effect of groundwater flow (mixing) on the varied isotopic ratio in yearly precipitation (Gat, 1971). Further homogenization of isotope values occurs in the deeper saline water as shown by the decrease in oxygen isotopic variability with depth (see Figure 5.24). The same phenomenon was exhibited by oxygen and tritium isotopes in the deep groundwaters found in the fractured aquifer at Cheju Island, Korea (Davis et al., 1970).

The oxygen-18 vs Cl plot (Figure 5.23) suggests mixing between isotopically light shallow groundwaters (wells), characteristic of mean annual local precipitation, and isotopically-enriched lake water, similar to trends indicated by major-ion data (eg. Figure 5.5). A second mixing trend, between isotopically light deeper saline waters and slightly more $\delta^{18}O$-enriched shallow dilute waters (Figure 5.23), also mimics mixing trends seen in major-ion data (Figure 5.8).

Samples that lie above the deep/shallow groundwater mixing line (DH-33,76; circled on Figure 5.23) may indicate local mixing of deep oxygen-18 depleted groundwater with more enriched near-surface groundwaters or lake water along fracture conduits. DH-

Figure 5.24 A decrease in the variation of $\delta^{18}O$ with depth is typical of fracture-flow dominated aquifers.

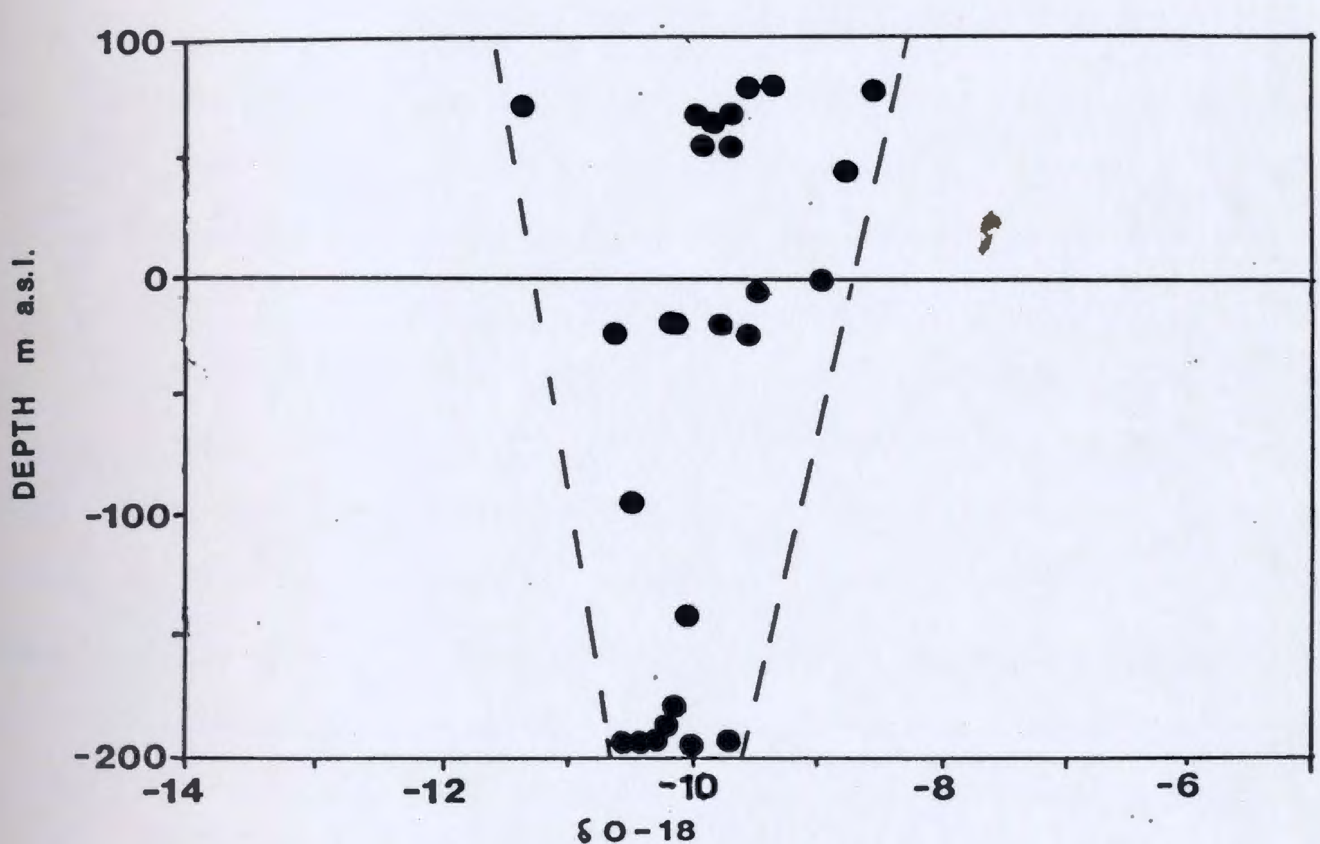

77 is a sample from a deep drill hole (see Section 5.3.1) but lies above this mixing line, also suggesting a mixture between saline water and lake water or shallow groundwater. High tritium contents in DH-77 and 33 support this local mixing hypothesis (see Section 5.3.4.2).

As shown in Figure 5.23, $\delta^{18}O$ decreases with increasing Cl. Although the deep/shallow mixing line has a very shallow negative slope, this line (y-intercept = -9.74) has a correlation coefficient of 0.81 indicating that this slope is statistically significant giving good evidence for the argument that there is indeed a decrease in oxygen-18 with increasing Cl in the deep mine groundwater. Possible reasons for this are 1) different sources for shallow and deep groundwaters and 2) isotopic exchange between deep groundwater and rock. However, isotopic exchange between groundwater and carbonate rock would result in an increase in the heavier isotope (Faure, 1977) and not a decrease which is found in the deep groundwaters of the Newfoundland Zinc Mine. Therefore, the low oxygen-18 values exhibited by saline groundwaters probably reflect a different recharge environment than that for the dilute shallow groundwaters. The lower $\delta^{18}O$ may be the result of an altitude effect (Eriksson, 1983) and thus an inferred higher elevation of recharge. The Long Range Mountains represent such a possible environment. Groundwaters which recharge in the mountains and discharge near the coast would belong to a regional flow system (eg: Toth, 1963).

T-Zone groundwaters may belong to a regional flow system; they may have obtained their salinity by mixing with modern/ancient seawater or dissolution of sulphate-type minerals and salts. A possible saline source could be ancient seawater that was trapped by isostatic depression during the last glacial advance (see Section 3.5). Water sources associated with glacial periods have lower $\delta^{18}O$ values reflecting recharge under cooler climatic conditions (Gat, 1971), suggesting that T-Zone groundwaters may have been recharged during the last ice age.

5.3.4.2 Tritium and carbon isotopes

Groundwater age can be defined as the time since infiltrating water became isolated from the atmospheric tritium/radiocarbon reservoir. When infiltrating water enters the saturated zone its radioactive isotope content will decrease due to radioactive decay. Apparent piston ages (t) for groundwater samples were calculated by assuming no mixing/dispersion, and substituting known atmospheric tritium levels typical for eastern North America (I.A.E.A., 1981; I.A.E.A., 1983a; I.A.E.A., 1986), and measured tritium concentrations from Table 5.3 into the radioactive decay equation. Because of the variability in tritium levels in atmospheric precipitation during the past 35 years due to fallout from thermonuclear testing in the 1950's and 1960's (Freeze and Cherry, 1979) groundwater samples have a wide range of tritium contents.

Generally the presence of tritium above 4 T.U. in northern latitudes indicates the presence of 'young' waters that have been recharged since the initiation of thermonuclear testing in the 1950's (Freeze and Cherry, 1979). Any tritium level above 20 T.U. implies that a component of the water has been recharged since 1961 (pg. 59 I.A.E.A., 1983b).

Estimated ages from tritium data indicates relatively young groundwater in the deep and shallow levels of the mine which vary from 13 to 33 years. Generally, the variation in tritium levels throughout the mine and between sampling years supports the concept of groundwater flow through an anisotropic aquifer (Davis et al., 1970), with permeability in the rock mass dominated by individual faults and major joint and bedding-plane systems. These conduits conduct shallow groundwater to the deeper parts of the mine at different rates, resulting in a range of measured tritium levels.

Initially, radiocarbon analysis of groundwater was undertaken to determine transit times for Daniel's Harbour groundwaters, but in light of all the 1986 tritium age estimates of less than 33 years, radiocarbon data would not contain any useful quantitative information on the ages of the groundwaters.

However, carbon-14 analyses may give some measure of the carbon-14 dilution caused by dissolution of carbonate rocks which have essentially no radiocarbon content. Of the three samples analyzed for radiocarbon only one sample, DH-25 (see Table 5.3) shows significant 'dead' carbon dilution. DH-25 contains half as much % radiocarbon as the other samples which are downgradient from it. These observations further emphasize the pecularities of this sample mentioned earlier in Section 5.3.1. Its lower radiocarbon content cannot be interpreted as a simple increase of dead carbon with length of flow path. An increase in 'dead' carbon in DH-25 may be due to the previously stated process of local sphalerite oxidation producing acidic conditions which in turn cause more carbonate dissolution. DH-27 and DH-85 have relatively high radiocarbon contents (Table 5.3) and show little dead-carbon dilution if one assumes the recharge radiocarbon content was lower than 85 % modern (Vogel, 1970) due to the presence of carbonate minerals in the soil zone. The relatively low dilution for these samples is consistent with the hypothesis that these groundwaters belong to a local flow system. DH-27 has a slightly lower radiocarbon content than DH-85 consistent with flow gradients and proposed flow paths originating north of, and flowing towards the L-Zone.

Carbon-13 in conjunction with DIC (dissolved inorganic carbon) can provide clues to the evolutionary paths of groundwaters. The $\delta^{13}C$ of groundwater in carbonate terranes is a function of the $\delta^{13}C$ acquired during recharge (soil zone CO_2 $\delta^{13}C$= -20 to -24 $^{o}/oo$) and the $\delta^{13}C$ of local carbonate rocks ($\delta^{13}C$ = -1.0 to -1.5 $^{o}/oo$; Lane, in prep.). The $\delta^{13}C$ values (-12.46 to -5.42 $^{o}/oo$; Table 5.3) for inorganic carbon in most mine groundwaters fall within the range typical for natural groundwater (-15 to -8 $^{o}/oo$; Fritz, 1983), but others are heavier than what is expected for the equivalent DIC in carbonate groundwater (-19 to -15 $^{o}/oo$; Deines et al., 1974).

Figure 5.25 is a plot of $\delta^{13}C$ vs the reciprocal of dissolved inorganic carbon (DIC). Half the samples analyzed show a large discrepancy between field DIC measurements (alkalinity titrations performed in the field laboratory) and laboratory DIC measurements (DIC measured on the $\delta^{13}C$ extraction line). The remainder of the samples showed little or no difference between the field or lab DIC and are plotted as an average of these two values (circled dots). Lab DIC for samples DH-27, 28, 30, 35 and 77 are consistently lower than the field DIC, possibly as a result of CO_2 degassing. Degassing may have occurred at the sample collection site or during storage. Most of the above samples were taken from drill hole valves and degassing may have occurred if bubbles formed as water poured from the valve. In general, the mine environment may promote groundwater degassing in drill holes and fracture seeps. Sensitivity calculations of pH error effects on calcite and dolomite saturation indices indicate that T-Zone samples are near or at a state of equilibrium and show little or no degassing at the sample site (see Section 5.5.1.2). Thus, the observed difference between field and lab DIC may be from leakage during storage of the bottles.

Assuming that the lab DIC and measured $\delta^{13}C$ for samples DH-27, 28, 30, 35, 77, and 78 result from CO_2 loss and subsequent carbon-13 fractionation, an attempt to correct for this was made by a simple Rayleigh calculation. The original $\delta^{13}C$ of ground-

Figure 5.25 Relationship between $\delta^{13}C$ and $1/C_t$ (total dissolved inorganic carbon). The scatter of data may be partly the result of CO_2 degassing during storage. The solid arrow represents calculated fractionation effect due to 20% gas loss at 5°C. Black dots represent calculated $\delta^{13}C$ and field DIC, assuming CO_2 gas loss (see text). Circled dots represent waters with no discrepancy between field and lab DIC. The high $\delta^{13}C$ for T-Zone samples may be the result of mixture with seawater. Symbols are as follows:

L = L-Zone, T = T-Zone samples.

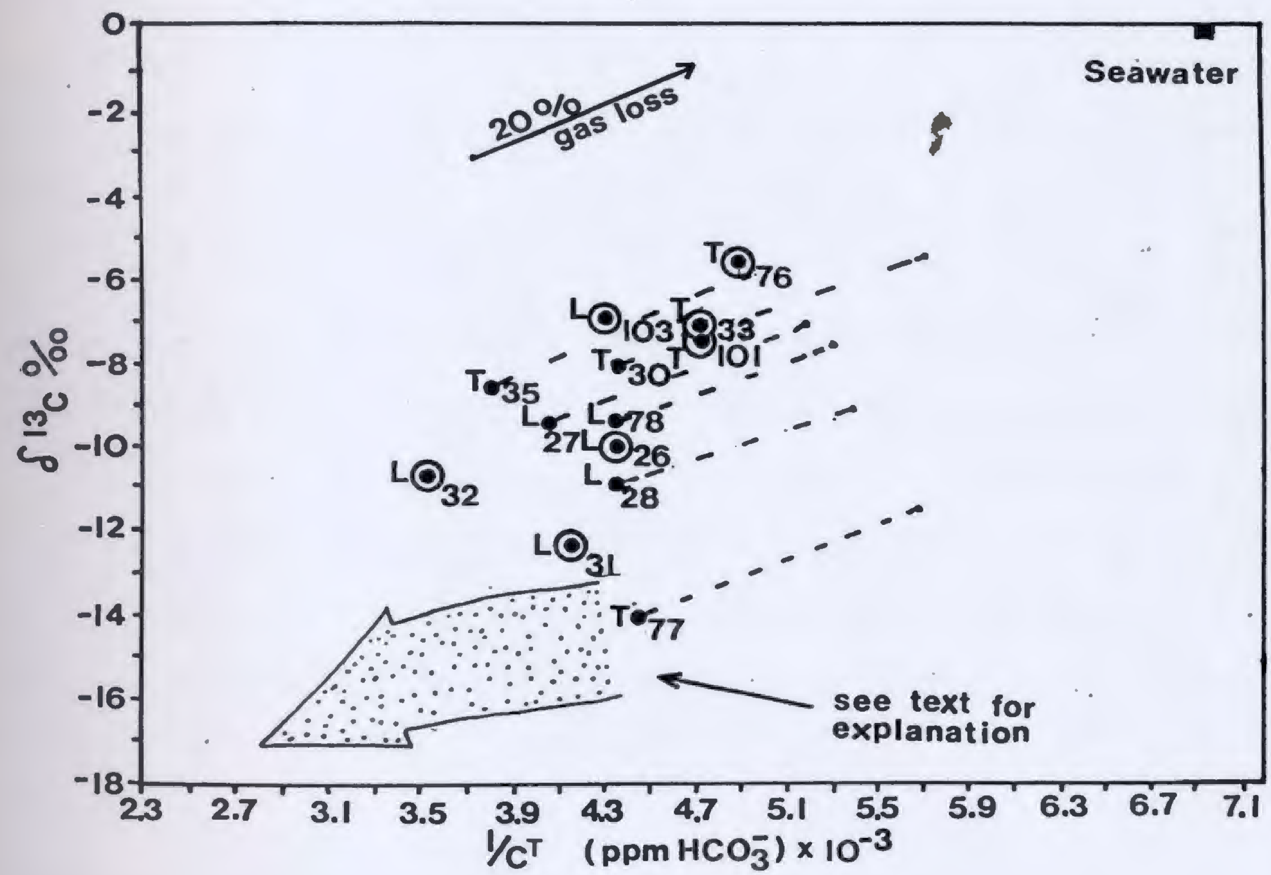

water was found by using the fractionation factor for CO_2-HCO_3 = 0.98975 at 5°C (Mook et al., 1974), and assuming that the ratio of lab to field DIC is the fraction of gas remaining. The field DIC and the calculated $\delta^{13}C$ are plotted as solid dots in Figure 5.25 with a trajectory back to the measured $\delta^{13}C$ and lab DIC.

The expected relationship in most carbonate terranes would be an increase in DIC for the deeper groundwater samples (eg. DH-76) which is the opposite of the trend suggested in Figure 5.25. An alternative hypothesis is that L-Zone groundwater evolved differently or has a different source than the T-Zone waters, and a mixing relationship is indicated. This would be consistent with mixing relationships suggested by major ions and $\delta^{18}O$ values.

L-Zone groundwaters are overall, closer to the $\delta^{13}C$ range and expected DIC for groundwaters that have dissolved carbonate rocks ($\delta^{13}C$ = -15 to -19 ‰; Deines et al., 1974). The $\delta^{13}C$ data suggest that T-Zone groundwaters may have obtained their higher $\delta^{13}C$ and lower DIC by mixing with seawater thereby supporting a seawater source for T-Zone salinity as indicated by $\delta^{18}O$ data.

5.4 Synopsis

The groundwaters of the Newfoundland Zinc mine and environs are basically of two groundwater types based on major-ion chemistry:

1) calcium-bicarbonate type--shallow, oxidizing, low total dissolved solids typical of surface wells and shallow

mine inflows

2) sodium-chloride type--reducing, high dissolved solids, saline groundwater found in the deeper parts of the mine.

The occurrence of gypsum, celestite, and barite in the mine and the shelf-type depositional environment of carbonate rocks which may host evaporite lenses, provide possible sources for the elevated salt content in these waters. High salinities may also be derived from relict seawater preserved in the deep groundwaters. Carbon-13 data argue against the dissolution of sulphate-type minerals and salts in carbonates as a source for T-Zone salinity and support seawater as a source of the salts.

Major-ion and trace-element chemistry, dissolved oxygen and oxygen-18 trends support the hypothesis that the deep saline T-Zone waters represent a regional groundwater flow system. Recharge for such a regional flow system may occur in the Long Range Mountains, as suggested by the oxygen-18 depletion in deeper groundwater samples.

Local dissolution of soluble minerals, and oxidation of sphalerite appear to control trace element concentrations. Isolated anomalies of zinc and other metal ions associated with zinc ore are restricted to shallow oxidizing groundwaters near known occurrences of developed and undeveloped sphalerite. Contours of high dissolved Zn concentrations indicate that local, shallow groundwater flows from Mike Lake south to Spring Lake.

5.5 Chemical Modelling

Two major questions can be asked in light of the geochemistry of Daniel's Harbour groundwaters: 1) How exactly do the shallow carbonate groundwaters evolve and what does this reveal about the hydrogeology? and 2) Do the saline groundwaters derived from ancient seawater that has mixed with groundwater belong to a regional flow system?

The purpose of this section is to establish possible evolutionary paths for the shallow carbonate groundwaters and origins for the deep saline waters of the Daniel's Harbour area, using the computer program PHREEQE (Parkhurst et al., 1980). The computer program calculates individual species concentrations, activities, saturation indices of possible minerals, and allows limited reaction-path modelling. PHREEQE is applicable for water temperatures from 0 to <100 degrees C. Activity coefficients are calculated by the extended Debye-Huckel method. The relevance of PHREEQE modelling results to real groundwaters is dependent on the thermodynamic data used, the validity of the extended Debye-Huckel activity coefficients, the choice of possible ion pairs, and the applicability of equilibrium calculations to natural systems.

Basic principles for developing geochemical models were implemented in the following modelling strategy (Plummer et al., 1983). Equilibrium speciation calculations were used to determine calcite and dolomite saturation indices and pCO_2 of the groundwater samples. These values were then used as constraints on the carbonate evolution and saline source groundwater models. Mixing of waters as a modelling procedure was done in the saline groundwater source models. Available geochemical evidence such as Ca/Mg and other molar ratios, oxygen-18 and trace-element data were used to constrain the choice of models. Mineral phases and reactions were chosen in light of the geology of the area and in no way represent the only possible models in this system, since one can model any final groundwater chemistry by choosing a variety of phases and reactions. Thus, a possible although not unique reaction path is suggested, using this type of modelling approach (Plummer et al., 1983). Models that will be discussed in the following text are: chemical speciation calculations, sensitivity analysis on saturation indices, shallow groundwater evolutionary paths, and saline groundwater origins.

5.5.1 Chemical speciation calculations

5.5.1.1 Characterization of groundwaters

As an initial step, chemical parameters (Eh, pH and T) and ion analyses were specified for each groundwater sample and the chemical speciation, saturation indices for relevant minerals and pCO_2 were calculated by PHREEQE. Results are listed in Table 5.5 for some of the water samples collected in 1985 and 1986. The chemical analysis entered for each of the samples was charge balanced using the elements Br and Ba since these do not complex significantly with the major species. The field temperature of each sample was used in the equilibrium speciation calculations.

Table 5.5 PHREEQE species modelling results for selected samples taken in 1985 and 1986. The saturation indices and log pCO_2 values found here were used as constraints in later models. Samples are sorted according to sample location/type. Symbols used in this table are:

- * rainwater sample used as the initial solution for modelling of evolutionary paths
- L groundwater samples from the L-Zone
- T groundwater samples from the T-Zone
- M mid-zone depth between the L and T Zones
- B borehole or well
- S sump discharge

Type	Spl#	Ca/Mg	pH	Eh	pe	SI_c	SI_d	$\log(pCO_2)$
1985:								
*	DH-023	1.67	5.82	218	3.68	<.01	<.01	-3.49
L	DH-009	1.03	7.29	255	4.30	0.38	0.09	-2.04
L	DH-010	1.17	7.55	332	5.60	0.66	0.25	-2.32
L	DH-011	1.14	7.30	337	5.70	0.59	0.19	-1.94
M	DH-013	1.32	7.20	53	0.90	0.30	0.04	-1.38
M	DH-014	1.10	7.25	12	0.20	0.34	0.07	-2.00
T	DH-005	0.72	7.41	-35	-0.60	0.41	0.15	-2.07
T	DH-006	0.88	7.42	83	1.40	0.51	0.19	-2.09
T	DH-007	0.93	7.52	-65	-1.10	0.64	0.29	-2.33
T	DH-008	0.90	7.51	-65	-1.10	0.56	0.23	-2.27
T	DH-012	0.71	7.48	-53	-0.90	0.55	0.28	-2.35
1986:								
B	DH-025	1.36	7.13	538	9.09	0.55	0.16	-1.93
S	DH-080	1.20	7.66	187	3.16	1.11	0.65	-2.39
B	DH-082	1.11	7.29	236	3.98	0.74	0.38	-1.94
B	DH-086	1.04	7.57	20	0.34	0.93	0.68	-2.23
L	DH-028	1.15	7.57	534	9.02	0.75	0.29	-2.31
L	DH-029	1.72	7.60	545	9.37	1.38	0.67	-2.31
L	DH-031	1.18	7.60	416	7.03	0.92	0.43	-2.32
L	DH-032	1.09	7.38	362	6.11	0.81	0.02	-2.04
L	DH-078	1.21	7.34	195	3.30	0.60	0.21	-2.07
L	DH-081	1.07	7.13	246	4.15	0.33	0.07	-1.86
L	DH-103	1.18	7.28	158	2.66	0.49	0.14	-2.01
M	DH-026	1.07	7.88	439	7.42	1.61	1.53	-2.62
M	DH-030	1.01	7.71	16	0.27	1.25	0.96	-2.47
M	DH-077	1.02	7.27	-188	-3.17	0.46	0.13	-2.04
M	DH-102	0.80	7.31	-104	-1.76	0.35	0.09	-1.99
T	DH-033	0.74	7.79	-20	-0.33	1.07	1.02	-2.60
T	DH-034	1.03	7.82	45	0.76	1.20	0.89	-2.58
T	DH-035	0.85	7.87	34	0.58	1.20	1.08	-2.56
T	DH-076	0.72	7.45	-189	-3.19	0.50	0.23	-2.27
T	DH-101	0.74	7.81	-113	-1.91	1.21	1.34	-2.62

The degree of mineral saturation is expressed by the saturation indices in the following format:

$S.I._c = [Ca^{2+}][CO_3^{2-}]/K_{sp}(\text{calcite})$
$S.I._d = [Ca^{2+}][Mg^{2+}][CO_3^{2-}]^2/K_{sp}(\text{dolomite})$
$S.I. = 1$ or $\log(S.I.) = 0$ is a state of saturation
$S.I. < 1$ or $\log(S.I.) < 0$ is a state of undersaturation
$S.I. > 1$ or $\log(S.I.) > 0$ is a state of supersaturation.

The log pCO_2 for these waters (see Table 5.5) is generally higher than that of the atmosphere indicating derivation of CO_2 from the soil zone (Freeze and Cherry, 1979). These groundwaters are more saturated with respect to calcite than to dolomite. This could be the result of the slower rate of dolomite dissolution (Rauch and White, 1970). Calcite supersaturation in a dolomite-water system can occur at temperatures observed in Daniel's Harbour groundwater (Palmer and Cherry, 1984).

Although saturation with respect to calcite and dolomite is typical of groundwaters in carbonate terrain and soil zones with abundant carbonate minerals (Thrailkill, 1968), many Newfoundland Zinc Mine samples deviate from this condition. Generally, saturation indices calculated using PHREEQE (Table 5.5) show that 1985 groundwaters were less saturated than 1986 groundwaters. Some 1985 samples were much more undersaturated than samples taken at the same site in 1986 (eg. DH-11 vs DH-32). None of the 1985 (L-and T-Zone) samples were saturated with respect to calcite and dolomite, whereas half of the 1986 L-Zone samples were saturated within calculation uncertainity limits (see Section 5.5.1.2). Most 1986 T-Zone samples were saturated to supersaturated with respect to calcite and dolomite. The fact that DH-29 was supersaturated with calcite and had δ^2H and $\delta^{18}O$ shifted along an evaporation slope supports the hypothesis that some L-Zone groundwaters are derived from the supersaturated Spring Lake waters.

The undersaturated groundwaters may be explained by dissolution kinetics or by the mine hydrogeology. As long as 16 days may be required for a solution to reach equilibrium with calcite (Plummer et al., 1979) and dolomite dissolution can take much longer (Rauch and White, 1970). Undersaturation could be the result of slow kinetics of dissolution versus the high flow rates that were experienced in 1985 (mine pumpage up to 38,000 l/min) in response to higher rainfall (see Figure 4.2). The 1986 summer drought caused lower groundwater inflows (24,000 l/min); lower velocities may have allowed more time for groundwaters to equilibrate with mineral phases (Freeze and Cherry, 1979).

Another explanation for this undersaturation is the occurrence of secondary processes such as mixing and dilution. This theory is in agreement with the mine mixing relationships indicated by major-ion trends (Section 5.3.1). Initially saturated groundwater that mixes with another saturated groundwater of different pH and pCO_2, or a more dilute undersaturated water, may cause undersaturation of the resultant groundwater (Plummer, 1975). Higher rainfall during 1985 and subsequent greater mine inflows may have caused shallow groundwater to mix more with T-Zone groundwater and with rainwater (dilution). Supersaturation of 1986 T-Zone samples may also be due to degassing at the sample site or a result of HCO_3/pH measurement errors (see Section 5.5.1.2).

5.5.1.2 Sensitivity analysis on saturation indices

It was suggested previously that the calculated 1985 and 1986 saturation indices (Table 5.5) may be different for hydrogeological reasons but their difference could also be due to pH, temperature or alkalinity errors.

The saturation index for calcite is defined by the following formula:

$$S.I._{calcite} = \frac{\dfrac{[Ca^{2+}]\,[HCO_3^-]\,K_{HCO3-}}{[H^+]}}{K_{sp}(calcite)}$$

Uncertainties for each of the above measured parameters add up to an estimated accumulated uncertainity of +/- 10 % for the saturation index. This is assuming a 0.2 % error for Ca (+/- 0.1 ppm; see Section 2.1.4), and 4.0 % uncertainity for alkalinity and pH measurements (assuming +/- 0.02 pH unit error); in addition, a possible error introduced by a change in temperature from the time of sampling to the actual time of measurement (5 ^oC = 15 % change in S.I. calcite; see Figure 5.26) must be considered. However, if degassing at the sample site is significant, as suggested by some DIC samples (Section 5.3.4.2), then an even larger effect on the calcite saturation indices would be expected. As CO_2 evolves from solution, the resultant pH rise would cause an increase in CO_3^{2-} concentration and hence an increase in the saturation index of carbonate minerals.

A sensitivity analysis was done on 16 mine samples from 1985 and 1986 to test the susceptibility of saturation indices to pH error; results are given in Table 5.6. The pH input to PHREEQE was changed by small increments to simulate possible errors for a given pH measurement. The measured temperature of each sample was used in the sensitivity calculations.

Most of the 1986 T-Zone groundwater samples have very similar pH-crossover points for both saturation indices (<0.07 pH units deviation) indicating conditions near or at equilibrium. Representative samples, DH-33, 35 and 101 have been plotted on Figure 5.26. Samples DH-30, 34 are also close to a state of equilibrium (<0.1 pH unit difference). DH-76 and DH-12 are exceptions since they have very close calcite and dolomite crossover points but not at the measured pH. Aqueous phases in these samples could be in equilibrium with calcite and dolomite

Table 5.6 Results from an analysis of the sensitivity of calcite and dolomite saturation indices to errors in pH. Samples considered at or near saturation had < 0.1 pH unit between the crossover points for saturation indices at equilibrium and measured pH. Groundwaters truly undersaturated had a difference >0.10 pH unit. A pH measurement error of 0.3 pH units may be the cause of disequilibrium for the samples DH-12 and 76. ΔpH = measured pH - calculated pH for equilibrium

Truly Saturated			Truly Undersaturated			Probably Undersaturated		
Spl.#	Location	ΔpH	Spl.#	Location	ΔpH	Spl.#	Location	ΔpH
DH-30	Mid-Zone	0.10	DH-09	L-Zone	-0.43	DH-12	T-Zone	-0.26
DH-33	T-Zone	0.03	DH-10	L-Zone	-0.18	DH-76	T-Zone	-0.30
DH-34	T-Zone	0.08	DH-11	L-Zone	-0.23			
DH-35	T-Zone	0.08	DH-14	Mid-Zone	-0.47			
DH-101	T-Zone	0.08	DH-28	L-Zone	-0.13			
			DH-32	L-Zone	-0.11			
			DH-103	L-Zone	-0.31			
			DH-08	T-Zone	-0.24			

Figure 5.26 Sensitivity analysis of pH error on saturation indices (S.I.) of calcite and dolomite. The measured pH for each sample is given in the upper left corner of the figure. T-Zone samples in this figure have similar measured pH crossover points for log(S.I.) of calcite and dolomite, indicating these samples are in, or close to a state of equililbrium. Symbols and the error bar (due to a maximum 5°C shift in temperature) also apply to Figure 5.27. Temperature for sensitivity calculations was the field measured temperature for each sample.

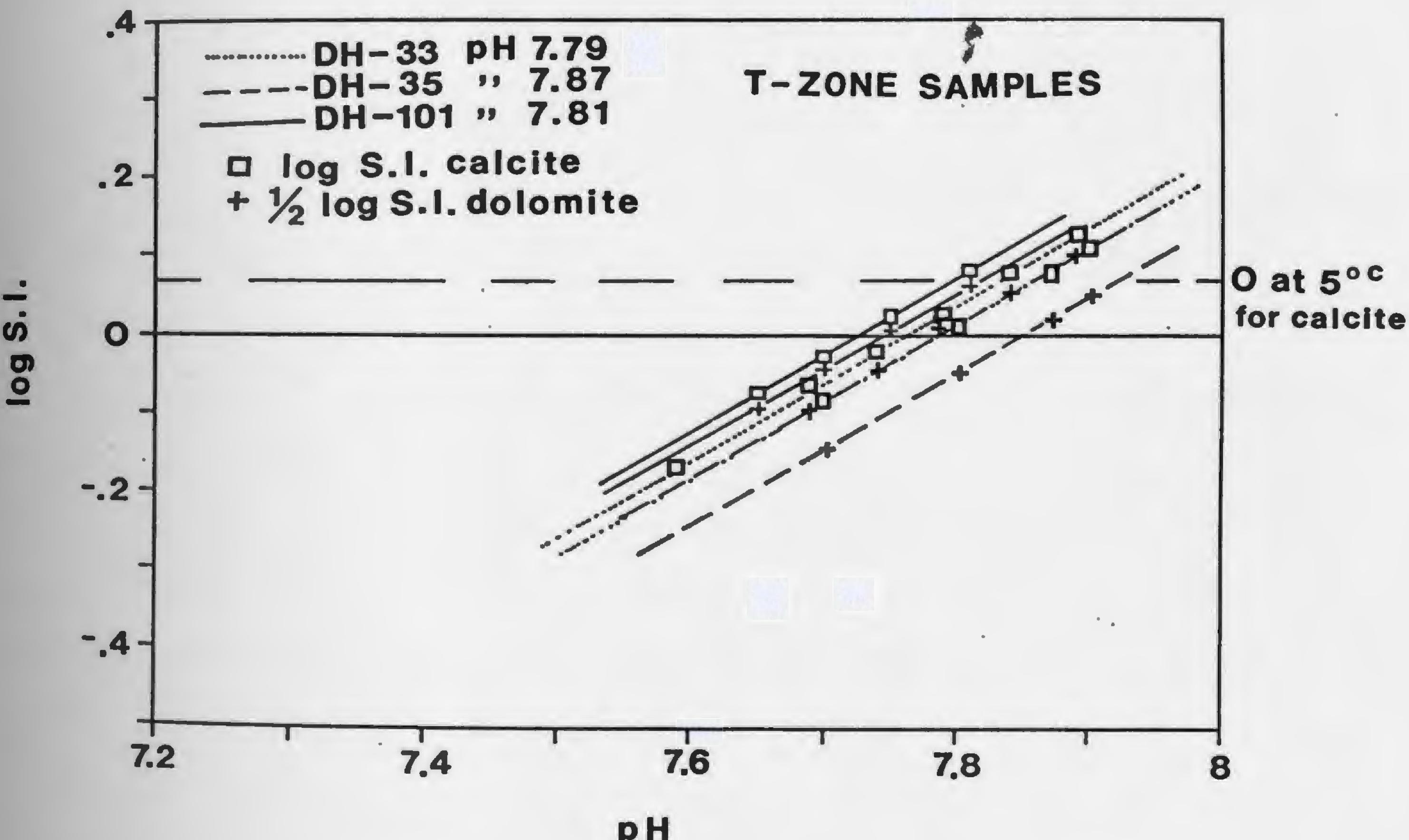

if a large pH measurement error of - 0.30 pH units was made (i.e. if measured pH was too low). But this error is much greater than the reported precision of +/- 0.02 pH units.

Samples that are truly in a state of disequilibrium have a difference between measured pH and saturation crossover point equal to or greater 0.10 pH unit (see Table 5.6). DH-9, 28 and 32 are plotted on Figure 5.27 as examples.

The following conclusions can be made from the sensitivity analysis: All 1986 shallow (L-Zone) groundwater samples tested are in a state of disequilibrium with respect to calcite and dolomite. Generally, 1986 T-Zone samples are near or at calcite/dolomite saturation. T-Zone samples DH-30 and DH-35 show large differences between field and lab DIC (see Section 5.3.4.2). Since these samples are not supersaturated then the lower lab DIC suggests CO_2 loss during storage rather than at the sample collection site. Results for L-Zone samples may suggest secondary disequilibrium caused by groundwater mixing. Only one sample (DH-12) from 1985 could be in a state of equilibrium with the carbonate minerals (if a large error of 0.26 pH units was assumed). The state of disequilibrium (with respect to calcite and dolomite) in most 1985 groundwaters may be a result of the fast flow rates for this 'wet' year or increased mixing due to higher water table elevations in 1985.

5.5.2 Shallow groundwater evolutionary paths

It was established in Section 5.5.1.2 that shallow mine

Figure 5.27 L-Zone groundwater samples appear to be in a state of true disequilibrium since their log(S.I.) vs pH crossover points are greater than 0.10 pH unit. The measured pH is consistently lower than what is required for calcite or dolomite saturation.

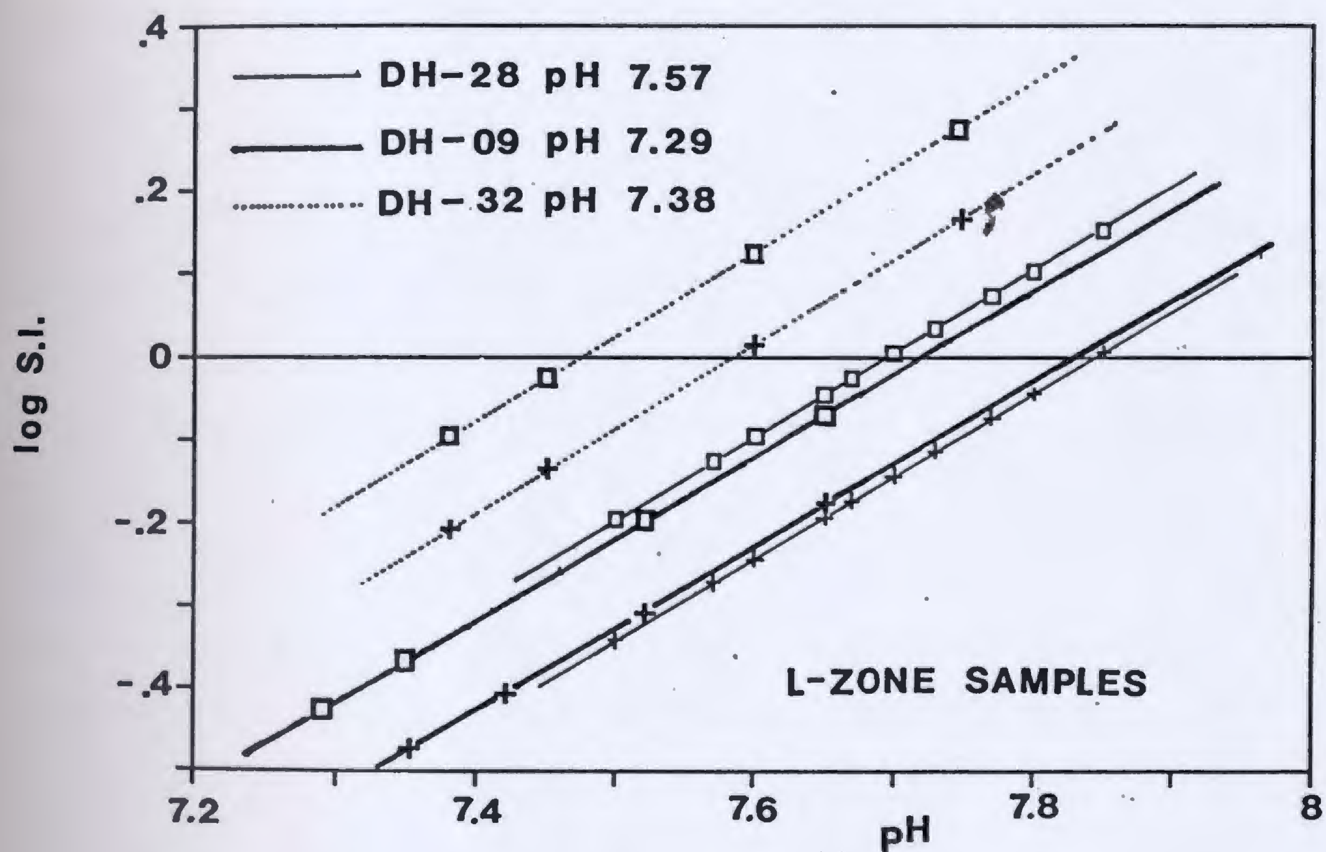

groundwaters (L-Zone) are indeed undersaturated with respect to calcite. Two possible evolutionary paths for the shallow groundwaters were tested in this modelling exercise to account for their observed chemical compositions: 1) closed-system dissolution of carbonate minerals to partial equilibrium (assuming groundwater infiltration along fractures allowing only partial dissolution of calcite/dolomite below water table) and 2) open-system dissolution to equilibrium followed by mixing/dilution (assuming infiltrating groundwater equilibrated with carbonate minerals in the soil zone).

Several assumptions were made in modelling these possible evolutionary paths. It was assumed: 1) that groundwaters flowed through dolostones and limestones, hence dolomite and calcite were the mineral phases chosen; and 2) that aqueous phases reacted with pure minerals (Mg-calcite was not used in the models).

The initial water used to dissolve the various minerals was represented by a sample of rainwater (DH-23) collected at the mine site. The log pCO_2 for rainwater in equilibrium with the atmosphere was assumed to be -3.5. In each model the Eh is held constant at the value measured in the field. Two average waters were chosen to represent (A) groundwaters of the L-Zone, and (B) deeper saline groundwater of the T-Zone (see Table 5.7). Modelling results were judged by how well they compared with average groundwaters. The reaction steps that were modelled are typical for carbonate terranes: an acidic rainwater equilibrating

Table 5.7 Averages and ranges of some chemical parameters for A) dilute shallow and B) deep saline groundwater, used in evolutionary models and for comparison of saline water source models. Ranges of the most important parameters are included for comparison. Average molar ratios were calculated from average element concentrations, not from an average of all calculated ratios. Samples used for the shallow groundwater average are DH -28,31,32,78,81,82,83,84,87,103 and for the saline groundwater average DH-5,6,7,8,12,33,34,35,76,101.

* only 1986 samples in Table 5.6 used for this average,
** only L-Zone mine samples used for this average
*** range does not include 33 and 76 (see Figure 5.23)

	A) SHALLOW GROUNDWATER		B) T-ZONE SALINE GROUNDWATER	
parameter	average	range	average	range
pH	7.4	(7.13-7.60)	7.61	(7.41-7.87)
Eh (mvolts)	288	(148-496)	-37	(-177 to -78)
T (^{o}C)	5.7 **	(4.1-10.8)	5.84	(4.6-6.7)
log pCO_2	-2.12	(-1.86 to -2.32)	-2.14	(-2.62 to -2.07)
$S.I._c$	0.656	(0.33-0.92)*	1.169	(0.5-1.21)*
$S.I._d$	0.242	(0.02-0.43)*	1.083	(0.23-1.34)*
Ca/Mg	1.2	(1.01-1.44)	0.79	(0.71-1.03)
Ca (ppm)	65.55	(52-83)	63.6	(38-98)
Mg "	34.14	(27-41)	48.1	(28-84)
Na "	13.47	(11-17)	367	(107-500)
HCO_3 "	226.00	(217-276)	231	(207-284)
SO_4 "	43.20	(13-62)	172	(58-310)
Cl "	21.22	(10-39)	505	(115-988)
Sr "	0.178	(0.04 - 0.290)	0.299	(0 - 1.046)
δO-18 (^{o}/oo)	-9.84	(-11.31 to -8.52)	-10.21	(-10.59 to -10.03)***
NO_3 (ppm)	4.00		7	
K "	1.80		21	
Fe "	0.03		0.1	
Mn "	0.01		0.0	
Al "	0.20		0.3	
Ca/Cl	3.22		0.11	
Mg/Cl	2.63		0.13	
Na/Cl	1.13		1.12	
Na/K	12.59		29.72	
SO_4/Cl	0.99		0.13	
Sr/Ca	0.0012		0.0021	

with soil-zone CO_2, dissolving calcite/dolomite while pCO_2 decreases and pH and saturation indices of the water increase (Palmer and Cherry, 1984). The observed saturation indices for 1986, were used as reaction end-point constraints in the modelling.

5.5.2.1 Closed-system model

Assumptions and conditions

The undersaturation of L-Zone groundwaters may represent a partial approach to equilibrium due to the kinetics of carbonate dissolution. Kinetic factors would be most effective if recharge occurred dominantly through joints, sinkholes and faults where the ratio of rock surface area to volume of water is low. Consequently, higher flow velocities and minimal rock/water contact in these fractures would prevent or delay the infiltrating groundwater from reaching equilibrium with calcite/dolomite in the soil zone, even if abundant carbonates were present in the soil zone. Thus, little carbonate dissolution would occur, even in the presence of a continuous supply of CO_2 (soil zone), and most dissolution would occur beneath the water table under closed-system conditions (restricted supply of CO_2). High flow velocities have been documented as a major control causing undersaturated conditions in carbonate terrains (Thrailkill, 1968).

For the first modelling phase, carbonate undersaturation is assumed to be a function of slow kinetics of dissolution, and is approximated by a partial approach to equilibrium. Five separate scenarios were modelled to cover the possible mineral sequences encountered by infiltrating water. These are listed below:

Model 1 - calcite dissolution only
Model 2 - dolomite dissolution only
Model 3 - dolomite and calcite dissolution simultaneously
Model 4 - dolomite then calcite dissolution
Model 5 - calcite then dolomite dissolution.

Palmer and Cherry (1984) emphasized that the sequence of minerals encountered by water is an important influence on the chemical evolution of groundwaters.

To simulate the lack of attainment of equilibrium under closed-system conditions, rainwater was equilibrated initially with specified pCO_2 levels and then was allowed to dissolve carbonate minerals to specified saturation states characteristic for shallow groundwater: calcite to a S.I. of 0.656 and dolomite to a S.I. of 0.242 (Model 3, 4, 5) or 0.246 (Model 2). The range for the log pCO_2 for the soil zone (initial log pCO_2) was chosen to be -1.4 to -1.2, characteristic of northern North American topsoil (Palmer and Cherry, 1984; Deines et al., 1974). Field log pCO_2 measurements are unavailable for Newfoundland soils; but soil log pCO_2 values calculated from shallow groundwater chemical data collected from eastern Newfoundland are high and range from -0.87 to -1.37 (S. Schillereff, personal communication). The temperature was held constant at the average temperature for shallow groundwater (5.7^{o}C).

Results

Selected results from closed-system modelling are listed in Table 5.8 and summarized in Figure 5.28. The model numbers listed in column 1 of Table 5.8 refer to the five mineral scenarios specified previously. Initial soil-zone log pCO_2 of -1.4 to -1.2 gave the most reasonable ranges for the final pCO_2 observed in the Daniel's Harbour groundwaters (log pCO_2 -1.86 to -2.32; Table 5.7A). From preliminary modelling it was determined that at a higher temperature (15^oC) an initial soil-zone log pCO_2 of -1.3 would give the best approximation of the observed shallow groundwater parameters. This value is close to the lowest values calculated for eastern Newfoundland soils (S. Schillereff, personal communication). Lowering the temperature to 5^oC raises the bicarbonate, Ca and Mg concentrations and has about the same effect on the HCO_3^- concentration as raising the log pCO_2 by 0.1. The final dolomite saturation index for Model 4 is slightly higher than what was initially specified because of the sequence of mineral dissolution. After the groundwater reached the prescribed state of equilibrium with dolomite it then dissolved calcite which increased the Ca concentrations and thus the S.I. of dolomite.

Models # 1 and 5 can be discarded on the basis of very high Ca/Mg ratios and their inappropriate saturation indices for dolomite. In Model 1, the Ca/Mg ratio is large and the dolomite S.I. is too low because pure calcite was the only mineral dissolved and there was no additional source of Mg except the

Table 5.8 Selected results from closed-system carbonate dissolution models. Initial pCO_2 conditions were varied in each model. These models assumed that L-Zone carbonate groundwater had not reached equilibrium with carbonate minerals due to kinetic factors and so observed S.I.'s were specified to approximate partial attainment of equilibrium. Symbols are as follows:

ASG	average shallow groundwater (for comparison)
*	in ppm
^	models plotted on Figure 5.28
$S.I._c$	saturation index for calcite
$S.I._d$	saturation index for dolomite
i,f	initial and final pCO_2

Mdl#	log pCO_2i	log pCO_2f	molar Ca/Mg	Ca*	Mg*	HCO_3*	pH	$S.I._c$	$S.I._d$
1	-1.3	-1.84	59.4	88.1	0.9	315	7.18	0.656	0.005
2	-1.4	-2.20	1.0	42.0	25.5	269	7.50	0.624	0.246^
2	-1.3	-1.99	1.0	49.8	30.2	330	7.37	0.624	0.246
2	-1.2	-1.80	1.0	58.4	35.4	404	7.24	0.624	0.246
3	-1.4	-2.15	1.1	44.4	24.0	269	7.50	0.656	0.242^
3	-1.3	-1.97	1.1	52.6	28.4	330	7.37	0.656	0.242
3	-1.2	-1.78	1.1	61.6	33.4	403	7.24	0.656	0.242
4	-1.4	-2.21	1.0	42.5	25.4	270	7.51	0.656	0.269^
4	-1.3	-2.00	1.0	50.4	30.1	331	7.38	0.656	0.268^
4	-1.2	-1.81	1.0	59.3	35.4	405	7.25	0.656	0.267
5	-1.3	-1.85	59.4	88.1	0.9	315	7.18	0.656	0.005
	ASG	-2.12	1.2	65.6	34.1	226	7.40	0.656	0.242

Figure 5.28 Comparison of shallow groundwater evolutionary models under open and closed pCO_2 conditions. The best approximation of the average shallow groundwater is obtained by models 2, 3, and 4. The bar represents parameter ranges found in shallow groundwater of the mine and serves as a comparison with the possible evolutionary paths represented by the selected models. Shallow groundwaters included in this range are DH -28,31,32,78,81,82,83,84,87,103. Closed-system Models 2, 3, 4 and Models 2 and 4 from the mixing models (open-system) have been plotted. Initial and final pCO_2 are also included for comparison.

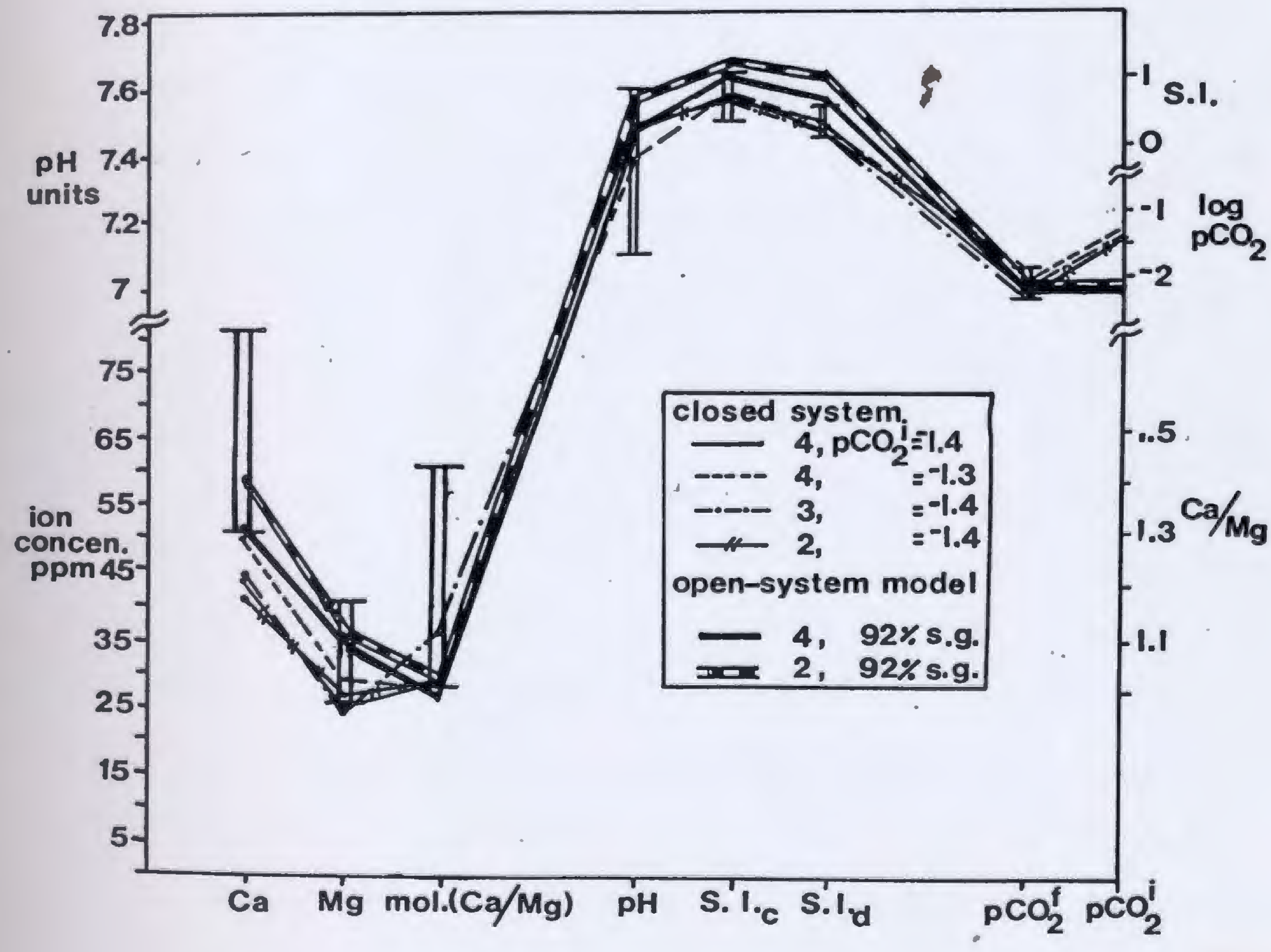

initial rainwater. Groundwaters that flow through limestone become saturated with calcite and when they reach dolomite, already laden with Ca^{2+}, they become supersaturated with respect to calcite as very little dolomite is dissolved. In Model 5 the Ca/Mg ratio is large and the final dolomite S.I. is too low because not enough dolomite was able to dissolve in order to increase the Mg concentration under the specified conditions.

With the exception of the high HCO_3^- content, closed-system models 2, 3, and 4 at log pCO_2 between -1.4 and -1.3 approximate the observed shallow groundwater carbonate chemistry. The most realistic final log pCO_2, Ca, Mg and HCO_3 values are obtained with an initial log pCO_2 of -1.4 and these scenarios are plotted in Figure 5.28. Lower HCO_3^- concentrations could be obtained by using an initial log pCO_2 lower than -1.4 but this would also lower the Ca and Mg levels. Ca and Mg contents do not match exactly the 'Shallow Groundwater' in Table 5.7A but they are close to the lowest observed concentrations, indicating that reasonable Ca and Mg concentrations can be obtained from models that always dissolved dolomite in the modelling scenario. Higher Ca concentrations were obtained in Models 1 and 5 but observed levels of Mg are not obtained since calcite is dissolved first. Raising the pCO_2 would obtain higher Ca and Mg concentrations but this would result in too high HCO_3^- concentrations, producing a lower than representative pH and generating an unrealistic final pCO_2. The average saturation indices may not approximate the system as well as they were intended and a more suitable (greater) index could be chosen to better approximate the equilibrium state and the Ca and Mg concentrations for the shallow groundwaters. However, this would not help in distinguishing between the 3 best models, thus requiring other constraints for subsequent elimination of the remaining models.

5.5.2.2 Open-system model

Assumptions and conditions

In the second phase of modelling, carbonate undersaturation in shallow groundwaters is assumed to be the result of secondary processes: mixing and dilution of initially saturated groundwaters. Groundwaters would attain equilibrium quickly if they were recharged through overburden containing carbonate minerals (see Section 3.5). Thus, carbonate dissolution would occur under open-system conditions (continuous supply of CO_2) in the soil zone.

In the first step of this modelling phase, saturated shallow groundwater, produced by equilibrating rainwater with carbonate minerals at an initial log pCO_2 value of -2.12, was mixed with saturated average T-Zone groundwater. The lower initial pCO_2 as compared to closed-system models, was necessary for open-system carbonate dissolution (continuous supply of CO_2) if the models were to approximate observed pCO_2 values in shallow groundwaters. An average log pCO_2 value of -2.12 is still a reasonable value for North American soils. A low log pCO_2 value of -2.12 for closed system modelling would result in lower Ca, Mg and HCO_3

concentrations than what is observed in shallow groundwater and thus higher initial pCO_2 values were required in the closed system models since the CO_2 reservoir is diminished and not replenished as groundwaters dissolve aquifer minerals.

The T-Zone endmember was found in a separate exercise by taking an average T-Zone groundwater in Table 5.7B and equilibrating it with calcite and dolomite. The resultant solution from the mixture of shallow and T-Zone groundwaters was not re-equilibrated with the carbonate minerals. For these models, the major source of Cl in shallow groundwater would be T-Zone water with minor contributions from rain. Thus, the range of Cl concentrations in shallow groundwater (10-39 ppm, average=21ppm) was used as a constraint on mixing proportions. For example, to obtain the maximum L-Zone Cl content of 39 ppm, 0.92 parts shallow groundwater was mixed with no more than 0.08 parts T-Zone groundwater.

In the second step of this modelling phase, Cl was assumed to be derived only from rainwater. The constraints on mixing would be mixing proportions that result in Cl concentrations of 10 to 21 ppm. In this scenario, shallow carbonate groundwater is produced by rainwater dissolving carbonate minerals to equilibrium under open-system conditions and then mixing with a second solution, the chemistry of which was rainwater.

Only the most reasonable mineral sequences (models 2, 3, and 4) from the initial closed-system modelling (see Section 5.5.2.1) were repeated in the open-system modelling. All the modelling was done at a temperature of 5.7°C.

Results

Results from the open-system mixing models are listed in Table 5.9. The only source of Cl in models that mixed saturated shallow carbonate groundwater with rainwater is the rainwater itself. Hence, observed L-Zone Cl concentrations greater than 0.5 ppm cannot be obtained by simply equilibrating rainwater with carbonate minerals and then mixing the resultant water with rainwater. Low Cl concentrations observed in shallow groundwaters could be obtained by mixing with T-Zone groundwater in lower proportions (0.98 in Table 5.9). However, this did not result in undersaturation of the final groundwater. Higher Cl levels could have been obtained by a two-stage mixing process: 1) mixing of L- and T-Zone groundwaters followed by 2) mixing with rainwater. This hypothesis was not tested.

Table 5.9 shows that when shallow groundwater was mixed with T-Zone groundwater in the most appropriate proportions (0.92-0.96) the resulting groundwater was only slightly undersaturated with respect to calcite and dolomite in Models 3 and 4, and saturated with respect to calcite in Model 2. The one example of rainwater mixing (see Table 5.9) best approximated the undersaturation observed in shallow groundwaters, but its Ca/Mg and Cl concentration were too low. This may indicate that dilution with rainwater as well as mixing with saturated T-Zone groundwater was responsible for calcite/dolomite undersaturation

Table 5.9 Results from open-system carbonate dissolution models. Mixing initially saturated shallow groundwater with T-Zone type (saturated) water. One model representing a mixture of saturated shallow groundwater and rainwater (undersaturated) is also given. The resultant groundwater for most models is slightly undersaturated with respect to calcite and dolomite. Initial log pCO_2 of -2.12 (average for shallow groundwater) and T=5.7°C. Symbols are the same with the following exceptions:

f	final pCO_2
^	these models have been plotted on Figure 5.29
*	in ppm
**	in this model Cl = 0.5ppm for a 80% S.G. and 20% rainwater mixture
S.G.	shallow groundwater
ASG	average shallow groundwater

Mdl#	Portion S.G.	log pCO_2f	molar Ca/Mg	Ca*	Mg*	HCO_3*	Cl*	pH	$S.I._c$	$S.I._d$
^2	0.92	-2.14	1.0	57.7	36.5	360	41	7.56	1.205	0.957
2	0.96	-2.13	1.0	57.7	35.8	365	21	7.56	1.230	0.977
2	0.98	-2.13	1.0	57.7	35.4	367	11	7.55	1.245	0.989
3	0.92	-2.14	0.6	46.1	44.2	363	41	7.56	0.977	0.955
3	0.96	-2.13	0.6	45.6	43.7	368	21	7.56	0.989	0.975
3	0.98	-2.13	0.6	45.3	43.6	370	11	7.56	0.993	0.986
^4	0.92	-2.14	0.9	51.5	36.5	341	41	7.54	0.971	0.697
4	0.96	-2.13	0.9	51.3	35.8	345	21	7.54	0.984	0.705
4	0.98	-2.13	0.9	51.1	35.4	347	11	7.53	0.991	0.709
3	0.80**	-2.19	0.6	36.4	34.9	298	0.5	7.54	0.690	0.519
ASG		-2.12	1.2	65.6	34.1	226	21	7.40	0.656	0.242

in the shallow groundwaters. In that case, the saturation index would not be the most sensitive criterion to determine the best representative model for the evolutionary path of the shallow groundwater.

All three models approximated observed values for final log pCO_2, exhibited higher than average pH values and Mg concentrations (although still within L-Zone range) and very high HCO_3^- concentrations. As a result, the most sensitive indicators in open-system modelling are Ca/Mg ratio and Ca content which indicate Model 2 (dolomite dissolution) and Model 4 (dolomite then calcite dissolution) represent the evolution of shallow groundwater better than Model 3 (dolomite and calcite dissolution simultaneously).

5.5.2.3 Comparison of results from evolutionary path models

The best runs from both closed- and open-system modelling are plotted in Figure 5.28. These models approximate the lower limit of the ranges for Ca and Ca/Mg observed in shallow groundwaters of the Newfoundland Zinc Mine. The shallow groundwaters with very high Ca concentrations (>85 ppm; DH-25,29,85) were excluded from the range shown in Figure 5.28. This is an arbitrary cut-off and samples included in the range with relatively high Ca (65-85 ppm) may not be representative of calcite dissolution, and other processes such as local salt-type mineral dissolution may be involved (see Section 5.3.1).

Each model run represents a submodel (referred to as Models

2, 3 or 4) from either closed- or open-system modelling that was run at different pCO_2 or mixing proportions, respectively. Only one mixing ratio (0.92) for Models 2 and 4 is plotted in Figure 5.28 since differing mixing proportions for each open-system mixing model changed the carbonate chemistry very little.

Under closed-system conditions, dissolution of mineral sequences represented by Models 2, 3, and 4 results in solutions having chemical compositions similar to shallow groundwaters at the mine, provided the initial log pCO_2 is -1.3. Similarly, appropriate concentrations can be obtained by Models 2 and 4 under a continuous supply of CO_2 at log pCO_2 = -2.12 and if mixing proportions of saturated shallow and saturated saline groundwater are (0.92-0.96) and (0.08-0.04), respectively. Closed-system modelling results suggest that shallow groundwater may be the result of carbonate mineral dissolution to partial equilibrium by rainwater under a restricted supply of CO_2.

The most sensitive criterion in distinguishing between open- or closed-system models is the concentration of Ca. Ca/Mg ratios are very similar for both closed- and open-system models, with the exception of Model 3 (see Table 5.9) and the saturation indices were fixed in the closed-system modelling. The undersaturated state of shallow groundwaters could not be duplicated by the open-system models, arguing against single-stage mixing as a part of shallow groundwater evolution. However, the best absolute Ca concentrations were obtained by open-system modelling suggesting these models are oversimplified and multi-stage mixing could be responsible for the undersaturation. Closed-system models at log pCO_2 = -1.4 reproduced the undersaturated state and approximated Ca content in shallow groundwaters. Thus, on the basis of this modelling and the stated criteria, shallow groundwaters from the mine may have evolved by dissolving dolomite only, dolomite and calcite simultaneously, or dolomite then calcite to undersaturation under a restricted supply of CO_2, or by dissolving the above mineral sequences to saturation and then mixing with a different type water under a continuous supply of CO_2. These simple models were useful in proving that dolomite is necessary in the mineral dissolution sequence and that a more complex evolution than what has been modelled thus far is necessary to duplicate observed values for all diagnostic parameters.

Based on geological evidence it is more realistic to assume that open rather than closed conditions exist at the mine site. Open-system conditions would occur in the carbonate rocks above the depressed water table and in the glacial overburden which contains carbonate minerals (Section 3.5). Geologically, closed-system dissolution of carbonates is unlikely because it would restrict recharge to the relatively rare fractured outcrops in the area and infiltrating water would assuredly encounter carbonate minerals before reaching the depressed water table. However, Deines et al. (1974) established that closed-system rather than open-system dissolution of carbonate rocks resulted in $\delta^{13}C$ similar to L-Zone groundwaters (-9 to -12.5). This information suggests that recharge at the mine site is dominated by joint and sinkhole conduits and not by more diffuse modes of flow that would occur in the glacial deposits.

Simultaneous dolomite and calcite dissolution (Model 3) is physically quite possible due to the lateral facies changes between limestone and dolostone within an assigned unit. Models 1 and 5 (closed sytem) and Model 3 (open system) were discarded after preliminary modelling indicated that shallow groundwaters most likely evolved by dissolving dolomite first. Thus, the sequence of mineral assemblages encountered is important in the evolution of these groundwaters (eg. calcite dissolution cannot precede dolomite dissolution).

The hydrogeological implication of this conclusion is that the shallow groundwater must have first dissolved dolostone and was not recharged in limestone (ie. not along the anticlinal axis; see Figure 3.3). This limits groundwater recharge to areas underlain by dolostone. The association of known sinkholes with dolostone areas suggests that groundwaters are recharged through sinkholes, which in turn supports the assumption that kinetics are a cause of disequilibrium. The Mike Lake-Zinc Lake-Lead Lake basin (see Figure 4.1) appears to be a logical area of recharge since it is underlain by dolostone and has known sinkholes (e.g. Lead lake sinkhole that may have an underground connection to the mine; Acres, 1974). Most of the L-Zone workings are overlain by dolostone implying possible direct recharge to the mine from above.

One would expect that groundwater encountering dolostone first, would have a lower Ca/Mg ratio than groundwater that first encounters limestone. The opposite is the case for diamond drill hole DH-82 (collared in dolostone) and DH-86 (collared in limestone; see Table 5.5). With this limited information from drill samples it is difficult to draw conclusions about the evolution of the shallow groundwaters in light of the local variations seen in the groundwaters (DH-25) already discussed in previous sections. More data from other wells in both limestone and dolostone areas would be needed to determine if there is indeed a connection between the chemistry of the groundwaters and the major rock type at the well collar location. In these modelling exercises the Ca/Mg ratio was a sensitive indicator in determining the best model that represented the mineral dissolution sequence in shallow groundwater evolution.

5.5.3 Dilute seawater/shallow groundwater mixing model

5.5.3.1 Assumptions and conditions

In this modelling section shallow groundwater/dilute seawater mixing was tested as a possible origin of the saline water found in the deeper parts of the mine. The source of seawater may be modern seawater encroaching inland, or ancient seawater now relict at deeper levels in the carbonate aquifer. A 1:18 seawater/shallow groundwater mixing ratio is needed to produce T-Zone chloride concentrations of 1000 ppm. This dilution can not reproduce $\delta^{18}O$ values of -10.3 $^{o}/oo$, typical of average T-Zone groundwater. Thus, direct mixing with seawater (seawater intrusion) can be ruled out on the basis of $\delta^{18}O$ values. However, a low $\delta^{18}O$, saline groundwater could have been produced by mixing seawater with groundwater recharged at a higher elevation in a regional flow system. Ancient seawater may have been trapped during the Wisconsinan ice age when this platform was inundated by seawater. This hypothesis is tested quantitatively in the following section.

The decrease in $\delta^{18}O$ values with increasing Cl concentrations in T-Zone groundwaters is assumed to be the result of a higher recharge elevation for the meteoric component of these waters. Since direct mixing of shallow groundwater with seawater can be ruled out on the basis of $\delta^{18}O$, it is proposed that T-Zone groundwater is a mixture of local shallow groundwater and a concentrated endmember, which in turn is a mixture of high-altitude recharge and seawater. For the mixing hypothesis, the dilute endmember was an average shallow groundwater (given in Table 5.7A). Assuming a maximum altitude effect of -0.5 $^{o}/oo$ per 100 m increase in elevation (Gat, 1981), a maximum depletion of 3 o/oo in $\delta^{18}O$ could be expected for the 600 m rise in elevation between the mine and the Long Range Mountains. Thus, for a mean $\delta^{18}O$ value of -9.8 $^{o}/oo$ for shallow groundwater, the high-altitude recharge should not have a $\delta^{18}O$ value lower than -12.8 $^{o}/oo$. Based on this value and assuming that the concentrated endmember is a mixture of seawater and high-altitude water, the concentrated endmember would have a maximum Cl concentration of

2230 ppm and $\delta^{18}O$ of -11.4 o/oo.

Samples collected recently (Welhar, pers. comm., 1989) revealed an even higher Cl concentration of 3600 ppm in deep flowing boreholes west of the mine. In light of these findings, it was reasoned that a more concentrated endmember than the 2230 ppm Cl component was more appropriate for the T-Zone modelling. It was assumed that an average of the highest Cl concentration observed west of the mine (3600 ppm) and the estimated endmember Cl concentration in the T-Zone (2230 ppm), would be a more appropriate Cl content for the concentrated endmember in the immediate mine area. The estimated saline endmember (Table 5.10), thus has a Cl concentration of 2900 ppm and $\delta^{18}O$ of -11.9 o/oo. The $\delta^{18}O$ of the high-altitude recharge component that would be required to mix with seawater to produce this concentrated endmember would be much lighter than contemporary high-elevation recharge (-14.0 o/oo). Thus, it is proposed that the seawater component may be relict, trapped during the last ice age, and mixed with a more $\delta^{18}O$-depleted paleo-meteoric water, recharged during glacial periods.

High-altitude recharge water was assumed to be similar in chemical composition to shallow groundwater with respect to the dissolved salt load content. This assumption is considered valid since the pH of groundwater that has dissolved silicate minerals can be as high as 7.23 (Palmer and Cherry, 1984) and dissolved Cl (2 to 20 mg/l) and SO_4 (1 to 11 mg/l) concentrations (Freeze and Cherry, 1979) are similar to those observed in shallow carbonate

Table 5.10 Chemical parameters for the endmembers (seawater and high-altitude groundwater) used in determining the CONCENTRATED ENDMEMBER which in turn was mixed with shallow groundwater to model T-Zone water (* average analysis from Parkhurst et al., 1980 and Hem, 1985). Endmember ion concentrations were determined by 0.15(seawater) and 0.85(high-altitude groundwater).

parameter/units	SEAWATER*	HIGH-ALTITUDE GROUNDWATER	CONCENTRATED ENDMEMBER (dilute seawater)
pH	8.22	7.4	7.24
T (^oC)	5.5	5.7	6
Eh (mvolts)	500	355	-37.9
Ca (ppm)	411	66	119
Mg "	1321	34	226
Na "	10634	13	1606
HCO_3 "	142	243	228
SO_4 "	2706	43	448
Cl "	19177	21	2900
K "	395	2	61
Sr "	8.1	.2	1.4
$\delta^{18}O$ ($^o/oo$ SMOW)	0.00	-14.0	-11.9
Ca/Mg	0.19	1.2	0.32
Na/Cl	0.85	1.1	0.84
SO_4/Cl	0.05	1.0	0.06
Sr/Ca	0.0090	0.0014	0.0054

groundwater.

A pH of 7.24 for the concentrated endmember used in the modelling was found by mixing (15 %) pure seawater and (85%) shallow groundwater. An Eh of -37.9 mvolts (typical of T-Zone waters) was chosen for the concentrated endmember and held constant throughout the simul-ations. Solutions were re-equilibrated to typical S.I. values for calcite (log S.I. = 0.0677) and dolomite (log S.I. = 0.0345) after mixing. Thus, groundwaters were allowed to precipitate carbonate minerals which would be expected in older, slower groundwaters where there is sufficient time for equilibration.

5.5.3.2 Results

Results for the mixing of shallow groundwater with the concentrated endmember in various proportions are given in Figure 5.29 and Table 5.11. The observed $\delta^{18}O$ range in T-Zone groundwaters was used to constrain the modelling results. The observed $\delta^{18}O$ values and SO_4/Cl and Ca/Cl ratios in T-Zone groundwaters are compared with results from the mixing models in Figure 5.29.

The mixed-water compositions listed in Table 5.11 are within observed ranges for saline groundwater (see Table 5.7B), but they do not match the average T-Zone ion concentrations exactly. Thus, it is possible to obtain T-Zone salinities by mixing 95% to 70 % shallow groundwater with 5 to 30 % dilute seawater.

Model 3 gave the closest match to average T-Zone groundwater. Sr in Model 3 (0.253 ppm) closely approximates the

Figure 5.29 Molar ratios of SO_4/Cl and Ca/Cl are plotted against $\delta^{18}O$ for dilute seawater modelling runs. Observed T-Zone range of $\delta^{18}O$ (dashed line) was used to constrain the possible ranges of mixed water compositions which are listed in Table 5.11. The ranges of observed Ca/Cl and SO_4/Cl ratios are also indicated.

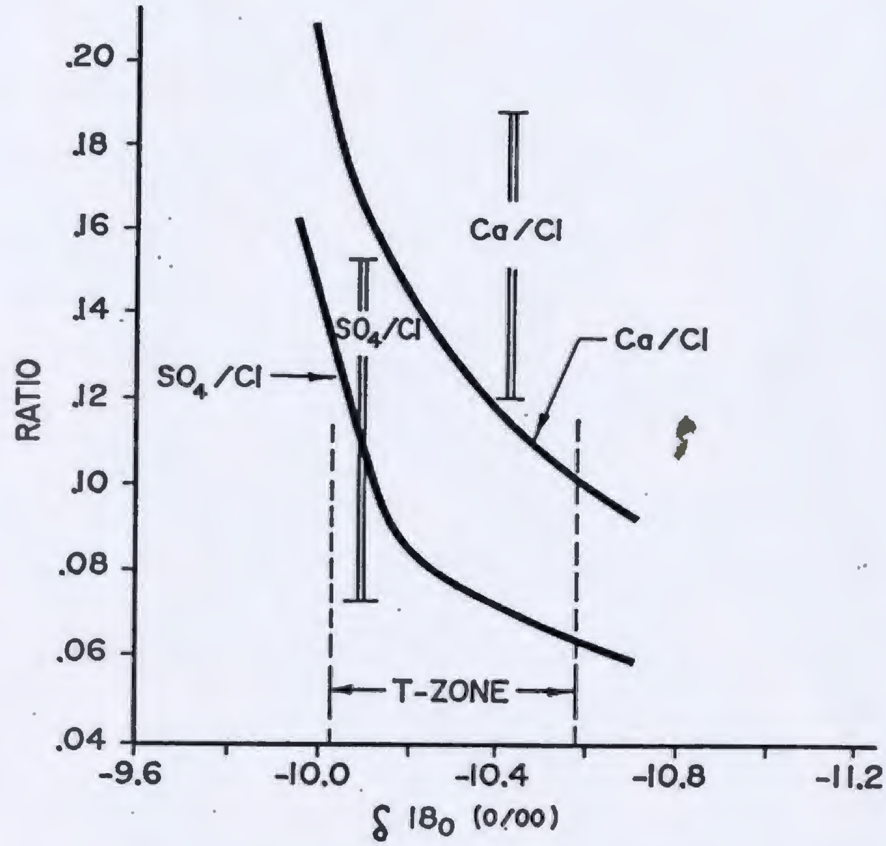

Table 5.11 Results from mixing dilute seawater with shallow groundwater. Explanation for symbols:
ADG = average deep groundwater of the T-Zone
* = Sr for model 3 is .253 ppm, Mg/Cl=0.18
S.G.= shallow groundwater

Mdl #	S.G. Portion		$\delta^{18}O$	Ca ppm	Mg ppm	Na ppm	K ppm	Cl ppm	SO_4 ppm	HCO_3 ppm	pH	SO_4/Cl { molar	Ca/Cl }
1	0.95		-9.94	67	51	93	5	165	70	278	7.62	0.16	0.36
2	0.85		-10.15	84	63	253	11	459	109	275	7.59	0.09	0.16
3	0.82	*	-10.21	89	66	302	13	547	121	274	7.58	0.08	0.14
4	0.80		-10.25	93	69	334	14	606	129	273	7.57	0.08	0.13
5	0.78		-10.29	96	71	366	15	664	137	272	7.57	0.08	0.13
6	0.70		-10.46	109	81	494	20	899	169	269	7.55	0.07	0.11
ADG			-10.27	64	48	367	21	505	172	231	7.61	0.13	0.11

average concentration in the T-Zone (0.299 ppm), suggesting a single seawater source for Sr, despite arguments presented in Section 5.3.2.4 for a local Sr source. Barium is dissolved in trace amounts in T-Zone groundwaters. Minerals that contain Ba (barite) probably do not contribute significantly to the salt load but it must be emphasized that local mineral occurrences may also explain the wide range in Ba (and Sr) found in the T-Zone.

The Na, Cl and K concentrations from Model 6 are near the maximum observed levels in the T-Zone but its SO_4 concentration remains below average. It appears that SO_4 has accumulated in T-Zone groundwaters in excess of amounts that would be produced solely from a seawater source, thus again suggesting dissolution of gypsum or oxidation of sphalerite. The HCO_3 content decreased with increasing salinity since seawater has a much lower bicarbonate content than shallow groundwater. The T-Zone DIC contents are indeed lower than the L-Zone DIC contents as discussed in Section 5.3.4.2, and these modelling results support the hypothesis that the observed increase in $\delta^{13}C$ for saline samples is due to mixing with seawater.

The results from mixing models also approximate the relative ion concentrations found in the T-Zone groundwaters and the best fit models (+) fall within the T-Zone groundwater fields in Figure 5.30. The resultant water from Model 3 is closest to the average T-Zone groundwater composition in all fields. The arrows in Figure 5.30 represent increasing proportions of the saline component in the mixing models. This figure illustrates that T-

Figure 5.30 Results from dilute seawater/shallow groundwater mixing models. Numerals refer to the respective runs of seawater mixing models (+) from Table 5.11 that most closely approximate the average T-Zone composition. Arrows indicate increasing salinity in the resultant groundwater.

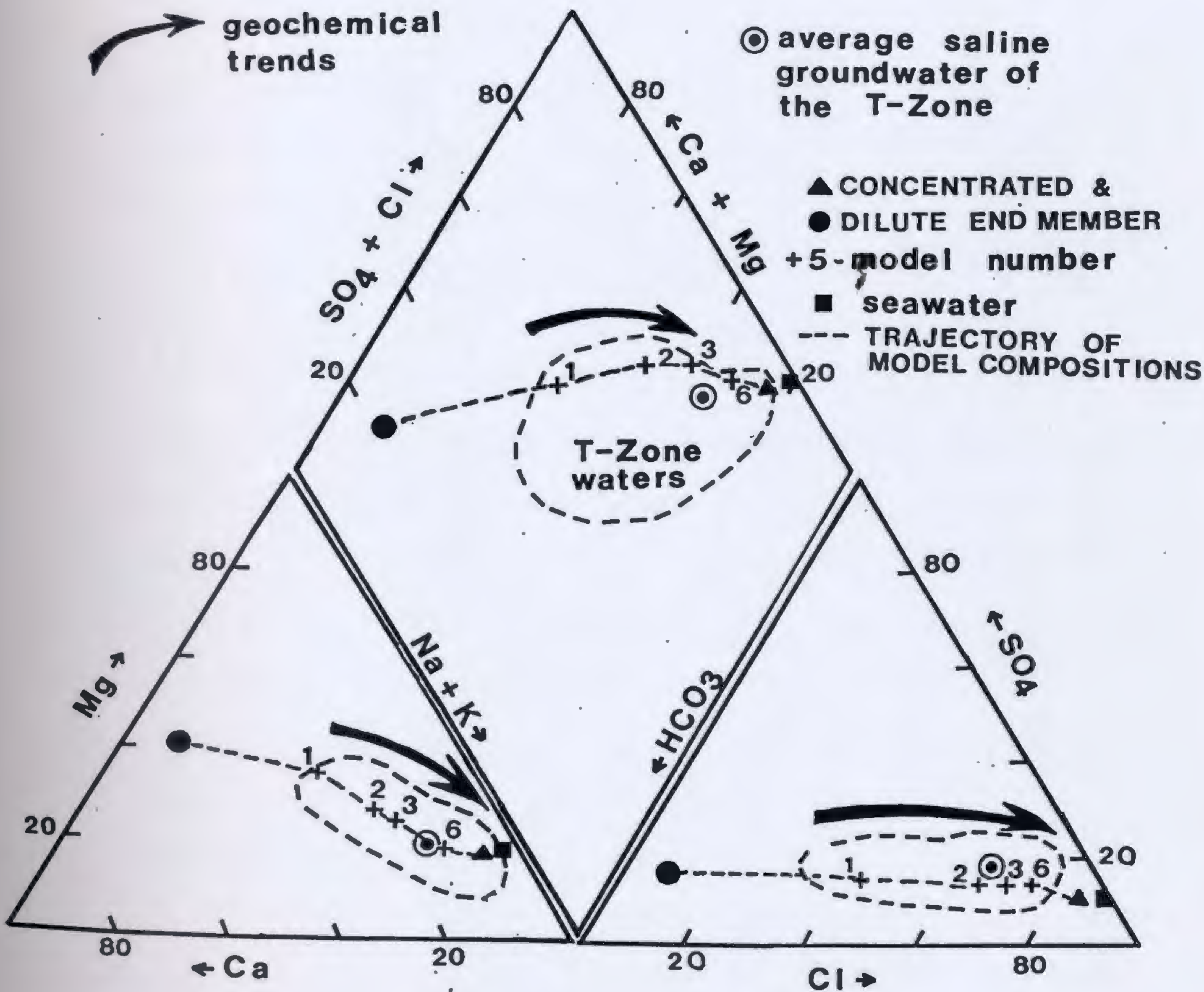

Zone groundwaters could indeed be the result of a mixture of dilute seawater and shallow groundwater in varying portions. Chloride and oxygen-18 mass balance arguments further suggest that mixing involves three endmembers, including isotopically light late Wisconsinan recharge water and relict seawater of similar age.

5.6 Conclusions from Hydrogeochemistry and Chemical Modelling

The Ca-HCO_3 type water of the L-Zone and the Na-Cl type water of the T-Zone mix in varying portions to produce the groundwater chemical compositions observed in the drawdown cone created over the Newfoundland Zinc Mine. This mixing trend is supported by major ion data, $\delta^{13}C-1/C_t$ and $\delta^{18}O$-Cl data and indicates vertical interconnectivity between the L- and T-Zone mining areas. Two flow systems make up the flow model in this mine environment as suggested by the dilute chemistry of the L-Zone (local flow system) and the salinity of the T-Zone groundwaters (regional flow system).

Dissolved oxygen, pH and $\delta^{18}O$ data support the hypothesis that the deep T-Zone groundwaters belong to a more chemically evolved regional flow system. The decrease in $\delta^{18}O$ with increasing Cl (Figure 5.23) is most likely due to a higher elevation of recharge for the dilute component of the regional groundwater.

Trace elements (I, V, Rb) appear to be controlled by residence-time in the deep flow system and their direct relationship with Cl supports accumulation of salt load in an evolving regional groundwater. However, high $\delta^{13}C$ values for DIC in T-Zone waters argues against evolution solely by carbonate dissolution, and suggests seawater mixing. Zinc, U, Mo, etc., are enhanced in the shallow groundwaters of the local flow system and appear to be related to dissolution and oxidation of specific sphalerite ore sources. Zinc distributions outline flow lines of a local flow system that are directed toward the L-Zone workings from surrounding areas. Barium and Sr concentrations also appear to be influenced by local occurrences of soluble minerals in vugs and to a lesser extent by dissolution of impure carbonates or mixing with seawater. Relatively high tritium values, and undersaturation of some T-Zone groundwater samples suggest direct mixing with dilute surface water along major conduits such as faults, individual joints or zones of increased permeability due to persistent joint patterns typical of karstified rocks.

Stable isotopes ($\delta^{13}C$ and $\delta^{2}H$) indicate that all the groundwaters have a meteoric origin, and they help to distinguish between waters of the same flow system. Major contributions to the mine inflow are from shallow groundwater. Calcite supersaturation and stable isotope "evaporation" shifts in mine samples nearest Spring Lake indicate that some mine inflows contain a component of evaporated surface water, and that at least some mine inflow originates from Spring lake.

Geochemical modelling indicates that the undersaturated nature of shallow carbonate groundwater sampled in 1985 and 1986 could have resulted from secondary processes such as mixing and dilution of two different types of water, or from kinetic factors related to rapid rainwater recharge through sinkholes etc.. However, other mixing scenarios, such as two-stage mixing/dilution, could also be responsible for observed disequilibrium. Due to (a) the prevalence of carbonate minerals in the overburden and (b) the depressed water table, some recharge most likely becomes equilibrated with calcite and dolomite above the water table under open-system conditions, whereas groundwaters recharged through major conduits (such as sinkholes and faults) would predominantly dissolve carbonate minerals below the water table under closed-system conditions.

Both open- and closed-system models could explain the undersaturated state of L-Zone groundwater. Modelling showed that shallow groundwaters evolved by dissolving dolomite first. Thus, shallow groundwater evolutionary modelling suggested that these waters were recharged in the Lead Lake basin area (underlain by dolostone, with a number of known sinkholes) and not in areas underlain by limestone (eg. along the axis of the anticline).

The Cl, Na, and K levels in T-Zone groundwaters can be reproduced by mixing shallow (L-Zone) groundwater with diluted seawater. Stable isotope-chloride mass balance calculations suggest that seawater is diluted with an isotopically light groundwater, probably of Late Wisconsinan age, so that the seawater source may be relict. The relatively high $\delta^{13}C$ and low

DIC values measured in T-Zone groundwaters support the hypothesis of a seawater source for the T-Zone salinity. Thus, it is possible that groundwater recharged in the Long Range Mountains flowed regionally and mixed with ancient seawater that was trapped within the submerged platform during the last ice age and that this regional groundwater in turn mixed with shallow local mine groundwater at or near T-Zone depths. Sulphate concentrations cannot be explained solely by a seawater mixture and Ba variability in T-Zone groundwaters suggests local occurrences of sulphate-type minerals in the mine area.

Chapter 6

CONCEPTUAL MODEL OF FLOW SYSTEMS

6.1 Physical Characterization of Mine Flow Regime

The Newfoundland Zinc Mine is situated in an highly anisotropic, moderately karstified, carbonate aquifer. Fracture mapping and analysis has determined two major joint sets with a mean plane orientation of 039/89 for Set 1 and 310/88 for Set 2. A third joint set was also distinguished but is less dominant than the first two sets. Underground conduit mapping showed that the closely spaced, long, sub-horizontal bedding planes which form the fourth fracture set, are an important water conducting feature in the mine. Undisturbed surface drainage follows the northeast regional (geological) trend and coincides with the prominent regional fault orientation of N028E. The axis of maximum transmissivity (calculated from pump-test data) is N63E and corresponds to an average orientation of the two documented major joint sets, the dominant regional NE trend, and an average of major local fault orientations. Extensive dissolution along these discontinuities, common in karstified carbonate terranes, contributes most to the permeability of this aquifer.

Carbonate dissolution is evident along the local anticlinal structure, along the regional lineaments where sinkholes are dominant, and along the joints, faults and bedding planes in the shallow L-Zone mine workings where large groundwater inflows occur. On a small scale, stylolites may localize dissolution by groundwater and decrease rock strength. Sinkholes have very limited areal influence as confirmed by dye tracer tests (Acres, 1974a) in which dye injected in the Spring Lake sinkhole was not detected in the nearby shallow L-Zone workings.

Permeability decreases with depth and is greatest near the ground surface weathering zone of the carbonate platform. This conclusion is supported by drill-core analysis, underground water -conduit and open pit mapping, packer testing, and a compilation of regional water well surveys. Hydraulic conductivity for the upper 10 m of the aquifer (greatest permeability) ranges from 1×10^{-2} to 1×10^{-3} cm/s (Acres, 1974a). Major individual conduits of groundwater flow are very significant locally for the permeability distribution in this carbonate aquifer. The highly variable tritium levels (1-41 T.U.), variation in $\delta^{18}O/Cl$ trends, and changing chemistry found in mid-depth groundwater sequential samples may be the result of localized flow controlled by major faults, joints or increased fracturing in zones. Geochemical evidence for mixing of L- and T-Zone waters, and the dominance of near-vertical joint sets and faults suggest excellent vertical connection between the shallow and deep parts of the mine.

The large drawdown cone centered over the mine is primarily a manifestation of dewatering operations. It has depressed the natural level of the water table by over 60 m. Hydraulic gradients around the L-Zone are towards this drawdown cone. Irregularities in its shape and the drawdown anisotropy observed in pump tests appear to be related to the above-stated fracture and fault geometry.

Mine pumping rates are directly related to seasonal variations in precipitation. Effects of mine dewatering on the local flow system are restricted to an area 1.5 km north and south of the eastern L-Zone workings and do not appear to extend to the T-Zone area. This is indicated by the reversal of the hydraulic gradients towards the west over the T-Zone area (in response to the topographic slope), and by the chemical homogeneity of the discharge zone near the T-Zone. The limited areal extent of pumping effects may be a function of the close proximity of this eastern area to increased permeability near the crest of the anticline and near the most extensive underground workings and pumping operations in the L-Zone.

6.2 Groundwater Geochemistry

Groundwaters sampled at the Newfoundland Zinc Mine and environs are of two types: 1) oxidizing, shallow waters with low total-dissolved-solids and chloride content (<125 ppm), and 2) reducing, deeper, saline waters of Na-Cl type with high chloride (700-1000 ppm) and sulphate (300-400 ppm) concentrations and low $\delta^{18}O$ values. Major-element relationships suggest mixing of these two types of groundwaters within the mine environment.

Higher than average SO_4 and K concentrations in some shallow groundwaters indicate local dissolution of gypsum, sylvite and other salts. However, sulphate in shallow groundwaters probably has 3 sources: local gypsum dissolution, sphalerite oxidation, and mixing with T-Zone groundwater. Variability in the 1986 Sr and Ba levels is controlled by more than one factor: dissolution of impure carbonate, mixing with low Sr groundwater, seawater mixing and local dissolution of sulphate-type minerals.

There are two types of trace elements: 1) those that are elevated in the T-Zone (I, V, and Rb) and related to high salinities indicative of control by groundwater residence-time; and 2) other elements such as Zn, Cd, Mo, and U which are more concentrated in shallow groundwaters and associated with sphalerite oxidation.

Shallow carbonate groundwaters carry up to 4457 ppb zinc near known sources of sphalerite mineralization. Zinc solubility in the groundwaters of the Newfoundland Zinc Mine is controlled by the availability of sphalerite in the carbonate host rock, by redox conditions (sphalerite oxidation), and to a lesser degree by carbonate-ion complexing.

Based on modelling results, it can be deduced that undersaturation due to 1) slow dissolution kinetics resulting from high flow rates and 2) secondary mixing of saturated but chemically different waters are both possible evolutionary paths for shallow groundwaters. Shallow carbonate groundwaters most likely evolved by dissolving dolomite first in the carbonate sequence. Rapid recharge through sinkholes situated in dolostone areas supports closed-system dissolution, but the widespread occurrence of carbonate minerals in the overburden implies open-system dissolution followed by mixing as a cause of disequilibrium. Thus, both open- and closed-system dissolution could produce the observed shallow groundwater geochemistry.

The decrease in $\delta^{18}O$ values with increasing Cl concentrations in deep mine waters suggests that saline groundwaters may have been recharged at a higher elevation (Long Range Mountains) and consequently may belong to a regional flow system. Saline groundwaters may have derived their elevated salt concentration from a deep regional flow system that has dissolved minerals such as gypsum, halite and sylvite. However, $\delta^{13}C$-1/DIC data argues against this hypothesis and the high $\delta^{13}C$ and lower DIC for T-Zone groundwaters suggest the possibility of mixing of shallow groundwaters with a seawater-type carbon source. The Quaternary record (inundation of the carbonate platform by seawater during the last ice age) implies a possible relict seawater source for the T-Zone salinity and DIC. Under the modelling constraints an average T-Zone groundwater can not be matched exactly by mixing a dilute seawater with shallow groundwater. The variable Ba, Sr and SO_4 contents in 1986 T-Zone samples supports some local dissolution of sulphate-type minerals suggesting a more complex model is necessary to explain the observed salinities.

6.3 Conceptual Model

The Newfoundland Zinc mine is situated in an aquifer that has both diffuse and conduit flow characteristics. The pervasive dominant joint sets imply that the aquifer has primarily diffuse characteristics with enlarged faults, joint and bedding-plane conduits controlling groundwater flow on a local scale. Figure 6.1 displays the interaction of the major conduits and natural controls on groundwater flow in this mining area. It emphasizes the role of the vertical joints and sinkholes in conducting surface recharge to more extensive bedding planes and faults in the subsurface. Increased dissolution near the anticlinal axis (eg. sinkholes) may serve to channel waters underground and emphasizes the importance of karstic processes in the hydrogeology of this mining area. The frequency of these discontinuities and the effects of weathering decrease with depth, resulting in a decrease in aquifer permeabililty. Mine dewatering increases hydraulic gradients and draws water along these conduits at a greater rate than in an undisturbed environment. This is evident from the permanent draining of Lead Lake and Zinc Lake since the commencement of mining, and the 60 m deep drawdown cone over the mine.

Groundwater flow rate can be as much as 2.3×10^{-2} m/s along major faults within the shallow L-Zone. Based on tritium analyses, portions of all analyzed groundwaters have been recharged within the last 33 years, illustrating the dynamic nature of this groundwater regime.

Local groundwater flow directions at the Newfoundland Zinc Mine are shown in Figure 6.2. These flow lines are based on the hydraulic-head maps and supported by well/mine water geochemistry and geochemical modelling. Flow directions are towards the L-

Figure 6.1 Sketch of major controls on groundwater flow in the Newfoundland Zinc Mine area. Vertical joints and sinkholes conduct surface recharge to solution-enlarged faults and laterally extensive bedding planes. Aquifer permeability decreases with depth.

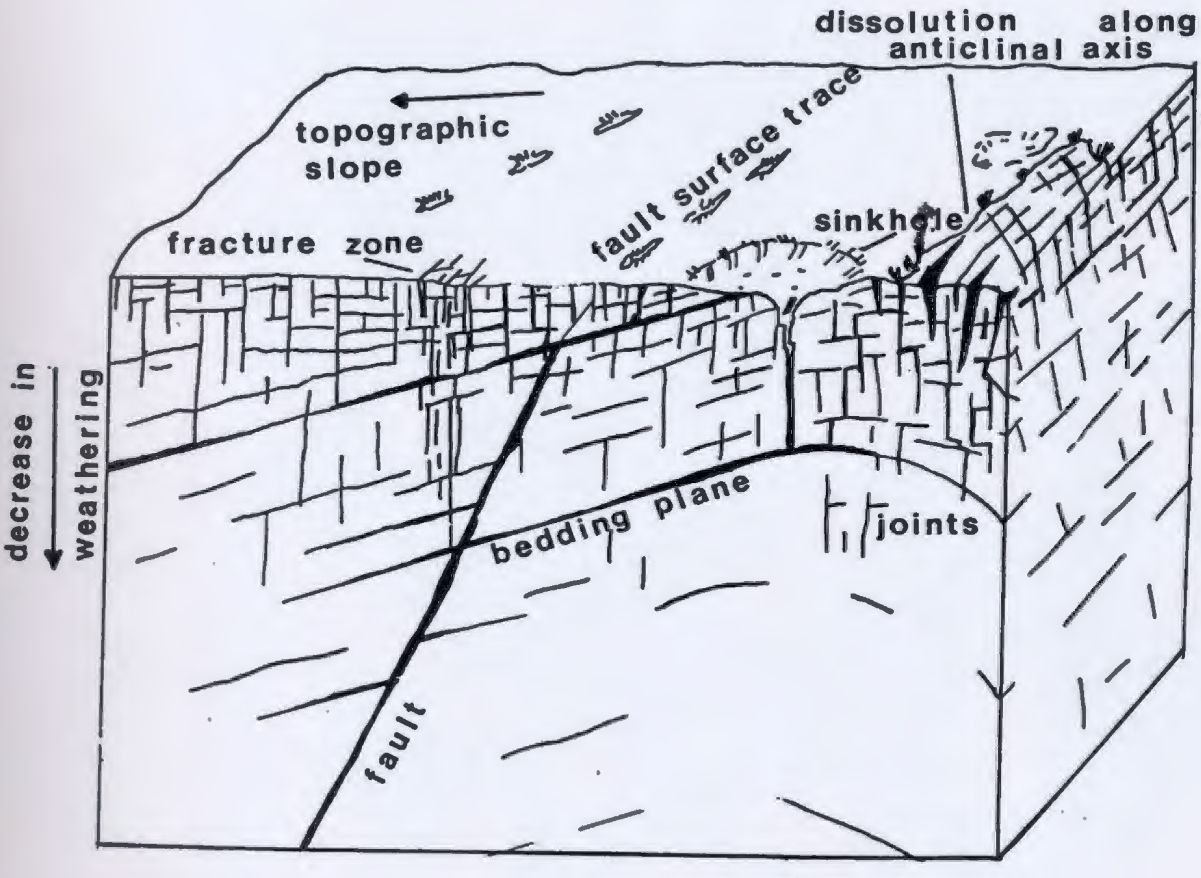

Figure 6.2 Deduced groundwater flow directions for the Newfoundland Zinc Mine area. Local flow system flow lines are based on hydraulic gradients calculated from 1985 and 1986 water-table surveys, geochemical maps and evolutionary modelling. Possible areas of recharge underlain by dolostone are also outlined on the map.

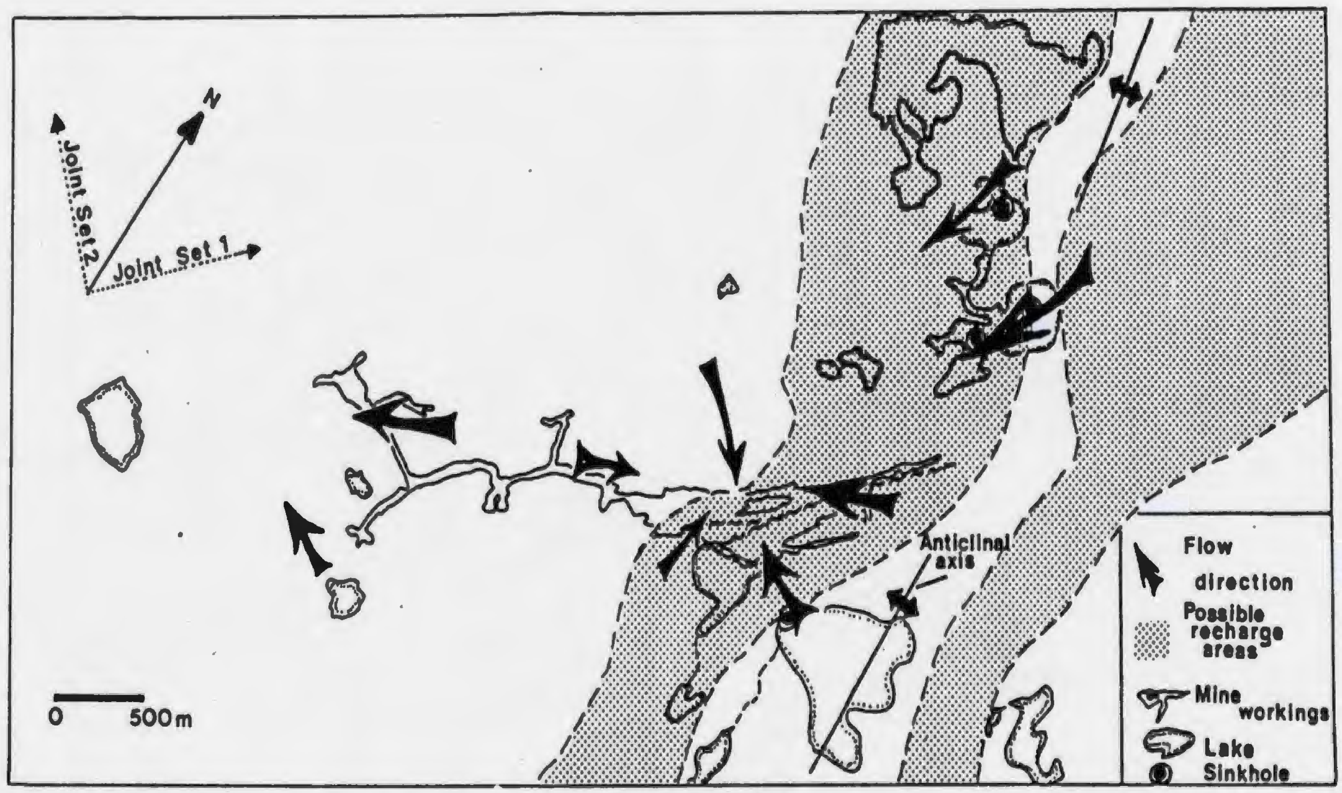
N
Joint Set 2
Joint Set 1
Anticlinal axis
0 500m
Flow direction
Possible recharge areas
Mine workings
Lake
Sinkhole

Zone mine workings. Only the area immediately surrounding the underground workings and an area 1.5 km north of these workings seems to be affected by the mine drawdown cone. Geochemical modelling suggests that shallow groundwaters were recharged in areas underlain by dolostone (see Figure 6.2), which restricts recharge to the Mike Lake-Zinc Lake-Lead Lake basin. Recharge consisting of lake water from Mike Lake and rainwater that enters the dry lake bottoms of Zinc Lake and Lead Lake via sinkholes, fractured outcrops and overburden, is drawn towards the L-Zone underground workings in response to the gradients imposed by underground pumping. Sinkholes are more prominent along the anticlinal axis and suggest greater dissolution due to increased permeability. The sinkholes coincident with dolomite areas, and their close proximity to the anticlinal axis, suggest that this lake basin is the principal recharge area for shallow mine inflows. Groundwater may also be recharged in a zone further east on the other limb of the anticline (Figure 6.2). The apparent contribution of evaporated surface water in shallow mine groundwater samples, and supersaturation in one L-Zone sample indicate that Spring Lake contributes directly to shallow mine inflows via joint and bedding planes intersecting the lake bottom or the lake's northwest edge (Figure 6.2).

The regional flow system proposed to account for the more saline groundwaters is assumed to be flowing below the local flow regime. The greater depth of the regional flow system suggests it to be less affected by mine dewatering. The Grenville basement, more than 1 km below the ground surface, is regarded as the regional flow-system boundary. Carbonate supersaturation in most lakes in the coastal region, and undersaturation in lakes elsewhere give evidence for both local and regional flow systems discharging near the coast of the carbonate platform on the Great Northern Peninsula of Newfoundland.

The following conclusions are based on stable isotope-chloride mass balances, DIC/carbon-13 data and geochemical modelling which support the seawater salinity source. It is suggested that the deep, saline (T-Zone) groundwaters of the mine result from a two-stage mixing process in which groundwater with low $\delta^{18}O$ values, recharged in the Late Wisconsinan at high altitudes in the Long Range Mountains, flows westward in a regional flow system and mixes with a paleowater. This paleowater appears to be relict seawater, trapped during isostatic rebound following the last ice age, when this platform was inundated with seawater. In the mine, mixing of shallow groundwater with this saline groundwater produces the observed range of salinities. Locally, dissolution of sulphate-type minerals may account for some of the T-Zone and L-Zone salinity.

REFERENCES

ACRES CONSULTING SERVICES, LTD. (1974a) Groundwater Study, Daniel's Harbour, 'L' Zone Orebody. Newfoundland Zinc Mines unpublished report, 22p.

ACRES CONSULTING SERVICES, LTD. (1974b) 'L' Zone Orebody decline, Estimate of well dewatering quantities. Newfoundland Zinc Mines unpublished report, 16p.

ACRES CONSULTING SERVICES, LTD. (1975a) Groundwater conditions. Newfoundland Zinc Mines unpublished report, 15p.

ACRES CONSULTING SERVICES, LTD. (1975b) Groundwater conditions 'L-Zone' Daniel's Harbour. Newfoundland Zinc Mines unpublished report, 9p.

ACRES CONSULTING SERVICES, LTD. (1976) Review of Groundwater Conditions, Daniel's Harbour. Newfoundland Zinc Mines unpublished report, 12p.

ACRES CONSULTING SERVICES, LTD. (1977) Review of the effect of mine water discharge on groundwater conditions. Newfoundland Zinc Mines unpublished report, 13p.

ACRES CONSULTING SERVICES, LTD. (1978) Pumping Requirement Estimates for future development, Daniel's Harbour Mine. Newfoundland Zinc Mines Ltd. unpublished report, 13p.

ACRES CONSULTING SERVICES, LTD. (1979) Review of groundwater conditions 1978-1979. Newfoundland Zinc Mines Daniel's Harbour Mine unpublished report, 11p.

ASTM (1978) D 2936-78 Standard test method for direct tensile strength of intact rock core specimens. ASTM (1979) D2938-79 Standard test method for unconfined compressive strength of intact rock core specimens. 466p.

ASTM (1980) D 2664-80 Standar test method for triaxial compressive strength of undrained rock core specimens without pore pressure measurements. 411p.

BACK W. and HANSHAW B. B. (1970) Comparison of chemical hydrogeology of the carbonate peninsula of Florida and Yucatan. Journal of Hydrology, 10, 330-368.

BARAKSO J. J. and BRADSHAW B. A. (1971) Molybdenum surface depletion and leaching. Geochemical Exploration, Special Volume, 11, C.I.M. 78-84.

BECK F. B. (1986) Groundwater monitoring considerations in karst on young limestones. in Proceedings of the Environmental

Problems in Karst Terranes and their Solutions Conferenc. 229p. National Water Well Association

BONI C. F. (1975) Recherches geologiques et geophysiques. in International Union of Geological Sciences Series B, Number 3. Hydrogeology of Karstic Terrains, Burger A. and Dubertret L. (editors) 91p. International Association of Hydrogeologists.

BROOK G. A. and ALLISON T. L. (1983) Fracture mapping and ground subsidence susceptibility modelling in covered karst terrain: Dougherty County, Georgia. in Environmental Karst, Dougherty P.H. editor, Geo Speleo Publications.

BROOKINS D. G. (1988) Eh - pH Diagrams for Geochemistry Springer -Verlag 176 p.

CANMET (1977) Pitslope manual: Supplement 3-1 Laboratory Classification tests. Energy mines and Resources Canada, 22-29.

CARTER F. B., MAHER M. L. J., ANNAN A. P. and RICHARD J. A. (1986) Specialized investigation techniques for defining Karstic Cavities. in Proceedings of the Environmental Problems in Karst Terranes and their solutions conference. Bowling Green, Kentucky, 345-367.

CAWOOD P. A. and WILLIAMS H. (1986) Northern extremity of the Humber Arm Allochthon in the Portland Creek area, western Newfoundland, and relationships to nearby groups. Current Research, Part A, Geological Survey of Canada, Paper86-1a, 675-682.

CHRISTIAN D. (1986) Diamond drilling at Holyrood and Daniel's Harbour Newfoundland. unpublished drillers report for J.E. Gale, Dept. of Earth Sciences, Memorial University.

COLEMAN, M.L., SHEPHERD, T.J., DURHAN, J.J., ROUSE, J.E. and MOORE, G.R. (1982) Reduction of water with zinc for hydrogen isotope analysis. Analytical Chemistry, 54, 993-995.

COLLINS J. A. and SMITH L. (1975) Zinc deposits related to diagenesis and intrakarstic sedimentation in the Lower Ordovician St. George Formation, Western Newfoundland. Bulletin of Canadian Petroleum Geology. 23, 393-427.

CORON C. R. (1982) Facies relations and ore genesis of the Newfoundland Zinc Mines Deposit, Daniel's Harbour, Western Newfoundland. unpublished Ph.D. Thesis,University of Toronto, 164p.

CRAIG H. (1961) Standard for reporting concentrations of deuterium and oxygen-18 in natural waters. Science, 133, 1833-1834.

CROSSLEY R. V. and LANE T. E. (1984) A Guide to the Newfoundland Zinc Mines Limited ore bodies, Daniel's Harbour. Newfoundland Department of Mines and Energy, Report 84-3, 45-51.

CUMMING L. M. (1968) St. George-Table Head Disconformity and Zinc Mineralization, Western Newfoundland. Canadian Institute of Mining and Metallurgy Bulletin, 721-725.

DAVIS S. N. (1969) Porosity and permeability of natural materials. Flow Through Porous Media, ed. R. J. M. De Wiest. Academic Press, New York, p. **.

DAVIS G. H., LEE C. K., BRADLEY E. and PAYNE B. R. (1970) Geohydrologic Interpretations of a volcanic Island from Environmental Isotopes. Water Resources Research, 6, 1, 99-109.

DEARIN C. (1976) The stratigraphy, diagenesis, and possible origins of the Lower Ordovician zinc deposits, Daniel's Harbour, Newfoundland. Maritime Sediments, 12, 1, 36p.

DEERE D. U. (1964) Technical description of rock cores for engineering purposes. Rock Mechanics and Engineering Geology. 1, 17-22.

DEERING M. F., MOHR E. T., SYPNIEWSKI B.F. and CARLSON E. H. (1983) Regional hydogeochemical patterns in ground water of northwestern Ohio and their relation to Mississippi Valley -type mineral occurrences. Journal of Geochemical Explortation, 19, 225-241.

DEINES P., LANGMUIR D. and HARMON R.S. (1974) Stable carbon isotope ratios and the existence of a gas phase in the evolution of carbonate groundwaters. Geochimica et Cosmochimica Acta, 38, 1147-1164.

DIGGLE P. J. and FISHER N. I. (1985) Sphere: A contouring program for spherical data. Computer and Geosciences. 11, 725-766.

ERIKSSON E. (1983) Stable isotopes and tritium in precipitation. in Guidebook on Nuclear Techniques in Hydrology, Technical Reports Series No. 91, I.A.E.A., Vienna, 439p. (19-33).

FAURE G. (1977) Principles of Isotope Geology, 464 p. John Wiley and Sons Inc.

FAUST, S.D. and HUNTER J.V. ed. (1967) Mineralogic factors in natural water equilibria by Bricker O.P. and Garrels R.M.

p.449-468 in Principles and Applications of Water Chemistry. 643p. John Wiley and Sons Inc.

FONTES J. -CH. (1983a) Dating of Groundwater. in Guidebook on Nuclear Techniques in Hydrology, Technical reports series No. 91, International Atomic Energy Agency, Vienna, 285-336.

FONTES J. -CH. (1983b) Groundwater in fractured rocks. in Guidebook on Nuclear Techniques in Hydrology, Technical reports series No. 91, International Atomic Energy Agency, Vienna. 337-350.

FREEZE R. A. and CHERRY J. A. (1979) Groundwater, 604p. Prentice-Hall.

FRITZ P. (1983) Environmental isotope hydrogeology: Tools to compliment the classical techniques of physical hydrology and geochemistry. Dept. of Earth Sciences, University of Waterloo, Ontario, 46p.

GALE J. E. and WITHERSPOON P. A. (1979) An approach to the fracture hydrology at Stripa, preliminary results. Lawrence Berkeley Laboratory Report LBL-7079, SAC-15.

GARRELS R. M. and CHRIST C. L. (1965) Solutions, Minerals, and Equilibria, 450 p. Harper and Row.

GAT J. R. (1971) Comments on the stable isotope method in regional groundwater investigations. Water Resources Research, 7, 4, 980-993.

GAT J. R. (1981) Chapter 10: Groundwater. in Stable Isotope and Oxygen-18 in the Water Cycle. Technical report series No. 210, (p. 223-229). I.A.E.A, Vienna, 337p.

GOLDER ASSOCIATES. (1983) Report to Newplan Consultants Ltd. Geological Assessment, Proposed Supplementary Water Supply Port au Chox, Newfoundland. Report # 831-5034, 21p.

GONFIANTINI R. (1981) Chapter 4. The δ-notation and the mass -spectrometric measurement techniques. in Stable Isotope Hydrology: Deuterium and Oxygen-18 in the Water Cycle, Technical Reports Series No. 210, (p.35-81) I.A.E.A., Vienna, 337p.

HANSULD J. A. (1966) Eh and pH in geochemical prospecting. in Proceedings, Symp. Geochemical Prospecting, Geological Survey of Canada, Dept. of Energy, Mines and Resources, paper 66-54, 172-187.

HAYWICK D. W. and JAMES N. P. (1984) Dolomites and dolomitization of the Lower Ordovician St. George Group of Western Newfoundland. Current Research, part A, Geological Survey of Canada, Paper 84-1A, 125-130.

HEALTH AND WELFARE CANADA (1987) Canadian Drinking Water Guidelines, 12-17.

HEATH R. C. (1983) Basic ground-water hydrology. United States Geological Survey Water-Supply Paper 2220. 84p.

HELZ G. R. and SINEX S. A. (1974) Chemical equilibria in the thermal spring waters of Virginia. Geochimica et Cosmochimica Acta, 38, 1807-1820.

HEM J. D. (1985) Study and interpretation of the chemical characteristics of natural water. United States Geological survey Water-Supply Paper 2254, 263p.

HOAG R. B. Jr. and WEBBER G. R. (1976a) Significance for mineral exploration of sulphate concentrations in groundwaters. CIM bulletin, 69, 776, 86-90.

HOAG R. B. Jr. and WEBBER G. R. (1976b) Hydrogeochemical exploration and sources of anomalous waters. Journal of Geochemical Exploration, 5, 39-57.

HORNBROOK E. H. W. , DAVENPORT P. H., and GRANT D. R. (1975) Regional and detailed geochemical exploration studies in glaciated terrain in Newfoundland. Newfoundland Department of Mines and Energy, Report 75-2, 116p.

HURLBUT JR. C.S. and KLEIN C. (1977) Manual of Mineralogy. 532 p., John Wiley and Sons.

INTERNATIONAL ATOMIC ENERGY AGENCY/I.A.E.A (1981) Statistical treatment of environmental isotope data in precipitation. Technical Reports Series No. 206, Vienna, 255p.

I.A.E.A. (1983a) Environmental isotope data no. 7: World survey of isotope concentration in precipitation (1976-1979). Technical Reports Series No. 226, Vienna, 241p.

I.A.E.A. (1983b) Isotope techniques in the hydrogeological assessment of potential sites for the disposal of high-level radioactive wastes. Technical Reports Series No. 228, Vienna, 151p.

I.A.E.A. (1986) Environmental isotope data no. 8: World survey of isotope concentration in precipitation (1980-1983). Technical Reports Series No.264, Vienna, 184p.

ISRM (1981) Brown, editor. Suggested method for determing indirect tensile strength by the brazil test. Pergamon Press 211p.

JAMES N. P. and STEVENS R. K. (1982) Excursion 2B:Anatomy and evolution of a lower paleozoic continental margin, Western Newfoundland. 11th International Congress on Sedimentology, McMaster University, Field Excursion Guidebook 2B, 75p.

JAMES N. P., STEVENS R. K., BARNES C. R. and KNIGHT I. (1989) Evolution of a Lower Paleozoic Continental-Margin Carbonate Platform, Northern Canadian Appalachians. in Society of Economic Paleontologists and Mineralogists Special Volume No. 44 Controls on Carbonate platform and basin development, editors Crevello P.D., Wilson, James L., Sarg J.F., Read J. 123-146.

KASTNING K.M. and KASTNING E.H. (1981) Fracture control of dolines, caves, and surface drainage: Mississippian Plateau, Western Kentucky, U.S.A. Proceeding's of the 8th International Congress of Speleology, 696-697.

KLAPPA C. F., OPALINSKI P. R. and JAMES N. P. (1980) Middle Ordovician Table Head Group of western Newfoundland: a revised stratigraphy. Canadian Journal of Earth Science, 17, 1007-1019.

KNIGHT I. (1977) Cambro-Ordovician platformal rocks of the Northern Peninsula, Newfoundland. Nefoundland Department of Mines and Energy, Report 77-6, 27p.

KNIGHT I. (1984) Mineralization in Cambro-Ordovician rocks, Western Newfoundland. In "Mineral Deposits of Newfoundland, a 1984 Perspective" H.S.Swinden (compiler) Newfoundland Department of Mines and Energy, Report 84-3, 37-44.

KNIGHT I. (1985) Geological mapping of Cambrian and Ordovician sedimentary rocks of the Bellburns (12I/5/6), Portland Creek (12I/4) and Indian Lookout (12I/3) map areas, Great Northern Peninsula, Newfoundland. Newfoundland Department of Mines and Energy, Report 85-1, 79-88.

KNIGHT I. and JAMES N. P. (1987) The Stratigraphy of the Lower Ordovician St. George Group, Western Newfoundland: The interaction between eustacy and tectonics. Canadian Journal of Earth Sciences, 24, 1927-1951.

KOCH JR. G. S. and LINK R. F. (1971) Statistical analysis of geological data. Vol. 2, 438 p., Dover Publications Inc.

KUNKLE D. (1986) Fracture system and hydraulic and acoustic properties of bedrock at Parson's Pond, Western Newfoundland, unpublished B.Sc. Thesis, Memorial University, Newfoundland.

LANE T. E. (1984) Preliminary classification of carbonate breccias, Newfoundland Zinc Mines, Daniel's Harbour, Newfoundland. Current Research, Part A, Geological Survey of Canada, Paper 84-1a, Report 84-1, 505-512.

LANE T. E. (in prep.) Ph.d. Thesis, Memorial University, Newfoundland. Dolomitization, brecciation and Zinc mineraliztion and their stratigraphic and structural framework, Upper St. George Group Daniel's Harbour Western Newfoundland.

LANGMUIR D. (1978) Uranium Solution-Mineral Equilibria at low temperatures with applications to sediment ore deposits. Geochimica et Cosmochimica Acta, 42, 547-569.

LATTMAN L. H. (1958) Technique of mapping geologic fracture traces and lineaments on aerial photographs. Photogrammetric Engineering, 24, 568-576.

LATTMAN L. H. and PARIZEK R. R. (1964) Relationship between fracture traces and the occurrence of ground water in carbonate rocks. Journal of Hydrology, 2, 73-91.

LEGRAND H. E. and STRINGFIELD V. T. (1971) Development and distribution of permeability in carbonate aquifers. Water Resources Research, 7, 5, 1285-1294.

MEMORIAL UNIVERSITY OF NEWFOUNDLAND (1987) Unpublished computer programs, Newfoundland.

MATTHESS G. (1974) Heavy metals as trace constituents in natural groundwaters and polluted. Geologie en Mijnbouw, 53, 4, 149-155.

MOOK W.G., BOMMERSON, J.C. and STAVERMAN W.H. (1974) Carbon isotope fractionation between dissolved bicarbonate and gaseous carbon dioxide. Earth Panetary Science Letters, 22, 169-176.

MOTYKA J. and WILK Z. (1986) Zone of nonlinear groundwater flow around mine workings in a karst-fractured rock massif and its significance for the reliability of mine water inflow predictions. Archiwum Gornictwa, 31, 2, 417-445.

MWENIFUMBO J. (1986) Personal communication. Borehole Geophysics Section, Mineral Resources Division, Energy, Mines and Resources Canada, Geological Survey of Canada, Ottawa, Ontario.

NOLAN, WHITE AND ASSOCIATES LTD. (1979) Hydrogeology of the Great Northern Peninsula. Water Resources Report 2-1 Groundwater Series, Dept. of Consumer Affairs and Environment, Water Resources Branch, Newfoundland, 68p.

PALMER C. D. and CHERRY J. A. (1984) Geochemical evolution of groundwater in sequences of sedimentary rocks. Journal of Hydrology, 75, 27-65.

PAPADOPULOS I. S. (1967) Non-steady flow to a well in an infinite anisotropic aquifer. in Proceedings, Dubrovnik Symposium on Hydrology of Fractured Rocks, International Association of Scientific Hydrology, 1, 21-31.

PARIZEK R. R. and SIDDIQUI S. H. (1970) Determining the sustained yields of well in carbonate and fractured aquifers. Ground Water, 8, 5, *.

PARKHURST D. L., THORSTENSON D. C. and PLUMMER L. N. (1980) PHREEQE - A computer program for geochemical calculations. U. S. Geological Survey, Water-Resources Investigations, 80 -96.

PIPER A. M. (1944) A graphic procedure in the geochemical interpretation of water analyses. Transactions American Geophysics Union, 25, 914-923.

PLUMMER L. N. (1975) Mixing of sea water with calcium carbonate ground water. in Quantitative studies in the geological sciences E.H.T. Whitten (editor) Geological Society of America, memoir 142, 219-236.

PLUMMER L. N., PARKHURST, D. L. and WIGLEY, T. M. L., (1979) Critical review of kinetics of calcite dissolution and precipitation. in: E.A. Jenne (Editor), Chemical Modelling in Aqueous Systems, Speciation, Sorption, Solubility and Kinetics. American Chemical Society Symposium. Ser. 93 537 -573.

PLUMMER L. N., PARKHURST D. L. and THORSTENSON D. C. (1983) Development of reaction models for groundwater systems. Geochimica Cosmochimica Acta, 47, 665-686.

PRICE N. J. (1966) Fault and Joint Development in Brittle and Semi-Brittle Rock. Oxford Pergamon Press, 176p.

PROUDFOOT D. N. and ST. CROIX L. (1987) Quaternary geology of the Bellburns (12I/5 and 6) map area. Current Research, Newfoundland Department of Mines and Energy, Report 87-1, 11-21.

RAUCH H. W. and WHITE W. B. (1970) Lithologic controls on the development of solution porosity in carbonate aquifers. Water Resources Research, 6, 4, 1175-1191.

ROSS R. J. and JAMES N. P. (1987) Brachiopod biostratigaphy of the middle Ordovician Cow Head and Table Head groups, western Newfoundland. Canadian Journal of Earth Science, 24, 70-95.

ROULEAU A. and GALE J.E. (1985a) Characterization of the fracture system at Stripa with emphasis on the ventilation drift. in Lawrence Berkeley Laboratory Technical Information Report, No. 52, 115p.

ROULEAU A. and GALE J. E. (1985b) Statistical characterization of the fracture system in the Stripa Granite, Sweden. Int. J. Rock mech. Min. Sci. and Geomech. Abstr., 22, 6, 353-367.

SALOMONS W. F. U. (1984) Metals in the Hydrocycle. 349p., Springer-Verlag Berlin, New York.

SANGSTER D. F. (1968) Some chemical features of lead-zinc deposits in carbonate rocks. Geological Survey of Canada, Department of Energy, mines and resources, Paper 68-39, 17p.

SMART C. C. and FORD D. C. (1986) Structure and function of a conduit aquifer. Canadian Journal of Earth Sciences, 23, 919-929.

SPENCER E. W. (1977) Introduction to the Structure of the Earth, McGraw-Hill Book Company.

STENZEL S. R., KNIGHT I., and JAMES N. P. (1990) Carbonate platform to foreland basin: revised stratigraphy of the Table Head Group (Middle Ordovician), western Newfoundland. Canadian Journal of Earth Sciences, 27, 14-26.

STOJIC P., MILICEVIC M. and MILANOVIC P. (1976) Use of piezometers boreholes for karst investigations. in Karst Hydrology and Water Resources, Proceedings of the US -Yugoslavian Symposium, Dubrovnik, Volume 1, Karst Hydrology. Yevjevich V. (editor) 409-418, Water Resources Publications.

STRONG D. F. and LONGERICH H. P. (1985) Machinations: The Inductively Coupled Plasma/Mass Spectrometer (ICP/MS). Geoscience Canada, 12, 72-75.

THRAILKILL J. (1968) Chemical and hydrologic factors in the excavation of limestone caves. Geological Society of America Bulletin, 79, 19-46.

THRAILKILL J. (1986) Models and methods for shallow conduit-flow carbonate aquifers. in proceedings of the Environmental Problems in Karst Terranes and Their Solutions Conference, 17-31.

TOTH J. (1963) A theoretical analysis of groundwater flow in small drainage basins. Journal of Geophysical Research, 68, 4795-4812.

TOTH J. (1978) Gravity-induced cross formational flow of formation fluids, Read Earth Region, Alberta, Canada: analysis, patterns and evolution. Water Resources Research, 14, 5, 805-843.

VAN EVERDINGEN R. O. (1970) The Paint Pots, Kootenay National Park, British Columbia--acid spring water with extreme heavy-metal content. Canadian Journal of Earth Sciences, 7, 831-852.

VOGEL J. C. (1970) Carbon-14 dating of groundwater. in Isotope Hydrology, I.A.E.A., 215-223.

WELHAN J. A., MILLAR, W.D., GALE, J.E. (1988) Geochemistry of groundwater-lake interaction in a carbonate terrain: application to geochemical exploration. Abstracts of Geological Association of Canada, Mineralogical Association of Canada and Canadian Society of Petroleum Geologists joint Conference, St. John's.

WELHAN J. A. and GALE J. E. (1986) Hydrogeological approach to mineral exploration preliminary results from Newfoundland Zinc Mine and area, Daniel's Harbour, Newfoundland. unpublish report.

WILLIAMS H. (1979) Appalachian Orogen in Canada. Canadian Journal of Earth Sciences, 16, 792-807.

APPENDIX A

Diamond drill logs and RQD plots for 1986 Drill Holes

Basic information on diamond drill holes drilled during the 1986 field season (Christian, 1986), their drill logs and RQD/fracture frequency/mean core length plots are given in this appendix. Core from the newly drilled holes discussed in Section 2.1.1 was logged for rock quality designation, RQD (Deere, 1964). RQD is the percentage of core length that is longer than 10 cm. Fracture frequency, mean core length and rock lithology were also recorded along each drill core. A metre interval was used with a 20 cm "moving average approach" to measure the RQD and fracture frequency, adopted from methods used by Rouleau & Gale (1985a). Core was also logged for any distinguishing characteristics, for instance the presence of stylolites, mineralogy etc.. All drill holes were collared in the pseudobreccia unit and drilled vertically.

DANIEL'S HARBOUR
Diamond Drill Holes
(AW core)

Hole	Footage	Orientation	Top of casing elevation*	Location
DDH-1-86	50	vertical	303.1 m	Mike lake
DDH-2-86	45	vertical	303.0 m	Lead lake
DDH-3-86	47	vertical	317.7 m	H-Zone pit
DDH-4-86	34	vertical	300.2 m	Spring lake

* relative to Teck Exploration Datum

DDH-1-86

METERAGE FROM	TO	FORMATION	DETAILS
0	0.35	pseudobreccia	collar, stylolites, grey bed, 1 foot casing
0.35	1.29	pseudobreccia	35 % sparry pseudobreccia 10 % vuggy, 1mm--2cm range vug size, brecciation extensive, 1mm--4cm diameter black fragments
1.29	1.70	pseudobreccia	fg light grey mottled, white veining, stylolites perpen. to core axis at 1.55 interlayer with no vuggy sparite
1.70	3.05	pseudobreccia	'120' marker bed, similar to previous interval, 35-40 % sparry matrix, 5 % vugs within sparry dolomite
3.05	3.66	pseudobreccia	light grey interbed, with white blebs/mottling
3.66	4.16	pseudobreccia	20 % sparry matrix with < 5% vuggs
4.16	5.03	pseudobreccia	light grey white sparry minute veinlets, interbed, black with some stylolites
5.03	5.64	pseudobreccia	15 % white sparry matrix, < 1% vugs, 2% disseminated pyrite
5.64	6.86	pseudobreccia	fg light grey interbed with white sparry veinlets, same as previous interval
6.86	7.56	pseudobreccia	30 % white sparry matrix, 1-5% vuggs
7.56	8.11	pseudobreccia	mainly black fracture veinlets probably dolomitized stylolites, 2mm wide white sparry veinlets
8.11	8.72	pseudobreccia	15 % white sparry matrix, 5 % vugs
8.72	9.42	pseudobreccia	light grey, fg, mottled, 2-3 mm white sparry veins
9.42	9.91	pseudobreccia	15 % white sparry matrix, 5 % vugs, interconnection of vugs, rust in vugs
9.91	10.15	pseudobreccia	interbed with distinct stylolites that are perpen. to core axis, contact between vuggy matrix and interbed appears to be stylolite
10.15	10.64	pseudobreccia	25 % sparry matrix, 5% vugs,

			crystals in vugs and covered by pyrite grains, 10 cm of vug interconnection
10.64	11.73	pseudobreccia	fg, light grey, mottled interbed, small sparry matrix bed,occasional white spar veins
11.73	12.65	pseudobreccia	incipient white sparry dolomite, approaching ls contact, 5 % white sparry matrix, < 1% vugs
12.65	13.11	pseudobreccia	fg interbed, rare spar veins, mottled
13.11	14.14	pseudobreccia	contact, transitional pseudobx, < 5% sparry matrix, <1% of <1mm vugs
14.14	14.51	limestone	dolomite/ls transition,very smooth mottled light grey interbed?, blebs 3mm, circular fossil fragments. specks of pyrite, white sparry vein running core length
14.51	15.15	limestone	dolomite/ls transition, original limestone structure preserved, speckled, dolomitic limestone

RQD plot for DDH-1-86

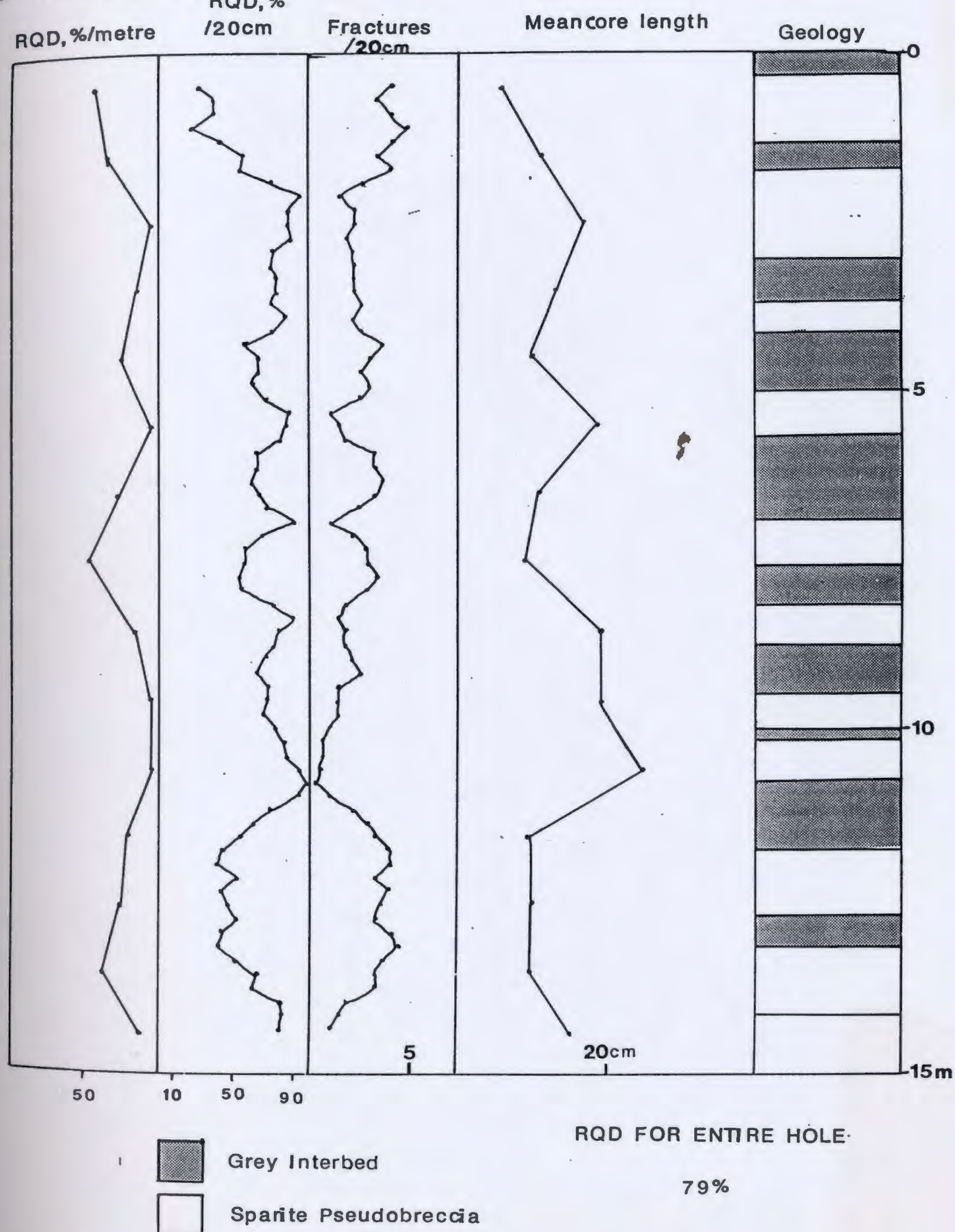

DDH-2-86

METERAGE FROM	TO	FORMATION	DETAILS
0	.305	Casing	bedrock setup
.305	.58	pseudobreccia	weathered pitted core, <15 % white spar, grey interbed, stylolites
.58	.85	pseudobreccia	5 mm, white ovoid shapes, light grey mottled interbed, stylolites
.85	1.55	pseudobreccia	10-15 % vugs, 35 % white sparry matrix, 7 cm of vug interconnection, fracture along stylolite surface at 2.6 m
1.55	2.09	pseudobreccia	light grey, smooth mottled interbed, stylolites form fracture surfaces, ovoid shapes
2.09	3.26	pseudobreccia	10-15 % open crystal vugs, occ stylolites, 15-20 % white spar, dark grey , very vuggy
3.26	3.76	pseudobreccia	light grey smooth, mottled interbed, white ovoid relect fossils, stylolites every 5 cm
3.76	5.68	pseudobreccia	top of '120'marker bed, 15-20 % vugs, fractures along vug connections, 33 % white sparry matrix
5.68	6.16	pseudobreccia	grey smooth, mottled interbed, stylolites perpend. to core axis, white spar ovoids
6.16	6.74	pseudobreccia	10 % vugs, 40% white sparry matrix, stylolites preserved
6.74	7.21	pseudobreccia	pitted grey interbed, stylolites weathered, <5% spar incipient pseudobx, 5.9m stylolites preserved in white pseudobreccia
7.21	7.98	pseudobreccia	smooth grey, mottled, many stylolites, large round ovoids ?fossils, grey interbed
7.98	9.01	pseudobreccia	10 % vugs, 30 % white sparry matrix,large vugs across diameter of core extent
9.01	9.60	pseudobreccia	light grey mottled interbed, white sparry veins, white small ovoids?fossils, dark stylolite form fractures perpend. to core axis
9.60	10.51	pseudobreccia	moderate pseudobrecciation 40 % white spar, 10 % vugs

			interconnection of vugs, fracture along stylolite contact, black infilling in stylolites
10.51	12.07	pseudobreccia	pitted, mottled grey interbed, black veinlets, stylolites, 2mm-10mm ovoid fossils
12.07	12.47	pseudobreccia	incipient pseudobreccia, 15 % white sparry matrix, 2% vugs,very tight matrix
12.47	12.56	pseudobreccia	small interbed, many stylolites
12.56	13.47	pseudobreccia	pitted surface, poorly developed pseudobx, 10-15% white sparry matrix
13.47			F.O.H.

RQD Plot for DDH-2-86

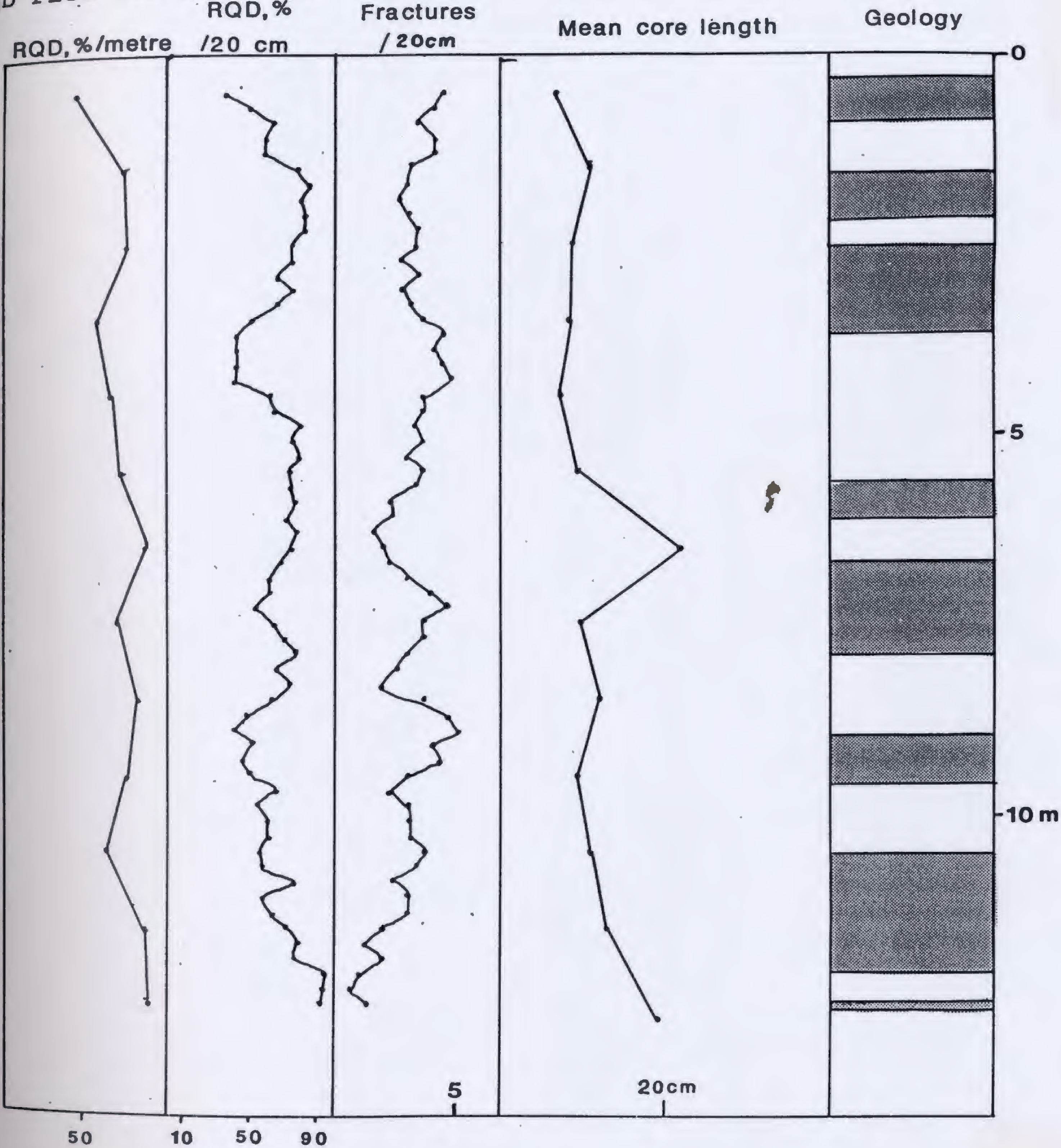

Grey Interbed

Sparite Pseudobreccia

RQD FOR ENTIRE HOLE

73%

DDH-3-86

METERAGE FROM	TO	FORMATION	DETAILS
0	0.305	pseudobreccia	collar,collared approx. 3 m below '120' marker bed
.305	0.62	pseudobreccia	45 % white sparry matrix, 2% vugs, small 3mm diameter
0.62	1.46	pseudobreccia	dark grey, irregular 2mm wide spar white veins, interbed, few stylolites and white ovoids
1.46	2.07	pseudobreccia	55 % white sparry matrix, fractured core, <1% disseminated sphalerite, 1 % vugs
2.07	2.62	pseudobreccia	irregular white dolomite veins occasional ovoids spar filled mottled interbed
2.62	3.14	pseudobreccia	40 % white spar matrix, fractured core oblique angle to core axis
3.14	3.86	pseudobreccia	interbed, white spar veinlets
3.86	4.30	pseudobreccia	45 % white sparry matrix, 2% vugs, mod.-good pseudobreccia
4.30	5.06	pseudobreccia	dark grey interbed, 8 cm of white spar matrix, white sparry veinlets causes brecciation of dark dolomite
5.06	5.32	pseudobreccia	very tight pseudobx, <15 % white sparry matrix, no vugs
5.32	5.82	pseudobreccia	dark grey interbed, 5mm white spar irregular veinlets, mottled black wispy layers
5.82	6.58	pseudobreccia	35 % white sparry matrix, rubbly core 6.56-6.58m,<1% vugs
6.58	8.70	pseudobreccia	pitted interbed, white ovoids, no veins, same bed as 13.1m in ddh-1-86, probably '150' marker bed, mottled
8.70	9.88	pseudobreccia	incipient pseudobx. with pitted texture, smooth light grey interbed with fossils at 8.7 -9.0m
9.88	10.67	pseudobreccia	light grey interbed with many white spar veins, occasional blebs of white spar, fracture zone 10.36-10.67
10.67	11.58	pseudobreccia	smooth light grey mottled interbed, white spar ovoids and occasional stylolites,fractured core 11.28-11.58m

11.58-13.99	lower limestone	contact, grey limestone, many black filled stylolites, occasional blebs of dolomite, white spar veins oblique to core axis
13.99		E.O.H.

RQD Plot for DDH-3-86

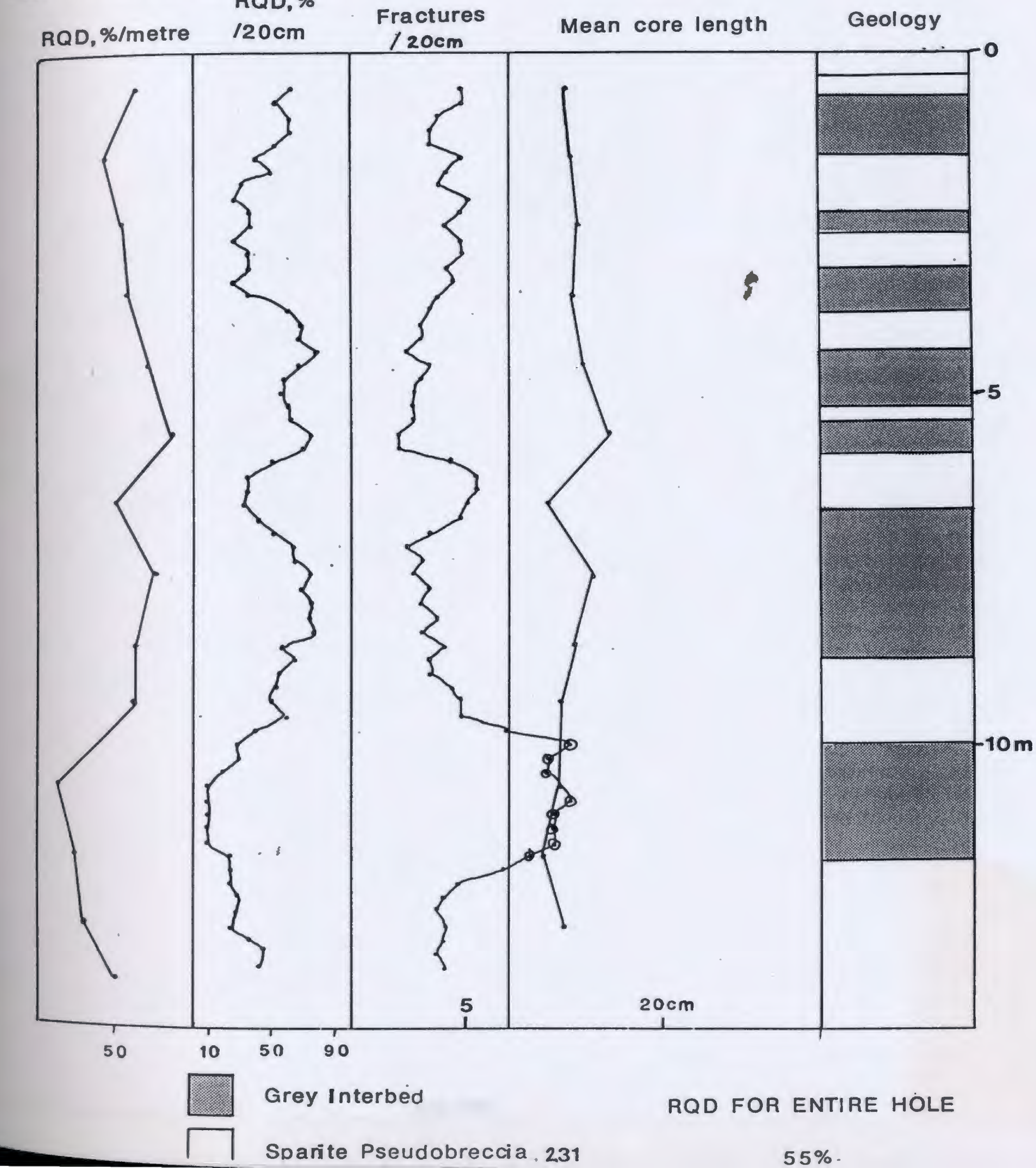

RQD FOR ENTIRE HOLE

55%

DDH-4-86

METERAGE FROM	TO	FORMATION	DETAILS
0	.305		casing
.305	1.11	pseudobreccia	buff grey dolomite, black rough stylolite ebery 1-2 cm, pitted core surface, rough fracture surfaces
1.11	1.87	pseudobreccia	grey mottled dolomite, occasional white dolomite blebs-possibly relict fossils
1.87	2.47	pseudobreccia	20-30% white sparry dolomite many black filled stylolites vuggy open 1mm-2cm diameter vug
2.47	2.91	pseudobreccia	dark grey mottled dolomite, many black irregular rough stylolites, <1mm diameter white spar blebs
2.91	3.94	pseudobreccia	35 % white spar dolomite, occasional preserved dark irregular stylolites
3.94	4.38	pseudobreccia	very mottled grey dolomite white spar blebs, many stylolites, few pyrite blebs
4.38	5.30	pseudobreccia	35 % white sparite with occasional stylolite, large 1 cm vugs joined by fracture perpend. to core axis, core breaks along vugs
5.30	5.56	pseudobreccia	dark grey mottled interbed, many stylolites, pyrite blebs
5.56	6.51	pseudobreccia	30% white spar, vugs 2mm occasional black stylolite
6.51	7.05	pseudobreccia	5mm dolomitized ovoid ?fossil dary grey interbed
7.05	7.30	pseudobreccia	small white spar interlayer 25-30% white sparite
7.30	9.50	pseudobreccia	dark grey mottled dolomite many stylolites, very pitted surface
9.50			E.O.H. many intervals of ground core so total length of core logged is less than was drilled

RQD Plot for DDH-4-86

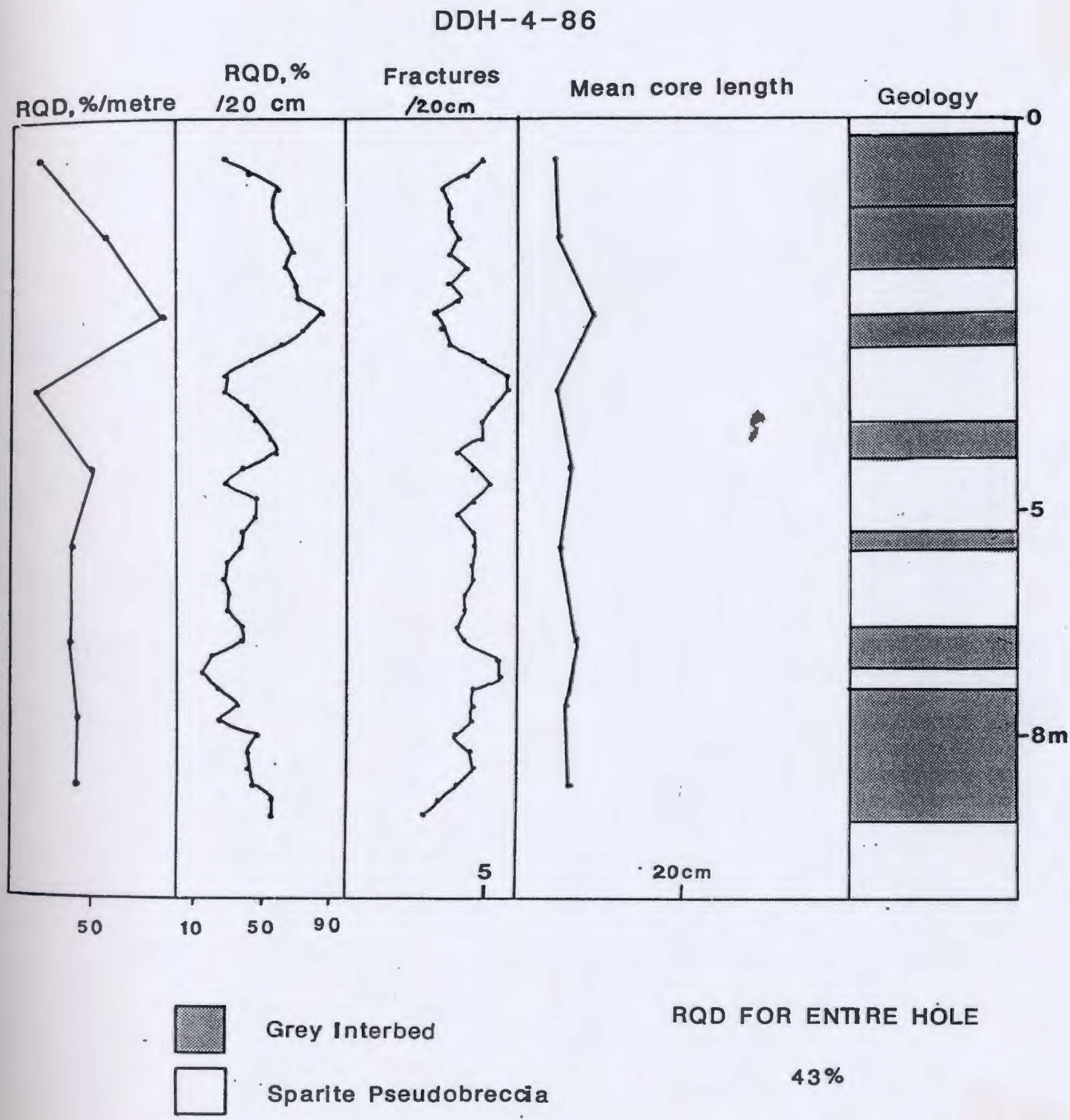

APPENDIX B

Underground water sampling site descriptions

Descriptions of each 1986 sampling site in the underground mine groundwater survey are given in the following table. (*-estimated flow rate only, lpm = litres per minute, ** -sequential sampling site, ***-photograph of this site given on plate 1).

SAMPLE NO.	MINE SAMPLE SITE DESCRIPTION		
	Location	Flow Rate*	Pertinent Notes
DH-26	L-Zone	225-455	-north side of L-Zone -proximal to pyrite zone -pipe flushed for 15 min.
DH-27	L-Zone	2	-iron oxide stained rock -organic scum in C-14 bottle -from blast hole north side
DH-28	L-Zone	23	-drinking water drill hole near portal decline -plastic pipe inserted into drill hole -DDH drilled vertical from surface,dry above DDH
DH-29	L-Zone	drip	-iron staining on rock face -very well defined bedding plane seep -tubing stuck in 2 cm wide fracture intersection
DH-30**	L-Zone	135-180	-DDH on floor near raise -rubber tubing stuck in valve -strong smell of sulfur -drilled to 150 m below floor into Trout Lake breccia body
DH-31	L-Zone	1-2	-near east drift sump -fractured zone in dark dolomite bed above pseudobx. -tube was not used
DH-32	L-Zone	23	-bedding plane seep -below major fault zone
DH-33**	T-Zone	18	-very strong sulfur smell -spl from bottom of 6 holes -hole is plugged with pipe with shut-off valve
DH-34	T-Zone	11	-white and rusty film on rock -60 cm above "66" marker bed -pipe has on/off valve
DH-35***	T-Zone	23	-rusty stain on rock from pipe with no shut-off valve -faint sulfur smell
DH-78**	L-Zone	drip	-bedding plane seep just below back, dripped into bottle a few cm below discharge area

APPENDIX C

<u>Fracture mapping overlays for open pits</u>

Fractures were drawn on overlays while field mapping progressed except in the case of the A-Zone open pits. These photos were not available and fractures were drawn on overlays after fractures were recorded in the field. Legend for symbols used in the fracture mapping technique is given below. There were no photos available of the underground drifts. The open pit locations are shown in Figure 3.3.

LEGEND:

V 056 00	Scanline label, azimuth, plunge
	Scanline
	Fracture
616	Fracture number (shown for first and last fracture intersecting each scanline)
	Exposed fracture face
	Limit of outcrop/rubble

A-ZONE Northeast facing pit wall

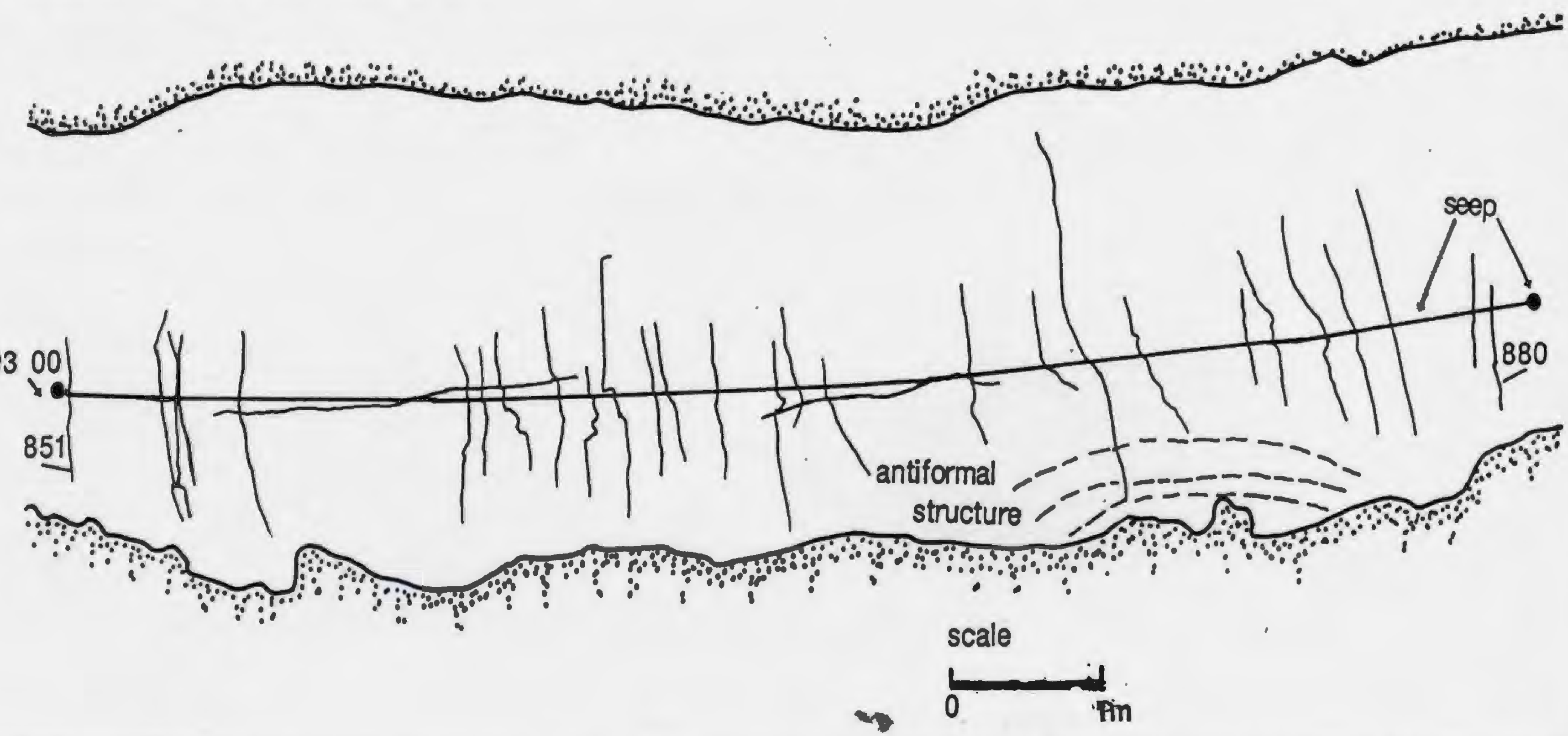

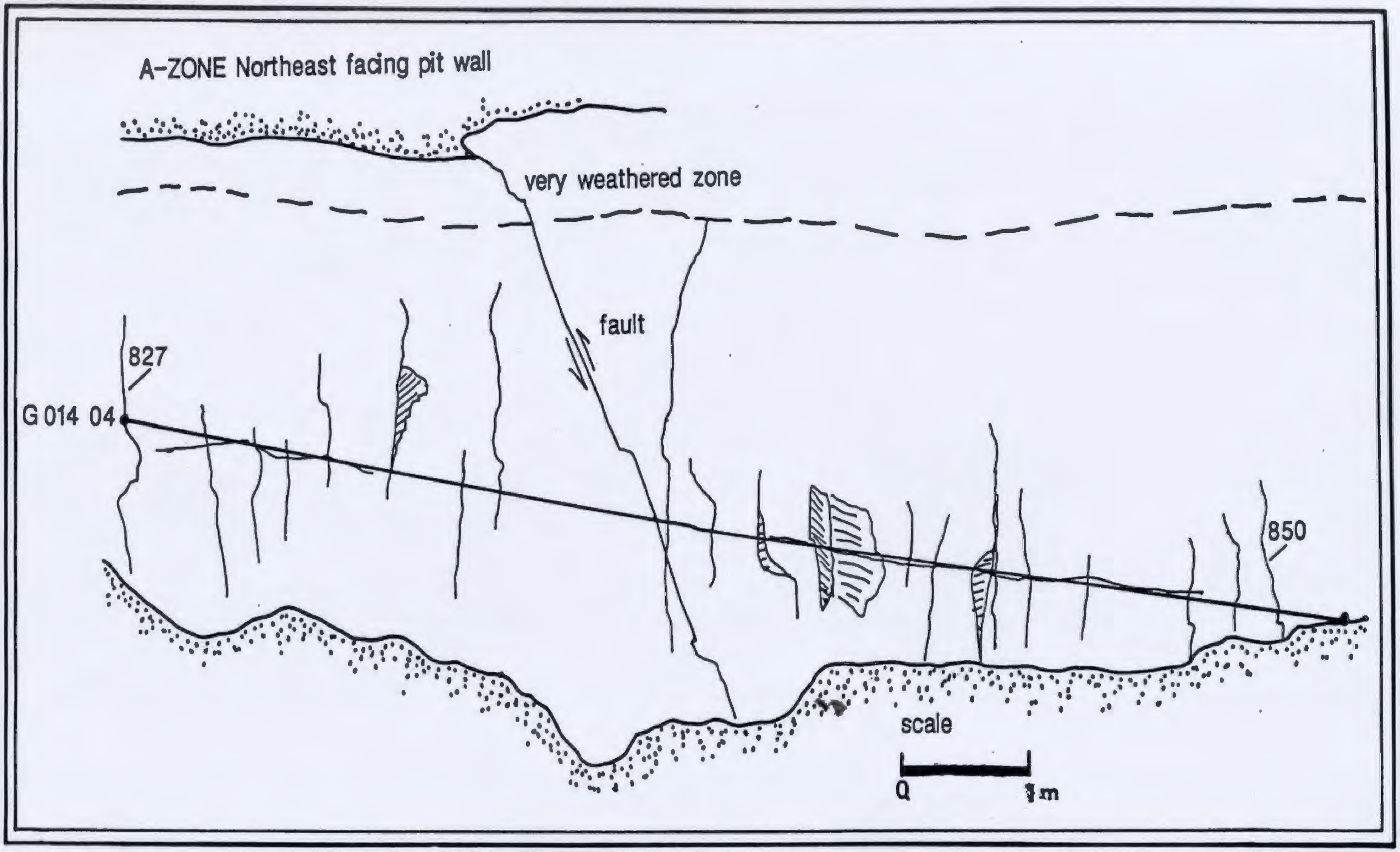
A-ZONE Northeast facing pit wall
very weathered zone
fault
827
G 014 04
850
scale
0
1 m

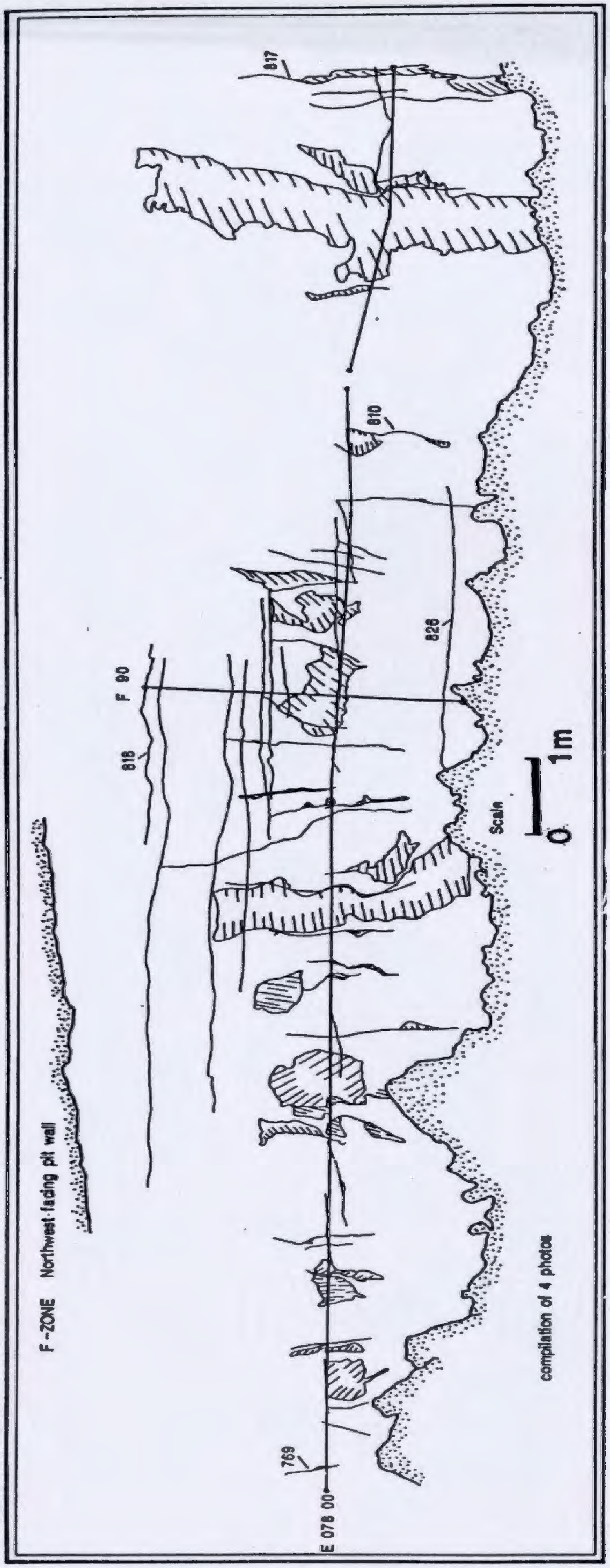
F-ZONE Northwest-facing pit wall
E 078 00
769
818
F 90
826
810
817
Scale
0
1m
compilation of 4 photos

H-ZONE Northeast facing pit wall

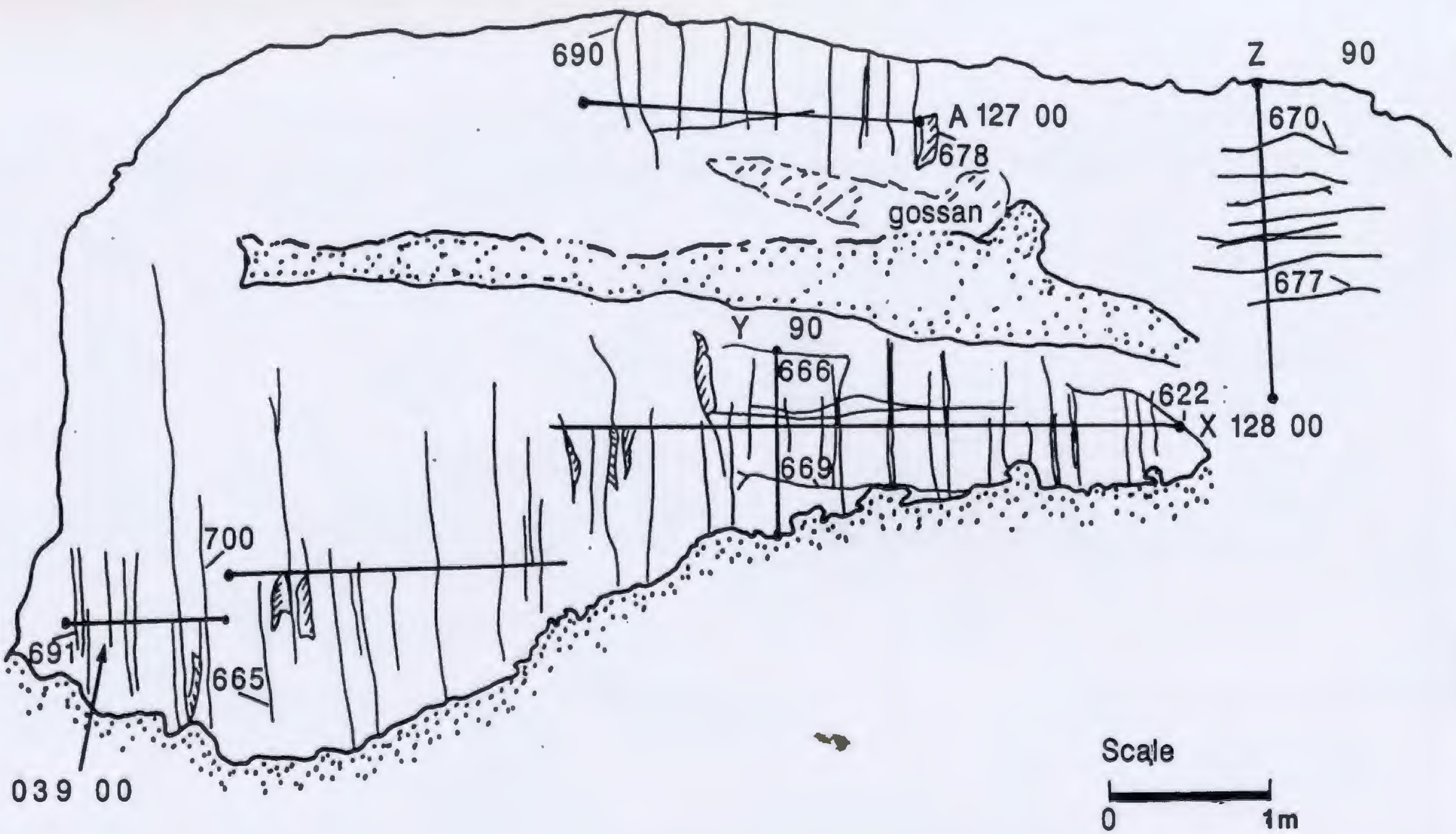

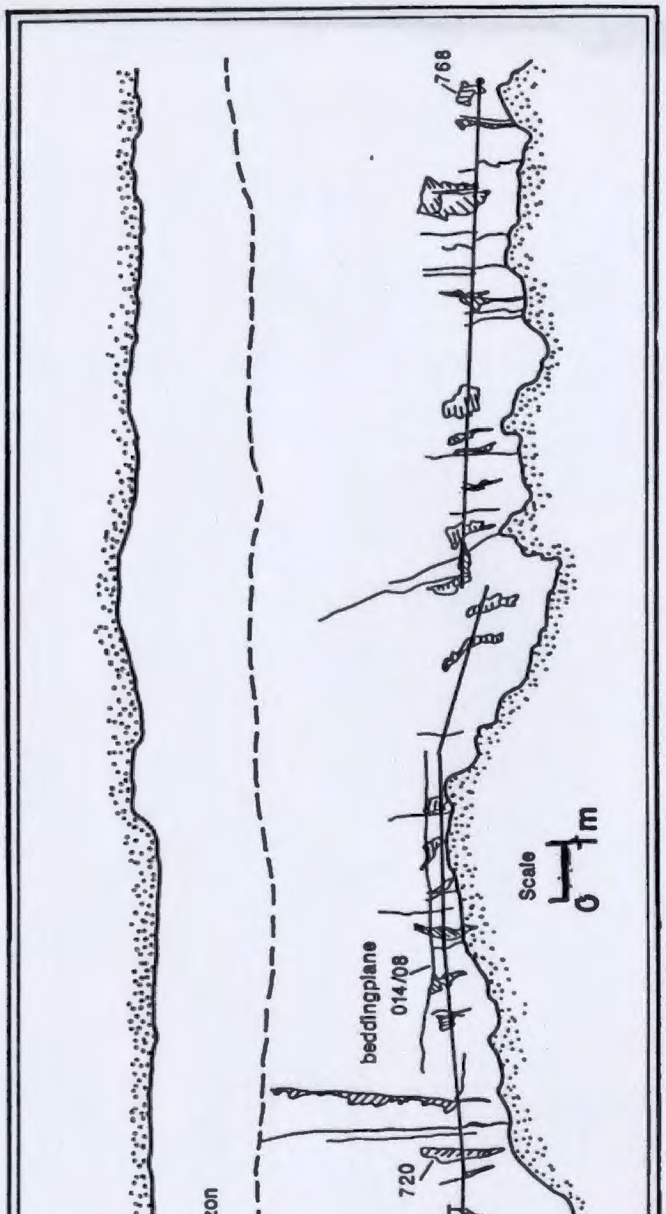
H-ZONE Northwest facing pit wall
Very weathered horizon
beddingplane
014/08
720
701
768
C 198 00
Scale
0
1m
compiled from 3 photos

H-ZONE Northwest facing pit wall

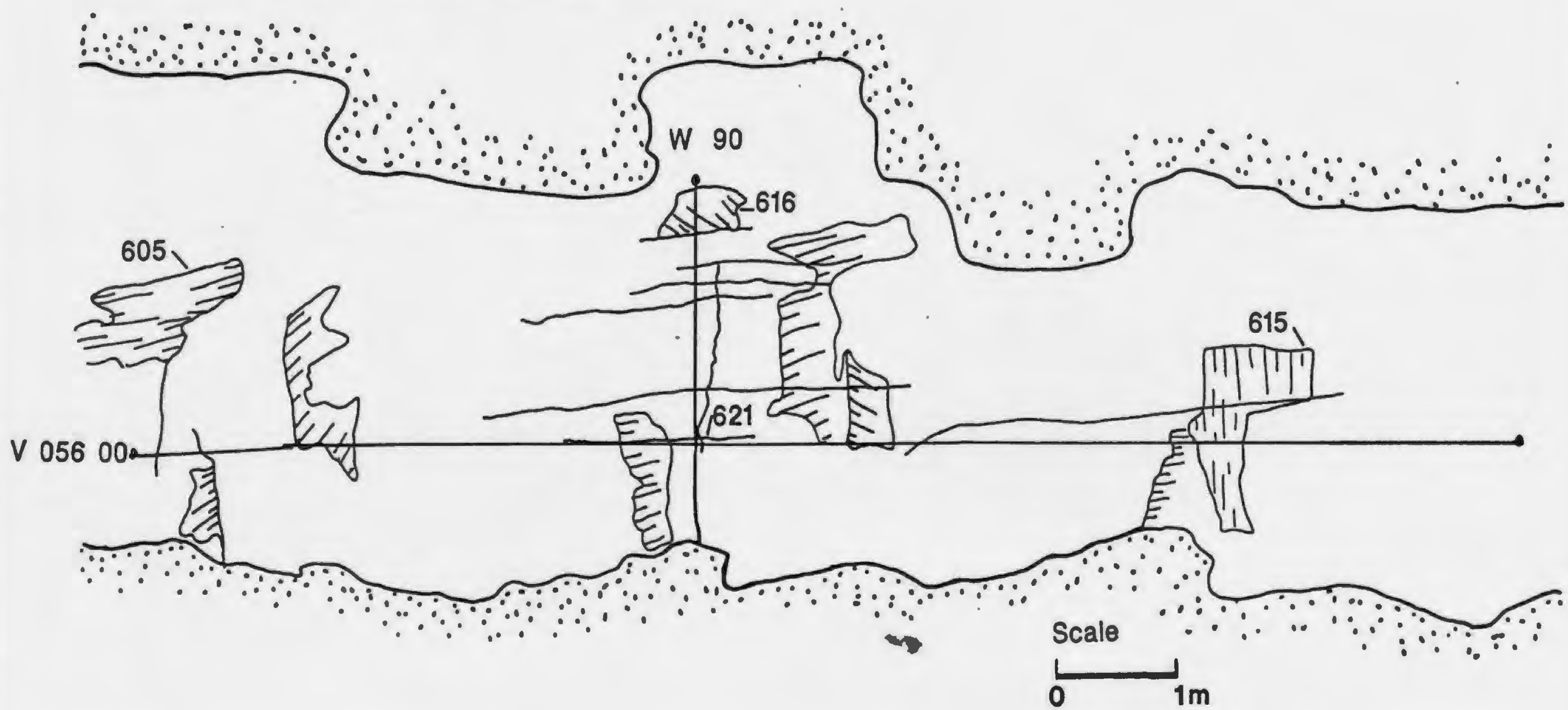

APPENDIX D

<u>Lead Lake outcrop fracture map</u>

The enclosed plate (see envelope) is a composite of all fracture overlays used in mapping the Lead Lake outcrop. A total of 15 photographs were used in this composite fracture map of the only horizontal surface mapped at the mine site. The location of the Lead Lake outcrop is given in Figure 2.4.

APPENDIX E

Fracture mapping codes and terms with their definitions

CODING CONVENTIONS-DANIEL'S HARBOUR FRACTURE MAPPING (adapted from Galé, 1981)

* FLAG - 11=data 22=scanline 33=comment
* PHOTO LOCATER - not used; 4 digits
* SCANLINE - use label A,B,C etc. one letter for each scanline on overlay
* SCANTREND - 0-360 azimuthal scanline trend (000 = true north)
* SCANPLUNGE - 0-90 inclination (0=horizontal)
* FRACTURE NUMBER - 1-999, sequential labels;mark on overlay;start number 1 at north or east end
* SCANLINE DISTANCE - distance in meters (+/- 1 cm) where fracture crosses scanline; start at north or east end
* FRACTURE TYPE - Joint - JT
  Vein - VN
  Bedding Plane - BP
* ORIENTATION - Dip direction 0-360 azimuthal bearing (000 = true north)
  Dip 0-90 inclination down to right side (RIGHT HAND RULE)
* TRACE LENGTH - to nearest 0.1 m; may continue off photo if exposed; minimum length = 0.5m (truncation length)
* CENSORING TYPE - 0 = both ends exposed
  1 = one end covered
  2 = both ends covered
* INFILLING - U=unknown R=rubble D=dolomite C=calcite
  (list in order of abundane; maximum of three)
* ROUGHNESS - Large scale (L) S= stepped U=undulating
  C= curved plane P=flat planar
  Small scale (S) R= rough K=slickensided S= smooth
* ROCK - rock types X= pseudobreccia(sparry dolomite) L= limestone
* TERMINATION STYLE - Blank= if censoring is 1 or 2
  0=both ends free
  1=T junction
  2=H junction
  3=splay
* COMMENT - pertinent details: age relationships, unusual rock types or structures, weathering-rusty,vuggs, etc.

APPENDIX F

Fracture data file

The following data files consist of the original fracture information used in the computer analysis.

```
33*****************************************************************
33*****************************************************************
33*******Daniel's Harbour Fracture Data*********************
33*******July-August 1986***********************************
33**********Lead Lake Outcrop*******************************
33**New Coding Conventions: Fracture Type BP=BEDDING PLANE****
33**Infilling D=DOLOMITE  Roughness=V=vuggy ROCK-L=limestone,*
33**D-DOLOMITE,X-PSEUDOBRECCIA******************************
33**************** length  start  finish  #frac  brkln ******
22    A15200 48  26.10                            0*********
33**FRACTURE MEASURE-BEARING OF DIP*************************
33***PAGE 1**************************************************
11              1  0.08JT 12287  3.7 OR   PRL0 July 21,1986,
11              2  0.62JT 31289  1.0 OR   PRL1
11              3  0.86JT 31290  6.6 OR   PRL1 July 28,1986
11              4  1.34JT 13385  5.7 OUR  CRL  partially filled
11              5  1.39JT 30080   .9 OU   PRL1
11              6  1.53JT 01088  1.0 OR   PRL2
11              7  2.36JT 13089  5.9 OR   PRL0
11              8  2.42JT 31280  2.7 OR   PRL1
11              9  2.98JT 31985  1.6 OR   CRL0
11             10  4.24JT 13085  3.8 OR   CRL2
11             11  4.40JT 00088  3.9 OR   PRL2    DIP?
11             12  4.54JT 14480   .8 OR   CRL1
11             13  5.70JT 00985  1.5 OR   PRL0
11             14  6.21JT 00689  1.6 OR   PRL2
11             15  6.76JT 30089 13.6 OR   PRL0   TENSION GASH
33****BLACK FILLING FG AT NORTH END OF FRACTURE**************
11             16  7.42JT 01890  1.3 OR   PRL3
11             17  8.06JT 31090 16.3 OR   PRL1
11             18  8.70JT 31289  5.2 OUR  PRL1  FG BLCK INFIL
11             19  9.03JT 11888  7.2 OR   PRL2
11             20  9.86JT 31290  5.5 OR   PRL0
11             21 10.01JT 35889  0.7 OR   PRL2    DIP?
11             22 10.54JT 30290  4.5 OR   URL3   JULY 30,1986
11             23 10.80JT 20289  0.6 OR   CRL0
11             24 11.03JT 10185  1.2 OR   CRL3
11             25 12.10JT 01786  1.4 1R   CRL3
11             26 12.22JT 30090  0.9 OR   PRL3
11             27 12.67JT 06090  1.8 OR   PRL
11             28 13.32JT 02190  5.5 ORU  CRL3   CARB INFIL?
33**********TENSION GASH?**********************************
11             29 13.71JT 18088  4.4 ORD  CRL3   DOLO. VRY
33*******RESISTANT INFILLING*******************************
11             30 13.87JT 00090  2.1 OR   CRL
11             31 14.14JT 30390  1.7 OR   PRL0
11             32 14.41JT 12585  4.3 OR   CR     OFFSET NORTH
33**END OF FRACTURE****************************************
33****PAGE 2***********************************************
11             33 15.23JT 24083  9.8 1R   CRL   #32 OFFSETS
33****#33/ #33 IS OLDER FRACTURE , INFILL IS EVEN LATER*****
11             34 15.23JT 02288  2.1 OR   CRL
11             35 15.86JT 12287 10.0 2R   CRL
11             36 16.37JT 17887  5.7 OR   CRL  SPLAY IN
33**MIDDLE OF FRACTURE*************************************
11             37 18.29JT 35485  5.3 OR   SRL
11             38 19.10JT 31390  3.2 OR   CRL    DIP? .
11             39 19.95JT 31587  2.7 OR   CRL3
11             40 20.79JT 30687 11.5 OR   PRL   FADED OUT
33**BOTH ENDS**********************************************
11             41 21.55JT 30590  5.1 OR   PRL0
11             42 22.14JT 13089  4.8 OR   SRL
33*******VERY ROUGH,RUBBLY*********************************
11             43 22.29JT 13288  2.3 OR   SRL
```

```
11              44 23.50JT 23285  4.2 OR   CRL3
11              45 24.10JT 30189  9.6 OR   SRLO     DIP?
11              46 24.62JT 13089  1.7 1R   RPL
11              47 25.68JT 12590  2.7 OR   CRL1
11              48 26.10JT 00490  2.1 1R   PRL
22    B15802    31 28.36
11              49  0.70JT 30690  3.9 1R   PRL
11              50  1.11JT 30490  1.6 OR   PRL
11              51  1.53JT 12275  5.2 1R   PRL    BLACKINFILL
11              52  1.66JT 30490  1.0 1R   PRL
11              53  1.93JT 12481  1.9 OR   PRL
11              54  2.72JT 13489  7.0 OR   PRL1
11              55  3.05JT 12887  1.6 1R   PRL
11              56  3.19JT 31082 15.3 1R   PRL
11              57  3.80JT 30185  8.1 1R   PRL
11              58  4.31JT 30283  9.4 1R   PRL
11              59  5.66JT 30885  4.7 OR   PRLO   DOLOMITEINFILL
11              60  6.34JT 12085  1.4 OD   PRLO  NOT WEATHERED-
33****OUT BLACK GANGE INFILLING PROBABLYN DOLOMITE***********
11              61  7.96JT 13288  2.0 2R   CRL
11              62  8.77JT 12688  1.7 2R   PRL
11              63 10.39JT 31390  1.4 1R   PRL
11              64 10.81JT 00272  2.3 2R   CRL
11              65 11.49JT 28090  0.7 1R   PSL
33******PAGE 3*********************************************
11              66 12.51JT 30890  2.8 1U   PSL  BLACK FILLED
33***GANGE NOT WEATHERED OUT ,,TENSION GASH*****************
11              67 13.20JT 12389  1.1 OU   PRLO
11              68 13.37JT 12489  2.7 OR   PRLO
11              69 14.30JT 30788  3.6 2R   PRL
11              70 14.68JT 30085  1.3 2R   PRL
11              71 15.48JT 30490  6.3 OR   PRLO  PARTIALLY
33************DOLOMITE FILLED*******************************
11              72 16.61JT 30790  5.6 1R   CRL
11              73 16.91JT 31087  1.9 1R   PRL
11              74 17.00JT 20883  2.5 1R   CRL
11              75 18.60JT 12482  6.3 ORU  PRL2  BLACK GANGE**
33****AND MOSS PARTIALLY FILLED FRACTURE,VERY ROUGH*********
11              76 19.50JT 31390  4.8 2RU  PRL
11              77 21.96JT 00090  0.8 2R   PRL
11              78 24.10JT 13289  2.1 OU   PRLO
11              79 28.36JT 12089  5.6 2R   SRL
22    C08402    37 32.52
11              80 00.14JT 30090  0.8 1R   SRL
11              81 00.51JT 06589  0.6 2R   CRL
11              82  1.27JT 30485  2.2 1D   PSL  VERY THIN FRACT.
33**********BLACK GANGE THAT IS NOT WEATHERED OUT*************
11              83  1.62JT 30888  1.1 1D   PSL  SAME AS ABOVE
11              84  1.83JT 00688  1.0 1R   CRL  WEATHERED / ****
33*****CROSSED BY LATER,WHITE DOLOMITE VEINLETS***************
11              85  3.10JT 30986  1.2 OD   PSL  VERY THIN BLACK*
33***GANGE , FRACTURED FILLED ,SPLAYS OFF OF THEM*************
11              86  4.10JT 30690  4.1 1R   SSL  WEATHERED FRACT*
11              87  5.20JT 19884  1.3 1R   CRL
11              88  5.29JT 26690  0.5 OR   CRLO
11              89  5.61JT 30489  3.2 1R   PRL
11              90  7.11JT 31090 16.3 OR   PRL1 SAME AS JT#17
11              91  7.26JT 01863  3.9 OR   CRLO
11              92  7.69JT 31289  5.2 OUR  PRL1 SAME AS JT#18
11              93  7.86JT 02580  0.7 OR   PRLO
11              94  8.36JT 11888  7.2 OR   PRL2 SAME AS JT#19
11              95  8.20JT 18189  0.7 OR   CRLO
11              96  8.67JT 01589  1.0 OR   CRLO
11              97  9.24JT 31290  5.5 OR   PRLO SAME AS JT#20
```

```
11            98 10.01JT 30290  4.5 OR   URL3 SAME AS JT#22
33******PAGE 4 ********************************************
11            99 11.80JT 20485  3.0 OR   CRL1
11           100 13.60JT 02090  2.1 OR   PRL1 LINEAR CHAIN OF
33*******POT HOLES ****************************************
11           101 14.74JT 31390  9.1 OR   CRL1
11           102 19.78JT 12487  2.6 OR   SRLO
11           103 20.46JT 32285  1.1 OR   CRLO  JULY 31,1986
11           104 21.20JT 31390  4.8 2RU  PRL   SAME AS JT#76
11           105 25.69JT 12986  4.5 1RD  PRL
11           106 28.41JT 31487  1.3 2R   CRL   MOSSFILLED WIDE
11           107 28.91JT 31288  2.1 1R   SRL
11           108 30.07JT 12885  4.9 1R   PRL
11           109 30.40JT 12889  3.3 1R   CRL
11           110 30.69JT 13386  2.2 2R   PRL
11           111 30.93JT 13387  1.6 2R   PRL
11           112 31.52JT 13089  1.2 OR   SRL   MOSSFILLED WIDE
11           113 31.77JT 13689  3.1 1R   CRL
11           114 32.16JT 13288  1.5 1R   CRL
11           115 32.39JT 30986  2.9 1R   CRL
11           116 32.52JT 31286  0.7 2R   PRL
22    D16100  41 23.18                      AUG. 2/86 LINE IS**
33*******35 CM OFF AIRPHOTO EDGE(NO COVERAGE).*******************
11           117  0.46JT 03790  1.1 OR   CRL1
11           118  0.78JT 31090  1.4 OU   PSLO  VERY THIN VEIN******
33*****NOT WEATHERED OUT, DOLOMITE FILLED MAYBE,TENSION PRODUCED?**
11           119  0.86JT 30889  0.7 1U   SSL    SAME AS ABOVE, 3MM
33******WIDE*****************************************************
11           120  1.70JT 31183  1.8 1R   PRL
11           121  2.27JT 13189  2.9 OR   PRL1   MOSS FILLED, WIDE
11           122  2.34JT 31788  0.8 OR   CRLO      SOLUTION JOINTS
33******WIDE,M THEY HAVE BEEN WEATHERED OUT CHAIN OF POTHOLES?*****
11           123  2.90JT 17886  4.2 OR   CRL1  MOSS FILLED, WIDE
11           124  3.80JT 12387  2.9 OR   CRL1
11           125  3.91JT 00086  1.8 1R   CRL
11           126  4.05JT 31387  2.7 1RD  PRL    MANY BLACK VEINLETS
33****OVERPRINTED BY DOLOMITE VEINLETS***************************
11           127  4.48JT 00188  3.1 OR   CRL3
11           128  5.69JT 01287  3.6 OR   CRL3   DIP? MOSSFILLEDWIDE
11           129  5.97JT 13287  1.3 OR   PRL3
11           130  6.30JT 30690  4.1 1R   SSL     SAME AS #86
11           131  6.66VN 35986  1.1 OD   PRLO    DIFF.WEATHERED WHITE
33****DOLOMITE VEIN**********************************************
33*****PAGE 5****************************************************
11           132  6.88JT 01089  1.1 OR   CRL2   ESTIMATE OF STRIKE
11           133  7.32JT 31086  1.3 2R   CRL     VERY ROUGH
11           134  7.51VN 00686  1.0 ORD  PRLO
11           135  7.53JT 11689  1.0 1R   CRL
11           136  8.93JT 13489  3.1 2R   PRL
11           137  9.42VN 18089  1.1 OD   SRLO
11           138  9.60JT 23086  2.7 OR   CRL3   MOSS FILLED
11           139  9.75VN 35889  2.9 1DR  PRL     DOLOMITE FILLED
33******5 CM WIDE***********************************************
11           140 10.00JT 13184  1.8 1R   PRL
11           141 10.44JT 17687  1.0 OR   PRL1
11           142 11.28JT 13089  3.4 1R   CRL    MOSS FILLED WIDE
11           143 11.95VN 00485  2.6 1DR  PSL   VERY GOOD MEASUREMENT
11           144 13.39VN 00485  1.1 1DR  PSL
11           145 13.64JT 30685  2.9 OR   PRL2
11           146 13.99JT 00490  1.4 1DR  PSL
11           147 14.27JT 12885  1.1 OR   PRL1
11           148 14.69JT 22589  4.4 1R   CRL
11           149 15.23JT 12687  2.1 OR   CRL1
11           150 15.76JT 30590  8.4 1R   PRL    WIDE MOSSFILLED JOINT
```

```
11          151 16.99JT 13388  3.9 OR   PRLO  PETTERS OUT AND CURVES
33*****AT ONE END*****************************************************
11          152 17.40JT 18386  1.1 OR   PRL2  VEIN-TYPE FRACTURE
11          153 18.09JT 12287 10.0 2R   CRL   SAME AS F#35 MOSSFILLED
11          154 19.74JT 31490  3.2 1R   PRL   WIDE MOSS FILLED
11          155 21.11JT 30988  0.7 OR   PSLO
11          156 21.53JT 31088  3.7 1R   PRL   PARTIALLY WIDE
33*******MOSS FILLED PETTERS OUT AT ONE END*************************
11          157 23.18JT 04288  3.5 2R   CRL  ARBITRARY JT,WIDE,MOSS
33*****FILLED, 25.23METERS TO END OF LINE*****************************
22    E19301   8 10.89
11          158  2.82VN 00290  1.0 OD   PSLO  VEIN IS WEATH. BLACK
33****** DOLOMITE****************************************************
11          159  2.89JT 04783  1.7 1R   PRL
11          160  3.62VN 18389  1.2 ODU  PSLO
11          161  4.74VN 18289  2.1 ODU  PRL1
11          162  4.95JT 04585  4.0 2R   CRL    VERY WIDE & RUBBLY
11          163  6.47VN 00690  3.1 ODU  PSLO
11          164  6.90JT 00287  2.8 OR   PRLO
33***********PAGE 6***************************************************
11          165 10.89JT 04389  3.0 2R   PRL   VERY APPROX.WIDE MOSS
33*****FILLED********************************************************
22    F17600 022 16.55
11          166  0.00JT 01890  0.7 1R   PRL1
11          167  0.43JT 29890  0.9 1R   CRL
11          168  0.95JT 29989  2.4 1R   SRL
11          169  3.42JT 11786  1.5 2R   CRL
11          170  3.53JT 00187  0.6 1R   PRL
11          171  3.69JT 33285  0.6 1R   CRL
11          172  3.94JT 04488  0.5 OR   CRL2
11          173  4.45JT 30390  3.0 1R   SRL
11          174  5.23JT 04285  1.3 2R   CRL  WIDE MOSS FILLED
11          175  7.78JT 13085  2.1 1R   PRL3 ONE SPLAY ENDING
11          176  8.87JT 30687  1.9 OR   PRL1 CHAIN OF SOLUTION
33*HOLES FRACTURE?????**********************************************
11          177  9.80JT 31190  2.8 1R   PRL
11          178 12.06JT 13088  5.5 1D   PSL  GASHLIKE 1-3MM WIDE
11          179 12.21JT 30990  5.7 1D   PSL  GASHLIKE 1-3MM WIDE
11          180 12.93JT 12785  0.8 OR   SRLO SOLUTION-HOLE CHAIN
11          181 14.04JT 21165  1.2 1R   CRL  SHALLOW-DIP TRUEFACE
11          182 14.65JT 22386  1.0 2R   PRL
11          183 14.76JT 31090  0.5 OR   PRL2
11          184 15.27JT 11188  1.7 OR   CRL2
11          185 15.71VN 13088  0.6 OUD  PSLO  3MMWIDE BLACK JOINS UP
33*WITH OTHER FRACTURE OF SIMILAR CHARACTER*************************
11          186 16.08JT 03290  0.7 OR   SRL1 VERY APPROXIMATE
11          187 16.55JT 18380  1.2 1R   SRL
22    G17000 019 15.60
11          188 00.11JT 13087  0.8 2R   PRL
11          189 00.77JT 20690  5.7 2R   PRL
11          190 01.80JT 11080  0.9 1R   PRL
11          191  2.16JT 05083  2.4 1R   CRL  WIDE,VARYING WIDTH,MOSS
11          192  3.77JT 30790  5.6 OR   PRL2   AUGUST 5, 1986
11          193  6.96JT 12288  7.3 2R   PRL   WIDE,MOSS FILLED
11          194  7.50JT 31089  5.8 OR   PRL3
11          195  8.70JT 21987  2.3 2R   CRL   WIDE,VERY
33********* APPROXIMATE AND EXTREMELY WEATHERED*********************
33*******PAGE 7*****************************************************
11          196 10.03JT 30290  2.4 OR   PRL1  SLIGHTLY CURVY,JAGGED
11          197 10.77JT 29690  1.8 1R   CRL
11          198 11.95JT 30186  6.9 2R   CRL
11          199 12.49JT 30990  5.0 1R   PRL
11          200 13.32JT 21468  3.2 2R   CRL  FAULT?WIDE MOSSFILLED
11          201 13.64JT 12389  4.9 1R   CRL  VERY ROUGH APPROXIMATE
```

```
11            202 14.03JT 30790  1.5 2R   CRL
11            203 14.26JT 12288  1.7 1RD  FRL
11            204 14.66JT 12589  0.9 1RD  PRL
11            205 15.44JT 30590  3.7 OR   PRLO
11            206 15.60JT 30890  0.7 1R   PRL
22     H24404  34 23.60
11            207  0.90JT 31088  1.0 1U   PSL
11            208  2.48JT 13088  5.2 OR   PSLO
11            209  2.49JT 23090  1.8 1R   CRL
11            210  2.72JT 05785  1.5 OR   CRL1
11            211  2.84VN 00690  3.1 ODU  PSLO   SAME AS F#163
11            212  3.34JT 21478  3.1 1R   CRL
11            213  4.77JT 04248  2.1 1R   CRL    WIDE,MOSSFILLED
11            214  5.15JT 04585  4.0 2R   CRL    SAME AS F#162,WIDE
11            215  5.80VN 00589  0.7 OD   SPL
11            216  5.93JT 30087  1.3 1R   CRL
11            217  7.03JT 30386  4.6 1R   CRL   WIDE MOSS FILLED
11            218  8.22JT 00186  1.5 1R   PRL  CHAIN OF SOL'N HOLES
11            219  9.43JT 04785  1.6 1R   CRL
11            220 10.99JT 29483  3.6 2R   CRL  WIDE,MAYBE 2 PARALLEL
33****FRACTURES***********************************************************
11            221 11.81JT 29389  1.0 1R   CRL
11            222 12.64JT 13085  2.1 1R   PRL SAME AS F#175,SPLAY END
11            223 12.65JT 03685  2.7 2R   PRL VERY ROUGH OPEN JOINTS
11            224 13.70JT 13087  1.3 1R   PRL
11            225 14.42JT 03570  1.9 2R   CRL
11            226 15.22JT 30288  1.2 OR   CRLO  SNAKE-LIKE FRACTURE
33******PAGE 8************************************************************
11            227 17.08JT 12389  4.9 1R   CRL  SAME AS F#201,AUG.6/86
11            228 17.59JT 30590  1.7 OUR  PRLO
11            229 18.65JT 30590  3.7 OR   PRLO  SAME AS F#205
11            230 18.98JT 30890  0.7 1R   PRL   SAME AS F#206
11            231 20.40JT 27287  0.8 2R   PRL   EDGE OF O/C,FELLAWAY
11            232 20.72JT 10278  1.1 2R   CRL
11            233 21.06JT 09073  0.8 OR   CRL3   MOSS FILLED
11            234 21.42JT 13388  0.8 1R   CRL    FRACTURE ZONE
11            235 21.65JT 09070  1.9 1R   CRL
11            236 21.70JT 31085  2.0 1R   PRL  MOSS FILLED FRAC.ZONE
11            237 22.04JT 31289  0.9 1R   PRL
11            238 22.35JT 31090  2.5 2R   PRL    WIDE,MOSSFILLED,
33********FRACTURE ZONE***************************************************
11            239 23.16JT 31586  1.2 1R   PRL    FRACTURE ZONE
11            240 23.60JT 13089  1.6 2R   PRL    FRACTURE ZONE
22     I16900 033 18.30
11            241 00.30JT 12983  0.5 1R   PRL   CHAIN OF SOL'N HOLES
11            242 00.81JT 05588  0.6 OR   PRL1  IRREGULAR FRACTURE
33*****WALLS A CHAIN OF SOLUTION HOLES************************************
11            243 00.86JT 30483  1.7 OR   PRL1  SAME COMMENT AS ABOVE
11            244  1.26JT 31090  2.3 OR   PRLO  SOLUTION HOLES ALONG
33****FRACTURE*********************************************************
11            245  3.05JT 29575  2.1 2R   PRL    DOL.FILLED BLACK
33*****3CM WIDE***********************************************************
11            246  3.80JT 30088  1.7 2R   PRL   15CM WIDE ,DOL.FILLED
11            247  4.22JT 19329  0.6 2R   PRL   SAME COMMENT AS ABOVE
11            248  4.95JT 30590  2.2 2R   PRL   SAME COMMENT AS ABOVE
33****ONLY 8CM WIDE*******************************************************
11            249  5.22JT 12488  1.3 1R   PRL   SAME COMMENT AS ABOVE
33******ONLY 4CM WIDE*************************************************
11            250  6.06JT 30070  5.7 2R   PRL   SAME COMMENT AS ABOVE
33*******ONLY 10CM WIDE***********************************************
11            251  6.77JT 30385  1.6 1R   SRL
11            252  6.99JT 31884  1.1 2R   CRL
11            253  7.47JT 13286  3.9 1R   CRL    WIDE BLACK DOL.FILLED
33***15CM WIDE SHALLOW FRACTURE DIP TOWARDS THE SOUTH EAST*********
```

```
11              254  7.91JT 04485  2.4 2R   CRL    WIDE DOL.FILL,15CMWIDE
11              255  8.21JT 03975  3.9 1R   CRL  SAME COMMENT AS ABOVE
11              256  8.67JT 30578  1.7 2R   CRL  SAME COMMENT AS ABOVE
11              257  9.46JT 31290  0.7 1R   PRL  THIN FRACTURE CAUSING
33*****SOLUTION HOLES TO DEVELOP***************************************
33*******PAGE 9********************************************************
11              258  9.71JT 13459  2.9 2R   PRL   WIDE 15CM,BLACK ***
33*****DOLOMITE FILLED************************************************
11              259 10.43JT 04389  0.5 1R   PRL
11              260 10.61JT 12385  1.4 1R   CRL   BLACK DOLOMITE FILLED
11              261 11.11JT 04472  0.8 2R   PRL   WIDE 20CM WIDE,DOLFILL
11              262 11.35JT 12483  8.1 2R   CRL   VERY WIDE 15-20CM
11              263 11.53JT 30686  0.7 1R   PRL
11              264 13.33JT 30480 12.6 1R   CRL   VERYWIDE LONG JT,20CMWD
11              265 14.11JT 31785  0.6 2R   PRL   THIN LINE OF SOLUTION
33********HOLES WITH FRACTURE*****************************************
11              266 14.19JT 03690  4.3 2R   CRL   FRACTURE? VERY WIDE SPA
33******CE ,5-10CM WIDE***********************************************
11              267 14.23JT 30385  0.7 1R   PRL
11              268 14.60JT 31090  7.2 1R   CRL  VERY WIDE 15-20CM FRCTR
11              269 15.10JT 11385  0.9 1R   CRL  NOT CONSTANT WIDTH,SOLN
33*****HOLES ALONG FRACTURE*******************************************
11              270 16.41JT 12580  4.4 0R   CRL3
11              271 16.95JT 12486  1.1 1R   SRL
11              272 17.43JT 30289  1.3 0R   SRLO  CHAIN OF SOLUTION HOLES
11              273 18.30JT 30085  2.1 1R   CRL   CHAIN OF SOLUTION HOLES
22     J07505 027 12.89
11              274  0.42JT 12687  3.6 2R   PRL   EITHER SIDE OF WIDE
33*****FRACTURE SPACE*************************************************
11              275  0.76JT 29990  1.2 2R   PRL   SAME COMMENT AS ABOVE
11              276  0.89JT 06687  0.7 0R   CRL   SOLUTION HOLE FRACTURES
11              277  1.01JT 21888  1.4 0R   CRL   SOLUTION HOLE FRACTURES
11              278  1.63JT 29890  1.4 0R   CRLO  SOLUTION HOLE FRACTURES
33******OFFSET BE FRACTURE********************************************
11              279  1.77JT 04790  1.2 0R   CRL1  SOLUTION HOLE FRACTURES
11              280  1.81JT 32288  1.6 0R   CRL1  SAME AS ABOVE
11              281  2.67JT 24490  1.2 2R   CRL   SAME AS ABOVE
11              282  3.41JT 14166  0.6 1R   PRL
11              283  4.00JT 30578  1.7 2R   CRL   MAPPED AS FR#256
11              284  4.47JT 03975  3.9 1R   CRL   MAPPED AS FR#255
11              285  4.92JT 22185  1.4 2R   CRL   FILLED WITH BLACK
33*****SEDIMENT,ORGANIC--SPACE FRACTURE*******************************
11              286  5.15JT 09488  1.1 2R   CRL   SAME COMMENT AS ABOVE
11              287  5.51JT 10089  1.1 0R   CRL3
11              288  6.70JT 06188  7.4 2R   CRL   SAME COMMENT AS ABOVE
33*****WIDE ABOUT 15CM************************************************
33*********PAGE 10****************************************************
11              289  7.09JT 12483  8.1 2R   CRL   MAPPED AS FR#262
11              290  7.48JT 13286  1.4 1R   CRL   TINY FRACTURE WITH
33****LINEAR CHAIN OF SOLUTION HOLES**********************************
11              291  8.36JT 14084  1.8 0R   CRL1  SOL'N HOLES WITH FRCT
11              292  9.43JT 04080  1.8 1R   CRL   WIDE 10-15CM JOINT
11              293  9.65JT 30480 12.6 1R   CRL   MAPPED AS FR#264
11              294 10.63JT 11085  2.2 1R   URL
11              295 10.67JT 06685  1.3 2R   CRL   WIDE DEEP WEATHERED
11              296 10.98JT 10981  1.7 2R   PRL   WIDE DEEP WEATHERED
11              297 11.19JT 11888  0.7 1R   URL
11              298 11.91JT 32590  1.8 1R   URL
11              299 12.07JT 10483  1.4 1R   URL
11              300 12.89JT 11188  1.5 1R   CRL
22     K17100 023 10.72
11              301  1.17JT 21088  2.3 2R   CRL   WIDE OPEN,10CM WIDE
11              302  1.57JT 11260  0.7 2R   CRL
11              303  1.79JT 30286  1.7 1R   CRL
```

```
11            304   2.20JT 12082   1.1 1R    CRL
11            305   2.68JT 02177   1.2 2R    URL
11            306   3.06JT 11784   1.3 1R    PRL
11            307   3.49JT 14187   0.6 OR    PRLO
11            308   4.00JT 18687   1.9 2R    CRL   5-10CM WIDE FRACTURE
11            309   4.12JT 30589   2.4 1R    CRL
11            310   4.39JT 12884   1.4 1R    PRL
11            311   4.58JT 11780   3.9 2R    PRL   10CM WIDE FRACTURE
33****SPACE***********************************************************
11            312   5.12JT 12288   1.1 2R    PRL
11            313   5.58JT 12688   2.2 1R    PRL
11            314   5.80JT 04080   1.8 1R    CRL  MAPPED AS FR#292
11            315   6.03JT 13785   0.9 OR    PRLO
11            316   6.54JT 14084   1.8 OR    CRL  MAPPED AS FR#291
11            317   7.62JT 13275   1.0 2R    PRL
11            318   7.95JT 30480  12.9 1R    CRL  MAPPED AS FR#264
11            319   8.10JT 30590   0.9 1R    CRL
33*********PAGE 11*****************************************************
11            320   8.60JT 26482   1.6 2R    URL  IRREGULAR JAGGED FR.
11            321  10.10JT 30980   2.9 1R    URL  20 CM WIDE FRACTURE
33*****CALLED A SPACE FRACTURE MAYBE 2 FRACTURES WEATHERED OUT*****
11            322  10.29JT 06188   7.4 2R    CRL  MAPPED AS FR#288
11            323  10.72JT 00673   0.6 2R    PRL  END OF SCANLINE 12.45M
22     LO7003 032  10.08
11            324   0.88JT 12588   3.0 2R    CRL   MOSS+PLANT FILLED
11            325   1.02JT 04184   1.2 2R    URL
11            326   1.20JT 12685  10.9 1R    PRL   WEATHERED COMPLETELY
33******OUT. FRACTURE GOES OFF THE AIRPHOTO ONTO NEXT ONE***********
11            327   1.40JT 31090   1.0 1R    URL   SOLUTION HOLES
11            328   1.66JT 30588   1.8 1R    CRL   SOLUTION HOLES
11            329   1.76JT 21989   0.5 1R    PRL   SOLUTION HOLES WITH JT
11            330   2.00JT 13083   1.0 OR    PRL2
11            331   2.41JT 12475   3.5 1R    CRL
11            332   2.86JT 22285   0.9 1R    CRL
11            333   2.97JT 11688   2.2 1R    PRL
11            334   3.23JT 13377   1.3 OR    PRLO
11            335   3.40JT 13073   2.0 OR    PRLO
11            336   3.80JT 13083   1.4 2R    PRL
11            337   4.11JT 29583   0.5 OR    PRL2
11            338   4.38JT 31284   5.5 2R    PRL    WIDE.AUGUST 9,1986
11            339   4.96JT 12885   6.1 1R    URL   WIDE OPEN DEPTH 6 INCH.
11            340   5.53JT 13285   1.5 OR    CRL3
11            341   6.20JT 13075   2.6 1R    PRL
11            342   6.44JT 12385   0.8 2R    PRL
11            343   6.80JT 06075   2.1 1R    SRL   VARIABLE DIP?
11            344   7.01JT 12786   1.1 OR    PRL2
11            345   7.15JT 12883   0.8 ODR   PRLO  PARTIALLY WEATHERED
11            346   7.29JT 30580   4.7 OR    PRLO  WEATHERED WIDE
11            347   7.27JT 23178   1.1 1R    URL   WIDE, VARIABLE
33**************DIP AND STRIKE*******************************
11            348   7.90JT 03175   2.1 1R    URL   WIDE,VARIABLE***
33******AND STRIKE*******************************************************
11            349   8.00JT 15485   1.7 OR    URL1
11            350   8.33JT 24070   1.8 1R    URL   VARIABLE DIP + STRIKE
33*************PAGE 12*************************************************
11            351   8.59JT 30690   0.9 OR    URLO
11            352   8.96JT 11580   5.6 1R    PRL    CURVED AT ONE END
11            353   9.16JT 08980   1.3 OR    URL1
11            354  10.03JT 10085   1.2 1R    CRL
11            355  10.08JT 04283   1.8 2R    URL
22     MO9005 041  15.50
11            356   1.09JT 30785   3.2 2R    CRL
11            357   1.47JT 12685   1.4 2R    PRL
11            358   1.83JT 29583   1.6 2R    PRL
```

11		359	2.19JT	30380	0.8	1R	PRL	
11		360	2.41JT	11383	3.7	OR	URLO	
11		361	2.82JT	12986	1.7	OR	PRL1	
11		362	3.41JT	03082	2.2	1R	URL	
11		363	3.51JT	12280	4.8	1R	CRL	
11		364	3.66JT	31090	2.1	OR	PRLO	
11		365	4.13JT	12789	4.2	1R	PRL	
11		366	4.26JT	02685	0.7	1R	CRL	
11		367	4.90JT	30990	2.4	OR	PRL1	
11		368	5.00JT	02570	2.8	OR	CRL2	
11		369	5.17JT	30386	2.0	OR	PRLO	
11		370	5.31JT	12680	6.1	OR	PRLO	
11		371	5.56JT	02585	1.7	2R	PRL	WIDE,FILLED WITH MOSS
11		372	5.69JT	11685	3.9	1R	PRL	
11		373	6.06JT	21090	0.9	OR	URL2	APPROXIMATE DIP+STRIKE
11		374	6.12JT	11884	1.5	1R	PRL	
11		375	6.18JT	30990	1.2	1R	PRL	
11		376	6.45JT	12487	4.0	1R	PRL	
11		377	7.36JT	30490	2.6	1R	CRL	
11		378	7.81JT	12481	0.9	1R	CRL	APPROXIMATE DIP?
11		379	8.10JT	30390	1.8	2R	PRL	ROUGH FRACTURE
11		380	8.29JT	12785	1.4	1R	PRL	
11		381	8.62JT	03680	1.1	2R	URL	
33**************PAGE 13**								
11		382	8.69JT	12286	7.6	1R	PRL	
11		383	9.86JT	30290	1.5	1R	SRL	
11		384	11.37JT	30490	1.0	1R	SRL	
11		385	12.00JT	12085	1.6	2R	URL	
11		386	12.42JT	29990	2.0	1R	PRL	
11		387	13.10JT	05080	1.5	1R	URL	
11		388	13.17JT	12088	2.7	2R	PRL	
11		389	13.26JT	30385	0.9	1R	PRL	
11		390	13.51JT	30090	0.5	1DR	PRL	
11		391	13.62JT	12285	3.0	1R	PRL	
11		392	13.65JT	12086	1.1	1R	PRL	
11		393	14.02JT	12882	2.8	1R	PRL	
11		394	14.43JT	12186	3.5	OR	PRLO	
11		395	14.90JT	30890	3.3	OR	PRL1	
11		396	15.50JT	11383	0.5	1R	PSL	END OF LINE 15.67M
22	N07603	028	8.87					
11		397	0.54JT	10376	0.7	1R	PRL	SMALL FRACT. ZONE
11		398	0.91JT	10270	1.3	1R	PRL	SMALL FRACT. ZONE
11		399	0.76JT	09868	0.9	2R	PRL	SMALL FRACT. ZONE
11		400	2.45JT	29086	0.7	1R	PRL	
11		401	2.94JT	11179	2.2	1R	URL	
11		402	3.05JT	29490	0.9	1R	PRL	
11		403	3.27JT	10377	0.6	1R	CRL	TAPERED FRACTURE
11		404	3.53JT	30184	0.8	1R	CRL	
11		405	4.05JT	29185	2.0	OR	URLO	
11		406	4.50JT	12985	1.2	OR	PRLO	
11		407	4.52JT	03086	0.8	2R	URL	APPROX. DIP&STRIKE
11		408	4.70JT	11377	1.1	1R	URL	
11		409	4.96JT	21280	1.1	2R	URL	
11		410	5.33JT	11486	0.5	2R	CRL	
11		411	5.67JT	09475	1.5	1R	CRL	VERY APPROX. MEASUREM.
11		412	5.89JT	10075	1.8	1R	CRL	VERY APPROX. MEASUREM.
33******************PAGE 14***								
11		413	6.13JT	12282	1.2	1R	CRL	
11		414	6.35JT	03586	2.3	1R	URL	
11		415	6.59JT	22870	0.6	1R	CRL	
11		416	6.91JT	13086	0.9	1R	CRL	
11		417	6.97JT	30090	0.7	1R	PRL	
11		418	7.08JT	11584	2.5	OR	URL1	
11		419	7.61JT	30790	3.6	2R	CRL	

```
11          420  7.89JT 05985  1.0 2R   URL
11          421  7.99JT 12884  1.0 1R   PRL
11          422  8.18JT 03587  2.2 2R   URL
11          423  8.72JT 12388  1.2 1R   CRL
11          424  8.87JT 03789  0.9 1R   URL   E.O.L. 9.2 METERS
22    016701 053 29.90
11          493  0.55JT 12489  3.2 OR   CRL   AUGUST 11,1986
11          494  0.62JT 12689  1.4 OR   PRL
11          495  0.74JT 02680  1.4 2R   URL
11          496  1.60JT 12186  1.6 OR   URLO
11          497  2.94JT 03490  1.9 1R   URL   VERY APPROX. DIP?
11          498  3.68JT 12288  7.3 2R   PRL   MAPPED AS FR# 193
11          499  4.49JT 12789  1.7 1DR  PRL
11          500  5.48JT 22080  2.8 2R   URL   VERY APPROXIMATE
11          501  6.27JT 17487  2.2 1DR  PRL
11          502  7.26JT 18488  3.4 ODR  PRLO
11          503  7.30JT 12585  1.9 OR   URLO
11          504  8.09JT 11685  1.3 OP   DRLO
11          505  8.88JT 17688  2.6 OD   PSLO
11          506 10.13JT 12389  4.9 1R   CRL    MAPPED AS FR#201
11          507 10.94JT 30590  3.7 OR   PRLO   MAPPED AS FR#205
11          508 12.16JT 30290  0.9 1R   URL    NO PHOTO COVERAGE
11          509 12.53JT 30890  4.7 1R   PRL    NO PHOTO COVERAGE
11          510 13.73JT 19787  1.1 1R   URL    NO PHOTO COVERAGE
11          511 14.00JT 11480  3.8 1R   CRL    PARTIAL PHOTO COV.
33*******************PAGE 15*********************************
11          512 14.92JT 27485  1.9 OR   CRLO   NO PHOTO COVERAGE,
33****RUBBLE IN FRACTURE 15.1-16.1 METERS************************
11          513 16.83JT 20886  0.9 2R   URLO   PHOTO COVERAGE?
11          514 17.03JT 12980  0.9 2R   PRL
11          515 17.79JT 11084  0.7 OR   URL1   APPROX. DIP?
11          516 18.35JT 12485  1.9 1R   CRL
11          517 18.89JT 02988  1.2 1R   CRL
11          518 19.19JT 11685  1.2 1R   SRL
11          519 19.45JT 21188  2.8 2R   CRL
11          520 20.13JT 11689  0.8 OR   CRLO
11          521 20.22JT 13088  0.5 OR   CRL1
11          522 20.99JT 13086  0.9 1R   CRL   MAPPED AS FR#416
11          523 21.04JT 30090  0.7 1R   PRL   MAPPED AS FR#417
11          524 21.17JT 11584  2.5 OR   URL1  MAPPED AS FR#418
11          525 21.87JT 30290  0.6 1R   CRL
11          526 21.95JT 03586  2.3 1R   URL   MAPPED AS FR#414
11          527 22.39JT 11685  3.9 1R   PRL   MAPPED AS FR#372
11          528 22.76JT 12185  2.3 1R   PRL
11          529 22.78JT 20787  1.2 OR   CRL2
11          530 23.12JT 12086  0.8 1R   PRL
11          531 23.38JT 30187  1.0 2R   PRL
11          532 24.19JT 11487  3.3 2R   PRL   VERY APPROX.DIP?
11          533 25.22JT 12587  6.8 2R   PRL
11          534 25.86JT 12286  7.6 1R   PRL   MAPPED AS FR#382
11          535 26.05JT 03683  1.7 2R   PRL
11          536 26.52JT 12388  8.4 1R   PRL
11          537 26.92JT 12785  2.4 1R   PRL
11          538 27.09JT 03790  1.0 OR   URL1    APPROX. DIP?
11          539 27.28JT 11885  2.4 1R   PRL
11          540 27.99JT 30590  3.0 1R   PRL
11          541 28.15JT 12385  3.7 2R   PRL
11          542 28.29JT 21089  1.6 1R   URL
11          543 28.42JT 15088  0.6 1R   PRL
33*********PAGE 16*********************************************
11          544 29.62JT 30890  1.9 1R   PRL
11          545 29.90JT 04485  4.1 1R   URL   E.O.L. 30 METRES
33********** VERY APPROX. STRIKE AND DIP***********************
22    P16000 035 18.76
```

```
11          546 00.00JT 13286  4.0 2R   PRL
11          547  0.12JT 13189  0.9 OR   URL1
11          548  0.39JT 13287  5.6 2R   PRL
11          549  0.54JT 31388  3.9 1R   SRL
11          550  1.05JT 12788  2.0 OR   PRL3
11          551  1.52JT 30890  3.7 OR   PRLO
11          552  2.02JT 30890  1.8 OR   URLO
11          553  2.29JT 12089  1.8 1R   PRL
11          554  2.62JT 01090  1.5 OR   URLO
11          555  3.78JT 13485  3.2 OR   PRLO
11          556  4.24JT 13289  4.8 OR   PRL1
11          557  5.14JT 31082 15.3 1R   PRL  MAPPED AS FR#56
11          558  5.53JT 13088  4.6 1DR  PRL
11          559  6.15JT 19086  1.4 OR   URLO
11          560  6.42JT 19786  1.8 OR   CRL1
11          561  6.49JT 13187  6.4 ODR  PRLO
11          562  7.07JT 13186  1.0 OR   PRL1
11          563  7.56JT 13589  2.7 OR   PRL1
11          564  7.93JT 30089 13.6 OR   PRLO MAPPED AS FR#15
11          565  8.35JT 13185  9.1 1R   PRL
11          566  9.03JT 30290  0.9 OR   PRLO
11          567  9.50JT 03690  2.3 1R   CRL  APPROX.DIP+STRIKE
11          568  9.67JT 31090 16.3 OR   PRL1 MAPPED AS FR#17
11          569 10.71JT 13285  3.2 1DR  PRL
11          570 11.02JT 13087  0.8 1DR  PRL
11          571 11.13JT 31389  1.6 1D   PSL
11          572 12.31JT 19886  2.0 OR   PRL2  DIP IS APPROX.
11          573 12.89JT 12287  4.1 1DR  PRL
11          574 13.35JT 12988  1.1 OR   PRL1
33****PAGE 17***************************************************
11          575 13.43JT 18989  1.4 OR   PRLO
11          576 14.20JT 31190  5.5 2R   PRL  APPROX.DIP+STRIKE
11          577 14.86JT 30990  0.6 OD   PSLO
11          578 15.58JT 35590  0.6 OD   PSLO
11          579 16.67JT 31390  9.1 OR   CRL1 MAPPED AS FR#101
11          580 18.76JT 17885  1.7 1D   PSL  E.O.L. 19.9M
33******PAGE 18*********************************************
22     Q20000 023 30.19
11          881  1.69JT 13086  2.2 2R   PRL
11          882  2.32JT 13385  0.5 OR   PSLO
11          883  5.35JT 31090  4.8 OR   PRL1
11          884  5.59JT 05689  3.9 1R   URL
11          885  7.17JT 06087  1.3 1R   URL
11          886  8.46JT 31390  4.8 2RT  PRL  MAPPED AS FR#76
11          887 10.89JT 00587  1.3 1R   PRL
11          888 12.75JT 04485  2.7 1R   URL  APPROX.DIP+STRIKE
11          889 13.06JT 22488  2.2 1R   URL  APPROX.DIP+STRIKE
11          890 14.00JT 18889  1.5 ORD  URLO PARTIALLY VEIN FIL
11          891 15.53JT 01090  3.9 ODR  PSLO PARTIALLY VEIN FIL
11          892 18.74JT 02285  5.1 1R   URL  APRROX.DIP+STRIKE
11          893 22.09JT 04185  3.6 2R   PRL  MAPPED AS FR#33
11          894 22.31JT 29885  0.9 1R   URL  APPROX.DIP+STRIKE
11          895 22.55JT 03585  2.8 OR   URLO
11          896 23.64JT 30189  9.6 OR   SRLO MAPPED AS FR#45
11          897 24.85JT 22388  2.8 1R   URL
11          898 25.84JT 02090  1.0 OR   PRL1
11          899 25.95JT 05090  1.2 OR   URL1
11          900 27.59JT 04488  1.7 OR   PRL1
11          901 28.39JT 24388  3.3 1R   CRL  APPROX. DIP+STRIKE
11          902 29.84JT 06090  0.9 OR   PRLO
11          903 30.19JT 31590  2.7 1R   PRL  E.O.L. 30.42 METRES
33**************PAGE 19*****************************************
22     R18000 020 11.77
11          904  0.69JT 21582  1.1 2R   PRL
```

11	905	1.OOVN	35290	1.2	2D	PSL	
11	906	1.65JT	13084	1.6	1R	CRL	
11	907	2.76JT	18287	0.6	OR	PRLO	
11	908	2.92JT	24285	3.0	1R	URL	
11	909	3.65JT	30590	1.1	OR	CRLO	
11	910	4.60JT	18889	1.9	ORD	PRL1	
11	911	4.78JT	30386	4.6	1R	CRL	MAPPED AS FR#217
11	912	6.73JT	18884	3.7	ORD	PRLO	
11	913	7.49JT	18388	1.6	ODR	PRLO	
11	914	7.76JT	12880	2.8	1R	PRL	
11	915	8.32JT	12789	1.3	2R	PRL	
11	916	8.39JT	31685	1.8	2D	PSL	
11	917	8.99JT	12087	1.7	1R	URL	
11	918	9.36JT	18085	1.6	1R	PRL	
11	919	9.74JT	31087	2.8	1R	PRL	
11	920	10.25JT	31288	3.6	ODR	PRL1	
11	921	10.60JT	12087	0.8	1R	CRL	
11	922	11.39JT	31085	1.3	1R	PRL	
11	923	11.77JT	12785	2.5	1R	PSL	E.O.L. 13.40METRES

```
33*****************************************************************
33********DANIEL'S HARBOUR FRACTURE ********************************
33**********JULY-AUGUST 1986***************************************
33**********MINE UNDERGROUND DRIFT *********************************
33****NEW CODING CONVENTIONS: Fracture Type BP=Bedding Plane,*****
33****Infilling D=Dolomite, Roughness V=vuggy, Rock; L=Limestone**
33****D=Dolomite, X=Pseudobreccia *********************************
33*************Page 20****RUSTY BEDDING PLANE SEEP ON MAIN DECLINE
22      S24708
11             425 00.50BP 30410 04.6 2  U PSL   CENSORING?
11             426  1.60JT 32775  0.6 1  U USL   CENSORING?BLAST FRC.?
11             427  3.50JT 35075  0.6 1  U PSL   CENSORING?
11             428  3.90BP 32014  4.6 1  U PSL   CENSORING?SAMEAS 425
11             429  6.00BP 33410  5.0 2  U PSL   CENSORING?LENGTH?
11             430  6.40BP 33314  5.0 2  U PSL   CENSORING?LENGTH?
11             431  6.90JT 20365  1.6 1  U USL   CENSORING?
11             432  7.30JT 11877  0.6 1  U PSL   CENSORING?
11             433  7.50JT 31243  1.0 1  U PSL   CENSORING?
11             434  4.90JT 12052  0.7 1  U PSL   CENSORING?
11             435  5.00JT 13084  2.0 1  U PSL   CENSORING?
33************PAGE 21*****PORTAL DECLINE WEST SIDE**************
22      T00607
11             436  0.24JT 14684  0.6 2  U SPL
11             437  0.25BP 27621  7.9 2  U UPL
11             438  0.76JT 12689  1.0 2  U PSL
11             439  0.84JT 13285  0.8 2  U PSL
11             440  0.95JT 13685  0.7 2  U PSL
11             441  1.00JT 13085  0.8 2  U PSL   RUBBLY ROCK 1.1-1.5M
11             442  1.42JT 13183  0.6 2  U PSL
11             443  1.50JT 13076  0.9 1  U USL
11             444  1.80BP 30615  2.4 1  R USL
11             445  2.20JT 12682  1.7 1  U PSL
11             446  2.26JT 15986  0.8 1  U PSL
11             447  2.64JT 24070  0.5 1  U PSL
11             448  2.73JT 13286  0.8 0  U PSLO
11             449  3.40JT 24568  0.8 1  D PSL
11             450  4.52BP 27715  1.2 1  R USL
11             451  5.10JT 31189  1.0 1 DR PRL
11             452  5.54JT 32587  1.5 1 D  PSL
11             453  7.23JT 13386  0.6 1 U  PSL
11             454  7.69JT 24190  0.7 0 U  PSL
11             455  7.84BP 16215  0.9 1 R  URL
11             456  7.92JT 22090  1.2 2 U  PSL
11             457  8.51JT 30680  0.8 0 U  PSLO
11             458  8.63JT 33785  0.5 1 U  USL
11             459  8.97JT 31075  0.7 0 U  PSLO
11             460  9.00BP 27016  2.4 1 R  USL
11             461 11.10JT 30585  1.1 0 U  PSLO
11             462 11.50JT 30384  0.8 1 U  PSL
11             463 11.67JT 31387  1.2 1 U  PSL
11             464 11.70JT 23690  0.9 1 U  CRL
11             465 11.95JT 31090  1.2 2    PSL
11             466 12.64JT 22587  0.6 0 U  CSL2
11             467 13.20JT 30590  1.2 2 U  PSL
33********PAGE 22*************************************************
11             468 14.20JT 31090  1.4 1 U  PSL
11             469 14.70BP 10420  4.1 1 R  URL
11             470 15.05JT 31585  0.9 1 U  PSL  SHORT FRACTURE
33****SET OF ALL ORIENTAT. 15.10-17.30*****************************
11             471 17.44JT 30988  0.6 1 U  PSL
11             472 18.31JT 05086  0.5 1 U  PSL
11             473 18.80JT 27307  1.0 0 U  CSLO  SHORT FRACTURE
33****SET OF ALL ORIENTATIONS 18.70-20.20*************************
11             474 20.23JT 14027  0.7 2 U  PSL
```

```
11           475 21.40JT 05080  0.6 2 U  PSL
11           476 21.70JT 13386  0.9 1 U  PSL   SHORT FRACTURE
33****SET OF ALL ORIENTATIONS 22.50-23.71**************************
11           477 23.60JT 09840  1.0 1 D  USL
11           478 24.72JT 13584  2.4 0 U  PSL1  CEMENT TUBE AT 24.9M
33*****THESE FRACTURES SEEM TO STOP AT BEDDING PLANE 478,479,480-82**
11           479 26.60JT 13883  1.8 1 U  PSL
11           480 26.84JT 13381  1.5 1 U  PSL
11           481 27.15JT 13683  2.1 1 U  PSL
11           482 27.40JT 13987  1.9 1 U  PSL
11           483 27.69JT 13687  2.5 1 U  PSL
11           484 28.16JT 13789  1.8 0 U  PSL1
11           485 28.17BP 25711  1.4 1 U  USL
11           486 28.45JT 11284  1.2 0 U  PSL1
11           487 28.55JT 11385  2.3 0 U  PSL2
11           488 28.93JT 33087  2.0 0 U  PSL2
11           489 29.00JT 32088  1.8 0 U  PSL2
11           490 30.00JT 31189  3.6 1 U  PSL
11           491 31.80JT 29890  2.2 2 U  PSL
11           492 32.00BP 29518  4.0 1 DU PSL   END OF LINE 32M,GOOD
33****BEDDING PLANE*************************************************
33****PAGE 23*****DEEPER PART OF L-ZONE********************************
22     UO5400
11           581 00.00JT 12586  1.0 1    PSL
11           582  0.50JT 13484  1.2 1    PSL
11           583  1.00JT 30888  1.5 1    PSL
11           584  1.50JT 32090  0.9 1    PSL
11           585  1.78JT 31080  1.0 1    PSL
11           586  2.50JT 31088  1.4 1    PSL
11           587  3.15JT 02581  0.6 1    PSL
11           588  3.39JT 32078  0.8 1 D  PSL
11           589  3.73JT 31588  2.5 1    PSL
11           590  3.97JT 13087  0.8 1    PSL
11           591  4.10JT 31890  0.7 1    PSL
11           592  4.95JT 14088  1.2 0    CRL1
11           593  5.20JT 31688  2.0 1    PRL
11           594  5.75JT 13385  1.2 1    PSL
11           595  6.24JT 30586  0.5 1    PSL
11           596  7.20JT 32188  1.4 1    PSL
11           597  8.80JT 32188  0.9 2    PSL
11           598  9.75JT 22578  1.1 1    PRL
11           599 11.10JT 12578  3.0 2    PRL  END OF LINE 14METRES
33***BREAK IN THE SAME LINE*******************************************
11           600 19.70JT 33084  8.0 2    PRL   WATER FILLED SEEPING
11           601 20.70JT 31083  4.0 2    PRL   WATER FILLED SEEPING
11           602 21.10JT 31087  1.1 1    PSL   WATER FILLED SEEPING
11           603 21.90BP 31587  2.4 2    PSL   WATER FILLED SEEPING
11           604 23.00BP 31513  4.5 2    PRL   WATER FILLED SEEPING
```

```
33*************************************************************************
33******DANIEL'S HARBOUR FRACTURE DATA**************************************
33********JULY-AUGUST 1986 *************************************************
33********PIT #1(H-ZONE), PIT #2(F-ZONE), PIT #3(A-ZONE)*******************
33********NEW CODING CONVENTIONS; Fracture Type BP=Bedding Plane*********
33********Infilling D=Dolomite, Roughness V=vuggy, Rock L=Limestone******
33********D=Dolomite, X=Pseudobreccia*************************************
33********PAGE 24 PIT #1 LARGE PIT IN H-ZONE, WHERE DH-3-86 IS LOCATED***
22     VO5600
11            605 OO.7OJT 31886 O1.2 2 C  PRX
11            606  1.24JT 31285 OO.8 2 C  PRX
11            607  1.89JT 13890  1.4 2 C  PRX
11            608  4.10BP 14807  1.3 1 RD PRX
11            609  4.35JT 28886  1.0 1CRT PRX  RT=RUST
11            610  4.95JT 08086  1.5 1U   USX
11            611  5.55JT 31084  1.8 1C   PRX
11            612  6.09JT 31086  0.8 1C   PRX
11            613  7.35BP 14015  3.0 1R   PRX  VUGGY=V
11            614  8.48JT 11584  0.9 1DC  USX
11            615  8.71JT 13789  1.2 ORTD PSX1  END OF LINE IS 11.25M
22     W00090
11            616  0.34BP 14808  1.5 1RD  PRX  2.42M LENGTH OF SC.LINE
11            617  0.59BP 15015  1.4 1RD  URX  VUGGY,INTERSECTS AT
33******4.95METRES ON THE PREVIOUS SCANLINE
11            618  0.70BP 15010  1.4 ORD  PRXO  APPROX. STRIKE/DIP
11            619  0.81BP 14910  1.3 OU   PSXO
11            620  1.42BP 15506  3.2 ORT  CRXO
11            621  1.73BP 14807  1.3 1RD  PRX    SAME AS BP#608
22     X12800
11            622  0.49JT 31685  0.6 2U   PSX
11            623  0.70JT 31088  0.6 1U   PSX
11            624  0.92JT 13090  0.8 2U   PSX
11            625  1.40JT 13290  1.0 2RC  PSX
11            626  1.46JT 31685  0.7 1C   PSX
11            627  1.62JT 13390  0.6 1U   PSX
11            628  1.75JT 13485  1.1 1U   PSX
11            629  2.06JT 14285  0.6 1U   USX
11            630  2.45JT 14490  1.2 2C   PSX
11            631  2.68JT 13490  0.7 1C   PSX
11            632  3.08JT 31688  1.2 1C   CSX   MAYBE DOLOMITE VEIN
11            633  3.11JT 32086  1.5 2C   PSX   MAYBE DOLOMITE VEIN
11            634  3.26JT 14086  1.5 2C   USX
33**********PAGE 25*****************************************************
11            635  3.72JT 13387  1.3 2U   USX  STRIKE/DIP APPROXIMATE
11            636  3.76JT 13090  1.1 1C   PSX
11            637  4.46JT 31089  1.3 1U   USX
11            638  4.58JT 31286  1.2 1U   CSX
11            639  4.70JT 13884  0.6 OU   PSXO
11            640  4.96JT 13288  0.8 OU   CSXO
11            641  5.43JT 32089  1.0 1    PRX
11            642  5.62JT 30985  1.2 1SP  PSX
11            643  5.75JT 30885  1.6 1C   PSX
11            644  6.02JT 30689  1.0 2RT  PSX
11            645  6.50JT 14189  1.5 2R   PSX
11            646  6.80JT 12685  0.7 1C   PRX
11            647  7.02JT 19685  0.8 1C   PRX
11            648  7.04JT 13485  0.6 1D   PSX
11            649  7.10JT 13088  1.1 1D   CSX
11            650  7.26JT 14086  1.0 OD   PSXO
11            651  7.44JT 13284  0.7 1U   PRX
11            652  7.82JT 14588  0.8 OC   PSX1  BREAK IN ROCK AND LINE
33***ROCK HAS SHIFTED****************************************************
11            653  7.95JT 33388  1.1 1C   PSX
11            654  8.02JT 14085  1.1 1C   PSX
```

```
11            655  8.30JT 14890  2.7 2D   PRX
11            656  8.99JT 15090  2.5 2RT  PRX   WEATHERED
11            657  9.46JT 14590  1.1 1R   USX
11            658  9.86JT 32585  1.6 2U   PSX
11            659  9.90JT 32288  0.9 1U   PSX
11            660 10.24JT 31488  1.8 2C   PSX
11            661 10.30JT 22683  0.5 1    PSX
11            662 10.49JT 31683  0.7 1C   USX
11            663 10.65JT 32689  3.7 1R   USX
11            664 11.20JT 22284  0.7 1U   PSX
11            665 11.70JT 30089  0.8 1C   PSX   END OF LINE AT
33**********11.70 METRES LONG*******************************************
33*****PAGE 26**********************************************************
22     Y00090
11            666 00.00BP 33205  4.0 2R   URX  INTERSECT LAST SCANLINE
33******AT 5.12 METRES*************************************************
11            667  0.53BP 22808  1.9 2R   URX
11            668  0.56BP 33306  5.2 2R   URX
11            669  1.22BP 22007  2.9 1R   URX  END OF LINE IN BOTTOM
33************** OF RUBBLE**********************************************
22     Z00090
11            670  0.33BP 33009  1.2 1RRT URX  STRIKE/DIP? UPPER WEATH-
33*****ERED ZONE OF PIT*************************************************
11            671  0.67BP 30009  1.4 1RRT URX  STRIKE/DIP?
11            672  0.91BP 25408  1.6 1RRT URX
11            673  1.15BP 29013  1.4 2RRT URX
11            674  1.25BP 26411  1.8 1RRT URX
11            675  1.32BP 28008  1.6 1RRT URX
11            676  1.63BP 22510  3.4 1RRT USX
11            677  2.00BP 22414  1.7 2RRT PSX  END OF LINE 2.22METRES
22     A12700
11            678  0.00JT 13886  0.6 2C   PRX
11            679  0.06JT 13886  1.2 2C   PRX
11            680  0.36JT 14890  0.9 1U   PSX   WEATHERED FRACTURE
33*********ZONE AROUND BEDDING 0.37-1.09METRES**********************
11            681  0.63JT 14084  0.7 1D   PRX   DOLOMITE VEIN?
11            682  0.68JT 14083  0.9 1D   PSX
11            683  0.95BP 14008  3.0 2R   URX
11            684  1.15JT 32289  1.7 2R   PRX
11            685  2.12JT 14085  0.9 1U   PSX
11            686  2.48JT 13890  1.2 1C   CSX
11            687  2.66JT 31088  0.8 1D   PRX
11            688  3.12JT 14085  1.0 2D   PSX
11            689  3.53JT 30489  1.0 2R   URX
11            690  3.89JT 30385  0.8 2D   PSX
22     B03900
11            691  0.52JT 14087  1.1 1C   PRX   SHORT LINE ON THE SOUTH
33******EAST FACING SLOPE*********************************************
11            692  0.75JT 31590  1.6 1C   PRX
11            693  1.11JT 31786  0.7 1C   PRX
11            694  1.41JT 14085  1.3 1U   USX
11            695  1.78JT 31989  1.7 1R   USX
33********PAGE27********************************************************
11            696  1.83JT 12789  1.6 1R   USX
11            697  2.39JT 22185  0.5 2D   PSX
11            698  2.80JT 32287  3.8 2RTD CSX
11            699  3.40JT 31590  1.3 1U   CSX
11            700  3.80JT 15089  2.4 2R   SSX  END OF LINE 3.8M LONG
33********PAGE 28******************************************************
22     C19800
11            701  0.36JT 11089  1.4 1U   USX
11            702  0.40JT 34135  0.7 1U   USX  PARALLELS VEIN
11            703  0.65JT 32728  1.0 1D   USX  SLICKS(MOVEMENT)VEIN
11            704  0.78JT 31984  0.5 0D   PSX1
```

```
11             705  0.93JT 32185  0.7 1U   PSX
11             706  1.34JT 32187  1.3 OD   PSXO
11             707  3.39JT 32288  1.7 1U   PSX
11             708  3.78BP 11308  6.8 OD   PSXO
11             709  4.95JT 13288  1.9 1U   PSX
11             710  5.74JT 12885  0.9 OC   PRXO
11             711  6.29JT 31488  1.1 OCD  PSX1
11             712  6.46JT 32084  2.1 OU   URXO
11             713  8.74JT 27478  1.2 OU   PRX2
11             714  9.11JT 24070  4.0 OU   URX2   STRIKE/DIP APPROX.
11             715  9.69JT 30584  0.5 OD   PSXO
11             716  9.72JT 05979  6.7 O    PRX1
11             717 10.48JT 22174  0.7 1U   URX
11             718 10.68JT 31982  0.7 1U   SPX
11             719 11.04JT 23979  1.0 1R   SRX
11             720 11.19JT 12589  1.2 OD   PSX1  CUTOFF AT TOP END
33*****BY BEDDING PLANE*********************************************
11             721 11.98JT 11685  2.5 OU   PSX1
11             722 12.22JT 29589  4.0 1D   PSX
11             723 12.78JT 29280  4.0 1C   URX   FRACTURES PARALLEL
33***TO ROCK FACE***************FRACTURE IS LONGER THAN 4METRES***
11             724 13.02JT 12224  0.8 OU   PSXO
11             725 14.15JT 13085  0.5 2D   PSX
11             726 14.35JT 24586  0.5 OU   URX1  STRIKE/DIP APPROX.
33*****IT COULD BE A BLAST FRACTURE*******************************
11             727 14.96JT 31780  0.8 2C   URX
11             728 15.62JT 19264  0.5 OD   PSX1
11             729 15.99JT 32685  1.0 1D   PSX
11             730 16.40JT 32189  1.3 1U   PSX
11             731 16.82JT 16089  0.7 OD   CSX1
11             732 17.00JT 12184  0.7 OD   SSX1
33******PAGE 29**************************************************
11             733 18.00JT 12990  1.0 2D   PSX
11             734 18.60JT 00790  1.1 OU   URXO  APPROX.DIP/STRIKE
11             735 18.73JT 13274  0.5 2D   PRX
11             736 20.43JT 20785  0.7 1R   PRX   WALL ROCK DISLODGED
11             737 21.49BP 11507  3.2 2R   PRL  APPROX.DIP/STRIKE
11             733 23.03JT 14875  1.1 2U   PRX
11             739 23.49JT 14287  0.9 1U   PRX
22      D19700
11             740 00.00JT 17373  2.6 2R   PRX
11             741  0.01JT 23270  1.2 2C   URX   FAULT WITH SLICKEN.
11             742  0.32JT 18065  3.1 2U   PSX
11             743  0.69VN 32805  1.1 1D   PSX
11             744  1.00JT 14487  0.9 1C   PSX
11             745  1.40JT 14885  0.7 OU   PSX1
11             746  1.93JT 09462  0.5 2U   PSX
11             747  2.01JT 15085  0.5 1U   PSX
11             748  2.64JT 03790  1.8 1U   PRX  SMALL FRACTURE ZONE
11             749  2.83JT 13476  0.8 2C   PSX
11             750  3.29JT 12873  1.0 1C   PSX
11             751  4.10JT 12580  1.0 2C   PRX
11             752  6.03JT 19681  1.2 OU   USXO
11             753  6.23JT 12890  1.1 2U   PSX
11             754  6.52JT 14090  1.7 2U   PSX
11             755  6.56JT 21588  0.9 2U   URX
11             756  6.66JT 32187  0.7 2U   USX
11             757  7.35JT 13488  1.2 OD   PSX1
11             758  7.46JT 14086  1.8 1D   PSX
11             759  7.94JT 12680  1.4 1U   USX  APPROX.STRIKE/DIP
11             760  8.29JT 23086  1.1 OR   PRX2
11             761  8.90JT 32286  1.1 1D   PRX
11             762  9.29JT 23589  0.9 1U   PRX
11             763  9.49JT 30585  1.1 1D   PSX
```

```
33******PAGE30*************************************************************
11            764 10.04JT 31285  1.5 1U   PRX
11            765 10.07JT 23009  2.5 1U   USX
11            766 10.94JT 02380  0.5 OU   CRXO
11            767 11.07JT 25189  1.4 1R   PSX
11            768 11.72JT 31887  0.5 2DRT PSX   END OF LINE 11.90M
33****PIT#2   PAGE 31*******************************************************
33**************************************************************************
33**************************************************************************
22     E07800
11            769 00.40JT 00880  0.5 2U   PRX
11            770  0.95JT 23673  0.5 1U   PSX
11            771  1.10JT 12770  0.5 1U   SSX
11            772  1.29JT 33015  1.0 OD   PRXO  VUGGY/DIP&STRIKE APPROX
11            773  1.35JT 32288  0.6 2U   PSX
11            774  2.00JT 33289  0.7 2U   PRX
11            775  2.10JT 28485  0.8 1U   PRX
11            776  2.69JT 32086  0.6 2U   PSX
11            777  2.97JT 31889  0.7 1D   PSX
11            778  3.29JT 19616  1.2 1CD  USX  APPROX. STRIKE/DIP
11            779  3.37JT 07885  0.5 1U   CSX  APPROX.STRIKE/DIP
11            780  3.49JT 14488  0.9 1U   URX
11            781  4.52JT 33610  2.3 OD   PSXO   AUGUST 16/86MAYBE BEDP
11            782  5.25JT 32085  0.9 2D   PSX
11            783  5.50JT 31280  1.0 1U   PSX
11            784  5.69JT 32290  1.4 1D   PSX
11            785  5.82JT 32089  1.6 1D   PSX
11            786  6.65JT 30212  0.7 OU   USXO
11            787  6.71JT 32083  1.8 1U   PSX
11            788  7.59JT 32090  1.2 1D   PSX
11            789  7.79JT 12288  0.8 OD   PSXO
11            790  8.29JT 14087  1.3 OU   URX3
11            791  8.39JT 32490  2.6 2D   PRX    SLICKS ROUGH
11            792  8.93JT 12085  1.7 1D   URX
11            793  9.15JT 13286  0.8 2D   PRX
11            794  9.89JT 14475  2.8 1DRT URX   VERY RUSTY
11            795 10.00JT 13486  0.8 1D   CSX
11            796 10.05JT 13378  0.7 1U   USX
11            797 10.24JT 10680  1.0 1U   PSX
11            798 10.65BP 25505  3.4 1U   USX   VERY GOOD SHALLOW
33*****MEASUREMENT OF BEDDING PLANE*********************************
11            799 10.72JT 08984  1.8 OU   URX1
11            800 10.94JT 23680  0.9 OR   URX1  APPROX.STRIKE/DIP
33******PAGE  32****************************************************
11            801 10.92JT 33485  1.0 1U   PRX
11            802 11.98JT 25174  1.1 1U   CRX  APPROX.MEASUREMENTS
11            803 12.24JT 32690  0.9 OU   PSX1
11            804 12.93JT 14789  0.9 1U   PSX
11            805 13.14JT 26070  1.1 OU   URX1
11            806 13.32JT 25485  0.6 OR   URX1
11            807 13.42JT 25260  0.5 OU   CRX2
11            808 13.43JT 30624  1.3 OU   USX1
11            809 14.08JT 25785  1.5 1R   PRX
11            810 14.65JT 32890  1.1 1U   PSX
11            811 16.75JT 32885  0.6 2U   PSX
11            812 17.07JT 31785  4.6 2DC  PRX
11            813 18.75JT 33085  1.8 1D   PSX
11            814 19.48JT 11106  2.5 1DR  USX  APPROX.DIP/STRIKE
11            815 19.90JT 06788  2.1 1R   PRX  SMALL FRACTURE ZONEBLAST
11            816 20.06JT 24486  1.2 1U   PRX
11            817 20.26JT 33685  3.3 1U   PSX  END OF LINE 20.65M
22     F00090
33*******THIS SCANLINE IS ON JOINT FACE,FACING 140DEGREES SOUTH
11            818 00.00BP 31210  2.9 1U   PSX  CENSORING?
```

```
11          819 OO.14BP 13005  7.4 1U   PSX  CENSORING?
11          820 OO.82BP 12208  6.1 1U   PSX  CENSORING?
11          821 OO.97BP 11607  4.6 1U   PSX  CENSORING?
11          822   1.14BP 112C5  3.3 1U   PSX  CENSORING?
11          823   1.22BP 13708  2.8 1U   PSX  CENSORING?
11          824   1.42BP 08805  1.0 1U   PSX  CENSORING?
11          825   1.90BP 10707  3.9 1U   PSX CENSORING?SAMEAS 798
11          826   2.96BP 10406  3.4 1U   PSX  CENSORING?
33*******PAGE 33 PIT#3*****************************************
33**************************************************************
33****************************************************************
22    GO1404                                    LINE ON 100DEGREES
33**** FACING WALL EAST OF FAULT PHOTOS TAKEN*******************
11          827   0.00JT 30890  1.8 2U   PSX
11          828   0.80JT 34008  1.5 OU   URXO  IT ENDS AT 2M FLAG
11          829   0.94JT 31080  1.3 1R   USX
11          830   1.00JT 25875  0.5 2C   PSX
11          831   1.55JT 30676  1.4 1C   PSX
11          832   1.85JT 31872  0.8 OC   PSXO
11          833   2.25JT 31482  0.8 1U   PSX
11          834   2.69JT 32189  0.7 OC   PSX2
11          835   2.78JT 31484  1.0 1R   PRX
11          836   4.21JT 11985  4.5 1C   PRX  FAULT,REVERSE
11          837   4.49JT 32077  3.8 2R   PRX
11          838   4.63JT 31584  0.8 OC   PSXO
11          839   5.08JT 31488  1.2 1C   USX
11          840   5.89JT 31785  2.4 1DC  PRX
11          841   6.02JT 13388  0.7 1D   PSX
11          842   6.29JT 03574  0.5 1U   PRX
11          843   6.75JT 13489  1.0 1CD  PSX
11          844   6.88JT 30588  0.9 1C   PSX
11          845   7.08JT 22588  0.9 OC   PSX2
11          846   7.20BP 15310  3.5 OR   URX3
11          847   7.73JT 31785  2.2 1CD  PSX
11          848   8.19JT 31987  0.9 1C   PSX
11          849   8.70JT 30984  1.4 2CD  PSX
11          850   9.15JT 31085  0.9 2U   PRX
33*****PAGE 34**************************************************
22    H29300                                    LINE RUNS ALONG TOP
33******OF SPECKLED PSEUDOBRECCIA BED****************************
11          851   0.07JT 12785  1.1 OC   PSX1
11          852   0.55JT 14085  0.7 1C   PSX
11          853   0.65JT 32084  0.9 2U   PRX
11          854   0.75JT 30385  1.0 1C   PRX  SMALL FRACTURE ZONE
11          855   1.13JT 24384  1.0 1U   PRX
11          856   2.06BP 34305  2.6 1U   URX  APPROX.DIP/STRIKE
11          857   2.27JT 13689  2.1 1U   USX
11          858   2.48JT 30085  0.5 OD   CSX2
11          859   2.67VN 34068  0.6 OD   PSXO
11          860   2.89VN 30787  0.9 1D   USX
11          861   3.10JT 21890  1.1 2U   PRX
11          862   3.15JT 05585  0.8 1U   PRX
11          863   3.29JT 31289  0.6 1C   PSX
11          864   3.79JT 30887  0.9 OCD  PSX1
11          865   3.95JT 05780  1.4 1U   URX
11          866   4.71JT 30986  2.0 1D   URX
11          867   5.29JT 31586  0.6 OU   PRX2
11          868   5.67JT 05288  0.6 OR   CRX1
11          869   6.37BP 03704  1.6 1C   PRX     VUGGS
11          870   6.92VN 29075  0.8 OD   USX1
11          871   7.39JT 29683  2.3 1D   PRX
11          872   7.63JT 07080  1.1 OU   URXO
11          873   8.00JT 29982  0.8 1R   PRX
11          874   9.40JT 09384  0.7 1R   PRX
```

```
11          875  9.58JT 06485  0.6 2U   CRX
11          876  9.81JT 04274  0.7 2    CRX   WATER SEEPING FROM
33******FRACTURE*************************************************************
11          877  9.82JT 30486  1.3 1U   PSX
11          878 10.09JT 31282  1.9 1U   PSX
11          879 10.70JT 04087  0.8 1U   PRX
11          880 11.40JT 22790  0.6 2U   PRX  END OF THE SCANLINE
33*********AT 11.70METRES WATER SPRING AT 10.89 11.70 METRES
33******ALONG THIS SCANLINE*******************************************
33*******************************************************************
33*******************************************************************
33*******************************************************************
```

APPENDIX G

Stereoplots from the STRPLO program

Lower hemisphere pole diagrams of fracture orientations using the STRPLO program are given in this appendix for i) Total fracture set ii) Lead Lake outcrop only.

i)

ii)

DANIEL'S HARBOUR

LEAD LAKE OUTCROP

555 POLES TO FRACTURE PLANES

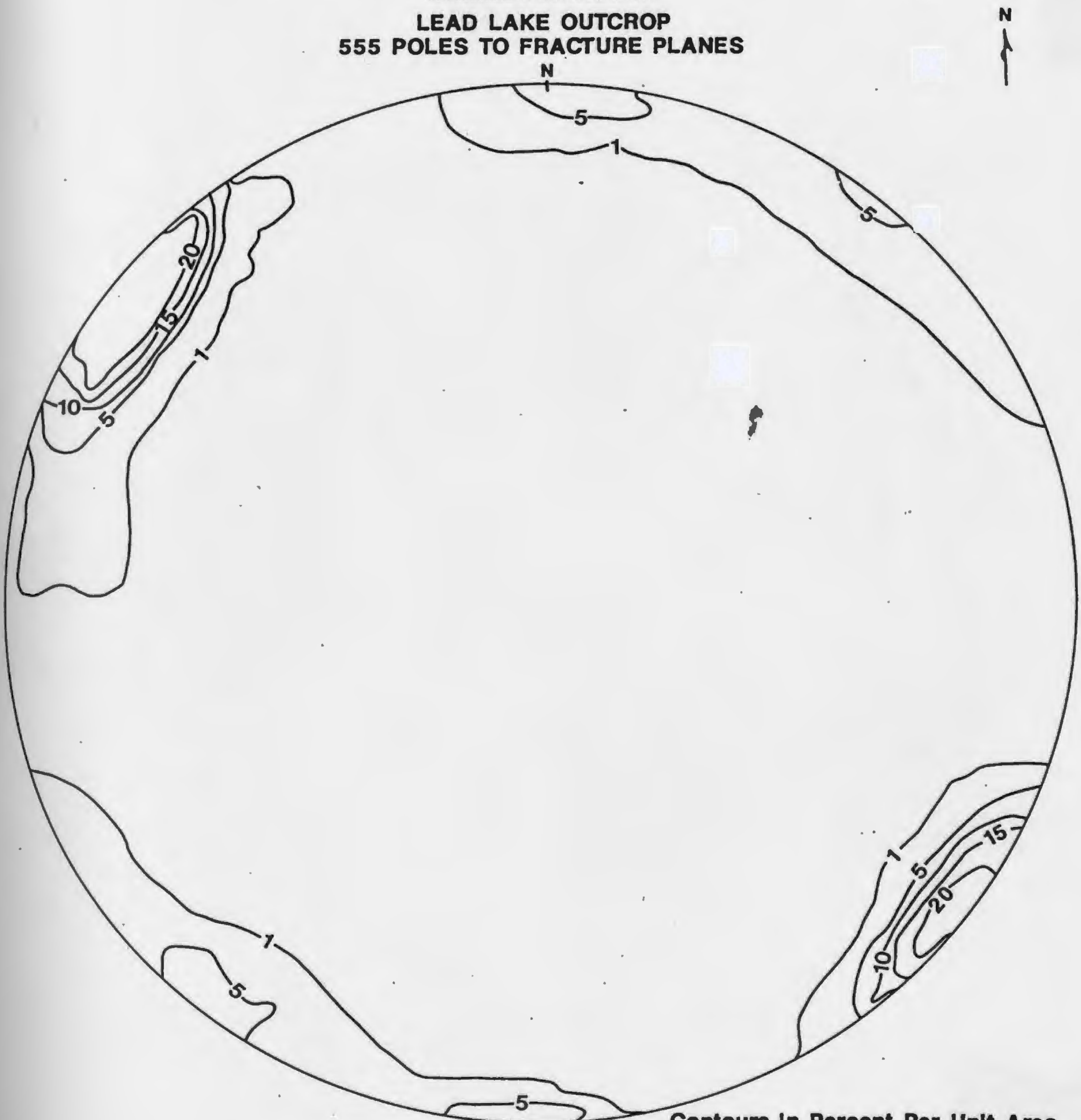

Contours In Percent Per Unit Area
Maximun 40.2%

APPENDIX H

Program listing of DHLOOK.FOR

```
C**********************************************************************
C
C DHLOOK.FOR                           W. MILLAR                 JUNE 1987
C
C THIS PROGRAM LOOKS THROUGH EACH FRACTURE DATA FILE OF DANIEL'S HARBOUR
C (MUST SPECIFY EACH FILE WITHIN THE PROGRAM) FOR FRACTURE ORIENTATION
C AND OUTPUTS A DATA FILE WITH A DIP, DIP DIRECTION FORMAT THAT CAN BE
C USED BY THE PLOTTING PROGRAM 'SPHERE'.
C
C**********************************************************************
C
      CHARACTER DATA*80
      INTEGER DPDR,DP,FLAG
C
      OPEN (10,FILE='DNSHAR.DAT',STATUS='OLD')
      OPEN (11,FILE='DNSHAR.OUT',STATUS='NEW')
C
C
15    READ(10,16,END=999) DATA
16    FORMAT(A)
      READ(DATA,17)FLAG
17    FORMAT(I2)
C
       IF (FLAG.NE.11) GO TO 15
C
            READ(DATA,30)DPDR,DP
30          FORMAT(25X,I3,I2)
            WRITE(11,40)DP,DPDR
40          FORMAT(' ',I2,2X,I3)
      GO TO 15
C
999   STOP
      END
```

APPENDIX I

<u>Results from fracture analysis using the SPHERE program</u>

Example of computer screen data output (i) from the SPHERE program. Tabulated results (ii) for each designated fracture set are also given together with a description of the rotation of pole clusters (iii).

i.

An example of the SPHERE output to the screen during the running of the program, for area 1 set 1. (SPH11)

Data analysis will be done on poles to planes 355

Eigen-analysis for 355 data points

Eigenvalues	0.9822	0.0115	0.0063

Eigenvectors as direction cosines

L:	0.5842	0.8023	0.1215
M:	0.8114	-0.5736	-0.1116
N:	-0.0198	0.1651	-0.9863

and as coordinates of end-points

plunge:	1.14	9.51	80.50
plunge azimuth:	305.75	215.56	42.56

Estimate of optimal smoothing constant from
Watson Bipolar model: 806.87
Cross-Validation method: 1030.97*

Plot 1
4 contours
0 equally spaced contours by function value
30 % probability contours

Minimum function value 0.0000
Maximum function value 1.2198

Contour heights 0.1525
0.4574
0.7624
1.0673

Plot 2

6 contours
0 equally spaced contours by function value

Minimum function value 0.0000
Maximum function value 1.2198

Contour heights 0.1016
0.3049
0.5082
0.7115
0.9148
1.1181

ii. RESULTS FROM THE ROTATION OF SETS FOR EACH AREA AT DANIEL'S HARBOUR THAT ARE DEFINED FROM SPHERE GENERATED CONTOUR PLOTS.

AREA	SET	# POLES	OPTIMAL SMOOTHING CONSTANT	EIGENVALUES			RESULTANT VECTOR* DIRECTION COSINES			PLUNGE	PLUNGE AZIMUTH
				S1	S2	S3	L:	M:	N:		
1	1	355	1030.97	0.9822	0.0115	0.0063	0.5842	0.8114	-0.0198	1.14	305.75
	2	100	162.93	0.9405	0.0519	0.0076	0.7880	-0.6146	0.0357	2.05	217.95
	3	52	819.46	0.9907	0.0065	0.0028	0.9989	-0.0464	-0.0054	0.31	2.66
2	1	58	274.12	0.9694	0.0233	0.0072	0.6816	0.7315	-0.0182	1.04	312.97
	2	12	388.91	0.9869	0.0092	0.0039	0.0947	0.1954	0.9761	77.46	115.86
	3	7	184.67	0.9753	0.0156	0.0091	0.6484	-0.7613	-0.0022	0.12	49.58
3	1	176	315.34	0.9630	0.0265	0.0105	0.0784	0.7058	0.0106	0.61	135.11
	2	37	451.79	0.9772	0.0197	0.0031	0.0172	0.0091	-0.9998	88.89	332.22
	3	32	98.55	0.9315	0.0523	0.0162	0.5386	-0.8414	-0.0444	2.54	57.38
TOTAL	1	581	614.85	0.9722	0.0203	0.0075	0.6281	0.7781	-0.0097	0.56	308.91
	2	132	190.12	0.9342	0.0577	0.0081	0.7593	-0.6501	0.0290	1.66	220.57
	3	54	805.05	0.9904	0.0064	0.0032	0.9984	-0.0559	-0.0010	0.06	3.2
	4	44	608.27	0.9713	0.0253	0.0034	0.0046	0.0140	0.9999	89.15	108.28

* THESE VALUES OF DIRECTION COSINES WERE USED IN THE SPACE.FOR PROGRAM TO CALCULATE SPACING VALUES BETWEEN FRACTURES OF THE SAME SET.

iii. EVALUATION OF ROTATION OF SETS RESULTS USING SPHERE PROGRAM

AREA	SET	# POLES	OPTIMAL SMOOTHING CONSTANT	CLUSTER OUTLINE			CLUSTER PEAKS			CLUSTER DENSITY			COMMENTS
				C	E	I	U	B	O	C	I	D	
1	1	355	1030.97	X			X			X			Well defined set
	2	100	162.93		X				X		X		Moderately defined set
	3	52	819.46		X		X				X		Moderately defined set, high smoothing constant
2	1	58	274.12		X		X				X		Moderately defined set
	2	12	388.91			X			X		X		Set not well defined, not enough points
	3	7	184.67			X			X			X	Set not well defined, not enough points
3	1	176	315.34			X	X				X		Moderately to well-defined set
	2	37	451.79		X			X		X			Moderately defined set symetrical may be 2 sets dipping in opposite dir.
	3	32	98.55			X		X				X	Poorly defined set
TOTAL	1	581	614.85		X		X			X			Well defined set
	2	132	190.12		X		X				X		Moderately defined set
	3	54	805.05		X		X			X			Moderately to poorly defined set
	4	44	608.27			X		X		X			Moderately defined set or two sets.

C - CIRCLE U - UNIMODAL C - COMPACT
E - ELLIPSE B - BIMODAL I - INTERMEDIATE
I - IRREGULAR O - OTHER D - DIFFUSE

FORMAT ADAPTED FROM DAVE BRIGGINS REPORT.

APPENDIX J

<u>Details on fracture analysis and manipulation.</u>

Sphere contour plots were generated for each fracture set and these sets or fracture clusters were rotated to the center of the sphere so an evaluation of the cluster distribution for each set could be made. One can obtain a true shape of the fracture cluster and its mean vector using the rotation option of SPHERE; see Appendix I for results of these plots. An even distribution would exhibit a cluster at the center in the shape of a circle.

The next stage in the fracture orientation analysis was the plotting of set distributions as frequency histograms using the program ORIENT.HIS; a program using the SPSSX batch system which is a comprehensive tool for managing and analyzing data. Two histograms were produced for each specified set; one for dip direction and the second for dip. Each histogram is accompanied by basic statistics which include variance, mean, sum, minimum and maximum value and standard deviation.

Standard statistics for trace length histograms are the same as produced by ORIENT.HIS. These statistics give results for only each length of fracture in a set, and disregard censoring and termination mode.

Further manipulation of trace length data was done using the SAS system programs available for histogram plots and statistics. The TRACE.SAS program decodes fracture data according to fracture type, length, censor, termination mode and set number. Histograms were produced first with distinction being made for censoring and then for termination mode. Univariant statistics on the entire file or set are printed with no regard to termination or censoring. Statistics given were mean, standard deviation, variance, minimum and maximum values, sum, skewness and kurtosis.

The SPACE.FOR program produced a list of fractures, their set number, scanline label, actual length, angle phi and the calculated spacing between consecutive fractures of the same set. In calculating the fracture spacing, first the direction cosines listed in Appendix I(ii) of the average plane for each fracture set (determined from sphere output, Appendix I(i)) was entered into the SPACE.FOR program. Secondly, the direction cosines (p,q,r) of the scanline were computed using the following formulae by Koch and Link (1971):

$p = \cos u \times \cos v$

$q = \sin u \times \cos v$

$r = \sin v$

where u is the bearing of the scanline in radians and v is the plunge of the scanline. The angle phi between the scanline and the average pole of the fracture set computed by the following formula:

$\cos \text{phi} = Ph \times Pf + Qh \times Qf + Rh \times Rf$

where the h refers to the scanline and f refers to the pole to the average fracture plane. Lastly, the true spacing between two consecutive fractures of the same set is calculated using the simple formula:

SPAC = l x cos phi

where l is the distance along the scanline between consecutive fractures of the same set (see Figure below for illustration).

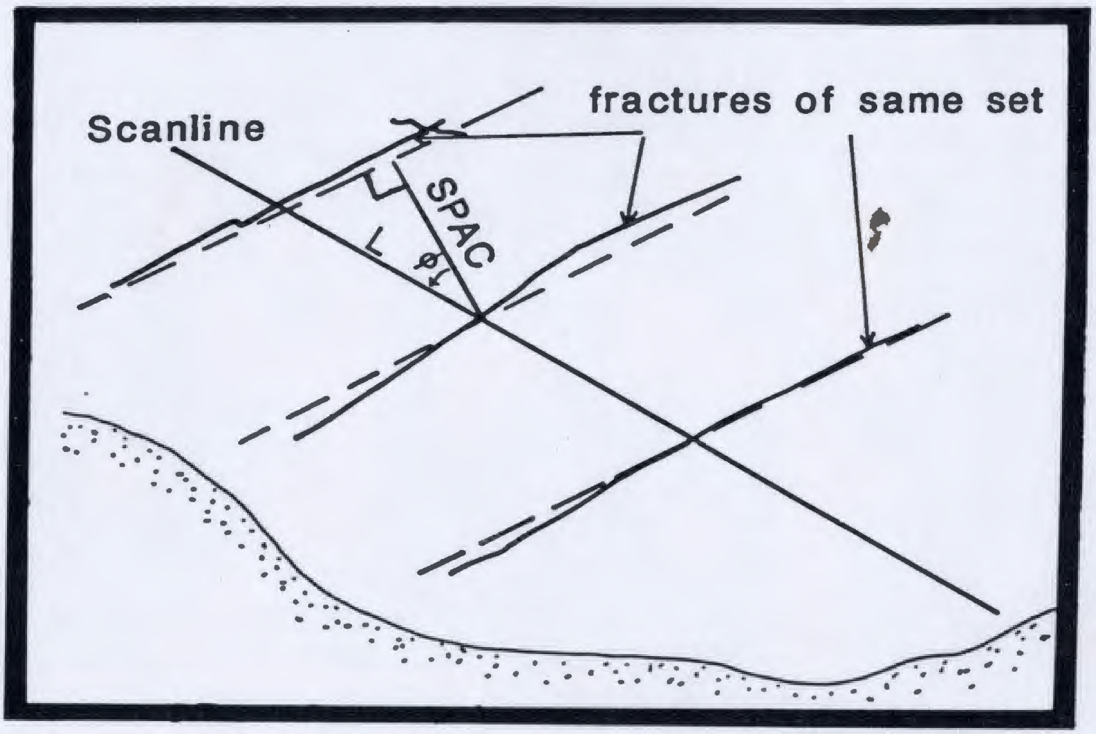

APPENDIX K

Statistics for fracture histograms

Trace Length statistics from Trace.his program, without consideration for censoring.

Data file	#	(m) Mean	(m) Std. dev.	(m) Min.	(m) Max.	(m) Sum	Comments
DNSHAR.DAT	555	2.72	2.54	0.50	16.30	1507.00	unimodal
Set 1	355	3.13	2.91	0.50	16.30	1112.10	unimodal
Set 2	100	2.19	1.60	0.50	9.80	219.20	unimodal
Set 3	52	1.92	1.22	0.60	5.70	99.90	unimodal
DNSHAR2.DAT	92	1.66	1.46	0.50	8.00	153.00	unimodal
Set 1	58	1.52	1.15	0.50	8.00	87.90	unimodal
Set 2	12	3.67	2.04	1.00	7.90	44.00	no peak
Set 3	7	0.80	0.27	0.50	1.20	5.60	unimodal
DNSHAR3.DAT	276	1.44	1.11	0.50	7.40	398.60	unimodal
Set 1	176	1.25	0.77	0.50	4.60	220.00	unimodal
Set 2	37	2.69	1.66	0.70	7.40	99.60	no peak
Set 3	32	1.23	1.10	0.50	6.70	36.00	unimodal
DNSHARTTL.DAT	923	2.23	2.19	0.50	16.30	2058.60	unimodal
Set 1	581	2.43	2.51	0.50	16.30	1409.60	unimodal
Set 2	132	1.90	1.56	0.50	9.80	250.60	unimodal
Set 3	54	1.92	1.23	0.50	5.70	103.90	unimodal
Set 4	44	2.81	1.72	0.70	7.40	123.80	no peak

Trace Length statistics for each data file (area) and their fracture sets, by degree of censoring (cens = 0, 1, 2).

Data file	Set 1			Set 2			Set 3		
DNSHAR.DAT									
Censoring	0	1	2	0	1	2	0	1	2
No.	129	163	63	29	39	32	37	14	3
Mean (m)	3.44	2.90	3.09	1.73	2.35	2.43	2.13	1.64	1.30
S. D. (m)	3.27	2.79	2.38	1.17	1.66	1.80	1.39	0.64	0.56
Min. (m)	0.50	0.50	0.50	0.50	0.60	0.60	0.60	0.60	0.80
Max. (m)	16.30	15.30	10.00	5.50	9.80	7.40	5.70	2.90	1.90
Sum (m)	444.2	473.1	194.8	50.1	91.5	77.6	78.7	23.0	3.9
DNSHAR2.DAT									
Censoring	0	1	2	0	1	2	0	1	2
No.	10	34	14	1	6	5	2	3	2
Mean (m)	1.54	1.33	1.96	1.00	2.67	5.40	0.65	0.83	0.90

S. D. (m)	0.60	0.68	2.02	/	1.37	1.42	0.07	0.31	0.42
Min. (m)	0.80	0.50	0.60	1.00	1.20	4.50	0.60	0.50	0.60
Max. (m)	2.40	3.60	8.00	1.00	4.60	7.90	0.70	1.10	1.20
Sum (m)	15.40	45.10	27.40	1.00	16.00	27.00	1.30	2.50	1.80

DNSHAR3.DAT

Censoring	0	1	2	0	1	2	0	1	2
No.	29	99	48	9	23	5	8	18	6
Mean (m)	0.95	1.29	1.35	2.41	2.66	3.36	1.55	1.08	0.70
S. D. (m)	0.45	0.76	0.90	1.91	1.65	1.40	2.09	0.46	0.25
Min. (m)	0.50	0.50	0.50	0.70	1.00	1.40	0.50	0.50	0.50
Max. (m)	2.50	4.50	4.60	6.80	7.40	5.20	6.70	2.10	1.10
Sum (m)	27.6	127.6	64.8	21.7	61.1	16.8	12.4	19.4	4.20

Spacing statistics for the individual areas and their sets.

DNSHAR.DAT

	Set 1	Set 2	Set 3
No.	338	82	42
Mean (m)	0.52	1.85	2.05
S. D. (m)	0.89	1.97	2.29
Min. (m)	0.01	0.00	0.14
Max. (m)	11.45	9.78	13.02
Sum (m)	174.34	152.08	86.16

DNSHAR2.DAT

No.	54	9	5
Mean (m)	0.25	1.54	0.42
S. D. (m)	0.42	1.23	0.56
Min. (m)	0.04	0.01	0.13
Max. (m)	8.53	1.19	3.18
Sum (m)	45.45	2.23	7.69

DNSHAR3.DAT

No.	167	26	24
Mean (m)	0.42	0.27	1.25
S. D. (m)	0.56	0.25	1.26
Min. (m)	0.00	0.03	0.05
Max. (m)	3.83	1.06	5.38
Sum (m)	70.73	7.10	29.97

APPENDIX L

<u>Hydraulic Head data for 1985 and 1986 surveys</u>

Water table elevation data is followed by (/) the depth below ground surface of the water table. Mine surveyed elevations are based on the datum of 104.6 m a.s.l. Symbols are: * = artesian wells, + = water above ground, ** = difference in drawdown between years; '-' decrease in 1986 relative to 1985.

DIAMOND DRILL #	1985 (m)	1986 (m)	(m)**
DDH-1		95.50/ 7.11m	
DDH-2		90.20/12.26	
DDH-3		106.40/10.71	
DDH-4		92.70/ 6.98	
GH-1		68.06/ 2.05	
367	<89.03/>15		
509	5.01/ 5.01		
584	<78.82/>28		
669	75.43/ 28.89		
715	65.01/ 45.87		
716	62.07/ 48.37		
824	90.94/ 8.34		
826		75.60/22.57	
1043	74.00/ 26.39		
1118		70.73/27.12	
1119		70.35/27.08	
1120		68.34/29.32	
1244		72.60/ 6.64	
1246	73.13/ 7.14	72.38/ 7.90	0.76
1248	76.79/ 4.11	76.93/ 3.96	-0.15
1249	73.75/ 2.06	73.54/ 2.28	0.22
1250		70.13/ 5.70	
1251	71.13/ 4.52	72.98/ 2.67	-1.85
1253		75.61/ 9.04	
1254		71.90/13.06	
1255		70.18/15.80	
1259		74.13/22.63	
1260	78.58/19.13	75.48/22.23	3.10
1261	79.90/17.80	76.27/21.44	3.64
1285	<88.43/>50		
1306		77.75/>18.29	
1307		80.31/>16.46	
1308		88.85/>11.58	
1315	<57.12/>50		
1316	58.42/48.58		
1322		116.62/ 7.13	
1323	89.97/11.04	83.33/17.68	6.64
1326		104.85/16.68	
1327	86.81/29.01	82.84/32.97	3.96
1328	84.19/34.61	79.67/39.13	4.52
1329	89.06/23.98		
1330		<64.10/>60	
1332		<76.17/ 8.12	
1388	94.03/21.31	78.53/36.81	15.50

1415		76.24/34.08	
1418	92.37/22.47		
1435		<78.76/>53	
1630	72.77/ 5.05		
1631	73.13/ 5.59		
1642		56.57*/0	
1646		70.77/ 3.69	
1647		67.12/ 3.81	
1698		111.08/14.61	
1699		110.66/13.46	
1700		110.45/14.88	
1751		74.25/27.49	
1752		76.59/25.12	
1756		76.59/24.53	
1758		76.39/25.49	
1759		76.40/25.62	
1761		76.02/26.46	
1762		76.42/25.64	
1767		75.93/25.02	
1770		80.07/21.60	
1863		68.93/ 0.02	
1864		69.36*/+0.20	
1867	69.62*/+0.20		
1868		69.47/ 2.90	
1869		70.14/ 2.67	
1870		67.41/ 0.0	
1871		>66.81*/0.0	
2201	71.40/4.17		
2202	73.61/0.0	73.61*/+0.31	
2204	76.16/0.0	76.22*/+0.06	
2235	59.77/0.0	>59.77*/ 0.0	
2236	61.01/0.33	>60.68*/ 0.0	
2237	70.40/2.94	70.35 / 2.98	0.04
2238	74.46/0.43	74.55 / 0.34	-0.09
2239	59.58/0.00	>59.58*/ 0.0	
2240		>59.72*/ 0.0	
2241	60.33/+0.50	>59.83*/ 0.0	
2273		108.35 /15.85	
2287		72.80 / 2.95	
2288		72.54 / 2.97	
2293		76.24 /12.98	
2294		79.37 /24.08	
2295		79.97 /29.05	
2296		81.65 /31.52	
2376		74.25 / 3.85	
2381		73.81 / 6.46	
2382		73.96 / 7.06	
2383		74.90 / 3.91	
2384		74.95 / 2.87	
2385		74.38 / 9.01	
2390		74.41 / 4.42	
Spring lake		99.55	

APPENDIX M

Strength analysis of core

A series of 5 rock-strength tests were done on samples of the vuggy pseudobreccia from underground and pit areas. Cores for the tests were drilled perpendicular and parallel to bedding directions. The tests included the direction tension test, uniaxial compressive test, and triaxial compressive test following the procedures outlined in the ASTM (1978 and 1980) standards publication; the Brazil (indirect tensile strength) test following the procedures in the ISRM (1981) guidelines; and the point load test following the CANMET (1977) standard procedure. The tests were repeated on at least five samples to obtain more representative results. Only one triaxial test was made due to the difficult procedure.

Results

Strength test results from Newfoundland Zinc Mine diamond drill core.

TEST TYPE	SPECIMEN #1	SPECIMEN #2
unaxial compressive strength	-100 MPa	-151 MPa
tensile strength (direct tension)	2.2 MPa	1.5 MPa
point load strenth index	5.9 MPa	6.4 MPa
Brazilian test (indirect tension)		8.5 MPa

Tensile strength was less if the test was done perpendicular to bedding. The compressive strength was less parallel to bedding as was expected in light of the inhomogeneities of this drill core (stylolites, veining, vugs = 10 % porosity, bedding plane surfaces). Stylolites decrease rock strenth and may localize dissolution by groundwater.

APPENDIX N

Primary permeability of dolomite and limestone belonging to shelf-type facies is assumed to be low (Boni, 1975) and in the order of 10^{-9} to 10^{-6} m/s (Davis, 1969). Permeability of the mine host rocks is more a function of secondary voids rather than the original porosity of the rock matrix and this is supported by evidence from other carbonate areas on the Northern Peninsula (Golder Associates, 1983). Carbonate rocks characteristically have an uneven permeability distribution, and dolomitization as well as ancient and present-day karstification of these platformal rocks accentuates this feature and increases permeability.

Relationship between groundwater flow and conduits

Major groundwater-bearing conduits in the mine workings are bedding planes, faults, and fractures. Other major sources of seepage include backs (ceilings of drifts), joint-bedding plane intersections and drill holes (Acres, 1975b).

Bedding planes are prevalent throughout the mine and about two-thirds of the backs are bedding plane surfaces (R. Crossley, pers. comm.). In the mine many bedding planes are intersected but only some of these conduct significant inflows and these surfaces may have been planes of slippage during regional compression (see Section 3.5.3.1). Bedding planes (Set #4) are consistently longer than any other fracture type (see Section 3.5.3.2), emphasizing the role of bedding planes in conducting groundwater to the mine despite their relatively low numbers. Wet lines appear on the backs where joints intersect the bedding planes and conduct water into the open drifts. In 1976 from May 14-15, over half of the total mine inflow was contributed by bedding planes (378 l/s from bedding planes "66" and "80") (Acres, 1979). Other inflows measured during this Acres survey are:

95 l/s from faults
71 l/s from rock bolts
38 l/s from diamond drill holes
58 l/s from raises

Large inflows occurred (Acres, 1977) in the mine where faults (subparallel to orebody) and three major bedding planes (9, 18 and 24 m below the worms marker horizon) (see Figure 3.2) intersected the L-Zone drifts. Faults with major inflows have an average orientation of 225/80 (Acres, 1975b). The importance of these faults was established in 1975 by dye tracer tests (Acres, 1975a). Dye injected elsewhere in the mine discharged soon afterwards at drift-fault intersections. Flow velocities of 2.3 x 10^{-2} m/s to 3.1 x 10^{-2} m/s were calculated, only an order of magnitude lower than maximum mean tracer velocities of 1.7×10^{-1} m/s for open-channel flow measured at Castleguard Meadows, Alberta (Smart & Ford, 1986).

In 1986, inflows from bedding planes were measured by timing the filling of a 500-ml container at various locations along 3 major bedding plane seeps (main decline near DH-27, see Figure 2.2). Seepage varied along the bedding planes and ranged from nil to 0.02 l/s every 3 m. A total inflow of 1.25 l/s over a length of 81 m was estimated. Golder Associates (1983), duringtheir pump testing at Port au Choix, also found distinct water-bearing zones that coincided with a geological contact between limestone (Catoche Formation) and the overlying dolostone (Aguathuna Formation).

The shallow east drift (NE of portal decline; Figure 3.3) was very wet in June 1975 and seepage from a zone of intense vertical jointing was observed (Acres, 1975a). In July 1986, the east drift was dry with the exception of minor seepage from a small joint zone near DH-31 (see Figure 2.2). In another part of the L-Zone where a major grouted fault (216/72) intersects bedding planes (vicinity of DH-32, see Figure 2.2) inflow of 9.8 l/s over a length of 14 m was measured in 1986. The number of water-conducting features decreases with depth in the L-Zone decline, which implies rock permeability decreases as well.

Permeability versus lithology

According to Nolan et al. (1979), no real aquifers exist in the surficial deposits of the Northern Peninsula, due to their thinness, discontinuous nature and low permeabililty (K of glacial drift = 10^{-2} to 10^{-10} m/sec, with yields of 0.03 to 0.17 l/s). Although the overburden and lake sediments around the mine site were not explicitly tested, a general consensus is that they have low permeability (Acres, 1975a; 1976) ranging from 10^{-12} to 10^{-6} m/s for glacial till (Davis, 1969).

RQD plots (see Appendix A) for the 1986 drill holes show that areas of dense fracturing do not appear to be related to specific (sparite) porous layers in the pseudobreccia unit. The lowest RQD values (dense fracture, low mean core length) consistently occur in the first 2-3 m of core and they are not restricted to the more vuggy sparite sublayers. This implies that permeability is not a function of lithology. Low vug interconnectivity may lessen the permeability of the sparite sub-layers. On a small scale, the pseudobreccia unit appears heterogeneous with respect to lithology and porosity; but the repetition of sub-layers makes this unit essentially homogeneous on a regional scale. Areas of increased permeability in carbonate rocks, caused by highly fractured water-conducting zones, can be found better by caliper logs in drilled holes

(Lattman and Parizek, 1964; Parizek and Siddiqui, 1970).

The following conclusions were derived from pressure-test data (Acres, 1974a). These tests were done on 8 diamond drill holes located 60 m from the northern shore of Trout Lake in the vicinity of the present L-Zone workings (see Figure 2.2). All wells were collared in either the siliceous dolomite (Aguathuna formation; see Section 3.2.3) or the Table Head formation. The pressure tests involved pumping pressurized water into a 3-metre perforated section sealed by double packers. Acres (1974a) suggested that in some holes, mud-filled voids may have been washed clean by this testing method. This method is also subject to errors if shallow and deep cavities interconnect a short distance from the well bore, allowing vertical leakage between successive zones of the aquifer, and producing exaggerated permeabilities (Parizek & Siddiqui, 1970).

A numerical listing of the permeability values was not given in the report (Acres, 1974a). Due to the poor quality of data presentation, a qualitative assessment of the permeability values versus depth was possible for only 3 of the holes tested. Two of the diamond drill holes, collared in the siliceous dolomite, were not tested every 3 m, due to caving of hole walls.

From these data it was concluded that the permeability of the siliceous dolomite tends to be greater than that of the underlying dark grey dolomite (Catoche Formation). The pseudobreccia unit gave some of the lowest permeability values in the tested section, but it is also lower down in the carbonate sequence and farther from the surficial weathering zone. The upper and lower contacts of the pseudobreccia commonly had high hydraulic conductivities of 1×10^{-3} m/s. The permeability variation can be larger within the same lithological unit than between different lithological units. These fluctuations may be caused by well bore intersections with major bedding planes or fracture seeps within each rock type. There is also as much a variation in permeability between holes laterally in the same formation, as between different lithologies in the same hole vertically. The lateral difference in permeability between piezometer holes is not great despite the known facies changes in lithologies throughout the area (T. Lane, pers. comm.; 1987). In individual units there is a minor trend to higher permeabilities laterally towards the east. This could be caused by an increase in the fracture size/or extent of dissolution as one gets closer to the crest of the anticline (see Figure 3.3).

The above information further substantiates Acres' conclusion that individual flow conduits such as bedding planes and fractures are very significant to the permeability distribution in the carbonate rock mass at the mine. The analysis of Acres data and the 1986 drill logs shows that permeability is not necessarily a function of lithology in this aquifer; at least not in the upper few hundred metres of the carbonate platform.

Permeability vs depth

Based on the compilation of data on yield and depth for 250 wells, Nolan et al. (1979) found that the most productive hydrogeologic unit on the Northern Peninsula is the St. George Group, with maximum recorded yields of 3 l/s. The shallower (less than 40 m) drilled wells maintained the highest yields and deep wells had low yields. They believe that the water-producing zones were of 2 types: fissures and solution cavities.

Large well yields may be obtained from fractured aquifers, especially at fracture intersections (Rauch and White, 1970) and at shallow depths (Thrailkill, 1986). The more weathered, highly fractured Table Head Limestone in the St. Anthony airport region was found to be more permeable than the underlying, less fractured St. George formation (Carter et al., 1986), which further emphasizes permeability as a function of depth and not lithology on the Northern Peninsula carbonate platform.

Permeability logs from the pressure tests (Acres, 1974a) show that the maximum permeability values occur in the upper 10 metres of the section, and most often in the upper 3 m regardless if the hole is started (collared) in Table Head limestone or siliceous dolomite. High permeability values occur sporadically down hole at bedding plane/geologic contacts and zones of fracture intersections (Acres, 1974a).

Acres further subdivided their quantitative permeability data into upper and lower zones. The first 45 to 60 m tested (upper zone) resulted in hydraulic conductivities of 1×10^{-5} to 1×10^{-6} m/s and lower horizons (underlying the ore zone) had hydraulic conductivities ranging from 1×10^{-6} to 1×10^{-7} m/s. Greater hydraulic conductivity of 8.0×10^{-4} m/s was calculated at ground surface from inflow measurements into the highly fractured K-Zone open pit (Acres, 1975a). In the upper 3 m of the open pits, fractures and bedding planes are more weathered and extensive. This is evidence for a layered permeability in the dolostone aquifer due to weathering rather than a permeability controlled by lithology.

Diamond drill core analyses by Acres (1974a) allowed a qualitative assessment of relative permeabilities in the rock sequence at the mine site. The upper 15 m of core exhibited the highest permeability due to solution-enlarged jointing and sinkholes. This conclusion is based on the following drillers' observations: loss of water, rod drops in the first 20 m, closely spaced fractures in upper sections of boreholes, low core recoveries and audible water flow into the hole. These observations correspond with the 1986 drilling results from 4 shallow holes (Appendix A) which had a total hole RQD range of 43.9 to 79 % and a low average of 62 %; indicating poor to fair rock mass conditions. Stylolites (perpendicular to core axis) were very common in the core, and some core sections could be broken by hand along these irregular suture-like subhorizontal discontinuities (see Appendix A). Stylolites decrease rock strength, as evidenced by rock strength tests (see Appendix M), and may localize dissolution by groundwater.

The Acres (1974a) drill core analysis indicated that rock horizons below 15 m and extending 45 to 60 m below the ground surface comprise a moderately permeable zone consisting of essentially homogeneous dolomite whose permeability gradually decreases near its bottom. This zone segregation is based on visual logging of core, fracture spacing, frequency of cavities and a RQD of 60%. In this phase of their study, Acres divided the permeability by lithological units with some regard to the weathering profile, but pressure testing later supported the hypothesis that permeability was not dependent on lithology. Thus, permeability decreases with depth as frequency and weathering of flow conduits decreases with depth.

Transmissivity and storativity

Two pump tests were undertaken in the same pumping well at different depths by Acres (1974a). Final drawdown cones and specifics for each pump test are given in Figure 4.6. The first water level measurement was taken 25 minutes after the pump test began and hence no early time data were recorded. Acres (1974a) employed analytical techniques based on the assumption of steady-state flow conditions. Transmissivities and hydraulic conductivities determined from each pump test range from 7.0×10^{-4} to 1.0×10^{-3} m^2/s, and from 5.7×10^{-6} m/s to 8.1×10^{-6} m/s respectively, for an aquifer thickness of 122 m.

Due to the number of observation wells, the Jacob distance-drawdown method (Heath, 1983) was the most applicable method for reanalyzing the pump test results since early time data necessary for Theis type curve analysis were unavailable. There is a large scatter in the plotted points on distance-drawdown plots, suggesting that this aquifer is anisotropic. Newly calculated transmissivity and storativity values are listed below:

Pump test #1 average T = 1.24 x 10 -3 m^2/s
Pump test #2 average T = 1.01 x 10 -3 m^2/s

Pump test # 1 S = 0.007
Pump test # 2 S = 0.002.

The new transmissivity values closely approximate and validate the values calculated earlier by Acres Consulting.

The axis of maximum transmissivity for the aquifer tested by pump test #1 (Acres, 1974a) was determined by Papadopolous' method (1967). This method determines directions of aquifer anisotropy using pump test data from a minimum of 3 observation wells. The N63E oriented axis (see Figure 4.6) corresponds to an average orientation between the two documented major joint sets in the mine area and the dominant regional NE trend (see Section 3.4.1). The previously mentioned major fault conduits have similar orientations as Joint set #1 and obviously contribute to the aquifer's anisotropy as well.

Other pump tests were done on the Northern Peninsula in the same rocks, by Golder Associates (1983). One can explain the disparity between Acres' transmissivities of 0.0007 to 0.001 m^2/s and Golder's values of 1.45 to 1.8 m^2/s by differing methods of analysis and by different water table levels in each case. At the beginning of the pump test the water table at Daniel's Harbour was 15 m below bedrock surface and much lower than at Port au Choix. Much of the water-producing section at Daniel's Harbour was lost, producing the lower transmissivity values. Groundwater was drawn from more of the bedrock's weathered portion at Port au Choix, as indicated by the perturbation in the drawdown curve after 200 minutes of pumping (Golder, 1983). Parizek and Siddiqui (1970) found in carbonate aquifers of Pennsylvania that a pumping well's yield is determined more by the position of the water table with respect to zones of increased permeability or openings than by the proportion of saturated rock that is transected by the well itself.

Aquifer Classification

Many authors have attempted to classify carbonate aquifers. (Beck, 1986; Legrand and Stringfield, 1971). The carbonate rocks of this region have characteristics that belong to all conceptual carbonate models introduced by Thrailkill (1986). Features such as: large well yields at shallow depths and dominant void space as fractures, the presence of sinkholes and the intimate association of aquifer flow with surface hydrology, the dominance of diffuse flow in an interconnected network of joints and bedding planes that are slightly enlarged by dissolution, are characteristics of The Weathered Fracture, Shallow Conduit-Flow Carbonate, and Deep Continuum-Flow Carbonate Aquifer Models, respectively (Thrailkill, 1986). The physical conceptual model for this study area, combining all these characteristics, may be called the Weathered Fracture-Shallow Conduit Carbonate Aquifer Model.

APPENDIX O

Calcium ICP/MS analysis

Water samples taken in 1986 were analyzed for trace elements on the ICP/MS as well as for calcium. Listed in this table are the Ca analysis in parts per million (ppm). These analyses were used in Figure 5.17 of the text.

DH25	119
DH26	60
DH27	56
DH28	45
DH29	79
DH30	65
DH31	52
DH32	67
DH33	57
DH34	46
DH35	34
DH71	58
DH76	56
DH77	71
DH78	57
DH79	60
DH80	55
DH81	53
DH82	63
DH83	58
DH84	71
DH85	91
DH86	39
DH87	59
DH88	30
DH101	61
DH102	37
DH103	57

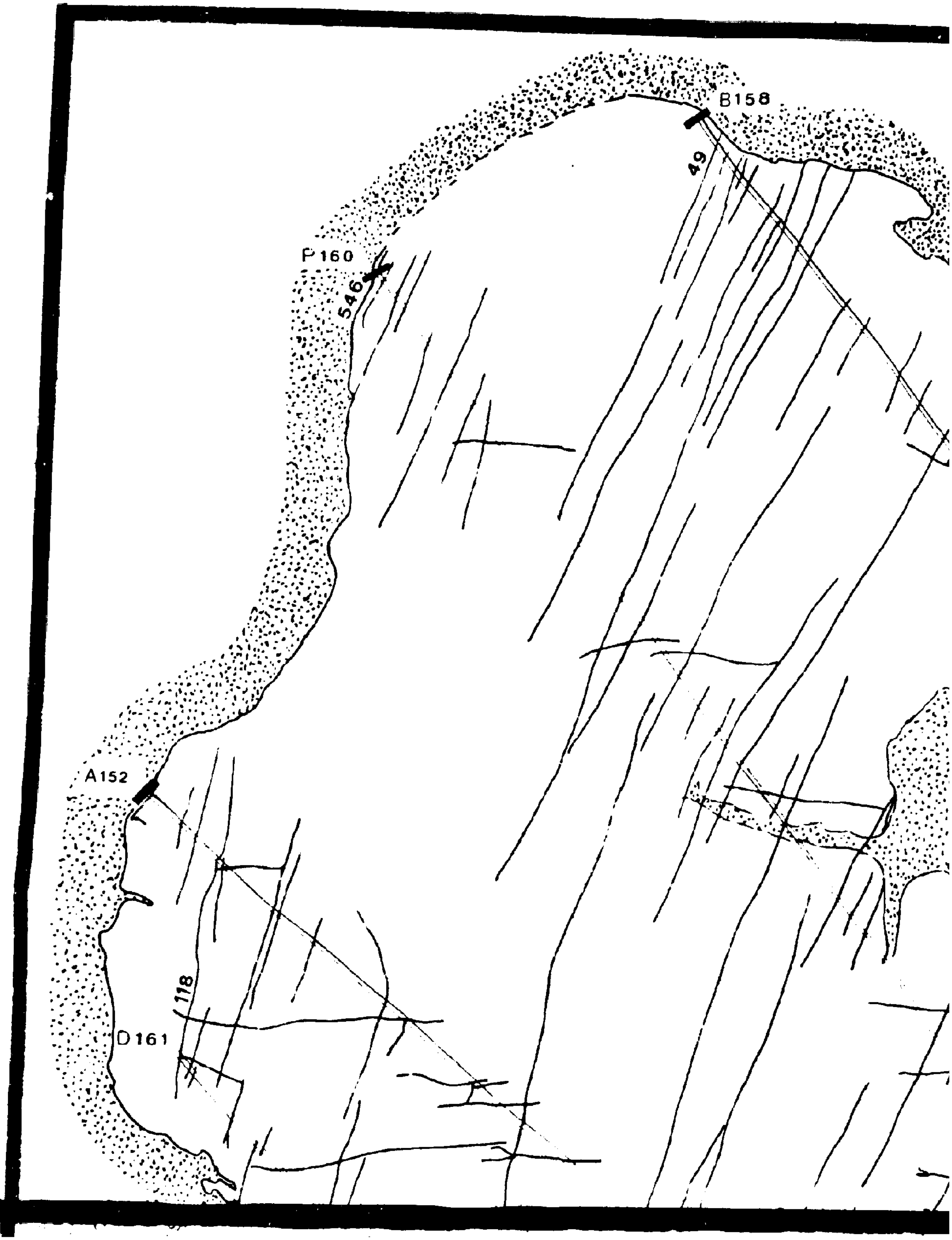

B158
49
P160
546
A152
118
D161

FRACTURE MAP OF THE LEAD

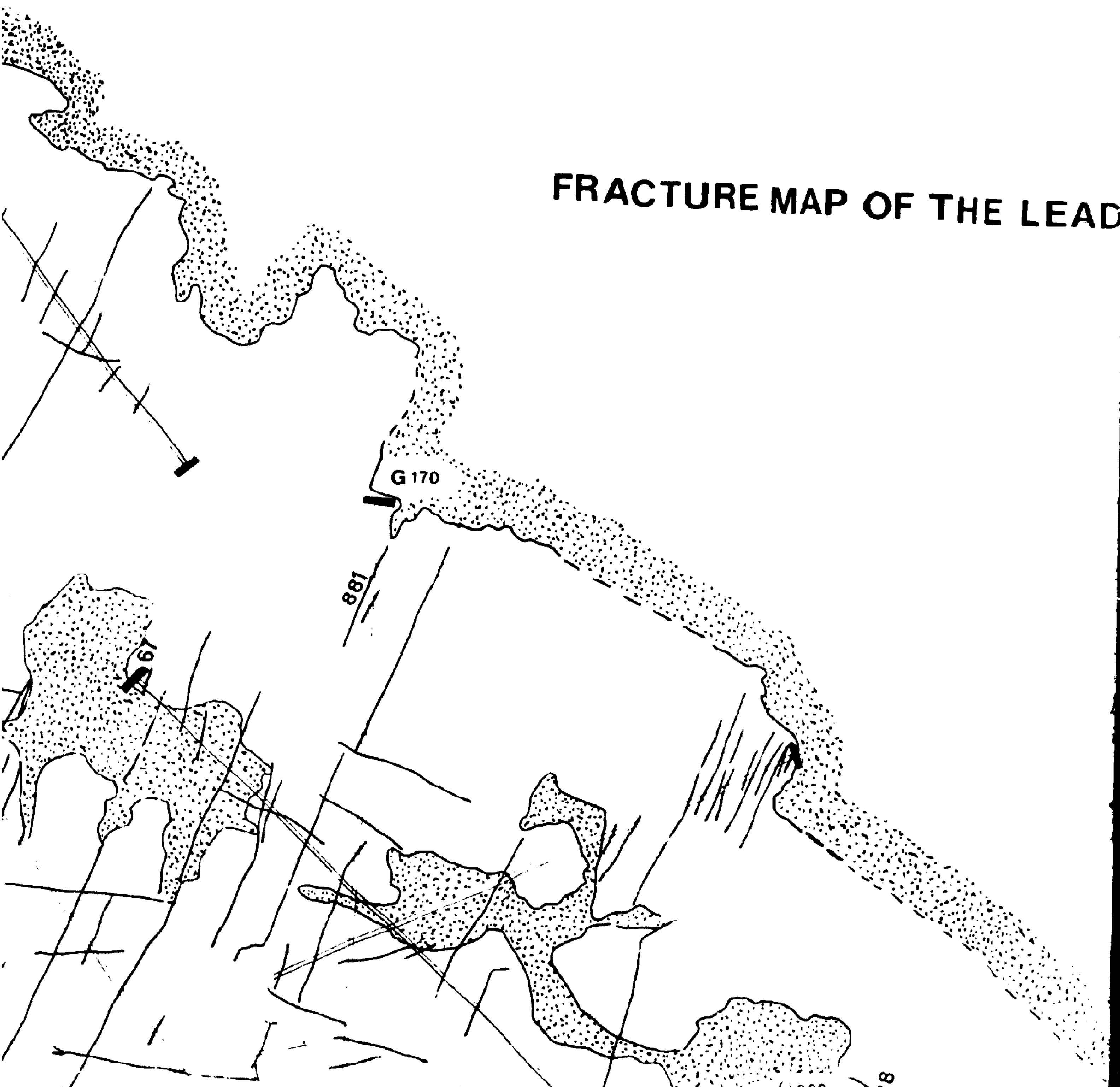

AP OF THE LEAD LAKE OUTCROP

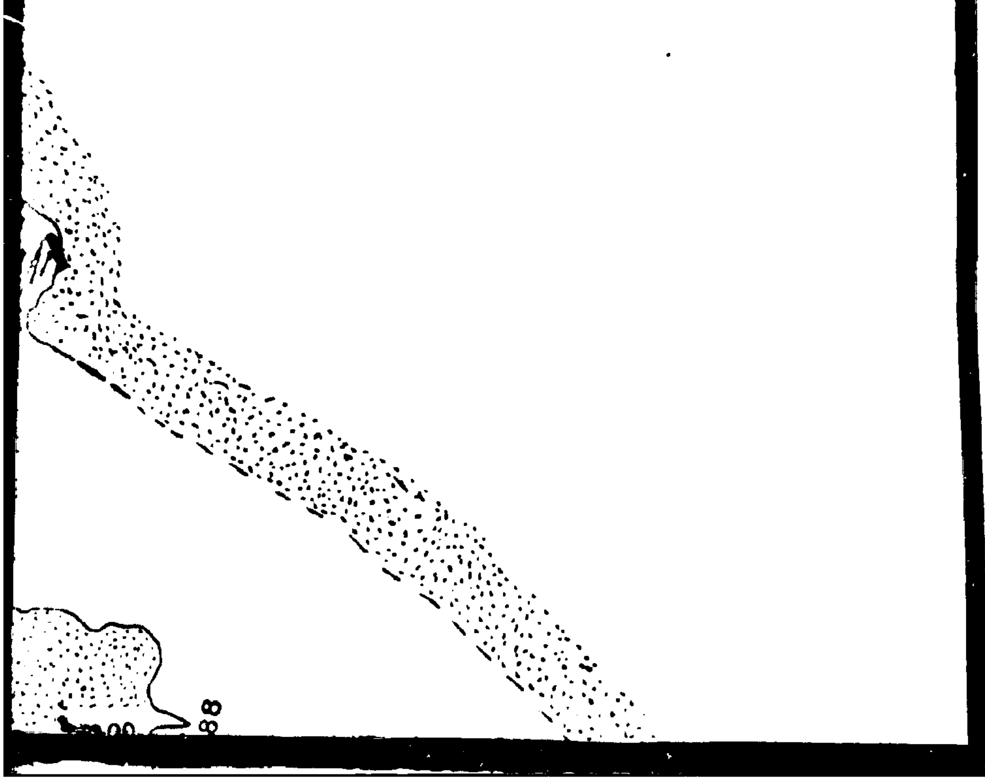

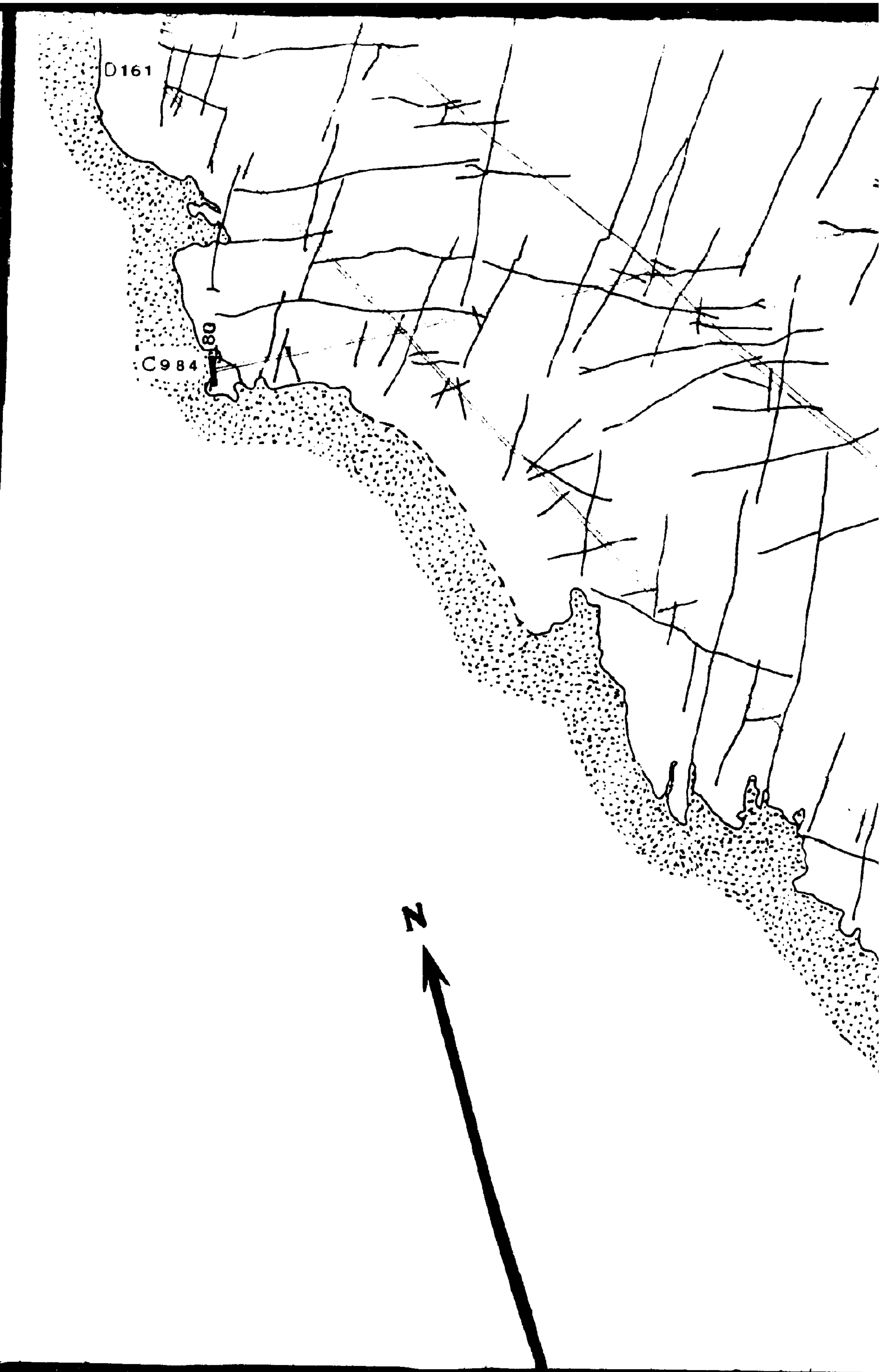
D161
C984
80
N

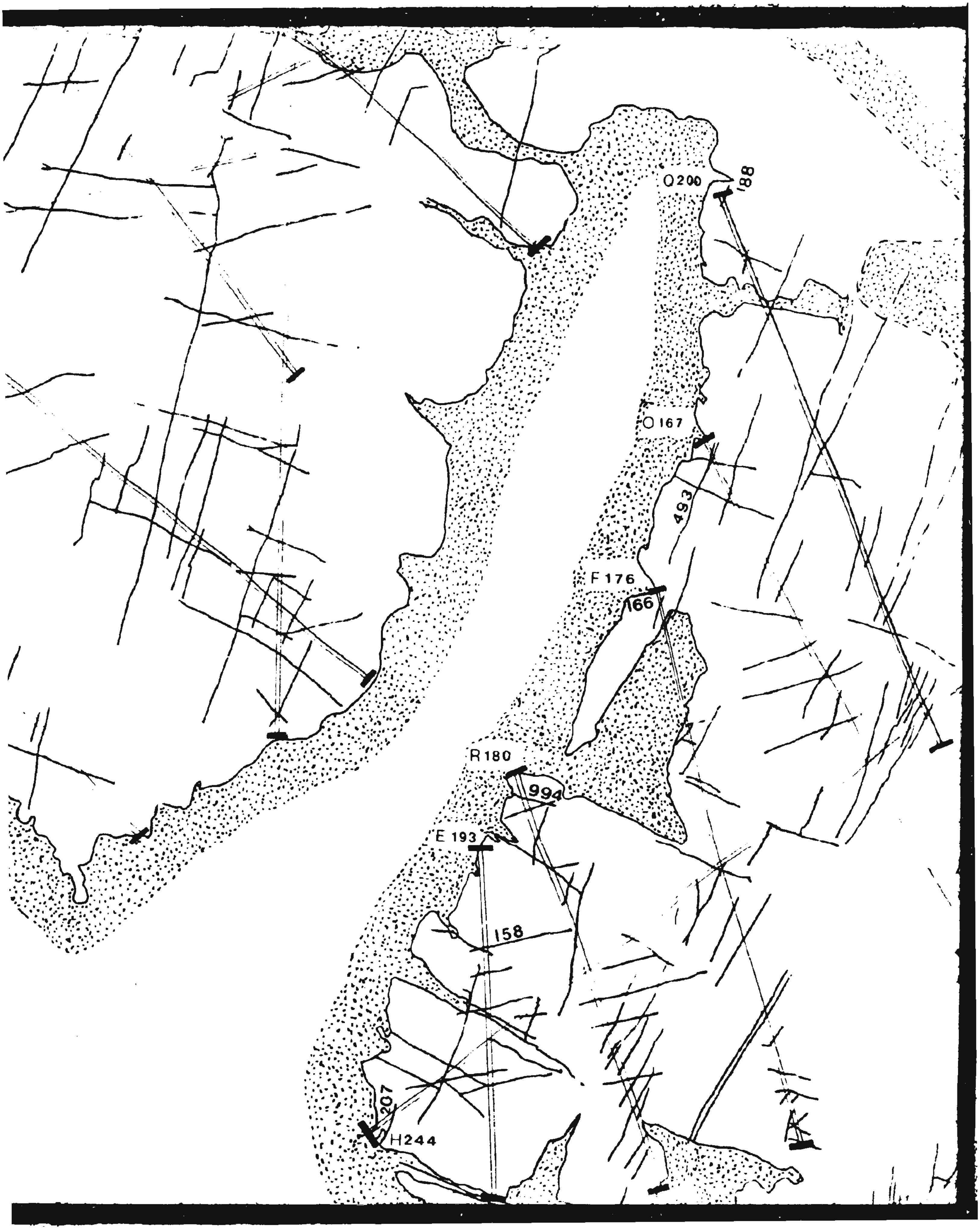
Q200
188
O167
493
F176
166
R180
994
E193
158
207
H244


188

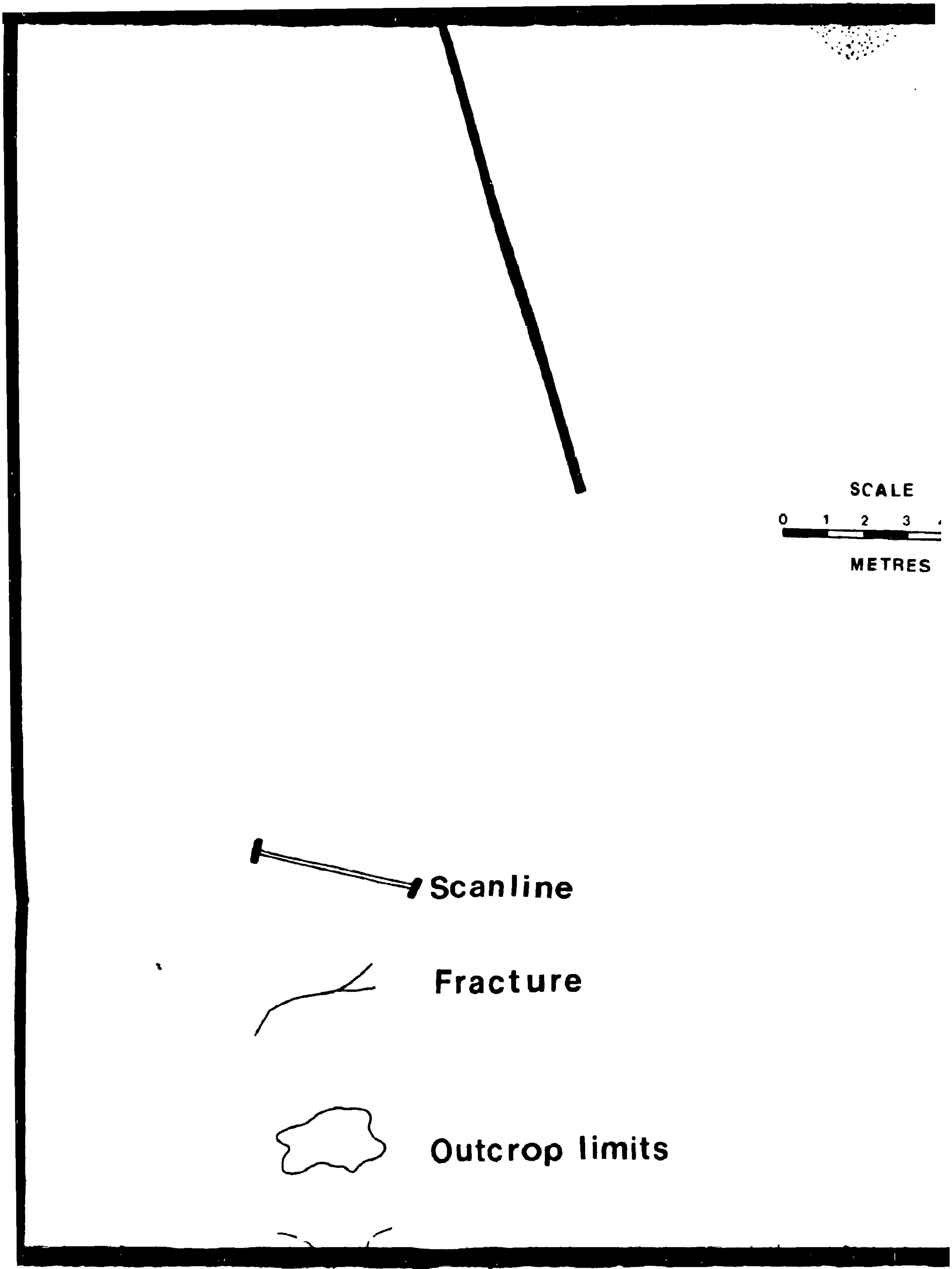
SCALE
0 1 2 3
METRES
Scanline
Fracture
Outcrop limits

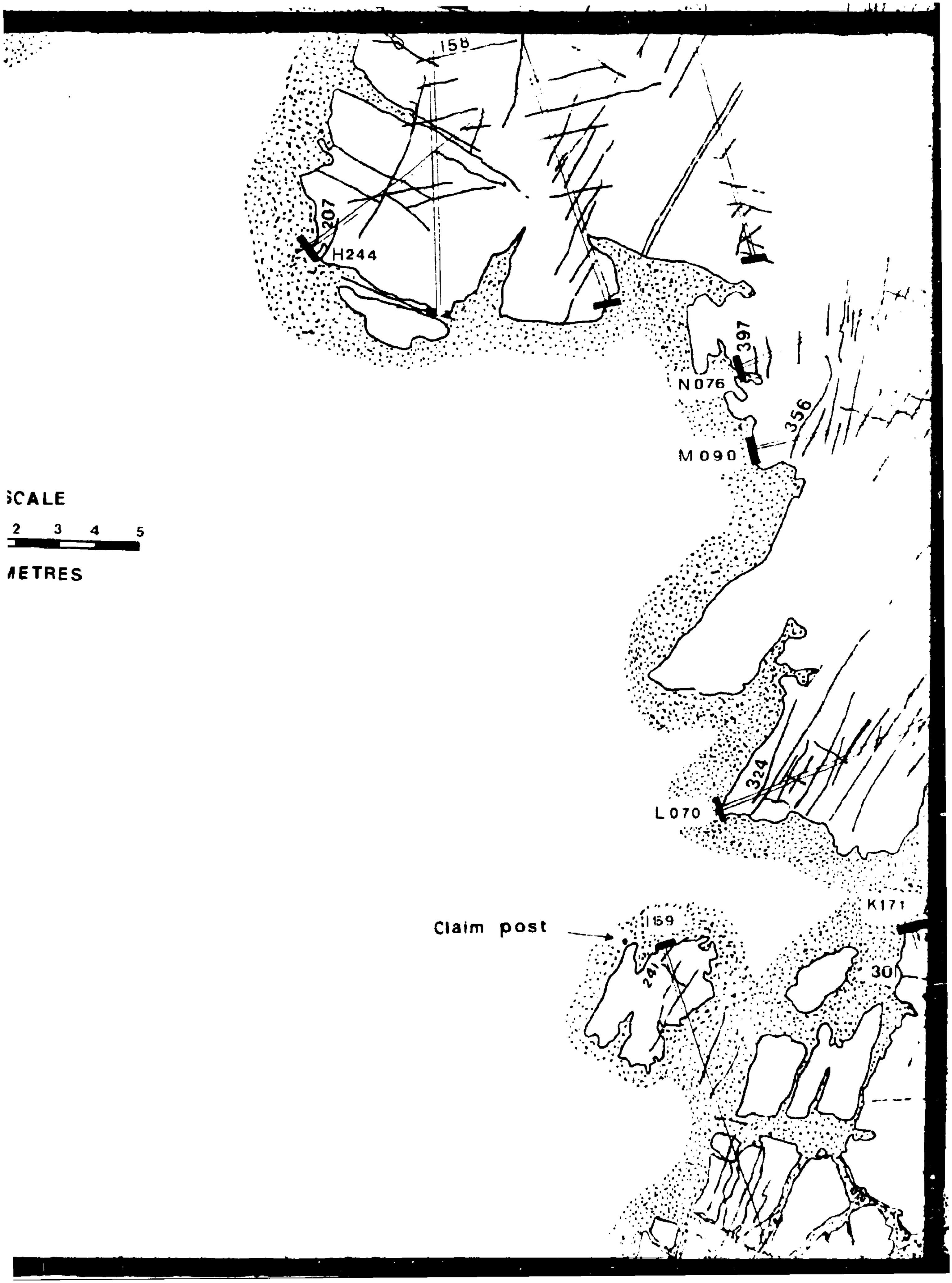

158
207
H244
397
N076
356
M090
SCALE
2 3 4 5
METRES
324
L070
K171
Claim post
I169
241
30

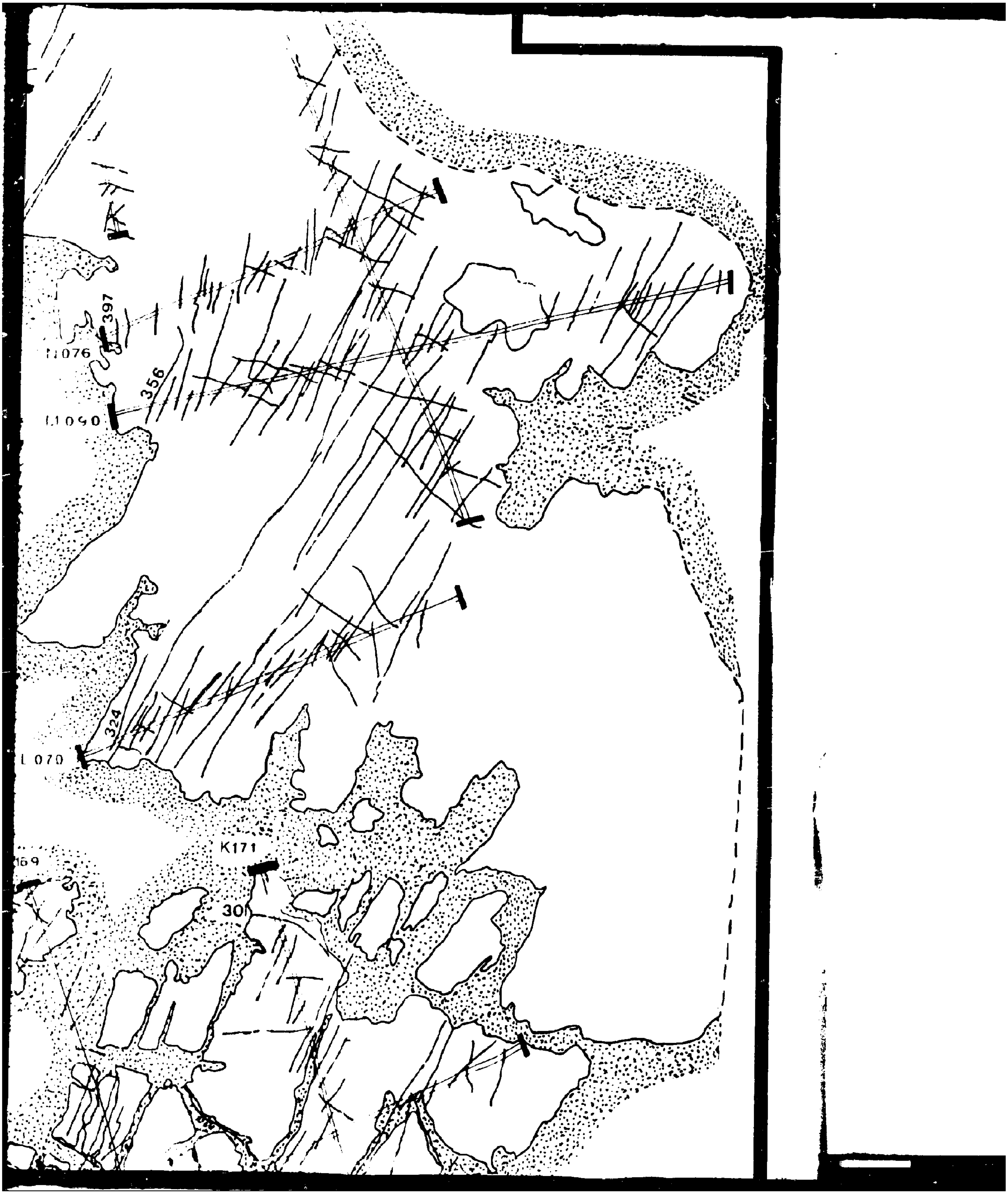

397
N076
356
L1090
324
L070
K171
169
30

Fracture

Outcrop limits

Estimated outcrop

R 176 Scanline leader and azi

167 Fracture number

(COM

imuth

PILATION

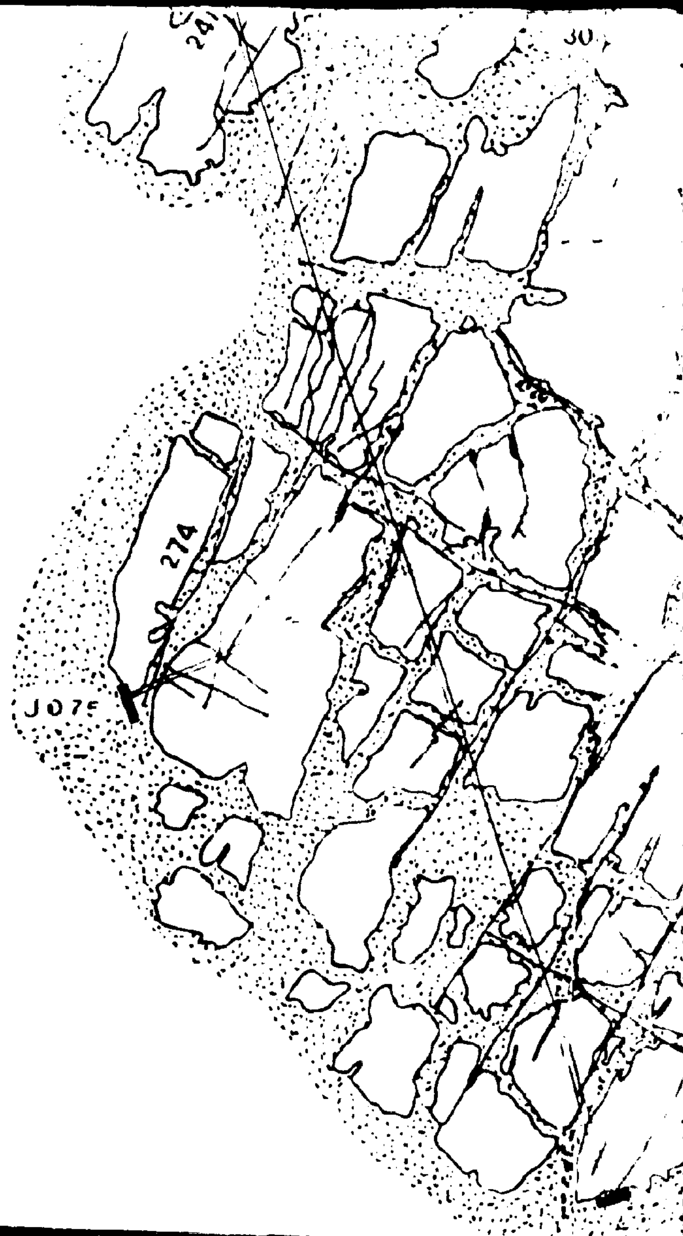


30